université PARIS-SACLAY

NNT: 2017SACLX051

Thèse de doctorat

Ab-initio description of optical nonlinear properties of semiconductors in the presence of an electrostatic field

Thèse de doctorat de l'Université Paris-Saclay
préparée à l'École Polytechnique

École doctorale №572 Ondes et matière
Spécialité de doctorat : Physique

Thèse présentée et soutenue à Palaiseau,
le 27 septembre 2017, par

Lucie Prussel

Composition du Jury :

Henri BACHAU Professeur, Université de Bordeaux	Président
Claudio ATTACCALITE Chargé de recherche, Aix-Marseille Université	Rapporteur
Christian BROUDER Directeur de recherche, UPMC	Rapporteur
Delphine MARRIS-MORINI Professeur, Université Paris-Sud	Examinateur
Julien TOULOUSE Maître de conférences, UPMC	Examinateur
Elena DEGOLI Professeur associé, UNIMORE	Examinateur
Valérie VÉNIARD Directeur de recherche, École Polytechnique	Directrice de thèse

Contents

Abreviations

(F)BZ	(First) Brillouin Zone
DFT	Density-Functional Theory
EFISH	Electric Field Induced Second-Harmonic
IPA	Independent-Particle Approximation
KS	Kohn-Sham
LDA	Local-Density Approximation
LEO	Linear Electro-Optic
LR	Linear Response
MTP	Modern Theory of Polarization
QEO	Quadratic Electro-Optic
RPA	Random Phase Approximation
SHG	Second-Harmonic Generation
SO	Scissor Operator
TDDFT	Time-Dependent Density-Functional Theory
THG	Third-Harmonic Generation
XC	Exchange-Correlation

Part I

Background

Chapter 1

Introduction

The context that brought up this thesis was the wish to provide a full ab-initio description of the second harmonic generation (SHG). So far, ab-initio calculations in solids of both bulk[1] and surfaces[2] were already available. The aim of this thesis was then to include in that description the SHG response induced by a static field, which can be especially important in some materials. This work will present this analytical calculation and application, which was first done for the linear response before applying it for SHG.

This chapter introduces the different nonlinear optical phenomena present in this thesis, in particular the linear electro-optic and electric-field induced second harmonic responses.

1.1 Nonlinear Optics

Optical properties of a material come from the interaction of light with matter, where the charged particles inside the medium interact with this electric field and create a polarization. Under usual circumstances, the response of a material induced by the electric field of the light is linear. With the invention of the laser in the 1960's, the optical power increased enough that the response of the medium started to deviate from this linear behavior (figure 1.1). Nonlinear optics (NLO) correspond

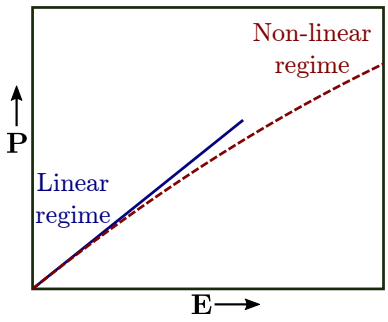

Figure 1.1: Evolution of the polarization with the strength of the input electric field **E**.

to phenomena where the polarization induced inside a material is not linear with respect to the electric field of the light. This can only be observed when the material is submitted to an intense light, such as the one provided by lasers. There is however some cases where it is possible to observe nonlinear optical processes without the presence of laser, such as (a) the static Kerr effect (also referred as the quadratic electro-optic effect) observed for the first time in 1875 by John Kerr[3], and (b) the Pockels effect discovered in 1893 by Friedrich Carl Alwin Pockels[3], that will later be referenced in this thesis as the linear electro-optic effect (LEO). Both these phenomena correspond to a change in the refractive

index of a material submitted to a static or low frequency electric field. They are often not counted among the nonlinear optical effects since they are still linear with respect to the field of the light and therefore, as previously stated, do not require a laser. The first nonlinear process obtained with a laser was in 1961, with the discovery of the second harmonic generation (SHG) by Peter Franken *et al.*[4], where they detected the frequency doubling of a red laser going through a nonlinear media. Many others nonlinear phenomena have since then been discovered, including the third harmonic generation (THG) by New *et al.*[5] in 1967 and the electric field induced second harmonic (EFISH) by Lee *et al.*[6], which will both be presented in more details later on in this chapter.

In the nonlinear regime, the polarization can be expanded in a Taylor series in terms of the total field. The induced polarization of the material is written as

$$\mathbf{P} = \chi^{(1)}\mathbf{E} + \chi^{(2)}\mathbf{EE} + \chi^{(3)}\mathbf{EEE} + \dots \tag{1.1}$$

where $\chi^{(1)}$, $\chi^{(2)}$ and $\chi^{(3)}$ are respectively the first, second and third order susceptibility and correspond to a tensor. This expansion of the polarization is correct if we are in the perturbation regime, meaning that the higher we go in the order of the susceptibility $\chi^{(n)}$, the less intense the response will be. This cease to be true when looking at high harmonic generation (HHG) where, past a certain point, the harmonics all reach the same intensity. This explains why a strong field is needed to be able to detect nonlinear effects. However, there is a limitation to how strong a field can be used. Indeed, if the field applied is too intense, the perturbation regime would not hold anymore. However for solids, applying a field that strong would usually provoke the destruction of the material.

There are many nonlinear optical processes which are partially referenced in table 1.1 for the second and third order. The highlighted blue rows correspond to the phenomena studied during this thesis. In general, susceptibilities exhibit different types of symmetry: time-reversal symmetry and

Nonlinear process		Susceptibilities[1]
Sum-Frequency Generation	SFG	$\chi^{(2)}(-(\omega_1+\omega_2);\omega_1,\omega_2)$
Difference-Frequency Generation	DFG	$\chi^{(2)}(-(\omega_1-\omega_2);\omega_1,-\omega_2)$
Second-Harmonic Generation	SHG	$\chi^{(2)}(-2\omega;\omega,\omega)$
Optical Rectification	OR	$\chi^{(2)}(0;\omega,-\omega)$
Linear Electro-Optic	LEO	$\chi^{(2)}(-\omega;\omega,0)$
Four-Wave Mixing	FWM	$\chi^{(3)}(-(\omega_1+\omega_2+\omega_3);\omega_1,\omega_2,\omega_3)$
Third-Harmonic Generation	THG	$\chi^{(3)}(-3\omega;\omega,\omega,\omega)$
Two-Photon Absorption	TPA	$\mathrm{Im}[\chi^{(3)}(-\omega;\omega,\omega,-\omega)]$
Quadratic Electro-Optic	QEO	$\chi^{(3)}(-\omega;\omega,0,0)$
Electric-Field Induced Second Harmonic	EFISH	$\chi^{(3)}(-2\omega;\omega,\omega,0)$

Table 1.1: Different second and third order optical phenomena that can occur when one or more beams are propagating inside nonlinear media.

permutation symmetry, which are fundamental properties of χ and symmetry in space, which reflects the structural properties of the medium. One of the consequence of the spacial symmetry is that even-order susceptibilities $\chi^{(2n)}$ are canceled in media with inversion symmetry in the electric dipole approximation. In such materials, the residual $\chi^{(2n)}$, due to higher multipole processes (quadrupolar polarization), is often too weak to be observed.

[1] We use the convention where the frequency of the emitted signal is written on the left side of a semicolon with a minus sign.

1.2 Linear Electro-Optic

The linear electro-optic effect (LEO) is a change in the dielectric properties, in particular the refractive index, of a material proportional to an electrostatic field $\boldsymbol{\mathcal{E}}$. This field can be created by appling a voltage on the material or already be present due to the structure of the material (see Figure 1.2).

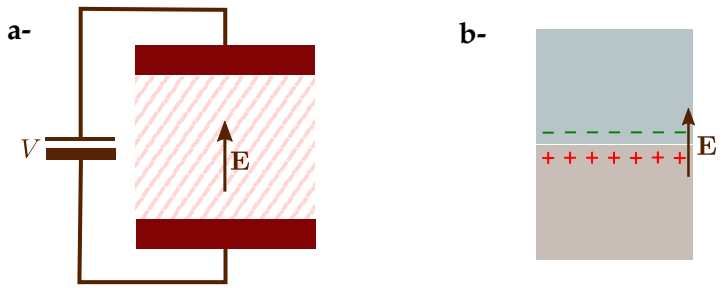

Figure 1.2: Creation of an dc-field inside the material by (a) applying a voltage on the material, (b) an accumulation of charge at an interface.

This phenomenon cannot be observed on every materials. Indeed it is calculated through a second order susceptibility $\chi^{(2)}$, hence it requires a lack of inversion symmetry to obtain a non-zero response. This susceptibility is not a simple scalar quantity. It connects the different components of the two electric fields $\mathbf{E}(\omega)$ and $\boldsymbol{\mathcal{E}}$ with the components of the polarization $\mathbf{P}$, which is why it can be considered as a rank 3 tensor $\chi^{(2)}_{ijk}$ with 27 components.

$$P_i(\omega) = \sum_{jk} 2\chi^{(2)}_{ijk}(-\omega;\omega,0)\; E_j(\omega)\; \mathcal{E}_k \tag{1.2}$$

where i, j, k are related to the axis orientation x, y, z and $\mathcal{E}_k$ is the dc-field along the k-direction. The factor 2 before the susceptibility appears when the two input frequencies are not equal, meaning for the sum- or difference-frequency generation (see Appendix A). Here this factor is not included in the susceptibility[7], so that we have the relation

$$\lim_{\omega\to 0} \chi^{(2)}_{SHG}(-2\omega;\omega,\omega) = \lim_{\omega\to 0} \chi^{(2)}_{LEO}(-\omega;\omega,0) \tag{1.3}$$

The refractive index corresponds to the ratio between the speed of light in vacuum and the one in a medium, which is slowed down by the interaction with the charge density inside the material. This can be altered by a static or low frequency electric field which would perturbe the electron distribution and therefore change the propagation of the light inside the material. This phenomenon can be tuned by changing the applied voltage. Such dc-tunable optical devices have a lot of applications. Most of which are electro-optic modulators (EOM), which control the light by changing the phase, amplitude or polarization of the beam. They usually contain one or two Pockels cells and possibly other optical elements such as polarizers. The simplest one is a phase modulator with only one Pockels cell (see Figure 1.3). EOM can also be used as fast optical switches where, instead of a gradual variation, the transmission is switched on or off. These different components are useful for optical communication or signal-processing applications.

The change in the refractive index is usually very small, but it can be significant for wave propagating on a distance far greater than the wavelength. This change is more important when materials have high intrinsic refractive indices.

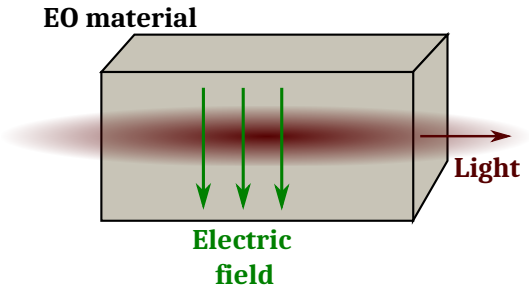

Figure 1.3: The static field changes the refractive index of the material, changing the light traveling though it.

The electro-optic effect can be considered as a correction to the linear response when the system is submitted to a dc-field. As such it needs to be included in the first order equation.

$$P_i(\omega) = \sum_{jk} \left[\chi^{(1)}_{ij}(-\omega;\omega) + 2\chi^{(2)}_{ijk}(-\omega;\omega,0)\ \mathcal{E}_k \right] E_j(\omega) \tag{1.4}$$

The linear optical properties of a material, which include phenomena such as absorption, dispersion, reflection and scattering, are obtained through the macroscopic dielectric tensor ε, which relates to the linear susceptibility $\chi^{(1)}(\omega)$ to the refractive index n by[2]

$$n^2(\omega) = \varepsilon(\omega) = 1 + 4\pi\chi^{(1)}(-\omega;\omega), \tag{1.5}$$

The real and imaginary part of the dielectric function (or refractive index) describe respectively the refraction and absorption of the light and is defined as

$$\mathbf{D}(\omega) = \mathbf{E}(\omega) + 4\pi\mathbf{P}(\omega) = \overleftrightarrow{\varepsilon}(\omega)\mathbf{E}(\omega), \tag{1.6}$$

where $\mathbf{D}$ is the electric displacement and $\mathbf{E}$ is the total electric field. If the medium is anisotropic, the dielectric constant is not a scalar quantity anymore and becomes a rank two tensor. When the static-field is turned on, we can define an effective dielectric function $\tilde{\varepsilon}_{ij}(\omega)$ that contains the electro-optic correction,

$$\tilde{\varepsilon}_{ij}(\omega) = \varepsilon_{ij}(\omega) + \sum_k 8\pi\ \chi^{(2)}_{ijk}(-\omega;\omega,0)\mathcal{E}_k, \tag{1.7}$$

which clearly shows that the variation of the refractive index will depend on the strength of the dc-field. The usual electro-optic coefficients are defined in term of the impermeability tensor $\eta_{ij}(\omega)$ [8], which is the inverse of the permittivity $\varepsilon_{ij}(\omega)$:

$$\eta_{il}(\omega)\ \varepsilon_{lj}(\omega) = \delta_{ij} \tag{1.8}$$

We then get a similar expression than eq. (1.7) for the impermeability,

$$\tilde{\eta}_{ij}(\omega) = \eta_{ij}(\omega) + r_{ijk}(\omega)\mathcal{E}_k, \tag{1.9}$$

where $r_{ijk}(\omega)$ is the linear electro-optic coefficient. The relation between the LEO susceptibility and coefficient is then given by:

$$\chi^{(2)}_{ijk}(-\omega;\omega,0) = -\frac{1}{8\pi}\ n_i^2(\omega)n_j^2(\omega)r_{ijk}(\omega) \tag{1.10}$$

[2]The equation are here written in atomic units, the 4π being absent from the formula in SI units.

where $n(\omega)$ is the refractive index of the medium.

The LEO correction is considered over a wide range of frequency. The presence of a static field usually induces a motion of the lattice. However, in the materials studied in this thesis, such as silicon or silicon carbide, this effect is quite weak and since we are only interested in the electronic part of the optical response, the motion of atoms is neglected. This corresponds to performing calculations with a near-static field that has a frequency high enough that the motion can be considered as frozen but low enough to avoid the dispersion induced by the field. Some early ab-initio calculations were already performed in the 90s, also using the "clamped lattice" approximation [7]. However the formalism used does not allow the inclusion of local fields or excitonic effects that will be discussed later.

1.3 Second-Harmonic Generation

Second harmonic generation (SHG) is one of the most widely used nonlinear optical phenomenon. It involves the absorption of two photons of the same frequency and the creation of a polarization at twice this frequency as shown in figure 1.4. It is a three-level interaction which takes place in a single

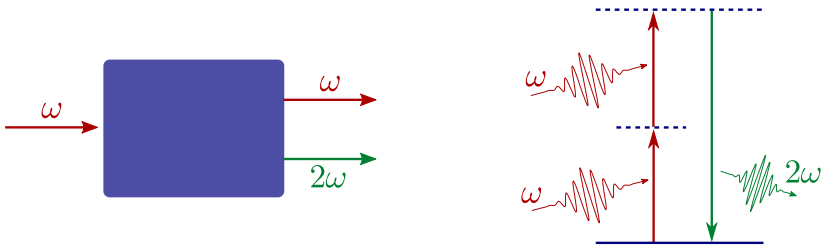

Figure 1.4: Scheme of SHG process: on the left, scheme of the material with the two transmitted beams at ω and 2ω; on the right, energy level description. The dashed lines represent virtual states.

step. It should not be confused with the two-photon absorption that comes from the imaginary part of a third order susceptibility $\chi^{(3)}$, and can be described by a similar sketch, in which the highest level would correspond to an excited state. In that case, there would be a true absorption of photons that would only occur if there is an excited state at twice the energy of the incoming photons. While in harmonic generation, several photons interact but without any actual absorption. In a real crystal, this three-level description is too simple, since many-body effects arise and more levels are involved. This phenomenon is described by a second-order susceptibility $\chi^{(2)}$, which, as for LEO, is a tensor with 27 components.

$$P_i(2\omega) = \sum_{jk} \chi^{(2)}_{ijk}(-2\omega;\omega,\omega)\, E_j(\omega)\, E_k(\omega) \tag{1.11}$$

The number of independent and non-zero components is entirely determined by the symmetry of the material studied. In the special case of SHG, the last two indices are interchangeable: $\chi^{(2)}_{ijk} = \chi^{(2)}_{ikj}$.

This optical process has found a lot of different applications over the years. One of the most heard of is the wavelength conversion of laser light, which can be used to reach frequencies where there is no regular laser sources available.

An important symmetry aspect of even-order susceptibility $\chi^{(2n)}$ is that it is canceled in media with inversion symmetry. For such materials, SHG is employed to probe surfaces and interfaces which are the only parts giving non-zero responses since they break the inversion symmetry. It is also used in microscopy, offering a contrast between molecules or particles with different symmetries, making it ideal for imaging tissues. However only dense non-centrosymmetric media can generate a second harmonic response, which can limit the applications. Experimentally, in order to have an efficient

response that is large enough to be detected, it is required to fulfill the phase-matching conditions $\Delta\mathbf{k} = \mathbf{k}_{2\omega} - 2\mathbf{k}_{\omega} = 0$, where $\mathbf{k}_{\omega}$ and $\mathbf{k}_{2\omega}$ are wave vectors for the incoming and outgoing photons, respectively. Otherwise, the incident power is not converted efficiently and part of the signal is lost due to interference, making it difficult to detect anything. If the system exhibits a resonance at ω_0, the SHG signal will display two resonances at ω_0 and $\omega_0/2$. Enhanced responses as well as dispersion effects are expected close to those resonances, as shown in figure 1.5. For a semiconductor, the resonant

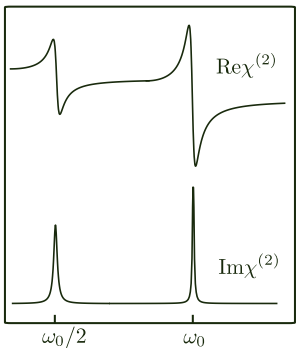

Figure 1.5: Variation of the real and imaginary part of SHG around the resonant frequencies.

frequency ω_0 corresponds to the gap between valence and conduction bands.

The ab-initio description of SHG for bulk and surfaces has already been well developed, including many-body effects[9;10]. But it is not yet the case for systems submitted to a static field.

1.4 Electric Field Induced Second Harmonic

Following the same idea as the linear electro-optic effect, which is a correction to the linear response when submitted to a static field, a similar phenomenon happens for the second harmonic called "Electric Field Induced Second Harmonic" (EFISH), which, as the name implies, corresponds to the generation of a second harmonic response in the presence of a dc-electric field. It is obtained through a third-order susceptibility, meaning that, unlike SHG, it does not depend on the centrosymmetry of the system.

$$P_i(2\omega) = \sum_{jkl} 3\chi^{(3)}_{ijkl}(-2\omega;\omega,\omega,0)\ E_j(\omega)\ E_k(\omega)\ \mathcal{E}_l \tag{1.12}$$

The factor 3 before the susceptibility comes from the fact that one of the input frequencies is different from the other two (see Appendix A). Regarding the EFISH susceptibility, the indices j and k are interchangeable, as in SHG, resulting in $\chi^{(3)}_{ijkl}(-2\omega;\omega,\omega,0) = \chi^{(3)}_{ikjl}(-2\omega;\omega,\omega,0)$.

When the material under measurements presents an inversion symmetry, SHG is typically used to probe surfaces or interfaces that break said symmetry since the usual more significant response from the bulk is zero. But when an interface is present in the system, as previously discussed for LEO, there is an accumulation of charges that occurs around it and a natural electrostatic field is created (see figure 1.2-b). And this static field induces an EFISH response from the bulk. Therefore, unlike SHG, EFISH is not surface-sensitive unless the static field only exists at the surface (or interface). The same phenomenon can occur with the laser, when performing experiments, which can also induce an accumulation of charges inside the material[11]. It then becomes necessary, when studying semiconductors where static fields are present, intrinsic to the material or voluntary applied, to be able to distinguish between SHG and EFISH contributions. This can be aided by the fact that, unlike SHG, EFISH has a clear voltage dependence. This also means that it can be a tool to study internal electric

fields. It is then essential, when aiming to provide accurate theoretical predictions for the second harmonic, to be able to determine this EFISH response.

Among the applications, EFISH has been widely used on molecular systems to investigate the second harmonic. In the experiments, the molecules are dissolved in a solvent and put in a optical cell with electrodes applied on both side. The generated electrostatic field orients the polar molecules and, by doing so, breaks the centrosymmetry of the system. It can then be used to probe the reorientation of molecules in an electric field[12]. Furthermore, EFISH was shown to be sensitive enough to the adsorption of molecule to be considered as a tool to monitor surface and interface contamination.

Since EFISH is considered as a correction to the second harmonic, it needs to be included in the second-order equation.

$$P_i(2\omega) = \sum_{jkl} \left[\chi^{(2)}_{ijk}(-2\omega;\omega,\omega) + 3\chi^{(3)}_{ijkl}(-2\omega;\omega,\omega,0)\ \mathcal{E}_l \right] E_j(\omega)\ E_k(\omega) \tag{1.13}$$

For a second-order response, the quantity describing the optical properties of the system is the macroscopic second order susceptibility $\chi^{(2)}$. In a similar fashion to equation (1.7) for the dielectric function $\varepsilon(\omega)$, an effective SHG susceptibility can be defined in the presence of a dc-field,

$$\tilde{\chi}^{(2)}_{ijk}(-2\omega;\omega,\omega) = \chi^{(2)}_{ijk}(-2\omega;\omega,\omega) + \sum_{l} 3\chi^{(3)}_{ijkl}(-2\omega;\omega,\omega,0)\ \mathcal{E}_l, \tag{1.14}$$

which then becomes dependent on the strength of the static field.

Although no ab-initio calculations have been previously done for EFISH, a general third-order formula with different frequencies was given by Aversa and Sipe[13]. However no spectrum was calculated using this formula, which has proven to be difficult for computational calculations, presenting a lot of convergence issues. Furthermore, as will be discussed later, the third order is much more sensible to the form of the expression than the lower order. Indeed, depending on the way the formula is written, the spectrum can be plagued by divergences in the energy terms that, if not cancelled properly, increase wrongly the intensity of the full spectrum.

1.5 Third-Harmonic Generation

The third harmonic generation (THG), often called 'frequency tripling', is a nonlinear optical phenomenon that involves the absorption of three photons at the same frequency and creates a polarization of thrice this frequency, as shown in figure 1.6. It is calculated through a third-order susceptibility,

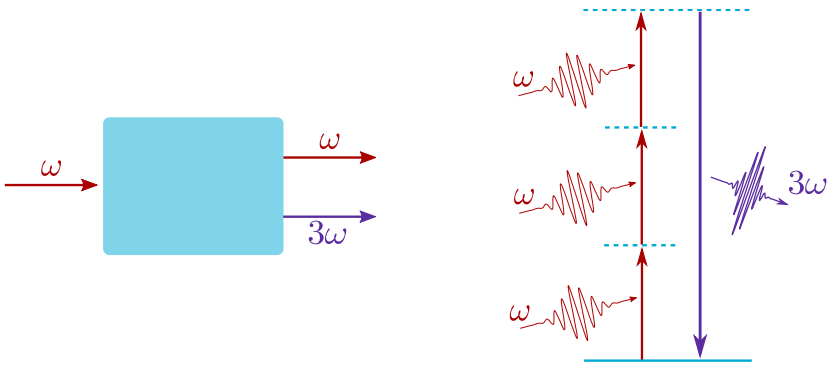

Figure 1.6: Scheme of THG process: on the left, scheme of the material with the two transmitted beams at ω and 3ω; on the right, energy level description. The dashed lines represent virtual states.

which corresponds to a $3 \times 3 \times 3 \times 3$ tensor of 81 components,

$$P_i(3\omega) = \sum_{jkl} \chi^{(3)}_{ijkl}(-3\omega;\omega,\omega,\omega)\ E_j(\omega)\ E_k(\omega)\ E_l(\omega), \tag{1.15}$$

where the three indices j, k, l are interchangeable: $\chi^{(3)}_{ijkl} = \chi^{(3)}_{ijlk} = \chi^{(3)}_{ikjl} = \chi^{(3)}_{iklj} = \chi^{(3)}_{iljk} = \chi^{(3)}_{ilkj}$. This specific phenomenon is of interest to us since it is a third-order process like EFISH, which give us the relation

$$\lim_{\omega\to 0} \chi^{(3)}_{THG}(-3\omega;\omega,\omega,\omega) = \lim_{\omega\to 0} \chi^{(3)}_{EFISH}(-2\omega;\omega,\omega,0) \tag{1.16}$$

This process is presented in this thesis in order to validate the range of intensity of the EFISH spectrum and confirm the value at $\omega = 0$. Furthermore, since it is a harmonic it is more easily calculated both analytically and computationally than a susceptibility with different frequencies like EFISH.

Also it has been calculated in order to compare it with EFISH, THG has nonetheless a lot of applications of its own. But, its applications are less spread than SHG due to the fact that this process is more difficult to observe since it is one order higher in the expansion (1.1), meaning that it far less intense. This is the reason why it is usually not used as such for the the tripling of the laser frequency into ultraviolet light. Instead, this is often realized in two steps. First, the input frequency is doubled and then frequency tripling is reached by a second-order process: sum-frequency generation of the original and doubled beam (see Figure 1.7).

Figure 1.7: Scheme of frequency tripling realized through SFG.

There are nonetheless applications using THG, for which the signal can be enhanced by several mechanisms such as a refractive index mismatch originated from an interface. Another one is resonance enhancement, where the wavelength of the produced THG signal is absorbed by the materials, leading to an increase intensity by resonance processes. One of the main application is THG microscopy, which uniquely provides 3D-imaging of the sample by detecting interfaces and heterogeneities. Since it is a nonlinear process, THG is induced only in close proximity to the focal point of the excitation laser, resulting in a high lateral resolution. Unlike SHG which is specific to centrosymmetry media, THG can be used on all materials since third-order susceptibilities are non-zero in any materials.

Some ab-initio calculations were already published for THG by C. Attaccalite and M. Grüning, using real-time approach[14;15] based on density-polarization functional theory. In that formalism, the polarization is not perturbative with respect to the field, meaning all orders are treated together, giving us access to all harmonics. However the results presented so far, using this method, do not include the value at $\omega = 0$ that we want.

Chapter 2

Density Functional Theory

This chapter reviews the basis of DFT, used to describe the electronic structure of many-body systems, as well as it time-dependent counterpart TDDFT, both of which are necessary for the calculation of optical properties.

2.1 Many-Body Problem

The many-body problem consists of a system of particles that all interact with each other, resulting in a coupled motion. It means that to solve the problem, one has to consider all the particles together, increasing considerably the difficulty of the problem with each new particle.

The starting point is the Hamiltonian describing a system of interacting electrons and nuclei in the non-relativistic limit,

$$\hat{H} = -\sum_i \frac{\hbar^2 \nabla_i}{2m_e} + \frac{1}{2}\sum_{i \neq j} \frac{e^2}{|\mathbf{r}_i - \mathbf{r}_j|} - \sum_I \frac{\hbar^2 \nabla_I}{2M_I} + \frac{1}{2}\sum_{I \neq J} \frac{Z_I Z_J e^2}{|\mathbf{R}_I - \mathbf{R}_J|} - \sum_{i,I} \frac{Z_I e^2}{|\mathbf{r}_i - \mathbf{R}_I|} \tag{2.1}$$

where the electrons are denoted by the subscript (i, j) and the nuclei by the upper case subscripts (I, J).

Born-Oppenheimer approximation

The mass of the nucleus M_I is considerably larger than the mass of an electron m_e, meaning that the motion of the electrons is much faster and can therefore be decoupled from the motion of the nuclei. In this approximation, when looking at the electronic part, the nuclei appear as frozen, which means that the nuclear positions $\mathbf{R}_I$ are described as constant parameters. The electronic Hamiltonian can then be written as

$$\hat{H} = -\sum_i \frac{\hbar^2 \nabla_i}{2m_e} + \frac{1}{2}\sum_{i \neq j} \frac{e^2}{|\mathbf{r}_i - \mathbf{r}_j|} - \sum_{i,I} \frac{Z_I e^2}{|\mathbf{r}_i - \mathbf{R}_I|} \tag{2.2}$$

where the three terms correspond in order to the kinetic energy $\hat{T}$, the electron-electron interaction $\hat{U}$ and the interaction $\hat{V}_{ext}$ with the static potential v_{ext} created by the ions.

$$\hat{V}_{ext} = \int d\mathbf{r}\, v_{ext}(\mathbf{r})\, \hat{\rho}(\mathbf{r}) \tag{2.3}$$

If we were to solve the previous equation (2.1) for a system of N particles, we would obtain wave-functions $\psi(\mathbf{r}_1, \ldots, \mathbf{r}_N)$ of 3N variables all interconnected. As a result, the complexity of the problem growths exponentially with the size of the system, which would make it impossible to solve realistic macroscopic system.

Many approaches exist to find an approximate solution to the many-body problem. One of them is the density functional theory (DFT) and its time-dependent counterpart (TDDFT), used to investigate respectively ground state and dynamical properties. In the following, we review the basis of the theory[16].

2.2 Density Functional Theory

Density functional theory (DFT) has become the method of choice for the investigation of medium and large scale systems. The main idea of DFT is the introduction of the electronic density as a fundamental variable instead of the many-body wavefunctions, allowing DFT, while formally exact, to be computationally very efficient.

2.2.1 Hohenberg-Kohn theorems

The key quantity calculated is the electronic density which allows the basic description of materials through the ground-state. It is important to incorporate all the essential contributions to the kinetic and potential energies, while balancing with the efficiency of the calculations. DFT aims to describe the ground-state of a system of N electrons in the presence of the external potential v_{ext} of the ions, static in time. The total energy can be obtained by solving the time-independent Schrödinger equation,

$$\hat{H}\big|\psi_0\big\rangle = E_0\big|\psi_0\big\rangle \tag{2.4}$$

where $\hat{H} = \hat{T} + \hat{U} + \hat{V}_{ext}$ is the Born-Oppenheimer Hamiltonian written in eq. (2.2). Since $\hat{T}$ and $\hat{U}$ are the same for all physical system, the Hamiltonian is entirely determined by the potential v_{ext}, which is an external single-particle potential. This means that all the properties of the system are also determined by the external potential like the ground-state wavefunctions ψ_0 and density $\rho_0(\mathbf{r})$. The inverse is also true as stated in the first Hohenberg-Kohn theorem.

Theorem 2.2.1. (Hohenberg and Kohn I, 1964,[17])
The ground-state density $\rho_0(\mathbf{r})$ of a system of interacting particles in some external potential $v_{ext}(\mathbf{r})$ determines this potential uniquely, except for a constant.

Therefore every observables, as well as the ground state many-body wavefunctions ψ_0, become a functional of the density, in particular the total energy $E_{v_0}[\rho] = \big\langle\psi_0[\rho]\big|\hat{T}[\rho] + \hat{U}[\rho] + \hat{V}_0[\rho]\big|\psi_0[\rho]\big\rangle$. Thus reducing the Schrödinger equation (2.4) to a functional of ρ, a three-variables quantity. Originally for non-degenerate systems, this theorem has now been extended for different cases to include degenerate states and the spin. The Rayleigh-Ritz principle leads us to the second theorem.

Theorem 2.2.2. (Hohenberg and Kohn II, 1964,[17])
A functional for the total energy $E[\rho]$ of the electronic density $\rho(\mathbf{r})$ can always be defined for any external potential $v_{ext}(\mathbf{r})$. The density that minimizes this functional is the exact ground-state density $\rho_0(\mathbf{r})$ for a given $v_0(\mathbf{r})$: $E_{v_0}[\rho] \geq E_{v_0}[\rho_0]$.

We went from solving the Schrödinger equation (2.4) to minimizing the energy functional with respect to $\rho(\mathbf{r})$, a task that would prove trivial if this so-called functional was known. The difficulty of the problem is now to find a suitable approximation for $E_{v_0}[\rho]$.

Another theory, based on the same idea of using the density as the main variable, was already formulated in the late 1920s by Thomas and Fermi. While less accurate than DFT, it still presents a lot

of similarities. In this model, the electron-electron interaction $\hat{U}$ was approximated by the classical Hartree potential v_H and the kinetic energy $\hat{T}$ by the one of an homogeneous electron gas, using the local density approximation (LDA) also encountered in modern DFT. The electron correlation is also completely neglected as in the Hartree-Fock method. This theory yields good results for atoms but is rather inaccurate for more complex systems since it fails to consider the actual structure of atomic orbitals, which is needed to correctly describe molecular bonding. This approach could be considered as an approximation to the modern DFT theory.

2.2.2 Kohn-Sham equations

Kohn and Sham (KS), instead, introduced an auxiliary system of independent particles for which the electronic density and other properties would correspond to the ones of the real system. In principle, it should lead to exact calculations of those properties. However, in practice many approximations are needed to perform actual calculations. This is expressed as the following

Definition 2.2.3. (Kohn and Sham, 1965,[18])
Any systems of interacting particles in the external potential v_0 can be mapped to a system of fictitious, non-interacting Kohn-Sham particles in the effective local potential v_S such that both have the same ground state density ρ_0 : $\hat{H} = \hat{T} + \hat{U} + \hat{V}_0 \xleftrightarrow{\rho_0} \hat{H}_S = \hat{T}_S + \hat{V}_S$

The KS Hamiltonian $\hat{H}_S$ has the usual kinetic operator $\hat{T}_S$ and a local single-particle potential $v_s(\mathbf{r})$, with

$$\hat{V}_S = \int d\mathbf{r}\; v_s(\mathbf{r})\; \hat{\rho}(\mathbf{r}) \tag{2.5}$$

If this potential was known exactly, it would be easy to solve the Schrödinger equation (2.4) independently for each particle of the fictitious system. This would give us the KS wavefunctions $\phi_i(\mathbf{r})$, thus allowing the calculation of the ground-state density ρ_0,

$$\rho_0(\mathbf{r}) = \sum_i^N |\phi_i(\mathbf{r})|^2 \tag{2.6}$$

and all related properties. In the Kohn-Sham approach, as in the Thomas-Fermi model, the electron-electron interaction $\hat{U}$ is approximated by the Hartree energy E_H,

$$E_H[\rho] = \frac{1}{2} \int d\mathbf{r}\; d\mathbf{r}'\; \frac{\rho(\mathbf{r})\rho(\mathbf{r}')}{|\mathbf{r} - \mathbf{r}'|} \tag{2.7}$$

But DFT is an exact theory, so we introduce an exchange-correlation operator E_{XC}, containing all the electron correlation neglected in the Thomas-Fermi model, which is the difference between the interacting many-body Hamiltonian and the approximated non-interacting one,

$$E_{XC}[\rho] = T[\rho] + U[\rho] - T_S[\rho] - E_H[\rho] \tag{2.8}$$

However, the exact form of this operator is unknown and would need to be approximated, which would be the only fundamental approximation in DFT. The ground-state energy functional of the interacting system can then be written as

$$E_{v_0}[\rho] = T_S[\rho] + E_H[\rho] + V_0[\rho] + E_{XC}[\rho], \tag{2.9}$$

which becomes the same for the KS auxiliary system at their minimum when $\rho = \rho_0$.

$$\begin{aligned} v_S([\rho_0], \mathbf{r}) &= \left.\frac{\delta E_H}{\delta \rho(\mathbf{r})}\right|_{\rho=\rho_0} + v_0(\mathbf{r}) + \left.\frac{\delta E_{XC}}{\delta \rho(\mathbf{r})}\right|_{\rho=\rho_0} \\ &= v_H([\rho_0], \mathbf{r}) \; + v_0(\mathbf{r}) + v_{XC}([\rho_0], \mathbf{r}) \end{aligned} \tag{2.10}$$

Hence the problem is reduced to solving the single-particle Schrödinger equation where the KS potential $v_S([\rho], \mathbf{r})$ is found in a self-consistent way with respect to the density, as illustrated in Figure 2.1. This procedure would give the exact ground-state density, were the exchange-correlation

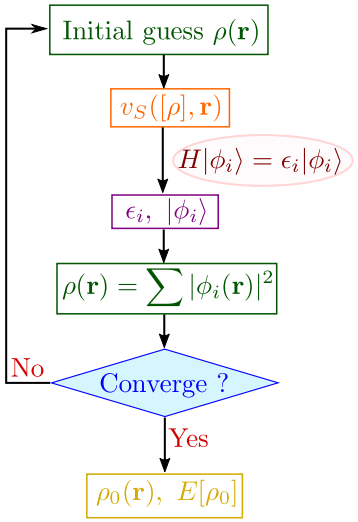

Figure 2.1: Self-consistent scheme in DFT

functional $E_{XC}[\rho]$ known.

2.2.3 Exchange-correlation potential

The long-range interaction is contained in the Hartree term. Therefore what remains in the exchange-correlation functional $E_{XC}[\rho]$ is nearly local. In its general form, it is written as

$$E_{XC}[\rho] = \int d\mathbf{r} \; \epsilon_{XC}([\rho], \mathbf{r}) \; \rho(\mathbf{r}) \tag{2.11}$$

where $\epsilon_{XC}([\rho_0], \mathbf{r})$ is the energy per electron depending on the density around $\mathbf{r}$. Since this term is not known, we need to use an approximation to evaluate it. Over the years, many approximations for the XC-functional have come to light with different degrees of accuracy. There is nowadays no universal XC-functional that works to calculate correctly all the properties of every materials. There is always a case where it fails. Here, we will only discuss the simplest one, which is the local density approximation (LDA), for which we consider that the exchange-correlation energy at one point $\mathbf{r}$ is the same as the one of an homogeneous electron gas with the same density in that point. The exchange-correlation functional $E_{XC}[\rho]$ can then be approximated as a local functional of the density.

$$E_{XC}^{LDA}[\rho] = \int d\mathbf{r} \; \epsilon_{XC}^{LDA}(\rho(\mathbf{r})) \; \rho(\mathbf{r}) \tag{2.12}$$

where $\epsilon_{XC}^{LDA}(\rho)$ is a local function of the density at $\mathbf{r}$ and not a functional. Usually it is split in an exchange and correlation part, $\epsilon_{XC}(\rho) = \epsilon_x(\rho) + \epsilon_c(\rho)$. The exchange part is given by the Dirac functional[19]. Various parametrizations exist to calculate $\epsilon_c(\rho)$ which are based on Monte Carlo simulations on homogeneous electron gases at different densities. The exchange-correlation potential v_{XC}

used in eq. (2.10) to determine the Kohn-Sham potential v_S can be written as

$$v_{XC}^{LDA}([\rho_0], \mathbf{r}) = \epsilon_{XC}^{LDA}(\rho_0(\mathbf{r})) + \rho_0(\mathbf{r}) \left. \frac{\delta \epsilon_{XC}^{LDA}(\rho(\mathbf{r}))}{\delta \rho(\mathbf{r})} \right|_{\rho=\rho_0} \tag{2.13}$$

In LDA the inhomogeneities in the density around $\mathbf{r}$ are completely neglected. But despite the drastic nature of the approximation, it can work quite well for extended systems due to the fact that it respects the sum rule for the exchange-correlation hole, stating that the hole should have the charge of one electron. However it is not accurate enough for molecules since it tends to overbind. Other approximations exist to overcome the failures of LDA like GGA (Generalized Gradient Approximation), where the inhomogeneities in the electron density are taken into account, or hybrid functionals, which correct the exchange part of the potential. Yet, for the purpose of this thesis, which is the calculation of optical properties of semiconductors, the quality of the XC-approximation in the ground-state is not so important and LDA is more than enough.

2.2.4 Bandstructure and band-gap problem

A well-known issue of DFT is the underestimation of the theoretical gap between valence and conduction bands compared to the experimental one. It is an important point for us since the correct relative eigenvalues of occupied and unoccupied states is required to calculate rather accurate optical responses, as it is aimed in this thesis. In fact, static DFT is not meant to describe excited properties of the system such as the optical band-gap. In theory, this correct band gap should be obtained at the TDDFT level had we had a good enough approximation for the time-dependent exchange-correlation potential. Moreover there is no physical interpretation for the KS eigenenergies with the exception of the highest occupied KS state in a finite system that should correspond to the ionization energy of the system in exact DFT. However, it is not always the case due to the self-interaction error (SIE) caused by the electron interacting with itself in equation (2.7). This error is introduced in the Hartree energy and not corrected by the xc-potential. In Hartree-Fock methods however, the exchange term is calculated exactly, which enables the cancellation of the Coulomb self-interaction. This could be partially solved by using hybrid functionals, which introduce a certain amount of Hartree-Fock exchange that cancels part of the SIE, thus leading to the relocalization of the density and increasing the band-gap.

In practice, including the correction to the band gap at the TDDFT level is not doable since we do not have an approximation for the time-dependent exchange-correlation potential that will treat this issue, which is why we want to start from the correct band gap before any TDDFT calculation. To obtain the real band-gap measured in photo-emission (PE) experiments, one should look at quasiparticle energies and not the Kohn-Sham ones. A common approach to access to the PE-band-gap consists in performing GW calculation. This method takes into account the fact that, when an electron is excited, it leaves a hole positively charged that attracts the surrounding electrons, which can be represented as a cloud of opposite charge particles. This can be interpreted as a screening of the hole. The particle and its screening cloud are referred to as quasiparticle. GW calculations are equivalent to performing an Hartree-Fock calculation that includes the screening. Therefore it does not contain the self-interaction error and it includes the interaction of particles, leading to a much better description of the band-gap, which usually agrees with experiments. For many systems the quasiparticle and KS bandstructures are actually quite similar regarding the shape of the bands and only differ in the size of the gap. Consequently, a much simpler procedure to solve the band-gap problem is to use the scissor approximation, where a rigid shift in energy is applied to the conduction band (see Figure 2.2), in the form of a non-local operator added to the Hamiltonian.

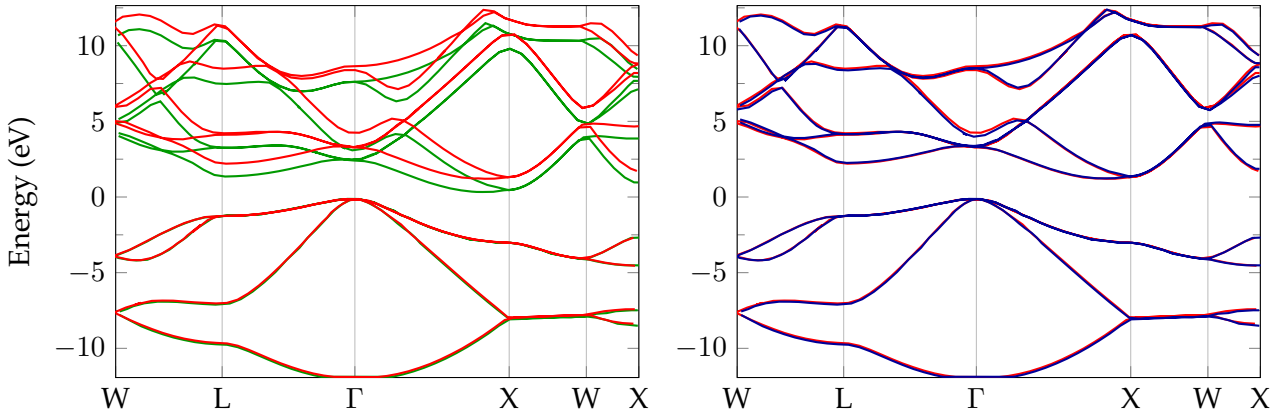

Figure 2.2: Bandstructure of silicon: (a) left panel: comparison between DFT (green) and G_0W_0 (red) calculation; (b) right panel: comparison between G_0W_0 (red) and DFT+scissor (blue), with a scissor $\Delta = 0.9$ eV.

2.3 Numerical details

Most of the density functional theory calculations performed on solids are based on pseudopotentials and a plane-wave basis set which includes explicitly periodic boundary conditions.

2.3.1 Bloch's theorem

To perform realistic calculations of electronic structure for solids, it is important to reduce the large number of electrons (proportional to the Avogadro number) by considering the periodicity of the system. This implies that the material under study is crystalline. In that case, only the atoms within the crystallographic unit cell are explicitly considered, and periodic boundary conditions are accounted for by exploiting the translational symmetry of the crystal. Such kind of approach is based on the Bloch's theorem which states that, for a potential with the periodicity of the lattice,

$$v_S(\mathbf{r}) = v_S(\mathbf{r} + \mathbf{R}), \qquad \text{where } \mathbf{R} \text{ is a lattice vector,} \tag{2.14}$$

the eigenstates of the single-particle Hamiltonian can be defined by,

$$\psi_{n,\mathbf{k}}(\mathbf{r}) = e^{i\mathbf{k}\cdot\mathbf{r}}\, u_{n,\mathbf{k}}(\mathbf{r}) \tag{2.15}$$

where $u_{n,\mathbf{k}}$ is a periodic function in the unit cell, ie. $u_{n,\mathbf{k}}(\mathbf{r}) = u_{n,\mathbf{k}}(\mathbf{r} + \mathbf{R})$. Bloch states of equation (2.15) are defined by two indices n and $\mathbf{k}$ which represent the band index and the crystal momentum, respectively. The dependence of the Bloch states which respect to $\mathbf{k}$ can be limited to the first Brillouin zone (FBZ) of the reciprocal space without any loss of information. Thanks to the Bloch theorem, the initial problem of solving the KS equations for an infinite number of electrons, ie. $n \to \infty$ in equation (2.9), transforms to calculating for a finite number of bands at an infinite number of $\mathbf{k}$-points, ie. to integrate the expression of the energy over the FBZ, that is

$$E_{\mathrm{KS}}[\rho] = \frac{1}{V_{\mathrm{FBZ}}} \int_{\mathrm{FBZ}} d\mathbf{k}\, E_{\mathbf{k}}[\rho_{\mathbf{k}}] \tag{2.16}$$

where V_{FBZ} is the volume of the first Brillouin zone. However, considering that energy and related properties are expected to smoothly vary with respect to $\mathbf{k}$, the integration over $\mathbf{k}$ can be approximated by a finite sampling of the FBZ.

2.3.2 Plane-wave basis set

The method used to solve equation (2.9) depends on the basis set used to expand the KS orbitals which, in equation (2.15) are defined by $u_{n,\mathbf{k}}$. Among the many possibilities, two families can be identified, which depend somewhat on the scientific background/culture. Chemists would prefer to expands KS orbitals in a sum of atom-centered functions using the standard "linear combination of atomic orbitals" (LCAO), whereas condensed matter physicists tend to use plane-wave as basis set. The use of plane-waves presents several advantages compared with localized basis functions: (i) their mathematical expression is very simple, (ii) they are mutually orthogonal, meaning that there is no overlap between them, (iii) they intrinsically account for periodic boundary conditions, and most importantly (iv) they allow for systematic —monotonic— convergence of the energy. The main drawback are related to their delocalized nature which (i) avoid "empty space" as required when dealing with 2D or 1D periodic systems, and (ii) they are not chemically intuitive —they are not atom-like functions— and involved development of relocalization algorithms to interpret KS orbitals or density in terms of chemical bonds. Using plane-wave basis set, the KS orbitals are expressed as,

$$\psi_{n,\mathbf{k}}(\mathbf{r}) = \sum_{\mathbf{G}} c_{n,k}(\mathbf{G})\, e^{i(\mathbf{k}+\mathbf{G})\mathbf{r}} \tag{2.17}$$

where the sum is performed over all possible reciprocal lattice vectors $\mathbf{G}$, and the set of coefficients $\{c_{n,\mathbf{k}}\}$ are determined by diagonalizing the matrix form of eq. (2.9) for each $\mathbf{k}$-point. To limit the expansion in equation (2.17), the sum over $\mathbf{G}$ is limited to a set of reciprocal lattice vectors contained in a sphere of radius $|\mathbf{k}+\mathbf{G}|$, which is usually defined by the kinetic energy cutoff,

$$\frac{\hbar|\mathbf{k}+\mathbf{G}|^2}{2m} \leq E_{cut} \tag{2.18}$$

Therefore, the convergence of the calculation is easily controlled by simply increasing the energy cutoff.

2.3.3 Pseudopotential approximation

Based on the fact that electrons principally involved in chemical bonding are those occupying the valence states, it is allowed to consider core electrons as spectators of the interactions of atoms in molecules or solids. The frozen-core approximation states that the core-electrons are not affected by their environment, ie. they are "frozen" and considered with the nuclei as rigid ion cores. This reduces the number of electronic degrees of freedom and decreases the computational time needed to solve the KS equations. Because atomic valence wavefunctions must be orthogonal to the core wavefunctions, they present strong oscillations (nodes) within the region close to the nucleus. This requires a large number of plane-waves to correctly reproduce this oscillating behavior. It is therefore more convenient to replace the nucleus and frozen core-electron potentials by an "ionic potential" also called pseudopotential which releases the constraints of orthogonality between valence and core states. The fact that core oscillations of valence electrons have now disappeared reduces the need for plane-waves with large kinetic energy components, and consequently reduces $\mathrm{E_{cut}}$ defined in equation (2.18). As depicted on Figure 2.3, the pseudo-wavefunctions vary smoothly in the core region and, unlike all-electron wavefunctions, present no nodes. The drawback of this approach is that most pseudopotentials are non-local to allow different states to feel different potentials. In contrast, local pseudopotentials act the same way on all the wavefunctions, making it less accurate and not very often used. The introduction of this non-local part in the potential means that the velocity operator $\hat{\mathbf{v}}$ is no longer the same as the momentum operator $\hat{\mathbf{p}}$. Indeed, we have

$$\hat{\mathbf{v}} = i[\hat{H}, \hat{\mathbf{r}}] = \hat{\mathbf{p}} + i[\hat{V}_{nl}, \hat{\mathbf{r}}] \tag{2.19}$$

where $\hat{V}_{nl}$ is the non-local contribution of the pseudopotential. This nonlocal contribution needs to be included in the optical response.

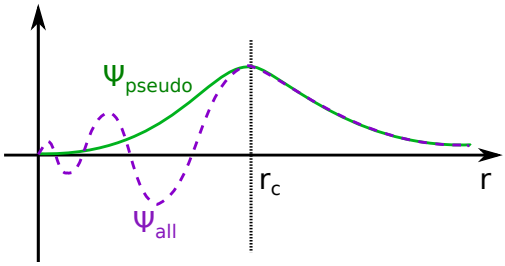

Figure 2.3: All-electron ψ_{all} (dashed line) vs pseudo-wavefunctions ψ_{pseudo} (solid line).

The two most common pseudopotentials used in plane-waves DFT codes are the norm-conserving (NCPP)[20] and ultrasoft (USPP)[21] pseudopotentials. During the generation of NCPP, the atomic pseudo-wavefunctions $\tilde{\phi}_i$ are enforced to respect the norm-conservation with respect to their all-electron analogues ϕ_i,

$$\int d\mathbf{r}\ \tilde{\phi}_i(\mathbf{r})\tilde{\phi}_j(\mathbf{r}) - \int d\mathbf{r}\ \phi_i(\mathbf{r})\phi_j(\mathbf{r}) = 0, \quad \text{for} \quad |\mathbf{r}| < r_c \tag{2.20}$$

and to match exactly above a certain cutoff radius r_c,

$$\tilde{\phi}_i(\mathbf{r}) = \phi_i(\mathbf{r}), \quad \text{for} \quad |\mathbf{r}| \geq r_c \tag{2.21}$$

Increasing r_c naturally tends to decrease the number of plane-waves needed to reach convergence. Due to the norm-conservation constraints, NCPP cutoff are generally small. For USPPs, which were not used in this thesis, the constraint of equation (2.20) is relaxed in order to limit the number of necessary plane-waves to the cost of introducing a generalized eigenvalue problem,

$$\hat{H}\big|\psi_i\big\rangle = \varepsilon_i \hat{S}\big|\psi_i\big\rangle, \tag{2.22}$$

where $\hat{S}$ is the hermitian overlap operator.

2.4 Time-Dependent Density Functional Theory

DFT has been extended by Runge and Gross in 1984 to include situations where the system is submitted to a time-dependent perturbation[22]. It is actually a generalization of the static Kohn-Sham method. I will briefly present it in this section, and afterwards its corrections since it was later proven to not be entirely correct.

2.4.1 Runge-Gross Theorem

We now start from the time-dependent Schrödinger equation:

$$i\hbar\frac{\partial}{\partial t}\big|\psi(t)\big\rangle = \hat{H}\big|\psi(t)\big\rangle, \qquad \hat{H} = \hat{T} + \hat{U} + \hat{V}_{ext}(t) \tag{2.23}$$

where the external potential $v_{ext}(\mathbf{r}, t)$ includes a time-dependent perturbation to the system in addition to the static ionic potential. As in DFT, one can establish a one-to-one mapping between the time-dependent electron density $\rho(\mathbf{r}, t)$ and the external potential $v_{ext}(\mathbf{r}, t)$.

Theorem 2.4.1. (Runge and Gross I, 1984,[22])
The density $\rho(\mathbf{r},t)$ evolving from an initial state $|\psi_0\rangle$ under the influence of a Taylor expandable potential $v_{ext}(\mathbf{r},t)$ determines this potential uniquely, except for a time-dependent constant.

This time-dependent constant only changes the random phase of the wavefunctions, which should not influence the calculation. This theorem is the time dependent equivalent to the first Kohn-Hohenberg theorem 2.2.1. However, it is not possible anymore to minimize the total energy with respect to the density, as it was done in DFT, since the energy is no longer a conserved quantity. Hence the quantum-mechanical action A is introduced as an analogue to the total energy in the static case and is defined as

$$A[\rho] = \int_0^T dt \Big\langle \psi[\rho] \Big| i\hbar \frac{\partial}{\partial t} - \hat{H}(t) \Big| \psi[\rho] \Big\rangle \tag{2.24}$$

The action is a unique functional of the density. The time-dependent Kohn-Sham equations can be derived from the principle of stationary action:

Theorem 2.4.2. (Runge and Gross II, 1984,[22])
For a given state $|\psi_0\rangle$, the action $A[\rho]$ becomes stationary at the density $\rho_0(\mathbf{r},t)$ that corresponds to the external potential $V_0(\mathbf{r},t)$.

This translates as

$$\left. \frac{\delta A_{v_0}[\rho]}{\delta \rho(\mathbf{r},t)} \right|_{\rho=\rho_0} = 0 \tag{2.25}$$

and means that, finding the density for which the action is stationary, corresponds to finding the solution of the system. Thus the minimization of the total energy is replaced by the search of the stationary points of the action. However the action is an unknown functional.

2.4.2 Kohn-Sham equations

To determine the action $A[\rho]$, in a similar fashion to the static case, Runge and Gross[22] introduced an auxiliary system of independent particles, that fulfill the time-dependent Schrödinger equation,

$$i\hbar \frac{\partial}{\partial t} |\phi_i(t)\rangle = (\hat{T}_S + \hat{V}_S) |\phi_i(t)\rangle \tag{2.26}$$

where $\phi_i(\mathbf{r},t)$ are the time-dependent Kohn-Sham wavefunctions, which are used to calculate the time-dependent density $\rho(\mathbf{r},t)$. As previously, the same density ρ_0 is solution of both the real and auxiliary system and is given by:

$$\rho_0(\mathbf{r},t) = \sum_i^N |\phi_i(\mathbf{r},t)|^2 \tag{2.27}$$

The action functional can be decomposed in the same fashion as the total energy in equation (2.9):

$$A_{v_0}[\rho] = T_S[\rho] + A_H[\rho] + A_0[\rho] + A_{XC}[\rho] \tag{2.28}$$

where A_{XC} includes all the non-trivial many-body parts of the action and is defined in similar way to equation (2.8) in the static case. When reaching the stationary point at the density $\rho_0(\mathbf{r},t)$, both the action of the real and KS systems become equal allowing us to write the following expression for the KS potential:

$$v_S([\rho_0],\mathbf{r},t) = v_H([\rho_0],\mathbf{r},t) \; + v_0(\mathbf{r},t) + v_{XC}([\rho_0],\mathbf{r},t) \tag{2.29}$$

This set of equations are self-consistent and can be solved iteratively with an approximation for the exchange-correlation potential v_{XC}. This self-consistency must be built into the time-propagation scheme. The time-dependent potential v_{XC} is more complex than the static one. Indeed, the dependence with the electron density is nonlocal in time and space. Moreover, in addition to its dependence on the density, v_{XC} formally also depends on the initial many-body and KS wavefunctions, $|\psi_0\rangle$ and $|\phi_i\rangle$. One of the easiest choice for the xc-functional is the adiabatic local-density approximation (ALDA), which is an extension of LDA in DFT. It greatly simplifies the problem since v_{XC} becomes local in time and space and the dependence on the initial conditions is neglected. However this simple approximation is known to fail when looking at the optical responses of solids. A more accurate alternative for optical spectra was found for f_{xc}, which is defined as $f_{xc} = \delta v_{XC}/\delta\rho$ and is applied through the Dyson equation, that is later introduced in section 2.4.4. This alternative consists in a long-range f_{xc}, also referred to as the α-kernel[23],

$$f_{xc}(\mathbf{q}) = -\frac{\alpha}{q^2}, \tag{2.30}$$

containing, as its name suggest, a long-range contribution (LRC), which is completely absent within ALDA. However there is no corresponding form for v_{XC}. One of the drawback of this kernel is that it is a static approximation with no frequency-dependence.

2.4.3 Correction to the Runge-Gross theorem

The one-to-one mapping between the density and the potential in the demonstration of the Runge-Gross theorem 2.4.1. was not entirely valid. It was only proven that for two systems with the same initial state ψ_0 and two-particle interaction $\hat{U}$, if they had different potentials then they could not have the same density (see Figure 2.4). It was then not proven that the same density $\rho(\mathbf{r}, t)$ could not

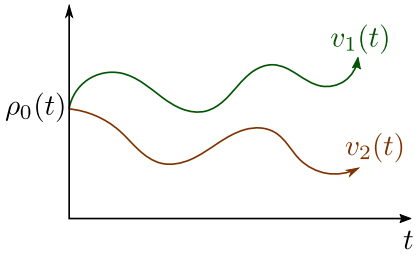

$$\psi_1(t_0) = \psi_2(t_0) = \psi_0$$
$$\hat{U}_1 = \hat{U}_2 = \hat{U}$$
$$\hat{V}_1(t) \neq \hat{V}_2(t) + c(t) \implies \rho_1(t) \neq \rho_2(t)$$

Figure 2.4: Runge-Gross theorem

be reproduced by the potential of a system with different ψ_0 and $\hat{U}$. Consequently any expectation value was a functional of the density and the initial state. However, in a non-interactive system, such as the KS auxiliary system, the interaction $\hat{U} = 0$, is usually different than the one in the real system $\hat{U} \neq 0$, meaning that, only considering the Runge-Gross theorem, for the same density, the two systems didn't necessarily have the same potential, and thus questioning the validity of the time-dependent KS approach. However, this is actually not a problem since this theorem was later extended by van Leeuwen[24] for systems with different initial states and two-particle interactions, providing the formal justification for the KS approach.

It was also demonstrated that the definition of the action in equation (2.24) led to causality-symmetry problem in the definition of the action derivative. Indeed, if as suggested by Runge and Gross, the potential was written as a functional derivative of the action, it would lead to

$$v_{ext}([\rho], \mathbf{r}, t) = \frac{\delta A[\rho]}{\delta\rho(\mathbf{r}, t)} \implies \frac{\delta v_{ext}([\rho], \mathbf{r}, t)}{\delta\rho(\mathbf{r}', t')} = \frac{\delta^2 A[\rho]}{\delta\rho(\mathbf{r}, t)\delta\rho(\mathbf{r}', t')}, \tag{2.31}$$

which is not possible since the derivative of the potential is causal, ie zero for $t' > t$, while the second derivative of the action is symmetric in term of t, t'. Furthermore, it was shown that the action functional, as it was defined, was actually not stationary[25]. So the variational principle for the density did not require it to be zero but equal to another functional, thus meaning that the potentials v_{ext}, v_S and v_{XC} are not merely functional derivatives of A_{v_0} but contain an additional term. Another approach was then developed by van Leeuwen[26] with a different definition of the action that avoid this causality-symmetry problem.

2.4.4 Linear response theory

In the following, I will show that to access the susceptibility, we don't actually need to solve the time-dependent equations presented in the previous sections, which would imply to evaluate the propagation in time of the wavefunctions as it is done, for instance, in the TDDFT code Octopus[27].

We consider a system previously in its ground-state, for which an external perturbation $v_{ext}(t)$ has been switch on at t_0. The density and wavefunctions of the ground-state for $t < t_0$ can be uniquely determined by DFT. If the perturbation is small, one could use perturbation theory, that will be fully described in the next chapter, instead of solving the full Kohn-Sham equations. In linear response theory, the goal is to evaluate the density-response χ of the fully-interacting system to the perturbation. The response of the fictitious Kohn-Sham system to the effective potential v_S is referred to as the independent-particle susceptibility χ_0.

$$\chi = \frac{\delta\rho}{\delta v_{ext}}, \quad \chi_0 = \frac{\delta\rho}{\delta v_S} \tag{2.32}$$

Since the densities of both the real and non-interacting systems are identical, we can link the two response functions,

$$\chi = \frac{\delta\rho}{\delta v_{ext}} = \frac{\delta\rho}{\delta v_S}\frac{\delta v_S}{\delta v_{ext}} = \chi_0 \frac{\delta(v_{ext} + v_H + v_{XC})}{\delta v_{ext}} = \chi_0 \left[1 + \frac{\delta v_H}{\delta\rho}\frac{\delta\rho}{\delta v_{ext}} + \frac{\delta v_{XC}}{\delta\rho}\frac{\delta\rho}{\delta v_{ext}}\right], \tag{2.33}$$

which gives us the Dyson-equation for the first order,

$$\chi = \chi_0 + \chi_0(v + f_{xc})\chi, \tag{2.34}$$

with $v = \delta v_H/\delta\rho$ and $f_{xc} = \delta v_{XC}/\delta\rho$. Similar equations could be written for every orders, each time increasing the difficulty by linking the n^{th}-order susceptibility $\chi^{(n)}$ with all the previous interacting and non-interacting susceptibilities $\chi^{(n-i)}$ and $\chi_0^{(n-i)}$. From the Dyson-equation, the simplest approximation is to set both v and f_{xc} to zero, which corresponds to the independent-particle approximation (IPA), where all the many-body effects are neglected, leaving only the Kohn-Sham response: $\chi^{(n)} = \chi_0^{(n)}$. Only putting $f_{xc} = 0$ and keeping the Coulomb interaction corresponds to the random-phase approximation (RPA), which includes the effects of the local fields induced by the perturbation inside the material. In both approximations, the exchange and correlation effects are still present at the DFT level, they are only neglected in TDDFT in the Dyson-equation.

At this point, one could also include in the Dyson equation a term representing the screening effect, instead of using GW or scissor approximations mentioned in section 2.2.4. However, as for f_{xc}, this screening term is a priori unknown and, how to evaluate it, is not so trivial. It has so far proven more effective to continue using either G_0W_0 or the scissor approximation, both introduced in the form of a non-local operator in the Hamiltonian and included in the IPA response χ_0.

Chapter 3

Theoretical framework

In this chapter, I describe the theoretical background needed in this thesis, which includes time-dependent perturbation theory as well as the link between macroscopic and microscopic response.

3.1 Perturbation Theory

We consider a system that we know how to solve and apply a small perturbation on it. Here "small" implies that the effect on the system is weak and that the quantum states would change very little. In that case, we can use perturbation theory to describe the change in the energy spectrum (see Figure 3.1), the aim being to express the perturbed solution as function of the unperturbed one.

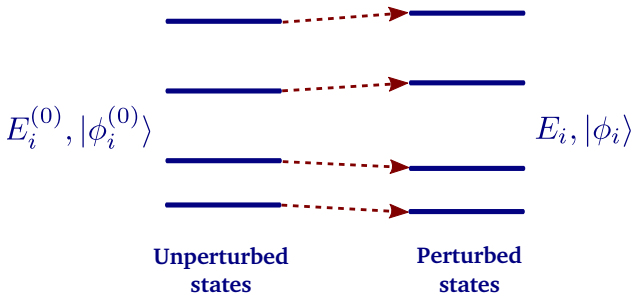

Figure 3.1: Effect of the perturbation on the energy levels using time-independent perturbation theory.

3.1.1 Interaction picture

In time-independent perturbation theory, the system is submitted to a perturbation which results in the addition of a term $\hat{H}^P$ to the Hamiltonian, $\hat{H} = \hat{H}_0 + \hat{H}^P$. One can then calculate the correction to the eigenvalues and eigenstates induced by this perturbation. With time-dependent perturbation theory, the goal is to look at the time evolution of this perturbed system, whether the perturbation itself depends on time or not. It is assumed that the unperturbed eigenvalues and eigenstates of the 'bare' Hamiltonian H_0 are known and usually constitute the starting point of the system.

In the Schrödinger picture, the propagator is attached to the state vectors $|\psi_S(t)\rangle$. The time evolution of these states is specified through the Schrödinger equation, while the observables $\hat{O}_S$ do not evolve in time,

$$i\hbar\frac{d}{dt}|\psi_S(t)\rangle = \hat{H}_S|\psi_S(t)\rangle, \qquad i\hbar\frac{d}{dt}\hat{O}_S = 0 \tag{3.1}$$

In most cases, it is usually more convenient to work in the interaction picture, where the time-dependence is split between the ket states and the operator. The transformation from the Schrödinger to the interaction picture is given as,

$$\begin{cases} \hat{H}_I^P(t) = e^{i\hat{H}_0 t/\hbar}\, \hat{H}_S^P\, e^{-i\hat{H}_0 t/\hbar} \\ \big|\psi_I(t)\big\rangle = e^{i\hat{H}_0 t/\hbar}\big|\psi_S(t)\big\rangle \end{cases}, \tag{3.2}$$

where $\hat{H}_0$ stays the same in every picture. Using both equations (3.1) and (3.2), we can then obtain the time evolution of the state in the interaction picture:

$$i\hbar\frac{d}{dt}\big|\psi_I(t)\big\rangle = \hat{H}_I^P(t)\big|\psi_I(t)\big\rangle \tag{3.3}$$

This corresponds to the Schrödinger equation in the interaction picture, which is similar to the one in the Schrödinger picture (3.1), except for the fact that the perturbed Hamiltonian is used instead of the total one. There is another picture developed by Heisenberg, working independently of Schrödinger, where the full propagator is, this time, attached to the observable, which will not be used in this thesis. The time dependence in the different pictures has been summarized in table 3.1.1.

picture	Schrödinger	Interaction	Heisenberg
observables	$\hat{O}_S$	$\hat{O}_I(t) = e^{i\hat{H}_0 t/\hbar}\, \hat{O}_S\, e^{-i\hat{H}_0 t/\hbar}$	$\hat{O}_H(t) = e^{i\hat{H} t/\hbar}\, \hat{O}_S\, e^{-i\hat{H} t/\hbar}$
state vector	$\big\|\psi_S(t)\big\rangle$	$\big\|\psi_I(t)\big\rangle = e^{i\hat{H}_0 t/\hbar}\big\|\psi_S(t)\big\rangle$	$\big\|\psi_H\big\rangle = e^{i\hat{H} t/\hbar}\big\|\psi_S(t)\big\rangle$

Table 3.1: Time-dependence and transformation for the three pictures.

At this point, we only have access to the unperturbed wavefunctions ψ_0. So we need to write the connection between them and the time-dependent wavefunctions in the interaction picture $\psi_I(t)$. They are related through the time-evolution operator $U_I(t)$, i.e. $\big|\psi_I(t)\big\rangle = U_I(t)\big|\psi_0\big\rangle$, which must satisfy equation (3.3) so that

$$i\hbar\frac{d}{dt}U_I(t) = \hat{H}_I^P(t)\, U_I(t) \tag{3.4}$$

Since we know the starting point $\big|\psi_0\big\rangle$, which is the state vector for t_0 in all the pictures, we can use the boundary condition $U_I(t_0) = 1$, to write equation (3.4) as an integral equation,

$$U_I(t) = 1 - \frac{i}{\hbar}\int_{t_0}^{t} dt'\; H_I^P(t')\, U_I(t'), \tag{3.5}$$

which is self-consistent for $U_I(t)$. Solving it iteratively provides us with the following expansion in powers of $\hat{H}_I^P$:

$$U_I(t) = 1 + \sum_{n=1}^{\infty}\left(\frac{-i}{\hbar}\right)^n \int_{t_0}^{t} dt' \int_{t_0}^{t'} dt'' \cdots \int_{t_0}^{t_{n-1}} dt_n\; \hat{H}_I^P(t')\, \hat{H}_I^P(t'') \ldots \hat{H}_I^P(t_n), \tag{3.6}$$

which is called the Dyson series. It is related to the full time-evolution operator $U_S(t)$, that links the Schrödinger wavefunctions $\big|\psi_S(t)\big\rangle$ to the time-independent ones $\big|\psi_0\big\rangle$, by the relation $U_S(t) = e^{-iH_0 t/\hbar}U_I(t)$. While the definition of an operator is different in every picture (cf. Table 3.1.1), the resulting expectation value needs to be independent of the chosen framework and should stay the same in all pictures. In the interaction picture, it is defined as follows:

$$O(t) = \Big\langle \psi_I(t)\Big|\hat{O}_I(t)\Big|\psi_I(t)\Big\rangle, \tag{3.7}$$

which can be recast using eq. (3.6),

$$O(t) = \langle\psi_0|\hat{O}_I(t)|\psi_0\rangle + \sum_{n=1}^{\infty}\left(\frac{-i}{\hbar}\right)^n \int_{t_0}^{t} dt' \cdots \int_{t_0}^{t_{n-1}} dt_n \left\langle\psi_0\middle|\left[\left[\hat{O}_I(t), \hat{H}_I^P(t')\right]\ldots, \hat{H}_I^P(t_n)\right]\middle|\psi_0\right\rangle \quad (3.8)$$

3.1.2 Response function

The response function corresponds to the change induced in the expectation value of an operator $\hat{\alpha}$ by a perturbation $v(t)$, which is not necessarily the same as the perturbed Hamiltonian $\hat{H}^P$. To obtain the response functions, we expand the observable $\hat{\alpha}$ with respect to the perturbation,

$$\begin{aligned}\hat{\alpha}_I([v],1) = \hat{\alpha}_0(1) + \int_{t_0}^{t_1} d2\, \frac{\delta\hat{\alpha}_I(1)}{\delta v(2)}\, v(2) + \frac{1}{2}\int_{t_0}^{t_1} d2 \int_{t_0}^{t_2} d3\, \frac{\delta^2\hat{\alpha}_I(1)}{\delta v(2)\delta v(3)}\, v(2)v(3) \\ + \frac{1}{6}\int_{t_0}^{t_1} d2 \int_{t_0}^{t_2} d3 \int_{t_0}^{t_3} d4\, \frac{\delta^3\hat{\alpha}_I(1)}{\delta v(2)\delta v(3)\delta v(4)} v(2)v(3)v(4) + \ldots \quad (3.9)\end{aligned}$$

where we adopt the notation $(1) \equiv (\mathbf{r}_1, t_1)$ to have a more concise expression. The expansion coefficients corresponds to the response function of the system $\chi_\alpha^{(i)}$,

$$\chi_\alpha^{(1)}(1,2) = \left\langle\psi_0\middle|\frac{\delta\hat{\alpha}_I(1)}{\delta v(2)}\middle|\psi_0\right\rangle, \qquad \chi_\alpha^{(2)}(1,2,3) = \left\langle\psi_0\middle|\frac{\delta^2\hat{\alpha}_I(1)}{\delta v(2)\delta v(3)}\middle|\psi_0\right\rangle, \qquad \ldots \quad (3.10)$$

They represent the variation of the operator $\hat{\alpha}$ with respect to the perturbation v but do not explicitly depend on the perturbing quantity. The form of these response functions depends on the coupling between the system and the perturbation. We consider the general case where this coupling is expressed through another operator $\hat{O}$ in the following way

$$\hat{H}_I^P(t) = \int d\mathbf{r}\, \hat{O}_I(\mathbf{r}, t)\, v(\mathbf{r}, t) \quad (3.11)$$

The linear response function $\chi_\alpha^{(1)}(1,2)$ depending on the coupling $\hat{O}$ becomes

$$\chi_{\alpha O}^{(1)}(1,2) = -i\theta(t_1 - t_2)\langle\psi_0|[\hat{\alpha}_I(1), \hat{O}_I(2)]|\psi_0\rangle \quad (3.12)$$

which was derived by Kubo in 1957[28]. $\theta(t)$ is the step function which is zero if $t < 0$ and 1 otherwise. The theory has later been generalized to higher order[29]:

$$\chi_{\alpha O}^{(n)}(1,2,\ldots,n) = (-i)^n\theta(t_1,t_2,\ldots,t_n)T\langle\psi_0|[[[[\hat{\alpha}_I(1), \hat{O}_I(2)], \hat{O}_I(3)]\ldots, \hat{O}_I(n)]|\psi_0\rangle \quad (3.13)$$

where $\theta(t_1,t_2,\ldots,t_n) = \theta(t_1-t_2)\theta(t_1-t_3)\ldots\theta(t_1-t_n)$ and T is the time-ordering operator that acts on indices $2,3,\ldots,n$. The response functions are causal and depend only on time differences and not on absolute times, as long as the perturbing field remains small, so that

$$\chi_{\alpha O}^{(n)}(\mathbf{r}_1,t,\mathbf{r}_2,t_2,\ldots,\mathbf{r}_n,t_n) = \chi_{\alpha O}^{(n)}(\mathbf{r}_1,\mathbf{r}_2,\ldots,\mathbf{r}_n,t_1-t_2,\ldots,t_1-t_n) \quad \text{for } t_1 > t_2,\ldots,t_1 > t_n \quad (3.14)$$

If we now consider the coupling to be the sum of different operator: $\hat{O} = \hat{\beta} + \hat{\gamma} + \hat{\delta}$, to get a more general form for the response functions, we obtain

$$\begin{aligned}\chi_{\alpha\beta}(1,2) &= -i\theta(t_1-t_2)\langle[\hat{\alpha}_I(1), \hat{\beta}_I(2)]\rangle \\ \chi_{\alpha\beta\gamma}(1,2,3) &= -\theta(t_1-t_2)\,\theta(t_1-t_3)\,T\langle\left[\left[\hat{\alpha}_I(1), \hat{\beta}_I(2)\right], \hat{\gamma}_I(3)\right]\rangle \\ \chi_{\alpha\beta\gamma\delta}(1,2,3,4) &= i\,\theta(t_1-t_2)\,\theta(t_1-t_3)\,\theta(t_1-t_4)\,T\langle\left[\left[\left[\hat{\alpha}_I(1), \hat{\beta}_I(2)\right], \hat{\gamma}_I(3)\right], \hat{\delta}_I(4)\right]\rangle\end{aligned} \quad (3.15)$$

where we use the notation $\langle\hat{O}\rangle = \langle\psi_0|\hat{O}|\psi_0\rangle$.

3.1.3 Light as a perturbation

In this part, the perturbation is chosen as the light that shines on the material and interacts with the system. The unperturbed Hamiltonian H_0 is the one-particle hamiltonian composed of kinetic and potential energies.

$$\hat{H}_0 = \sum_i \left[\frac{\mathbf{p}_i^2}{2m} + V(\mathbf{r}_i) \right] \tag{3.16}$$

The system is then put inside an electromagnetic field corresponding to the light, and represented by perturbing electric $\mathbf{E}^P$ and magnetic fields $\mathbf{B}^P$,

$$\mathbf{E}^P = -\nabla\varphi^P - \frac{1}{c}\frac{\partial \mathbf{A}^P}{\partial t}, \qquad \mathbf{B}^P = \nabla \times \mathbf{A}^P \tag{3.17}$$

where φ^P and $\mathbf{A}^P$ are respectively scalar and vector potentials. This interaction with the external field of the light means the addition to the total Hamiltonian of a vector potential that moves together with the momentum $\mathbf{p} \to \mathbf{p} - e/c\mathbf{A}(\mathbf{r}, t)$ and of a scalar potential, both associated with the perturbation.

$$\hat{H}(\mathbf{r}, t) = \frac{1}{2m}\sum_i \left[\mathbf{p}_i - \frac{e}{c}\mathbf{A}^P(\mathbf{r}_i, t) \right]^2 + \sum_i V(\mathbf{r}_i) + \sum_i e\varphi^P(\mathbf{r}_i, t) \tag{3.18}$$

We recast the perturbing Hamiltonian $\hat{H}^P(t)$ to be expressed as function of the charge density $\hat{\rho}$ and current density $\hat{\mathbf{j}}$,

$$\hat{H}^P(t) = -\frac{1}{c}\int d\mathbf{r}\ \hat{\mathbf{j}}(\mathbf{r})\mathbf{A}^P(\mathbf{r}, t) + \frac{e}{2mc^2}\int d\mathbf{r}\ \hat{\rho}(\mathbf{r}) \left[\mathbf{A}^P(\mathbf{r}, t)\right]^2 + \int d\mathbf{r}\ \hat{\rho}(\mathbf{r})\ \varphi^P(\mathbf{r}, t), \tag{3.19}$$

where the charge density operator $\hat{\rho}(\mathbf{r})$ and the current density operator $\hat{\mathbf{j}}(\mathbf{r})$ are defined as

$$\begin{cases} \hat{\rho}(\mathbf{r}) = e\ \sum\limits_i\ \delta(\mathbf{r} - \mathbf{r}_i) \\ \hat{\mathbf{j}}(\mathbf{r}) = \dfrac{e}{2m}\ \sum\limits_i\ \left[\mathbf{p}_i\ \delta(\mathbf{r} - \mathbf{r}_i) + \delta(\mathbf{r} - \mathbf{r}_i)\ \mathbf{p}_i\right] \end{cases} \tag{3.20}$$

To access the different susceptibility shown in table 1.1, we need to calculate the polarization of the system which is linked to the induced current density by the relation

$$\mathbf{j}_{ind}(\mathbf{r}, t) = \frac{\partial}{\partial t}\mathbf{P}(\mathbf{r}, t) \quad \xrightarrow{FT} \quad \mathbf{j}_{ind}(\mathbf{r}, \omega) = -i\omega\mathbf{P}(\mathbf{r}, \omega) \tag{3.21}$$

Moreover the charge and current densities induced by the external field are related together by the charge conservation law,

$$\frac{\partial}{\partial t}\rho_{ind}(\mathbf{r}, t) + \nabla \cdot \mathbf{j}_{ind}(\mathbf{r}, t) = 0, \tag{3.22}$$

making it equivalent for us to calculate one or the other. However this statement is only true if the field is longitudinal, which will be explained in section 3.3. They reflect the induced motion of particles inside materials as well as their spatial structure. Using equations (3.8) and (3.19), we get the expectation value for the induced current operator at the first order:

$$\begin{aligned} \mathbf{j}^{(1)}_{ind}(\mathbf{r}, t) = -\frac{e}{mc}\ \langle\hat{\rho}(\mathbf{r})\rangle\ \mathbf{A}^P(\mathbf{r}, t) - i\int dt'\ \theta(t - t')\int d\mathbf{r}'\ \left\langle\left[\hat{\mathbf{j}}_I(\mathbf{r}, t), \hat{\rho}_I(\mathbf{r}', t')\right]\right\rangle \varphi^P(\mathbf{r}', t') \\ + \frac{i}{c}\int dt'\ \theta(t - t')\int d\mathbf{r}'\ \left\langle\left[\hat{\mathbf{j}}_I(\mathbf{r}, t), \hat{\mathbf{j}}_I(\mathbf{r}', t')\right]\right\rangle \mathbf{A}^P(\mathbf{r}', t') \end{aligned} \tag{3.23}$$

We can identify the response function from their definition in equation (3.15) where α, β, γ and δ are either the current or density operator $\hat{\mathbf{j}}$ and $\hat{\rho}$. All the response functions are not independent of each other and can be related using gauge-invariance. It is more convenient for us to work in the frequency domain rather than in the time domain. After doing a time Fourier transform using the previously mentioned time translational invariance for the response functions $\chi_{\alpha\beta}(\mathbf{r}, t, \mathbf{r}', t') = \chi_{\alpha\beta}(\mathbf{r}, \mathbf{r}', t - t')$, we obtain for the induced current:

$$\mathbf{j}^{(1)}_{ind}(\mathbf{r}, \omega) = \frac{ie}{m\omega} \langle \hat{\rho}(\mathbf{r}) \rangle \, \mathbf{E}^P(\mathbf{r}, \omega) + \frac{i}{\omega} \int d\mathbf{r}' \, \chi_{\mathbf{jj}}(\mathbf{r}, \mathbf{r}', \omega) \, \mathbf{E}^P(\mathbf{r}', \omega) \tag{3.24}$$

This formula, expressed in terms of the electric field, is gauge-invariant and is formally obtained by replacing the potentials by[30]

$$\begin{cases} \bar{\varphi}^P = \varphi^P - \dfrac{1}{c} \dfrac{\partial}{\partial t} \Lambda(\mathbf{r}, t) \\ \bar{\mathbf{A}^P} = \mathbf{A}^P - \dfrac{\partial}{\partial \mathbf{r}} \Lambda(\mathbf{r}, t) \end{cases} \tag{3.25}$$

The passage from the potential to the electric field $\mathbf{E}^P$ creates an apparent divergence in ω. If left in the formula, that divergence will appear in the spectrum when $\omega \to 0$. However we know that for the first order, the correct spectrum of semiconductors should not be divergent. It is then important to remove this unphysical divergence by writing the formula in a different way. For metals though, there is a natural divergence. But it is important to note that all the formulae shown in this work are only for insulators or semiconductors since during the analytical calculation, we make the assumption that there is a gap.

The microscopic first order polarization is defined in terms of the perturbing field as

$$\mathbf{P}^{(1)}(\mathbf{r}, \omega) = \int d\mathbf{r}' \, \tilde{\alpha}^{(1)}(\mathbf{r}, \mathbf{r}', \omega) \, \mathbf{E}^P(\mathbf{r}', \omega), \tag{3.26}$$

where $\tilde{\alpha}^{(1)}$ is the linear quasipolarizability that can be expressed from equation (3.24) and (3.21) as

$$\tilde{\alpha}^{(1)}(\mathbf{r}, \mathbf{r}', \omega) = -\frac{1}{\omega^2} \left[\frac{e}{m} \langle \hat{\rho}(\mathbf{r}) \rangle \, \delta(\mathbf{r} - \mathbf{r}') + \chi_{\mathbf{jj}}(\mathbf{r}, \mathbf{r}', \omega) \right] \tag{3.27}$$

We can write similar expressions for the induced current density at the second and third orders:

$$\begin{aligned} \mathbf{j}^{(2)}_{ind}(\mathbf{r}, \omega) = &- \int d\mathbf{r}' \, d\mathbf{r}'' \int d\omega' \, d\omega'' \, \frac{\delta(\omega - \omega' - \omega'')}{\omega' \omega''} \, \mathbf{E}^P(\mathbf{r}', \omega') \, \mathbf{E}^P(\mathbf{r}'', \omega'') \\ &\times \left[\frac{e}{m} \, \chi_{\rho\mathbf{j}}(\mathbf{r}, \mathbf{r}', \omega') \, \delta(\mathbf{r} - \mathbf{r}'') + \frac{e}{2m} \, \chi_{\mathbf{j}\rho}(\mathbf{r}, \mathbf{r}', \omega) \, \delta(\mathbf{r}' - \mathbf{r}'') + \frac{1}{2} \, \chi_{\mathbf{jjj}}(\mathbf{r}, \mathbf{r}', \mathbf{r}'', \omega', \omega'') \right] \end{aligned} \tag{3.28}$$

$$\begin{aligned} \mathbf{j}^{(3)}_{ind}(\mathbf{r}, \omega) = i \int d\mathbf{r}' \, d\mathbf{r}'' \, d\mathbf{r}''' \int d\omega' \, d\omega'' \, d\omega''' \, \frac{\delta(\omega - \omega' - \omega'' - \omega''')}{\omega' \omega'' \omega'''} \, \mathbf{E}^P(\mathbf{r}', \omega') \, \mathbf{E}^P(\mathbf{r}'', \omega'') \, \mathbf{E}^P(\mathbf{r}''', \omega''') \\ \times \left[-\frac{e^2}{2m^2} \, \chi_{\rho\rho}(\mathbf{r}, \mathbf{r}', \omega' + \omega''') \, \delta(\mathbf{r}' - \mathbf{r}''') \, \delta(\mathbf{r} - \mathbf{r}'') - \frac{e}{2m} \, \chi_{\rho\mathbf{jj}}(\mathbf{r}, \mathbf{r}', \mathbf{r}'', \omega', \omega'') \, \delta(\mathbf{r} - \mathbf{r}''') \right. \\ - \frac{e}{4m} \, \chi_{\mathbf{jj}\rho}(\mathbf{r}, \mathbf{r}', \mathbf{r}'', \omega', \omega'' + \omega''') \, \delta(\mathbf{r}'' - \mathbf{r}''') - \frac{e}{4m} \, \chi_{\mathbf{j}\rho\mathbf{j}}(\mathbf{r}, \mathbf{r}', \mathbf{r}'', \omega' + \omega''', \omega'') \, \delta(\mathbf{r}' - \mathbf{r}''') \\ \left. - \frac{1}{6} \, \chi_{\mathbf{jjjj}}(\mathbf{r}, \mathbf{r}', \mathbf{r}'', \mathbf{r}''', \omega', \omega'', \omega''') \right] \end{aligned} \tag{3.29}$$

Regarding the second and third order response, we can only get rid of the apparent divergence in $\omega'\omega'' \ldots$ in specific cases, which include all the phenomena presented in this thesis, since some processes are known to present true divergences that have a physical meaning (see for instance the optical rectification).

Likewise, one could show similar formulae for the charge density.

3.2 Nonlocal operators

The addition of nonlocal operators to the Hamiltonian, introduced by pseudopotentials or the scissor approximation used to correct the band-gap, needs to be included within the IPA response. [1]

3.2.1 Pseudopotentials

The use of pseudopotentials in DFT calculations introduces a nonlocal part to the potential that was so far considered to be local. In practice it means that the potential V_{nl} does not commute with the position operator $\hat{\mathbf{r}}$ anymore, thus adding corrections to the momentum operator. The velocity operator is then defined as

$$\hat{\mathbf{v}} = [\hat{H}_0, i\mathbf{r}] = \hat{\mathbf{p}} - i[\hat{\mathbf{r}}, \hat{V}_{nl}] \tag{3.30}$$

A nonlocal potential is then added in the perturbing Hamiltonian[31] of equation (3.19),

$$\hat{H}^P(\mathbf{r},t) = -\frac{1}{2c}\left\{\mathbf{p}\cdot\mathbf{A}^P(\mathbf{r},t) + \mathbf{A}^P(\mathbf{r},t)\cdot\mathbf{p}\right\} + \frac{1}{2c^2}\left[\mathbf{A}^P(\mathbf{r},t)\right]^2 + \varphi^P(\mathbf{r},t) + V_{nl}^P, \tag{3.31}$$

where V_{nl}^P is defined as

$$\left\langle \mathbf{r}\middle| V_{nl}^P \middle|\mathbf{r}'\right\rangle = V_{nl}(\mathbf{r},\mathbf{r}')\sum_{k=1}^{\infty}\frac{1}{k!}\left(\frac{i}{c}\int_{\mathbf{r}'}^{\mathbf{r}}\mathbf{A}^P(\mathbf{x},t)\,d\mathbf{x}\right)^k \tag{3.32}$$

Since we are interested in calculating the third-order susceptibility $\chi^{(3)}$ for the EFISH response, we need to write the perturbing Hamiltonian up to the third-order.

$$\begin{aligned}
H^{(1)}(\mathbf{r},t) &= -\frac{1}{2c}\left\{\mathbf{p}\cdot\mathbf{A}^P(\mathbf{r},t) + \mathbf{A}^P(\mathbf{r},t)\cdot\mathbf{p}\right\} + \varphi^P(\mathbf{r},t) + \frac{i}{c}\,V_{nl}(\mathbf{r},\mathbf{r}')\int_{\mathbf{r}'}^{\mathbf{r}}\mathbf{A}^P(\mathbf{x},t)\,d\mathbf{x} \\
H^{(2)}(\mathbf{r},t) &= \frac{1}{2c^2}\left[\mathbf{A}^P(\mathbf{r},t)\right]^2 - \frac{1}{2c^2}\,V_{nl}(\mathbf{r},\mathbf{r}')\left(\int_{\mathbf{r}'}^{\mathbf{r}}\mathbf{A}^P(\mathbf{x},t)\,d\mathbf{x}\right)^2 \\
H^{(3)}(\mathbf{r},t) &= -\frac{i}{6c^3}\,V_{nl}(\mathbf{r},\mathbf{r}')\left(\int_{\mathbf{r}'}^{\mathbf{r}}\mathbf{A}^P(\mathbf{x},t)\,d\mathbf{x}\right)^3
\end{aligned} \tag{3.33}$$

When going through the charge density calculation, we have direct access to the density-response function $\chi_{\rho\rho}$, that we want to calculate in TDDFT, by putting $\mathbf{A}^P = 0$.

$$\rho_{ind}^{(1)}(\mathbf{r},\omega) = \int d\mathbf{r}'\,\chi_{\rho\rho}(\mathbf{r},\mathbf{r}',\omega)\,V^P(\mathbf{r}',\omega) - \frac{1}{c}\int d\mathbf{r}'\,\chi_{\rho\mathbf{j}}(\mathbf{r},\mathbf{r}',\omega)\,\mathbf{A}^P(\mathbf{r}',\omega) \tag{3.34}$$

To calculate the integral over $\mathbf{x}$, we use the long-wavelength approximation, mentioned in section 3.3.1, for which $\mathbf{A}^P(\mathbf{r},t) \to \mathbf{A}^P(t)$ and we obtain

$$\begin{aligned}
H^{(1)} &= -\frac{1}{c}\,\mathbf{A}^P(t)\,\hat{\mathbf{v}} + \varphi^P(\mathbf{r},t) \\
H^{(2)} &= \frac{1}{2c^2}\left[\mathbf{A}^P(t)\hat{\mathbf{r}}, \mathbf{A}^P(t)\hat{\mathbf{v}}\right] \\
H^{(3)} &= \frac{1}{6c^3}\left[\mathbf{A}^P(t)\hat{\mathbf{r}}, \left[\mathbf{A}^P(t)\hat{\mathbf{r}}, \mathbf{A}^P(t)\hat{\mathbf{v}}\right]\right]
\end{aligned} \tag{3.35}$$

When comparing the above expressions with the ones without this nonlocal contribution to the potential, we see that using pseudopotentials means that the momentum operator $\hat{\mathbf{p}}$ must be replaced by the velocity one $\hat{\mathbf{v}}$ in the Hamiltonian $\hat{\mathbf{p}} \to \hat{\mathbf{v}} = \hat{\mathbf{p}} - i[\hat{\mathbf{r}}, \hat{V}_{nl}]$. This statement stays true even for the third order and above since the commutator $[\hat{\mathbf{r}}, [\hat{\mathbf{r}}, \hat{\mathbf{p}}]]$ is zero, explaining why there is no third order Hamiltonian when the potential is local.

[1] From this point, atomic units are used ($e = m = \hbar = 1$).

3.2.2 Scissor operator

To include the screening in the following calculations and correct the band-gap problem as discussed in section 2.2.4, I will use the scissor approximation. In practice, this is done by adding a scissor operator $\hat{S}$ to the unperturbed Hamiltonian $\hat{H}_0^{KS}$:

$$\hat{H}_0^{\Sigma} = \hat{H}_0^{KS} + \hat{S} \tag{3.36}$$

This operator $\hat{S}$ is nonlocal and is used to apply a rigid shift Δ to the conduction bands. The value of this shift depends on the material and is based on a previous GW calculation. It is written in the form

$$\hat{S} = \Delta \sum_{\mathbf{k}} \sum_{n} (1 - f_{n,\mathbf{k}}) \big|\phi_{n,\mathbf{k}}\big\rangle\big\langle\phi_{n,\mathbf{k}}\big|, \tag{3.37}$$

where $f_{n,\mathbf{k}}$ is the occupation number of the band which is either 1 or 0. The unscissored and scissored Hamiltonian both satisfy a Schrödinger equation for the same set of wavefunctions and gives respectively unscissored and scissored energies.

$$\begin{cases} \hat{H}_0^{KS}\big|\phi_{n,\mathbf{k}}\big\rangle = E_{n,\mathbf{k}}\big|\phi_{n,\mathbf{k}}\big\rangle \\ \hat{H}_0^{\Sigma}\big|\phi_{n,\mathbf{k}}\big\rangle = E_{n,\mathbf{k}}^{\Sigma}\big|\phi_{n,\mathbf{k}}\big\rangle \end{cases} \tag{3.38}$$

The shift in the energies is given by

$$E_{n,\mathbf{k}}^{\Sigma} = E_{n,\mathbf{k}} + (1 - f_{n,\mathbf{k}})\Delta \tag{3.39}$$

Since the scissor operator is nonlocal, it is now included in the definition of the velocity operator in a similar fashion as for the nonlocal part of the pseudopotential.

$$\hat{\mathbf{v}}^{\Sigma} = [\hat{H}_0^{\Sigma}, i\hat{\mathbf{r}}] = \hat{\mathbf{p}} - i[\hat{\mathbf{r}}, \hat{V}_{nl}] - i[\hat{\mathbf{r}}, \hat{S}] \tag{3.40}$$

For the diagonal elements of the velocity matrix, there is no scissor effect.

$$\langle\phi_{n,\mathbf{k}}|\hat{\mathbf{v}}^{\Sigma}|\phi_{n,\mathbf{k}}\rangle = \langle\phi_{n,\mathbf{k}}|\hat{\mathbf{v}}|\phi_{n,\mathbf{k}}\rangle \tag{3.41}$$

It is important to note that, unlike for the linear case, implementing the scissor operator to higher order is not as straightforward as to swap every Kohn-Sham energies by their scissored counterparts and requires a lengthy analytical calculation that will be explained later on.

3.3 Longitudinal fields

In general, an electric field $\mathbf{E}$ is composed of a longitudinal and transverse component. Longitudinal and transverse fields propagate respectively along and perpendicular to the direction of the wave vector $\mathbf{k}$. Photons are described by a transverse field, illustrated in figure 3.2, while longitudinal fields can represent electrons in plasmon oscillations. Therefore, for optical response, both the incoming and outgoing fields should be transverse, which then corresponds, for the linear case, to the transverse-transverse component of the macroscopic dielectric tensor ε^{TT}.

$$\begin{pmatrix} D^L \\ D^T \end{pmatrix} = \begin{pmatrix} \varepsilon_M^{LL} & \varepsilon_M^{LT} \\ \varepsilon_M^{TL} & \varepsilon_M^{TT} \end{pmatrix} \begin{pmatrix} E^L \\ E^T \end{pmatrix} \tag{3.42}$$

Although a transverse field could also in principle create a longitudinal field, corresponding to the transverse-longitudinal component ε^{TL}, this is not the one we are interested in when looking at the optical response. Yet TDDFT is a theory that can only gives us access to the longitudinal-longitudinal part of the dielectric function ε^{LL}. The transverse part could be calculated through the current density $\mathbf{j}$ obtained from TDCDFT (Time-Dependent Current-Density-Functional Theory), which is far less developed than TDDFT.

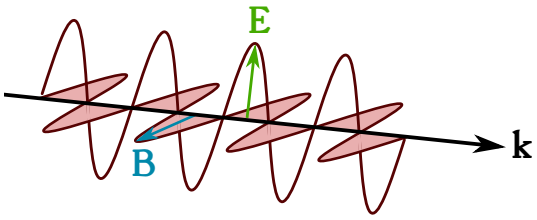

Figure 3.2: Scheme of an electromagnetic wave

3.3.1 Optical limit

The incident light used for the measurement and theoretical calculation of the optical response usually corresponds to visible or UV light with a wavelength of about $\lambda \sim 10^3$Å, while the typical size of the lattice parameter is of the order of 1Å. Since the wavelength of the light is large in comparison to the unit cell, it means that the field is almost constant over the cell. Therefore an approximation can be made that $\lambda \to \infty$, which is called the long-wavelength limit. For periodic crystals, the momentum vector $\mathbf{k}$ is defined as $\mathbf{k} = \mathbf{q} + \mathbf{G}$, where $\mathbf{q}$ is a vector of the first Brillouin zone and $\mathbf{G}$ is a reciprocal lattice vector. For an electromagnetic radiation, the wave vector $\mathbf{q}$, that indicates the direction of the light propagation, is related to the wavelength and the frequency ω by the relation

$$q = \frac{2\pi n}{\lambda} = \frac{n\omega}{c}, \tag{3.43}$$

where n is the refractive index of the medium. The long-wavelength limit, also referred as the optical limit, is then equivalent to say that $\mathbf{q} \to 0$. In that limit, the fields do not propagate anymore, which means that the transverse and longitudinal direction determined by $\mathbf{q}$ are no longer distinguishable. However the electric field still keeps a direction, which is the only meaningful one. Since, the dielectric tensor can be calculated in any basis, by choosing different $\mathbf{q}$, one could compute the entire dielectric tensor from a longitudinal response[1]. This means that TDDFT can be used to compute the different susceptibilities, assuming we are in the optical limit. Working in the framework of TDDFT means that we need to evaluate density response functions $\chi^{(1)}_{\rho\rho}$, $\chi^{(2)}_{\rho\rho\rho}$, $\chi^{(3)}_{\rho\rho\rho\rho}$, while in TDCDFT one would need to consider current response functions $\chi^{(1)}_{\mathbf{jj}}$, $\chi^{(2)}_{\mathbf{jjj}}$, $\chi^{(3)}_{\mathbf{jjj}}$. The full current response functions cannot be obtained with TDDFT since the charge conservation law only relates the charge density to the longitudinal part of the current,

$$\mathbf{q}\,\chi_{\mathbf{jj}}(\mathbf{q},\mathbf{q},\omega)\,\mathbf{q} = -\chi_{\rho\rho}(\mathbf{q},\mathbf{q},\omega). \tag{3.44}$$

3.4 Macroscopic response

In the previous section 3.1.3, microscopic response functions were introduced. But the quantities that can be compared with experiments are macroscopic. Making the link between the two requires to average the microscopic quantities over a large distance. They can be different due to fluctuations on a microscopic scale. However, in the independent-particle approximation, used in this thesis and introduced in section 2.4.4, they only differ by a factor that depends on the symmetry. Nonetheless it is important to talk about it to determine those coefficients for the different symmetries.

So far, the induced current, related to the microscopic polarization by equation (3.21), was expressed in terms of the perturbing field. We now want to express the macroscopic polarization in terms of the total field. For that, we need to find the link between the perturbing field and the total field. The perturbing field created by the incident light is defined from the external field $\mathbf{E}^{ext}$,

following the formalism of Del Sole *et al.*[32], as

$$\mathbf{E}^P = \mathbf{E}^{ext} + \mathbf{E}^{i,T} = \mathbf{E} - \mathbf{E}^{i,L} \tag{3.45}$$

where $\mathbf{E}$ and $\mathbf{E}^i$ are the total and induced field and the subscripts T and L stands for transverse and longitudinal. In that definition, the external and perturbing field are not the same since the induced transverse field $\mathbf{E}^{i,T}$, coming from the retarded electron interaction, is not accounted for in the unperturbed Hamiltonian H_0 and therefore must be included in the perturbation.

From Maxwell equation, we get the relation between the perturbing and total field in the reciprocal space,

$$\mathbf{E}^P_{\mathbf{G}}(\mathbf{q},\omega) = \mathbf{E}_{\mathbf{G}}(\mathbf{q},\omega) + 4\pi\, \widehat{\mathbf{q}+\mathbf{G}}\, P^L(\mathbf{q},\omega), \tag{3.46}$$

where $\widehat{\mathbf{q}+\mathbf{G}}$ is the direction of the momentum: $\widehat{\mathbf{q}+\mathbf{G}} = (\mathbf{q}+\mathbf{G})/|\mathbf{q}+\mathbf{G}|$. In practice, the macroscopic average in reciprocal space consists of putting $\mathbf{G} = 0$. After some analytical calculation that will not be detailed here but is explained in Ref. [9], we obtain the following relations when considering a longitudinal field,

$$\begin{cases} \mathbf{E}^P_{\mathbf{0}}(\mathbf{q},\omega) = \varepsilon^{LL}_M(\mathbf{q},\omega)\, \mathbf{E}_{\mathbf{0}}(\mathbf{q},\omega) \\ \mathbf{P}^{(2)}_M(\mathbf{q},\omega) = \varepsilon^{LL}_M(\mathbf{q},\omega)\, \mathbf{P}^{(2)}_{\mathbf{0}}(\mathbf{q},\omega) \\ \mathbf{P}^{(3)}_M(\mathbf{q},\omega) = \varepsilon^{LL}_M(\mathbf{q},\omega)\, \mathbf{P}^{(3)}_{\mathbf{0}}(\mathbf{q},\omega) \end{cases} \tag{3.47}$$

with the longitudinal dielectric function expressed as

$$\varepsilon^{LL}_M(\mathbf{q},\omega) = \frac{1}{1 - 4\pi\tilde{\alpha}^{(1),LL}_{\mathbf{0},\mathbf{0}}(\mathbf{q},\mathbf{q},\omega)} \tag{3.48}$$

and $\tilde{\alpha}^{(1),LL}_{\mathbf{0},\mathbf{0}}$ corresponds to the macroscopic component of the quasipolarizability defined in the reciprocal space as

$$\mathbf{P}^{(1)}_{\mathbf{G}}(\mathbf{q},\omega) = \sum_{\mathbf{G}_1} \tilde{\alpha}^{(1)}_{\mathbf{G},\mathbf{G}_1}(\mathbf{q},\mathbf{q},\omega)\, \mathbf{E}^P_{\mathbf{G}_1}(\mathbf{q},\omega) \tag{3.49}$$

3.4.1 Components

The second-order microscopic polarization is expressed as

$$\mathbf{P}^{(2)}_{\mathbf{0}}(\mathbf{q},\omega) = \sum_{\mathbf{q}_1} \delta_{\mathbf{q}-\mathbf{q}_1-\mathbf{q}_2} \int d\omega_1\, \delta(\omega-\omega_1-\omega_2)\, \tilde{\alpha}^{(2)}_{\mathbf{0},\mathbf{0},\mathbf{0}}(\mathbf{q},\mathbf{q}_1,\mathbf{q}_2,\omega_1,\omega_2)\, \mathbf{E}^P(\mathbf{q}_1,\omega_1)\, \mathbf{E}^P(\mathbf{q}_2,\omega_2) \tag{3.50}$$

Using equation (3.47), we can recast equation (3.50) to display the macroscopic polarization in terms of the total field, which is otherwise defined as

$$P^{(2),L}_M(\mathbf{q},\omega) = \sum_{\mathbf{q}_1} \delta_{\mathbf{q}-\mathbf{q}_1-\mathbf{q}_2} \int d\omega_1\, \delta(\omega-\omega_1-\omega_2)\, \hat{\mathbf{q}}\, \overleftrightarrow{\chi}^{(2)}(\omega_1,\omega_2)\, \hat{\mathbf{q}}_1 E_1(\omega_1)\, \hat{\mathbf{q}}_2 E_2(\omega_2), \tag{3.51}$$

where $\chi^{(2)}$ is the macroscopic second order susceptibility. Using the following relation,

$$\hat{\mathbf{q}}\, \tilde{\alpha}^{(2)}_{\mathbf{0},\mathbf{0},\mathbf{0}}(\mathbf{q},\mathbf{q}_1,\mathbf{q}_2,\omega_1,\omega_2)\, \hat{\mathbf{q}}_1\hat{\mathbf{q}}_2 = -\frac{i}{2}\, \chi_{\rho\rho\rho}(\hat{\mathbf{q}},\hat{\mathbf{q}}_1,\hat{\mathbf{q}}_2,\omega_1,\omega_2), \tag{3.52}$$

we can establish the link between $\chi^{(2)}$ and the fully-interacting density response function $\chi_{\rho\rho\rho}$,

$$\hat{\mathbf{q}}\, \overleftrightarrow{\chi}^{(2)}(\omega_1,\omega_2)\, \hat{\mathbf{q}}_1\, \hat{\mathbf{q}}_2 = -\frac{i}{2}\, \varepsilon^{LL}_M(\hat{\mathbf{q}},\omega)\, \chi_{\rho\rho\rho}(\hat{\mathbf{q}},\hat{\mathbf{q}}_1,\hat{\mathbf{q}}_2,\omega_1,\omega_2)\, \varepsilon^{LL}_M(\hat{\mathbf{q}}_1,\omega_1)\, \varepsilon^{LL}_M(\hat{\mathbf{q}}_2,\omega_2) \tag{3.53}$$

Using the second-order Dyson-like equation, within IPA, the ε_M^{LL} functions are compensated, leaving only

$$\hat{\mathbf{q}}\,\overleftrightarrow{\chi}^{(2)}(\omega_1,\omega_2)\,\hat{\mathbf{q}}_1\,\hat{\mathbf{q}}_2 = -\frac{i}{2}\,\chi_0^{(2)}(\hat{\mathbf{q}},\hat{\mathbf{q}}_1,\hat{\mathbf{q}}_2,\omega_1,\omega_2) \tag{3.54}$$

where $\chi_0^{(2)}$ is the IPA response function and $\mathbf{q}=\mathbf{q}_1+\mathbf{q}_2$. From there, one can evaluate the susceptibility of any symmetry. For instance, if we consider an hexagonal symmetry (6mm), the polarization is

$$P_M^{(2),L}(\mathbf{q},\omega) = \hat{\mathbf{q}}\begin{pmatrix} \chi^{(2)}_{xxz}(\omega_1,\omega_2)\,\hat{q}_{1x}\,\hat{q}_{2z} + \chi^{(2)}_{xzx}(\omega_1,\omega_2)\,\hat{q}_{1z}\,\hat{q}_{2x} \\ \chi^{(2)}_{yyz}(\omega_1,\omega_2)\,\hat{q}_{1y}\,\hat{q}_{2z} + \chi^{(2)}_{yzy}(\omega_1,\omega_2)\,\hat{q}_{1z}\,\hat{q}_{2y} \\ \chi^{(2)}_{zxx}(\omega_1,\omega_2)\,\hat{q}_{1x}\,\hat{q}_{2x} + \chi^{(2)}_{zyy}(\omega_1,\omega_2)\,\hat{q}_{1y}\,\hat{q}_{2y} + \chi^{(2)}_{zzz}(\omega_1,\omega_2)\,\hat{q}_{1z}\,\hat{q}_{2z} \end{pmatrix} E_1(\omega_1)E_2(\omega_2) \tag{3.55}$$

Depending on the value of $\mathbf{q}_1$ and $\mathbf{q}_2$, we can access any components. For example, by choosing $\mathbf{q}_1=\hat{\mathbf{x}}$ and $\mathbf{q}_2=\hat{\mathbf{z}}$, we would get

$$\chi^{(2)}_{xxz}(\omega,0) = -\frac{i}{\sqrt{2}}\,\chi_0^{(2)}(\frac{\hat{\mathbf{x}}+\hat{\mathbf{z}}}{\sqrt{2}},\hat{\mathbf{x}},\hat{\mathbf{z}},\omega,0), \tag{3.56}$$

which is true since $\chi^{(2)}_{zxz}$ is zero in this symmetry.

Similar equations to (3.50) and (3.51) can be written for the third-order response. We then define the third-order quasipolarizability in terms of the density response function $\chi_{\rho\rho\rho\rho}$ as

$$\hat{\mathbf{q}}\,\tilde{\alpha}^{(3)}_{\mathbf{0},\mathbf{0},\mathbf{0}}(\mathbf{q},\mathbf{q}_1,\mathbf{q}_2,\mathbf{q}_3,\omega_1,\omega_2,\omega_3)\,\hat{\mathbf{q}}_1\hat{\mathbf{q}}_2\hat{\mathbf{q}}_3 = \frac{1}{6}\,\chi_{\rho\rho\rho\rho}(\hat{\mathbf{q}},\hat{\mathbf{q}}_1,\hat{\mathbf{q}}_2,\hat{\mathbf{q}}_3,\omega_1,\omega_2,\omega_3), \tag{3.57}$$

which gives us the relation between the third-order susceptibility and the microscopic IPA response function,

$$\hat{\mathbf{q}}\,\overleftrightarrow{\chi}^{(3)}(\omega_1,\omega_2,\omega_3)\,\hat{\mathbf{q}}_1\,\hat{\mathbf{q}}_2\,\hat{\mathbf{q}}_3 = \frac{1}{6}\,\chi_0^{(3)}(\hat{\mathbf{q}},\hat{\mathbf{q}}_1,\hat{\mathbf{q}}_2,\hat{\mathbf{q}}_3,\omega_1,\omega_2,\omega_3). \tag{3.58}$$

For the cubic, hexagonal and tetragonal symmetries, the only non-vanishing components $\chi^{(3)}_{ijkl}(\omega_1,\omega_2,\omega_3)$ are of the type: $(i=j=k=l)$, $(i=j,\ k=l)$, $(i=k,\ j=l)$, $(i=l,\ j=k)$.

$$P_M^{(3),L}(\mathbf{q},\omega) = \hat{\mathbf{q}}\begin{pmatrix} \chi^{(3)}_{xxxx}\,\hat{q}_{1x}\,\hat{q}_{2x}\,\hat{q}_{3x} + \chi^{(3)}_{xxyy}\,\hat{q}_{1x}\,\hat{q}_{2y}\,\hat{q}_{3y} + \chi^{(3)}_{xzzx}\,\hat{q}_{1z}\,\hat{q}_{2x}\,\hat{q}_{3z} + \dots \\ \chi^{(3)}_{yyyy}\,\hat{q}_{1y}\,\hat{q}_{2y}\,\hat{q}_{3y} + \chi^{(3)}_{yyzz}\,\hat{q}_{1y}\,\hat{q}_{2z}\,\hat{q}_{3z} + \chi^{(3)}_{yxyx}\,\hat{q}_{1x}\,\hat{q}_{2y}\,\hat{q}_{3x} + \dots \\ \chi^{(3)}_{zzzz}\,\hat{q}_{1z}\,\hat{q}_{2z}\,\hat{q}_{3z} + \chi^{(3)}_{zzxx}\,\hat{q}_{1z}\,\hat{q}_{2x}\,\hat{q}_{3x} + \chi^{(3)}_{zyzy}\,\hat{q}_{1y}\,\hat{q}_{2z}\,\hat{q}_{3y} + \dots \end{pmatrix} E_1(\omega_1)E_2(\omega_2)E_3(\omega_3) \tag{3.59}$$

This gives two different cases:

(a) if all subscripts $ijkl$ are the same. For instance, we set $\mathbf{q}_1=\mathbf{q}_2=\mathbf{q}_3=\hat{\mathbf{z}}$

$$\chi^{(3)}_{zzzz} = \frac{1}{6}\,\chi_0^{(3)}(\hat{\mathbf{z}},\hat{\mathbf{z}},\hat{\mathbf{z}},\hat{\mathbf{z}},\omega,\omega,0) \tag{3.60}$$

(b) if the subscripts are equal two by two. For example, we choose $\mathbf{q}_1=\mathbf{q}_3=\hat{\mathbf{x}}$ and $\mathbf{q}_2=\hat{\mathbf{y}}$

$$\chi^{(3)}_{yxyx} = \frac{\sqrt{5}}{6}\,\chi_0^{(3)}(\frac{2\hat{\mathbf{x}}+\hat{\mathbf{y}}}{\sqrt{5}},\hat{\mathbf{x}},\hat{\mathbf{y}},\hat{\mathbf{x}},\omega,\omega,0) \tag{3.61}$$

Part II

Development and applications

Chapter 4

Microscopic response: IPA calculations

The simplest level of approximation for the calculation of the susceptibility $\chi^{(n)}$ is the independent particle approximation (IPA) where both the local field and excitonic effects are neglected and only the Kohn-Sham response is present. Despite its simplicity, IPA actually captures the main effect in the spectrum and can be a rather good approximation. Indeed, it is known to work quite well for the bulk response, since, for a large class of materials, the effect of the local fields is proven to be negligible, regarding both the linear and SHG computation. However this effect is rather large when looking at the surface response, which will not be the case here.

4.1 Polarized ground-state

The goal of this thesis was to calculate optical responses of materials under a static field. To evaluate such a response, two feasible ways emerged. Since a dc-field is a static perturbation with no time dependence, it should be possible to take it into account at the ground-state level and then calculate the response function of the $(n-1)$-order of the one desired. For instance, one could calculate the first order response function $\tilde{\chi}^{(1)}(\omega)$ of a polarized medium to obtained the linear electro-optic effect instead of having to calculate the second order susceptibility $\chi^{(2)}(\omega, 0)$ of an unpolarized medium. The quantity then calculated would contained all the orders in terms of the static field $\boldsymbol{\mathcal{E}}$ since it will not be treated as a perturbation.

$$\tilde{\chi}^{(1)}(\omega) = \chi^{(1)}(-\omega;\omega) + \chi^{(2)}(-\omega;\omega,0)\boldsymbol{\mathcal{E}} + \chi^{(3)}(-\omega;\omega,0,0)\boldsymbol{\mathcal{E}}\boldsymbol{\mathcal{E}} + \dots \tag{4.1}$$

Apart for the first term in the expansion, the response of the system depends on the dc-field. For a reasonable value of the static field, the dominating term is the unpolarized first order susceptibility $\chi^{(1)}(\omega)$, meaning that the accuracy on the remaining term of the expansion, much smaller, may not be as good.

It poses the problem of applying a static field on a periodic system, given that the scalar potential associated with the dc-field, $V(\mathbf{r}) = -e\boldsymbol{\mathcal{E}}\mathbf{r}$, is *non-periodic*, due to the position operator $\hat{\mathbf{r}}$. Furthermore, the matrix elements of $\hat{\mathbf{r}}$ are ill-defined with Bloch functions, that are commonly used for periodic systems. Moreover, the potential is also *unbound from below*, meaning that the energy of the system could always be lowered by Zener tunneling, illustrated in Figure 4.1, which corresponds to a charge transfer from the valence to the conduction bands at different momentums. It is rendered possible due to the tilting of the bands by the dc-field, shown in Figure 4.1. As a consequence, an infinite system submitted to a static field has no ground state. The importance of this Zener tunneling is linked to the strength of the static field. Therefore, if the field is small enough, this tunneling is negligible on

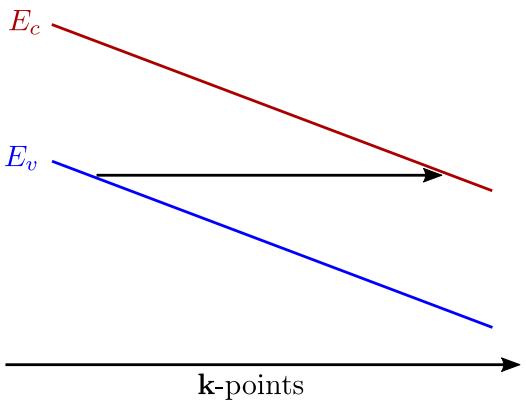

Figure 4.1: Zener tunneling: charge transfer from the valence to the conduction band.

the relevant time scale and the system remains in a polarized long-lived resonant state that retains its periodicity.

The problem of calculating the ground-state can then be solved for field-polarized Bloch functions by minimizing the energy functional, introduced in Ref. [33],

$$E[\{u_{n,\mathbf{k}}^{(\boldsymbol{\mathcal{E}})}\};\boldsymbol{\mathcal{E}}] = E^{(0)}[\{u_{n,\mathbf{k}}^{(\boldsymbol{\mathcal{E}})}\}] - \Omega\boldsymbol{\mathcal{E}}\cdot\mathbf{P}[\{u_{n,\mathbf{k}}^{(\boldsymbol{\mathcal{E}})}\}], \tag{4.2}$$

where $E^{(0)}$ is the Kohn-Sham energy of the system, Ω the unit-cell volume and $\mathbf{P}$ is the macroscopic polarization defined using the Modern Theory of Polarization (MTP)[34;35].

In the MTP, the total change in polarization per unit volume, induced by an adiabatic change in the potential, represented by the parameter λ, is defined as

$$\Delta\mathbf{P} = \int_{\lambda_1}^{\lambda_2} \frac{\partial\mathbf{P}}{\partial\lambda}\, d\lambda = \mathbf{P}^{(\lambda_2)} - \mathbf{P}^{(\lambda_1)}, \tag{4.3}$$

with the polarization $\mathbf{P}(\lambda)$ given as a sum over the occupied bands of Berry phases,

$$\mathbf{P}(\lambda) = -\frac{ie}{8\pi^3}\sum_n \int d\mathbf{k}\, f_{n,\mathbf{k}} \left\langle u_{n,\mathbf{k}}^{(\lambda)} \middle| \frac{\partial}{\partial\mathbf{k}} \middle| u_{n,\mathbf{k}}^{(\lambda)} \right\rangle, \tag{4.4}$$

where $f_{n,\mathbf{k}}$ is the occupation number. Here the parameter λ is the dc-electric field $\boldsymbol{\mathcal{E}}$. Thus both the KS energy and the polarization depends only on the occupied bands of the system. It means that minimizing the functional in equation (4.2) gives us access to the occupied field-polarized Bloch functions, which was already implemented in the DFT code ABINIT[36]. And the derivative of this functional with respect to the electric field can then provide static susceptibilities, also implemented in ABINIT.

Now, to go beyond the static response, one needs to determine the polarized-conduction bands as well, meaning that we have to diagonalized the Hamiltonian

$$H[\rho^{(\boldsymbol{\mathcal{E}})}] = H^{(0)}[\rho^{(\boldsymbol{\mathcal{E}})}] + H^{int}[\rho^{(\boldsymbol{\mathcal{E}})}]. \tag{4.5}$$

where $H^{(0)}$ is the usual KS Hamiltonian but calculated for the polarized density and H^{int} contains the interaction with the static field and corresponds to the scalar potential $V(\mathbf{r})$. The challenge, here, is then to determine this Hamiltonian H^{int}. In the rest of this section, I will present the two main attempts of finding a valid representation of H^{int} for Bloch functions. Although this way of calculating electro-optic responses was not successful in the end, I still present here the main difficulties I have faced.

4.1.1 Velocity operator

For convenience, the Hamiltonian (4.5) is written in the basis of the non-polarized wavefunctions, for which $H^{(0)}$ is diagonal. Since the position operator $\hat{\mathbf{r}}$ is ill-defined in periodic systems, we need to find a new way to write it:

$$\langle \phi_{m,\mathbf{k}'} | \hat{\mathbf{r}} | \phi_{n,\mathbf{k}} \rangle = \frac{\langle \phi_{m,\mathbf{k}'} | [H, \hat{\mathbf{r}}] | \phi_{n,\mathbf{k}} \rangle}{E_{m,\mathbf{k}'} - E_{n,\mathbf{k}}} = -i \frac{\langle \phi_{m,\mathbf{k}'} | \hat{\mathbf{v}} | \phi_{n,\mathbf{k}} \rangle}{E_{m,\mathbf{k}'} - E_{n,\mathbf{k}}}, \tag{4.6}$$

with the matrix elements set to zero when $E_{n,\mathbf{k}} = E_{m,\mathbf{k}'}$. In principle, one could think about using the velocity to represent the position operator as it is done for the calculation of optical response. However, in that case, a few issues arise.

During the diagonalization of the Hamiltonian, the eigenvalues are uniquely determined while the eigenstates depends on a phase which is randomly assigned: $|\widetilde{u}_{n,\mathbf{k}}\rangle = |u_{n,\mathbf{k}}\rangle e^{i\alpha_{n,\mathbf{k}}}$. In the calculation of optical responses, this phase is canceled with the others matrix elements $\langle \phi_{n,\mathbf{k}} | \hat{\mathbf{v}} | \phi_{m,\mathbf{k}} \rangle \langle \phi_{m,\mathbf{k}} | \hat{\mathbf{v}} | \phi_{n,\mathbf{k}} \rangle$. Looking at each individually, they may seem ill-defined, due to the discontinuity in their values occurring around degeneracies, as shown in Figure 4.2 around X for the bands 1 and 2 of silicon where the energies are equal. The full bandstructure was plotted in Figure 2.2. However it can be simply

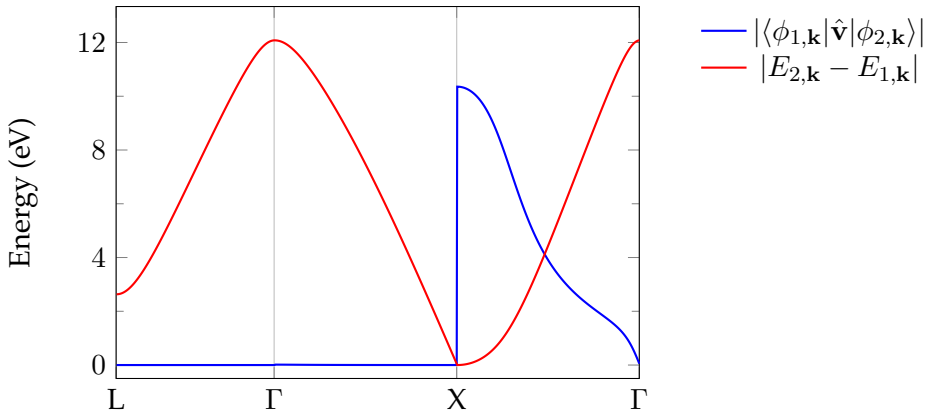

Figure 4.2: Plot of the matrix elements of the velocity operator (in blue) and the energy difference (in red) between the band 1 and 2 of silicon.

explained by the fact that the phase is brutally changed at the degeneracy while it is slowly varying in k-points everywhere else, since the basis is not uniquely determined at that point. We could expect this discontinuity in the phase to be a problem when solving the Hamiltonian. But actually, this should not matter considering that these phases are random and are not suppose to have specific relations between k-points. Indeed, using velocity matrix elements would lead to solve an Hamiltonian for one k-point of the form

$$H = \begin{pmatrix} H_{11} & H_{12}e^{i(\alpha_2-\alpha_1)} & H_{13}e^{i(\alpha_3-\alpha_1)} \\ H_{21}e^{i(\alpha_1-\alpha_2)} & H_{22} & H_{23}e^{i(\alpha_3-\alpha_2)} \\ H_{31}e^{i(\alpha_1-\alpha_3)} & H_{32}e^{i(\alpha_2-\alpha_3)} & H_{33} \end{pmatrix}, \tag{4.7}$$

where the phase are explicitly written and will be canceled during the diagonalization, leading to phase-free eigenvalues. Thus, finally, contrary to what one might think, the phase of the wavefunctions is not an issue here.

The problem resides in the division by the energy difference $(E_{n,\mathbf{k}} - E_{m,\mathbf{k}})$. Indeed, around a degeneracy, the term added to the Hamiltonian would tends to infinity and have a huge impact on the

bandstructure by creating divergences in energy there. Even if a tolerance was added on the energy differences, making $\langle\phi_{n,\mathbf{k}}|\hat{\mathbf{r}}|\phi_{m,\mathbf{k}}\rangle$ go to zero if $(E_{n,\mathbf{k}} - E_{m,\mathbf{k}})$ was bellow the tolerance, it would only shift the divergences that would still appear on the bandstructure and the shape would be highly depend on the value of this tolerance (see Figure 4.3). Thus this form of the matrix elements is not

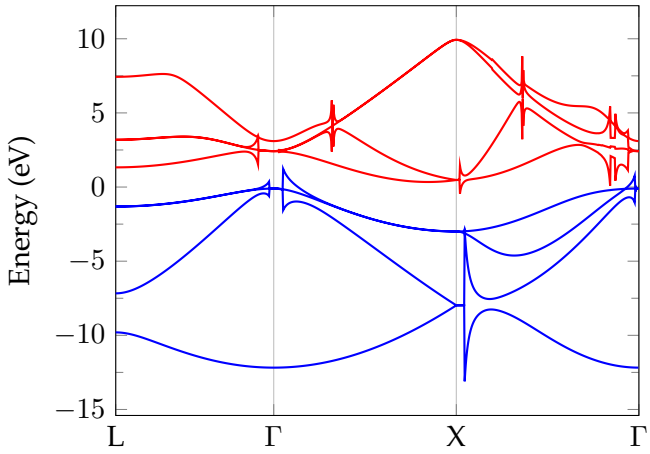

Figure 4.3: Field-polarized bandstructure of silicon using velocity matrix elements, with a tolerance of $2.5 \cdot 10^{-2}$ eV on the energy difference $|E_{n,\mathbf{k}} - E_{m,\mathbf{k}}|$ and with a static field of $2.6 \cdot 10^{6}$ V.cm^{-1}.

suitable here to replace the position operator.

4.1.2 Derivative over k: $\partial/\partial\mathbf{k}$

Another possibility would be to follow the idea of Ref. [33] to find the Hamiltonian H^{int} containing the interaction with the static field expressed for Bloch functions. The energy functional of equation (4.2) is develop using the definition of the polarization presented in equation (4.4),

$$E[\{u^{(\boldsymbol{\mathcal{E}})}_{n,\mathbf{k}}\};\boldsymbol{\mathcal{E}}] = \frac{1}{8\pi^3}\int d\mathbf{k}\sum_n f_{n,\mathbf{k}}\left[\left\langle u^{(\boldsymbol{\mathcal{E}})}_{n,\mathbf{k}}\middle|H^{(0)}_{\mathbf{k}}\middle|u^{(\boldsymbol{\mathcal{E}})}_{n,\mathbf{k}}\right\rangle + \left\langle u^{(\boldsymbol{\mathcal{E}})}_{n,\mathbf{k}}\middle|ie\boldsymbol{\mathcal{E}}\frac{\partial}{\partial\mathbf{k}}\middle|u^{(\boldsymbol{\mathcal{E}})}_{n,\mathbf{k}}\right\rangle\right], \tag{4.8}$$

which corresponds to the expectation value of the following operator:

$$H_{\mathbf{k}} = H^{(0)}_{\mathbf{k}} + ie\boldsymbol{\mathcal{E}}\frac{\partial}{\partial\mathbf{k}}, \tag{4.9}$$

where $H_{\mathbf{k}}$ is the Hamiltonian of the periodic part of the Bloch functions $u_{n,\mathbf{k}}$, defined by the relation on the eigenvalues, $E_{n,\mathbf{k}} = \langle\phi_{n,\mathbf{k}}|H|\phi_{n,\mathbf{k}}\rangle = \langle u_{n,\mathbf{k}}|H_{\mathbf{k}}|u_{n,\mathbf{k}}\rangle$. Furthermore, we know from Ref. [13] that the position operator can then be written as

$$\left\langle\phi_{m,\mathbf{k}'}\middle|\hat{\mathbf{r}}\middle|\phi_{n,\mathbf{k}}\right\rangle = \delta(\mathbf{k}'-\mathbf{k})\left\langle u_{m,\mathbf{k}}\middle|i\frac{\partial}{\partial\mathbf{k}}\middle|u_{n,\mathbf{k}}\right\rangle + \delta_{nm}\, i\frac{\partial}{\partial\mathbf{k}}\delta(\mathbf{k}'-\mathbf{k}) \tag{4.10}$$

This relation is easily obtained for $(m \neq n)$ and $(\mathbf{k} = \mathbf{k}')$ through the velocity operator

$$\langle\phi_{m,\mathbf{k}}|\hat{\mathbf{v}}|\phi_{n,\mathbf{k}}\rangle = \left\langle u_{m,\mathbf{k}}\middle|\left[\frac{\partial}{\partial\mathbf{k}}, H_{\mathbf{k}}\right]\middle|u_{n,\mathbf{k}}\right\rangle = -\left(E_{m,\mathbf{k}} - E_{n,\mathbf{k}}\right)\left\langle u_{m,\mathbf{k}}\middle|\frac{\partial}{\partial\mathbf{k}}\middle|u_{n,\mathbf{k}}\right\rangle \tag{4.11}$$

But in that case the random phase, mentioned before, may be an issue due to the derivative over $\mathbf{k}$:

$$\left\langle\widetilde{u}_{p,\mathbf{k}}\middle|i\frac{\partial}{\partial\mathbf{k}}\middle|\widetilde{u}_{n,\mathbf{k}}\right\rangle = \left[\left\langle u_{p,\mathbf{k}}\middle|i\frac{\partial}{\partial\mathbf{k}}\middle|u_{n,\mathbf{k}}\right\rangle - \delta_{pn}\frac{\partial\alpha_{n,\mathbf{k}}}{\partial\mathbf{k}}\right]e^{i(\alpha_{n,\mathbf{k}}-\alpha_{p,\mathbf{k}})}, \tag{4.12}$$

Indeed, the phase is here a problem for the diagonal part of the matrix elements, that were set to zero as a first approximation when using the velocity operator instead in the previous section. It is illustrated on a simple model.

Hubbard model

We use the same model as the one introduced in Ref. [33], which is a simple 1D two-site periodic model, displayed in Figure 4.4. The on-site terms are $-\Delta/2$ and $\Delta/2$ for the site 1 and 2 respectively,

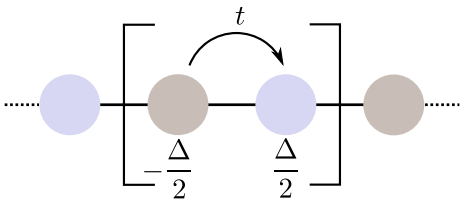

Figure 4.4: Sketch of the Hubbard model.

and the hopping between sites is characterized by the hopping integral t. The k-points sample the first Brillouin zone, between $-\pi/a$ and π/a, where a is the unit-cell period. To simplify the problem, we choose to have Δ and a equal to 1. This gives us the following Hamiltonian

$$H_k^{(0)} = \begin{pmatrix} -\frac{1}{2} & 2t\cos(\frac{k}{2}) \\ 2t\cos(\frac{k}{2}) & \frac{1}{2} \end{pmatrix} \tag{4.13}$$

The energy eigenvalues, obtained by diagonalization of this Hamiltonian (4.13) are given by

$$E_{v,k}^{(0)} = -\frac{1}{2}\left[1 + 16\,t^2\cos^2(\frac{k}{2})\right]^{1/2}, \qquad E_{c,k}^{(0)} = -E_{v,k}^{(0)} \tag{4.14}$$

and the corresponding eigenstates are

$$\left|u_{v,k}^{(0)}\right\rangle = \begin{pmatrix} \cos\Theta_k \\ \sin\Theta_k \end{pmatrix} e^{i\alpha_{vk}} \quad , \quad \left|u_{c,k}^{(0)}\right\rangle = \begin{pmatrix} \sin\Theta_k \\ -\cos\Theta_k \end{pmatrix} e^{i\alpha_{ck}} \tag{4.15}$$

with

$$\begin{cases} \cos\Theta_k = \dfrac{2t\cos(\frac{k}{2})}{\left[\left(2t\cos(\frac{k}{2})\right)^2 + \left(\frac{1}{2} + E_{v,k}^{(0)}\right)^2\right]^{\frac{1}{2}}} = \dfrac{2t\cos(\frac{k}{2})}{\left[E_{v,k}^{(0)}\left(2E_{v,k}^{(0)} + 1\right)\right]^{\frac{1}{2}}} \\ \sin\Theta_k = \dfrac{\frac{1}{2} + E_{v,k}^{(0)}}{\left[\left(2t\cos(\frac{k}{2})\right)^2 + \left(\frac{1}{2} + E_{v,k}^{(0)}\right)^2\right]^{\frac{1}{2}}} = \dfrac{\frac{1}{2} + E_{v,k}^{(0)}}{\left[E_{v,k}^{(0)}\left(2E_{v,k}^{(0)} + 1\right)\right]^{\frac{1}{2}}} \end{cases} \tag{4.16}$$

$e^{i\alpha_{nk}}$ is the random phase associated to the eigenstates $\left|u_{n,k}\right\rangle$ during the diagonalization of the Hamiltonian.

We now add the static field on the system

$$H_k = H_k^{(0)} + H_k^{int} = H_k^{(0)} + ie\,\mathcal{E}\frac{\partial}{\partial k}, \tag{4.17}$$

and write this Hamiltonian in a basis for which $H_k^{(0)}$ is diagonal,

$$H_k = \begin{pmatrix} E_{v,k}^{(0)} - e\mathcal{E}\frac{\partial\alpha_{vk}}{\partial k} & ie\mathcal{E}\frac{\partial\Theta_k}{\partial k}\,e^{i\Delta\alpha_k} \\ -ie\mathcal{E}\frac{\partial\Theta_k}{\partial k}\,e^{-i\Delta\alpha_k} & -E_{v,k}^{(0)} - e\mathcal{E}\frac{\partial\alpha_{ck}}{\partial k} \end{pmatrix} \tag{4.18}$$

with

$$\frac{\partial\Theta_k}{\partial k} = \frac{t\,\sin(\frac{k}{2})}{4(E_{v,k}^{(0)})^2} \tag{4.19}$$

One can notice that, in this model, the phase-free matrix elements $\langle u_{n,k}|\nabla_k|u_{n,k}\rangle$ of equation (4.12) are zero and only the derivative of the phase $\nabla_k\, e^{i\alpha_{n,k}}$ remains for the diagonal part. After diagonalizing this Hamiltonian, the calculated eigenvalues are

$$\begin{cases} E_{v,k}^{(\mathcal{E})} = E_{v,k}^{(0)} - e\mathcal{E}\,\dfrac{\partial\alpha_{vk}}{\partial k} + \dfrac{\left[e\mathcal{E}t\sin(\frac{k}{2})\right]^2}{\left[2E_{v,k}^{(0)}\right]^3} \\ E_{c,k}^{(\mathcal{E})} = E_{c,k}^{(0)} - e\mathcal{E}\,\dfrac{\partial\alpha_{ck}}{\partial k} - \dfrac{\left[e\mathcal{E}t\ \sin(\frac{k}{2})\right]^2}{\left[2E_{v,k}^{(0)}\right]^3} \end{cases} \tag{4.20}$$

Unlike, all the cases previously discussed, the eigenvalues here depend on the random phase of the wavefunctions. This leads to the discontinuity shown in Figure 4.5 for $k = 0$. This can be avoided if

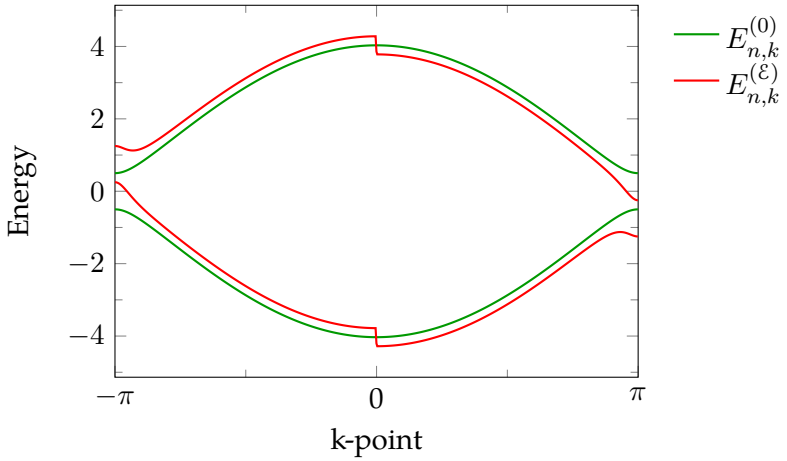

Figure 4.5: Bandstructure of the periodic two-site model with (red curve) and without (green curve) an electrostatic field. Parameters: $t = 2$, $\mathcal{E} = 0.5$, $\alpha_{vk} = \alpha_{ck} = \arcsin(\cos(k/2))$.

the derivative over k is done on a phase-free quantity such as $\frac{\partial}{\partial k}\left(|u_{m,\mathbf{k}}\rangle\langle u_{m,\mathbf{k}}|\right)$ as suggested in Ref. [33]. It can be done easily for the matrix elements between two different bands,

$$\begin{aligned} \left\langle u_{c,k}\middle|\frac{\partial}{\partial k}\middle|u_{v,k}\right\rangle &= \left\langle u_{c,k}\middle|\left(\frac{\partial}{\partial k}|u_{v,k}\rangle\langle u_{v,k}|\right)\middle|u_{v,k}\right\rangle \\ \left\langle u_{v,k}\middle|\frac{\partial}{\partial k}\middle|u_{c,k}\right\rangle &= \left\langle u_{v,k}\middle|\left(\frac{\partial}{\partial k}|u_{c,k}\rangle\langle u_{c,k}|\right)\middle|u_{c,k}\right\rangle, \end{aligned} \tag{4.21}$$

that do not pose any problem here but might when writing the derivative over $\mathbf{k}$ as a finite-difference expansion:

$$\frac{\partial}{\partial\mathbf{k}}|u_{n,\mathbf{k}}\rangle = \frac{1}{2\Delta_{\mathbf{k}}}\left(|u_{n,\mathbf{k}_+}\rangle - |u_{n,\mathbf{k}_-}\rangle\right), \tag{4.22}$$

with $\Delta_{\mathbf{k}} = \mathbf{k}_+ - \mathbf{k} = \mathbf{k} - \mathbf{k}_-$. But, as for in any gauge, the diagonal matrix elements are ill-defined and cannot be recast in such a way.

In a first approximation, the problematic diagonal part of H^{int} was set to zero, which seems like a good approximation for this model considering that the phase-free part of the diagonal elements is zero. However, when applied on real materials, the calculation appeared to be wrong since some components which were supposed to be zero due to the symmetry were not: the quantity $\widetilde{\chi}^{(1)} - \chi^{(1)}$ of equation (4.1) should be quadratic with the dc-field for bulk silicon, since $\chi^{(2)}$ is zero for this material and the dominating term is $\chi^{(3)}$, and it should be linear for silicon carbide, for which the leading term

is $\chi^{(2)}$. However, in the end, both showed a linear dependence with the static field, which would indicate that the calculation was erroneous. Moreover, the relations between the components of the $\chi^{(2)}$ tensor for SiC were not respected either.

It is important to note, even if it was not used in this thesis, that different papers treated the issue of the $\mathbf{k}$ derivation[37;38], and could potentially offer insights on understanding the problem in our calculation. However at this point, it was decided that we should follow a different route and directly calculate a $\chi^{(2)}$ and $\chi^{(3)}$ for LEO and EFISH, respectively.

4.2 From an unpolarized ground-state

In this section, the static field is considered as the limit of the time-dependent field,

$$\boldsymbol{\mathcal{E}} = 2\mathbf{E}(0) = \lim_{\omega \to 0} \mathbf{E}(\omega), \tag{4.23}$$

and is treated at the same level as the optical field.

In the framework of TDDFT, where the perturbation is described by a scalar potential, what we are interested in is the calculation of density response functions: $\chi_{\rho\rho}$, $\chi_{\rho\rho\rho}$, and $\chi_{\rho\rho\rho\rho}$, respectively for the first-, second- and third-order susceptibilities. There are two different ways to evaluate those quantities. It can be obtained directly from the charge density ρ or one could use the charge conservation law to get it through the current density $\mathbf{j}$. Either one of those calculations brings many challenges.

Indeed, if choosing the charge density path, taking the long-wavelength limit will require the use of the $\mathbf{k}\cdot\mathbf{p}$ perturbation theory in order to evaluate this kind of matrix elements: $\langle \phi_{n,\mathbf{k}} | e^{-i\mathbf{qr}} | \phi_{m,\mathbf{k}+\mathbf{q}} \rangle$, for which the analytical calculation can be quite lengthy. However, this kind of terms could also be evaluated by taking a very small and finite $\mathbf{q}$, representing then the difference between $\mathbf{k}$-points, $\mathbf{q} = \mathbf{k} - \mathbf{k}'$, usually from two different grids with one slightly shifted compared to the other. This works quite well for the first order but is much more complicated for the second order and require high numerical accuracy beyond single machine precision. Regarding the first order response, the expression contains the product of two matrix elements that should be proportional to q^2, while for the second order, it contains the product of three matrix elements that should be proportional to q^3 (assuming $q_1 = q_2$). For this to be true means that all previous order in q are zero. This exact cancellation, occurring when using the $\mathbf{k}\cdot\mathbf{p}$ theory, then needs to be reached numerically, meaning that the chosen grids should explicitly contain all the symmetry or they should directly be included in the formula.

On the other hand, if one were to choose to go through the calculation of the current density, the treatment of the long-wavelength limit response would be quite straightforward, but after using the charge conservation law,

$$-i\omega\, \rho_{ind}(\mathbf{q},\omega) + i\mathbf{q}\, \mathbf{j}_{ind}(\mathbf{q},\omega) = 0, \tag{4.24}$$

here written in the reciprocal space, the expression will show an apparent divergence in ω that one must get rid of before performing actual calculations.

Depending on the process, we followed either both routes to check the validity of the analytical calculation or just one when it became too complicated.

4.2.1 Linear Electro-Optic effect

For the LEO calculation, both paths were followed resulting in the same analytical formula. The LEO calculation from the current density is described in appendix C. Here, I will only discuss the

calculation using the second-order charge density,

$$\rho^{(2)}(\mathbf{r},\omega) = \frac{1}{2}\int d\mathbf{r}_1\, d\mathbf{r}_2 \int d\omega_1\, d\omega_2\; \delta(\omega-\omega_1-\omega_2)\; \chi_{\rho\rho\rho}(\mathbf{r},\mathbf{r}_1,\mathbf{r}_2,\omega_1,\omega_2)\varphi^P(\omega_1,\mathbf{r}_1)\; \varphi^P(\mathbf{r}_2,\omega_2) \quad (4.25)$$

where φ^P is the scalar potential of the perturbation introduced in section 3.1.3. Using perturbation theory, we obtain the non-interacting response function in the reciprocal space:

$$\begin{aligned}\chi_{\rho\rho\rho}(\mathbf{q},\mathbf{q}_1,\mathbf{q}_2,\omega_1,\omega_2) = \frac{1}{V}\sum_{n,m,p}\sum_{\mathbf{k}} \frac{\left\langle\phi_{n,\mathbf{k}}\middle|e^{-i\mathbf{qr}}\middle|\phi_{m,\mathbf{k}+\mathbf{q}}\right\rangle}{E_{n,\mathbf{k}}-E_{m,\mathbf{k}+\mathbf{q}}+\omega_1+\omega_2+2i\eta}\left\langle\phi_{m,\mathbf{k}+\mathbf{q}}\middle|e^{i\mathbf{q}_1\mathbf{r}_1}\middle|\phi_{p,\mathbf{k}+\mathbf{q}_2}\right\rangle \\ \times\left\langle\phi_{p,\mathbf{k}+\mathbf{q}_2}\middle|e^{i\mathbf{q}_2\mathbf{r}_2}\middle|\phi_{n,\mathbf{k}}\right\rangle\left(\frac{f_{n,\mathbf{k}}-f_{p,\mathbf{k}+\mathbf{q}_2}}{E_{n,\mathbf{k}}-E_{p,\mathbf{k}+\mathbf{q}_2}+\omega_2+i\eta}+\frac{f_{m,\mathbf{k}+\mathbf{q}}-f_{p,\mathbf{k}+\mathbf{q}_2}}{E_{p,\mathbf{k}+\mathbf{q}_2}-E_{m,\mathbf{k}+\mathbf{q}}+\omega_1+i\eta}\right) \\ +\big((\mathbf{q}_1,\omega_1)\leftrightarrow(\mathbf{q}_2,\omega_2)\big)\end{aligned} \quad (4.26)$$

with $\mathbf{q}=\mathbf{q}_1+\mathbf{q}_2$. This relation contains a symmetric term so that it is written as $\chi^{(2)}_{ijk}(-\omega;\omega_1,\omega_2)+\chi^{(2)}_{ikj}(-\omega;\omega_2,\omega_1)$. Both terms need to be present to account for the fact that we don't know which electric field was applied first. In the case of SHG, these two terms are equals. The variable η acts as a broadening but also determines the intensity of the spectrum near a resonance. It should have no effect however in the gap region – at low frequency.

Since we only work with cold semiconductors, we can neglect the momentum dependence in the occupation factor: $f_{m,\mathbf{k}+\mathbf{q}}\to f_m$. In the optical limit, $\mathbf{q}$ tends to zero, so we can do an expansion in terms of $\mathbf{q}$ for the matrix elements and for the energy denominators using $\mathbf{k}\cdot\mathbf{p}$ perturbation theory

$$\begin{aligned}\left\langle\phi_{n,\mathbf{k}}\middle|e^{-i\mathbf{qr}}\middle|\phi_{m,\mathbf{k}+\mathbf{q}}\right\rangle &= \langle\phi_{n,\mathbf{k}}|\phi_{m,\mathbf{k}}\rangle+\left\langle\phi_{n,\mathbf{k}}\middle|\mathbf{q}\,\phi^{(1)}_{m,\mathbf{k}}\right\rangle+\left\langle\phi_{n,\mathbf{k}}\middle|q^2\phi^{(2)}_{m,\mathbf{k}}\right\rangle \\ \frac{1}{E_{n,\mathbf{k}}-E_{m,\mathbf{k}+\mathbf{q}}} &= \frac{1}{E_{n,\mathbf{k}}-E_{m,\mathbf{k}}}+\frac{\mathbf{q}E^{(1)}_{m,\mathbf{k}}}{(E_{n,\mathbf{k}}-E_{m,\mathbf{k}})^2}\end{aligned} \quad (4.27)$$

Performing the above expansion around $\mathbf{q}=0$ to the first non-vanishing order is known as the dipole approximation. The first and second order Hamiltonian in terms of $\mathbf{q}$ are obtained by replacing $\mathbf{k}$ by $\mathbf{k}+\mathbf{q}$ in the expression of the band energies:

$$E_{n,\mathbf{k}+\mathbf{q}} = \langle\phi_{n,\mathbf{k}+\mathbf{q}}|H|\phi_{n,\mathbf{k}+\mathbf{q}}\rangle = \langle u_{n,\mathbf{k}+\mathbf{q}}|H_{\mathbf{k}+\mathbf{q}}|u_{n,\mathbf{k}+\mathbf{q}}\rangle \quad (4.28)$$

where the Hamiltonian is $H=p^2/2+V_{nl}$ with a nonlocal potential due to the pseudopotential as discussed in section 3.2.1 and $u_{n,\mathbf{k}}$ is the periodic part of the Bloch function defined in equation (2.15). We take the limit $\mathbf{q}\to 0$ to the second order for the term $e^{-i(\mathbf{k}+\mathbf{q})\mathbf{r}}\,V_{nl}\,e^{i(\mathbf{k}+\mathbf{q})\mathbf{r}}$ and obtain

$$\begin{aligned}H_{\mathbf{k}+\mathbf{q}} = \frac{1}{2}k^2+\mathbf{k}\cdot\mathbf{q}+\frac{1}{2}q^2-i\mathbf{k}\nabla-i\mathbf{q}\nabla-\frac{1}{2}\nabla^2+e^{-i\mathbf{kr}}\,V_{nl}\,e^{i\mathbf{kr}}+\left[e^{-i\mathbf{kr}}\,V_{nl}\,e^{i\mathbf{kr}},i\mathbf{qr}\right] \\ -\frac{1}{2}\,e^{-i\mathbf{kr}}\,V_{nl}\,e^{i\mathbf{kr}}\,(\mathbf{qr})^2+\mathbf{qr}\,e^{-i\mathbf{kr}}\,V_{nl}\,e^{i\mathbf{kr}}\,\mathbf{qr}-\frac{1}{2}\,(\mathbf{qr})^2\,e^{-i\mathbf{kr}}\,V_{nl}\,e^{i\mathbf{kr}}\end{aligned} \quad (4.29)$$

which gives us $H_1=\mathbf{q}\hat{\mathbf{v}}$ and $H_2=-\left[i\mathbf{q}\hat{\mathbf{r}},\mathbf{q}\hat{\mathbf{v}}\right]/2$. We then use perturbation theory to obtain the first and second order in the wavefunction expansion[1]:

$$\left|\mathbf{q}\phi^{(1)}_{n,\mathbf{k}}\right\rangle = \sum_{m\notin D_n}\frac{\langle\phi_{m,\mathbf{k}}|\mathbf{q}\hat{\mathbf{v}}|\phi_{n,\mathbf{k}}\rangle}{E_{n,\mathbf{k}}-E_{m,\mathbf{k}}}\left|\phi_{m,\mathbf{k}}\right\rangle \quad (4.30)$$

$$\begin{aligned}\left|q^2\phi^{(2)}_{n,\mathbf{k}}\right\rangle = \sum_{m\notin D_n}\sum_{p\notin D_n}\frac{\langle\phi_{m,\mathbf{k}}|\mathbf{q}\hat{\mathbf{v}}|\phi_{p,\mathbf{k}}\rangle\,\langle\phi_{p,\mathbf{k}}|\mathbf{q}\hat{\mathbf{v}}|\phi_{n,\mathbf{k}}\rangle}{(E_{n,\mathbf{k}}-E_{p,\mathbf{k}})(E_{n,\mathbf{k}}-E_{m,\mathbf{k}})}\left|\phi_{m,\mathbf{k}}\right\rangle-\frac{1}{2}\sum_{m\notin D_n}\frac{\langle\phi_{m,\mathbf{k}}|[i\mathbf{q}\hat{\mathbf{r}},\mathbf{q}\hat{\mathbf{v}}]|\phi_{n,\mathbf{k}}\rangle}{E_{n,\mathbf{k}}-E_{m,\mathbf{k}}}\left|\phi_{m,\mathbf{k}}\right\rangle \\ -\langle\phi_{n,\mathbf{k}}|\mathbf{q}\hat{\mathbf{v}}|\phi_{n,\mathbf{k}}\rangle\sum_{m\notin D_n}\frac{\langle\phi_{m,\mathbf{k}}|\mathbf{q}\hat{\mathbf{v}}|\phi_{n,\mathbf{k}}\rangle}{(E_{n,\mathbf{k}}-E_{m,\mathbf{k}})^2}\left|\phi_{m,\mathbf{k}}\right\rangle-\frac{1}{2}\sum_{m\notin D_n}\frac{|\langle\phi_{m,\mathbf{k}}|\mathbf{q}\hat{\mathbf{v}}|\phi_{n,\mathbf{k}}\rangle|^2}{(E_{n,\mathbf{k}}-E_{m,\mathbf{k}})^2}\left|\phi_{n,\mathbf{k}}\right\rangle,\end{aligned} \quad (4.31)$$

where D_n is the degenerate subspace with $|\phi_{n,\mathbf{k}}\rangle$. While it was shown that the commutator $[i\hat{\mathbf{r}}, \hat{V}_{nl}]$, appearing in the definition of the velocity, can have a significant role in the description of optical responses[39;40], this is not the case for the double commutator $[i\mathbf{q}\hat{\mathbf{r}}, [i\mathbf{q}\hat{\mathbf{r}}, \hat{V}_{nl}]]$, introduced in the second term of equation (4.31), which is very small with no visible impact on the spectrum[41] and will therefore be neglected in the following calculation.

In the two-band contribution, the terms containing a square or cube to the energy denominator $(E_{n,\mathbf{k}} - E_{m,\mathbf{k}} + \omega + i\eta)$ can be more difficult to converge in terms of $\mathbf{k}$-points and are therefore recast using the relation

$$\frac{-\Delta_{nm,\mathbf{k}}(\mathbf{q})}{(E_{n,\mathbf{k}} - E_{m,\mathbf{k}} + \omega + i\eta)^2} = \mathbf{q}\,\frac{\partial}{\partial \mathbf{k}}\,\frac{1}{(E_{n,\mathbf{k}} - E_{m,\mathbf{k}} + \omega + i\eta)}, \tag{4.32}$$

with $\Delta_{nm,\mathbf{k}}(\mathbf{q}) = \langle\phi_{n,\mathbf{k}}|\mathbf{q}\hat{\mathbf{v}}|\phi_{n,\mathbf{k}}\rangle - \langle\phi_{m,\mathbf{k}}|\mathbf{q}\hat{\mathbf{v}}|\phi_{m,\mathbf{k}}\rangle$, as a sum of three- and two-band terms.

As mentioned in section 3.4, the electric field is longitudinal meaning that its direction is along $\mathbf{q}$, therefore one can write $\mathbf{E}(\mathbf{q}) = \hat{\mathbf{q}}E(\mathbf{q})$. In the dipole approximation, the momentum $\mathbf{q}$ tends to zero, therefore its norm should be very small but its actual value is not relevant to the calculation, only its direction is important to determine the one of the electric field and consequently which components of the $\chi^{(2)}$ tensor will be calculated, as shown is section 3.4.1. After a lengthy calculation, detailed in appendix B, we obtain the final term for the IPA density-response function:

$$\begin{aligned}
\chi_0^{(2)}(\hat{\mathbf{q}}, \hat{\mathbf{q}}_1, \hat{\mathbf{q}}_2, \omega, 0) = \frac{1}{V}\sum_{\mathbf{k}}\sum_{n,m,p}\sigma_{n,m,p}\,\hat{\mathbf{r}}_{nm,\mathbf{k}}(\hat{\mathbf{q}})\Big[\hat{\mathbf{r}}_{mp,\mathbf{k}}(\hat{\mathbf{q}}_1)\,\hat{\mathbf{r}}_{pn,\mathbf{k}}(\hat{\mathbf{q}}_2)\Big(-\frac{f_{np}}{(E_{nm,\mathbf{k}}+\tilde{\omega})E_{np,\mathbf{k}}} \\
-\frac{f_{mp}}{(E_{nm,\mathbf{k}}+\tilde{\omega})(E_{pm,\mathbf{k}}+\tilde{\omega})} + \frac{1}{2}\,\frac{f_{nm}\,E_{np,\mathbf{k}}}{(E_{nm,\mathbf{k}}+\tilde{\omega})(E_{nm,\mathbf{k}})^2} - \frac{1}{2}\,\frac{f_{nm}\,E_{pm,\mathbf{k}}}{(E_{nm,\mathbf{k}}+\tilde{\omega})^2 E_{nm,\mathbf{k}}} \\
+\frac{1}{2}\,\frac{f_{mp}\,E_{np,\mathbf{k}}}{(E_{pm,\mathbf{k}}+\tilde{\omega})(E_{pm,\mathbf{k}})^2} + \frac{1}{2}\,\frac{f_{mp}\,E_{nm,\mathbf{k}}}{(E_{pm,\mathbf{k}}+\tilde{\omega})^2 E_{pm,\mathbf{k}}} + \frac{1}{2}\,\frac{f_{np}\,(E_{pm,\mathbf{k}}+E_{nm,\mathbf{k}})}{(E_{np,\mathbf{k}}+\tilde{\omega})(E_{np,\mathbf{k}})^2}\Big) \\
+\hat{\mathbf{r}}_{pn,\mathbf{k}}(\hat{\mathbf{q}}_1)\,\hat{\mathbf{r}}_{mp,\mathbf{k}}(\hat{\mathbf{q}}_2)\Big(-\frac{f_{np}}{(E_{nm,\mathbf{k}}+\tilde{\omega})(E_{np,\mathbf{k}}+\tilde{\omega})} - \frac{f_{mp}}{(E_{nm,\mathbf{k}}+\tilde{\omega})E_{pm,\mathbf{k}}} \\
+\frac{1}{2}\,\frac{f_{np}\,E_{pm,\mathbf{k}}}{(E_{np,\mathbf{k}}+\tilde{\omega})(E_{np,\mathbf{k}})^2} - \frac{1}{2}\,\frac{f_{nm}\,E_{pm,\mathbf{k}}}{(E_{nm,\mathbf{k}}+\tilde{\omega})(E_{nm,\mathbf{k}})^2} + \frac{1}{2}\,\frac{f_{nm}\,E_{np,\mathbf{k}}}{(E_{nm,\mathbf{k}}+\tilde{\omega})^2 E_{nm,\mathbf{k}}} \\
+\frac{1}{2}\,\frac{f_{np}\,E_{nm,\mathbf{k}}}{(E_{np,\mathbf{k}}+\tilde{\omega})^2 E_{np,\mathbf{k}}} + \frac{1}{2}\,\frac{f_{mp}\,(E_{np,\mathbf{k}}+E_{nm,\mathbf{k}})}{(E_{pm,\mathbf{k}}+\tilde{\omega})(E_{pm,\mathbf{k}})^2}\Big)\Big]
\end{aligned} \tag{4.33}$$

with $\sigma_{n,m,p} = 1$ if n, m and p are all different and $\sigma_{n,m,p} = 0$ otherwise and using the short notation

$$\begin{aligned}
f_{nm} = f_n - f_m, \qquad E_{nm,\mathbf{k}} = E_{n,\mathbf{k}} - E_{m,\mathbf{k}}, \qquad \tilde{\omega} = \omega + i\eta \\
\hat{\mathbf{r}}_{nm,\mathbf{k}}(\hat{\mathbf{q}}) = \langle\phi_{n,\mathbf{k}}|i\hat{\mathbf{q}}\hat{\mathbf{r}}|\phi_{m,\mathbf{k}}\rangle\,, \qquad \hat{\mathbf{v}}_{nm,\mathbf{k}}(\hat{\mathbf{q}}) = \langle\phi_{n,\mathbf{k}}|\hat{\mathbf{q}}\hat{\mathbf{v}}|\phi_{m,\mathbf{k}}\rangle
\end{aligned} \tag{4.34}$$

to shorten the formula. The different terms are colored depending on the kind of denominators they have. The red terms corresponds to interband contributions as defined in Ref. [42], while the rest corresponds to intraband transitions. The matrix elements of the position operator $\hat{\mathbf{r}}$ are calculated as matrix elements of the velocity operator $\hat{\mathbf{v}}$ and are defined as

$$\langle\phi_{n,\mathbf{k}}|i\hat{\mathbf{r}}|\phi_{m,\mathbf{k}}\rangle = \begin{cases} \dfrac{\langle\phi_{m,\mathbf{k}}|\hat{\mathbf{v}}|\phi_{m,\mathbf{k}}\rangle}{E_{n,\mathbf{k}} - E_{m,\mathbf{k}}} & \text{if } E_{n,\mathbf{k}} \neq E_{m,\mathbf{k}} \\ 0 & \text{if } E_{n,\mathbf{k}} = E_{m,\mathbf{k}} \end{cases} \tag{4.35}$$

It is interesting to note that in the LEO case, after modifying the problematic terms following equation (4.32), there is no two-band contribution left, unlike what could be observed for the second harmonic. The LEO and SHG formula are different and, while it is not so easy to prove analytically,

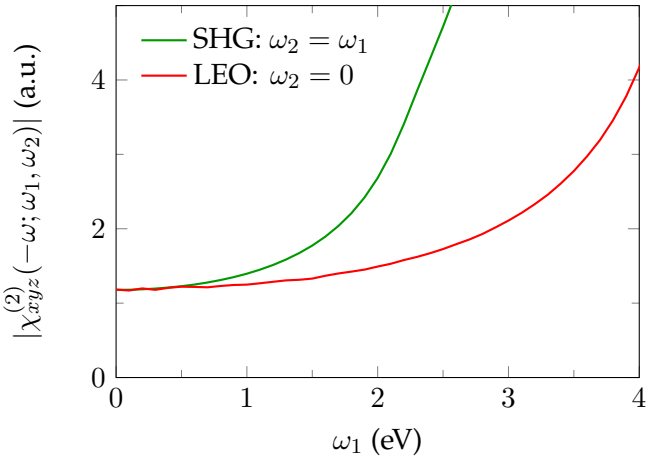

Figure 4.6: Comparison between second-order optical responses in 3C-SiC below the band gap: module of the xyz component of the LEO tensor $\chi^{(2)}_{xyz}(-\omega;\omega,0)$ (red line) and SHG susceptibility $\chi^{(2)}_{xyz}(-2\omega;\omega,\omega)$ (green line).

it appears obvious that the two should yield the same result for $\omega = 0$ (see equation (1.3)), which was confirmed computationally, as shown in figure 4.6. The SHG curve rises at lower frequency that LEO, which is expected since the resonance starts at half the gap for SHG.

Scissor operator

The scissor operator introduced in section 3.2.2 accounts for the screening of particles inside materials and is a correction to the IPA response. The matrix elements of the position operator $\hat{\mathbf{r}}$ remain unchanged when applying a scissor:

$$\langle \phi_{n,\mathbf{k}} | i\hat{\mathbf{r}} | \phi_{m,\mathbf{k}} \rangle = \frac{\langle \phi_{n,\mathbf{k}} | \hat{\mathbf{v}}^{\Sigma} | \phi_{m,\mathbf{k}} \rangle}{E^{\Sigma}_{n,\mathbf{k}} - E^{\Sigma}_{m,\mathbf{k}}} = \frac{\langle \phi_{n,\mathbf{k}} | \hat{\mathbf{v}} | \phi_{m,\mathbf{k}} \rangle}{E_{n,\mathbf{k}} - E_{m,\mathbf{k}}} \tag{4.36}$$

For the linear optical response, introducing a scissor operator is quite straightforward, since it amounts to simply replacing the KS energies in the denominator by scissored energies,

$$\chi_{\rho\rho}(\mathbf{q},\mathbf{q},\omega) = -\frac{1}{V}\sum_{\mathbf{k}}\sum_{n,m}(f_{n,\mathbf{k}} - f_{m,\mathbf{k}})\,\frac{\langle \phi_{n,\mathbf{k}} | i\mathbf{q}\hat{\mathbf{r}} | \phi_{m,\mathbf{k}} \rangle \langle \phi_{m,\mathbf{k}} | i\mathbf{q}\hat{\mathbf{r}} | \phi_{n,\mathbf{k}} \rangle}{E^{\Sigma}_{n,\mathbf{k}} - E^{\Sigma}_{m,\mathbf{k}} + \omega + i\eta}. \tag{4.37}$$

As a consequence, the peaks generated on the linear spectrum are simply shifted to higher energy, as illustrated in Figure 4.7 (first row). For second-order responses, however, it is not as straightforward [43], since more matrix elements are involved leading to larger consequences on the final spectrum. For instance, regarding the second harmonic response, applying a scissor introduce a shift to higher energy as well, but also changes the weight of the peaks (see 2nd row of Figure 4.7). In practice, regarding the analytical calculation, the difference only arises in terms containing the commutator $\left[i\hat{\mathbf{r}}, \hat{\mathbf{v}}^{\Sigma}\right]$ that appear in the second-order wavefunction correction $|\phi^{(2)}_{n,\mathbf{k}}\rangle$ and when modifying the two-band term using equation (4.32). The calculation is detailed in appendix B.3. As a consequence, the final two-band contribution is no longer zero when a scissor is applied,

$$\chi^{(2),2bnd}_{0}(\hat{\mathbf{q}},\hat{\mathbf{q}}_1,\hat{\mathbf{q}}_2,\omega,0) = \frac{1}{V}\sum_{\mathbf{k}}\sum_{n,m}\frac{f_{nm}}{(E^{\Sigma}_{nm,\mathbf{k}} + \tilde{\omega})}\Big[\Delta_{nm,\mathbf{k}}(\hat{\mathbf{q}}_1)\,\hat{\mathbf{r}}_{nm,\mathbf{k}}(\hat{\mathbf{q}}_2)\,\hat{\mathbf{r}}_{mn,\mathbf{k}}(\hat{\mathbf{q}})$$
$$+ \Delta_{nm,\mathbf{k}}(\hat{\mathbf{q}})\,\hat{\mathbf{r}}_{nm,\mathbf{k}}(\hat{\mathbf{q}}_2)\,\hat{\mathbf{r}}_{mn,\mathbf{k}}(\hat{\mathbf{q}}_1)\Big]\left(\frac{1}{(E^{\Sigma}_{nm,\mathbf{k}})^2} + \frac{1}{E^{\Sigma}_{nm,\mathbf{k}}\,E_{nm,\mathbf{k}}} - \frac{2}{(E_{nm,\mathbf{k}})^2}\right), \tag{4.38}$$

using the short notation of equation (4.34). And the three-band term becomes

$$\chi_0^{(2),3bnd}(\hat{\mathbf{q}},\hat{\mathbf{q}}_1,\hat{\mathbf{q}}_2,\omega,0) = \frac{1}{V}\sum_{\mathbf{k}}\sum_{n,m,p}\Bigg\{\hat{\mathbf{r}}_{nm,\mathbf{k}}(\hat{\mathbf{q}})\,\hat{\mathbf{r}}_{mp,\mathbf{k}}(\hat{\mathbf{q}}_1)\,\hat{\mathbf{r}}_{pn,\mathbf{k}}(\hat{\mathbf{q}}_2)\Bigg[-\frac{f_{np}}{(E^{\Sigma}_{nm,\mathbf{k}}+\tilde{\omega})E^{\Sigma}_{np,\mathbf{k}}}$$
$$-\frac{f_{mp}}{(E^{\Sigma}_{nm,\mathbf{k}}+\tilde{\omega})(E^{\Sigma}_{pm,\mathbf{k}}+\tilde{\omega})}-\frac{1}{2}\frac{f_{nm}E_{pm,\mathbf{k}}}{(E^{\Sigma}_{nm,\mathbf{k}}+\tilde{\omega})^2E_{nm,\mathbf{k}}}+\frac{1}{2}\frac{f_{mp}E_{nm,\mathbf{k}}}{(E^{\Sigma}_{pm,\mathbf{k}}+\tilde{\omega})^2E_{pm,\mathbf{k}}}$$
$$+\frac{f_{mp}E_{np,\mathbf{k}}}{(E^{\Sigma}_{pm,\mathbf{k}}+\tilde{\omega})E_{pm,\mathbf{k}}}\left(\frac{1}{E^{\Sigma}_{pm,\mathbf{k}}}-\frac{1}{2E_{pm,\mathbf{k}}}\right)+\frac{f_{nm}E_{np,\mathbf{k}}}{(E^{\Sigma}_{nm,\mathbf{k}}+\tilde{\omega})E_{nm,\mathbf{k}}}\left(\frac{1}{E^{\Sigma}_{nm,\mathbf{k}}}-\frac{1}{2E_{nm,\mathbf{k}}}\right)$$
$$+\frac{1}{2}\frac{f_{np}(E_{pm,\mathbf{k}}+E_{nm,\mathbf{k}})}{(E^{\Sigma}_{np,\mathbf{k}}+\tilde{\omega})(E_{np,\mathbf{k}})^2}\Bigg]$$
$$+\hat{\mathbf{r}}_{nm,\mathbf{k}}(\hat{\mathbf{q}})\,\hat{\mathbf{r}}_{mp,\mathbf{k}}(\hat{\mathbf{q}}_2)\,\hat{\mathbf{r}}_{pn,\mathbf{k}}(\hat{\mathbf{q}}_1)\Bigg[-\frac{f_{np}}{(E^{\Sigma}_{nm,\mathbf{k}}+\tilde{\omega})(E^{\Sigma}_{np,\mathbf{k}}+\tilde{\omega})}-\frac{f_{mp}}{(E^{\Sigma}_{nm,\mathbf{k}}+\tilde{\omega})E^{\Sigma}_{pm,\mathbf{k}}}$$
$$+\frac{1}{2}\frac{f_{nm}E_{np,\mathbf{k}}}{(E^{\Sigma}_{nm,\mathbf{k}}+\tilde{\omega})^2E_{nm,\mathbf{k}}}+\frac{1}{2}\frac{f_{np}E_{nm,\mathbf{k}}}{(E^{\Sigma}_{np,\mathbf{k}}+\tilde{\omega})^2E_{np,\mathbf{k}}}+\frac{f_{np}E_{pm,\mathbf{k}}}{(E^{\Sigma}_{np,\mathbf{k}}+\tilde{\omega})E_{np,\mathbf{k}}}\left(\frac{1}{E^{\Sigma}_{np,\mathbf{k}}}-\frac{1}{2E_{np,\mathbf{k}}}\right)$$
$$-\frac{f_{nm}E_{pm,\mathbf{k}}}{(E^{\Sigma}_{nm,\mathbf{k}}+\tilde{\omega})E_{nm,\mathbf{k}}}\left(\frac{1}{E^{\Sigma}_{nm,\mathbf{k}}}-\frac{1}{2E_{nm,\mathbf{k}}}\right)+\frac{1}{2}\frac{f_{mp}(E_{np,\mathbf{k}}+E_{nm,\mathbf{k}})}{(E^{\Sigma}_{pm,\mathbf{k}}+\tilde{\omega})(E_{pm,\mathbf{k}})^2}\Bigg]\Bigg\}, \quad (4.39)$$

following the same color code as in equation (4.33). If the scissor operator is zero ($\Delta = 0$ in equation (3.37)), scissored and unscissored energies become equal and this expression returns to equation (4.33).

The effect of the scissor on different susceptibilities is shown in Figure 4.7. For the first order, this effect corresponds to a shift of the spectrum towards higher energies, while for the second harmonic, the peaks are shifted but the weight repartition of each peak is also changed. This is due to the fact that, in the SHG formula, two types of denominators appear: $(E_{nm,\mathbf{k}}+2\omega)$ and $(E_{np,\mathbf{k}}+\omega)$, meaning that, for a given energy transition $E_{nm,\mathbf{k}}$, two peaks appear, one at $E_{nm,\mathbf{k}}$ and the other at $E_{nm,\mathbf{k}}/2$. By introducing the scissor, we change the weight of those two peaks. However for LEO, there is only one kind of denominator: $(E_{nm,\mathbf{k}}+\omega)$, creating only one peak. Therefore, in that case, the same weight redistribution is not possible since there is only one kind of peak.

Nonetheless since, for LEO, all eigenvalues $E_{n,\mathbf{k}}$ are not simply replaced by scissored ones $E^{\Sigma}_{n,\mathbf{k}}$ like for the first order, one could still expect some change in the shape of the spectrum due to the modification in the coefficients (cyan terms). However the effect of the scissor on the LEO plot, finally, just corresponds to a simple rigid shift of the peaks, displayed in Figure 4.7 (3$^{\text{rd}}$ row), like for the first order. And the effect of the presence of both scissored and unscissored energies is, in the end, simply negligible.

3C-SiC 2H-SiC

- **Linear response (LR)**

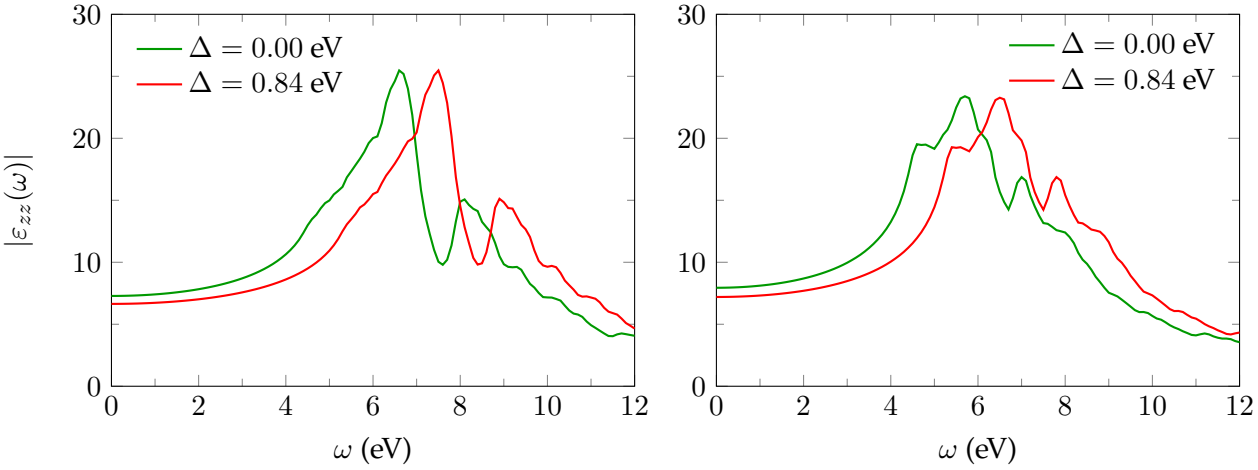

- **Second Harmonic Generation (SHG)**

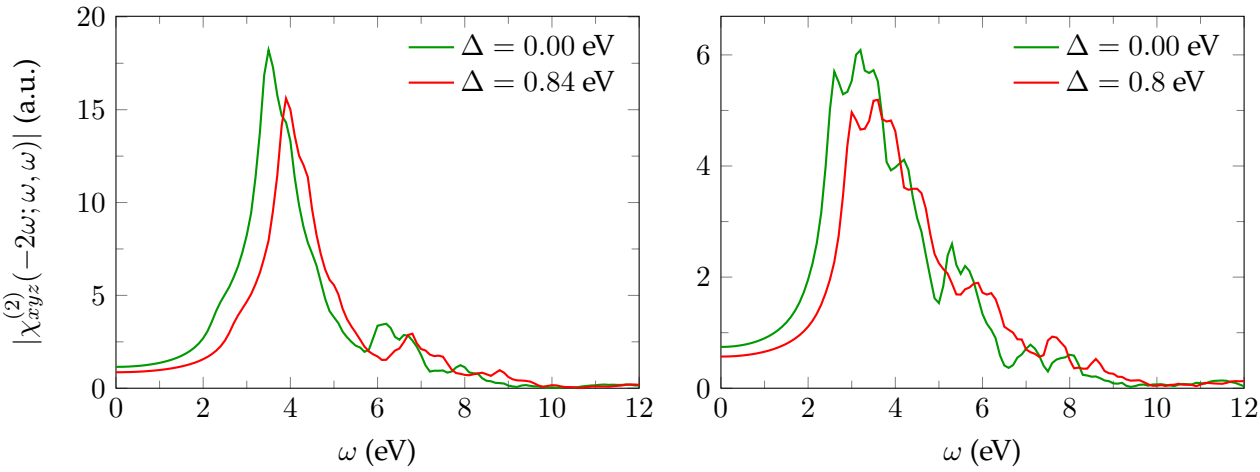

- **Linear Electro-Optic (LEO)**

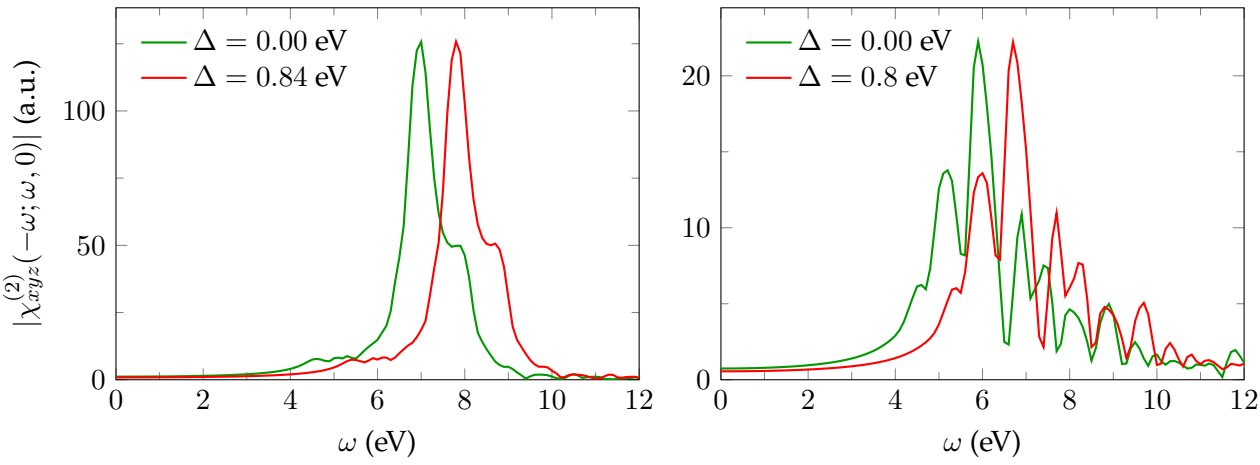

Figure 4.7: Effect of the scissor on the LR, SHG and LEO susceptibilities, respectively on the 1st, 2nd and 3rd row, applied on silicon carbide, cubic (3C-SiC) on the left and hexagonal (2H-SiC) on the right.

4.2.2 Third-order response

When regarding the calculation of the third order susceptibility, it appears, a priori, easier to go through the current density instead of the charge density, since the calculation of the optical limit in the charge density formula, using the $\mathbf{k}\cdot\mathbf{p}$ perturbation theory, is very long and complicated. For the current density, however, the long-wavelength limit can be done directly and the difficulty comes from removing the divergence in frequency in the formula. The third-order current density relates to the quasipolarizability by the relation,

$$\mathbf{j}^{(3)}_{ind}(\mathbf{q},\omega) = -i\omega \int d\omega_1 \int d\omega_2 \int d\omega_3\, \delta(\omega-\omega_1-\omega_2-\omega_3) \sum_{\mathbf{q}_1,\mathbf{q}_2,\mathbf{q}_3} \tilde{\alpha}^{(3)}(\mathbf{q},\mathbf{q}_1,\mathbf{q}_2,\mathbf{q}_3,\omega_1,\omega_2,\omega_3) \\ \mathbf{E}^P(\mathbf{q}_1,\omega_1)\,\mathbf{E}^P(\mathbf{q}_2,\omega_2)\,\mathbf{E}^P(\mathbf{q}_3,\omega_3). \quad (4.40)$$

From the continuity equation (4.24), one get the relation with the density response function:

$$\hat{\mathbf{q}}\,\tilde{\alpha}^{(3)}(\mathbf{q},\mathbf{q}_1,\mathbf{q}_2,\mathbf{q}_3,\omega_1,\omega_2,\omega_3)\,\hat{\mathbf{q}}_1\hat{\mathbf{q}}_2\hat{\mathbf{q}}_3 = \frac{1}{6}\,\chi_{\rho\rho\rho\rho}(\hat{\mathbf{q}},\hat{\mathbf{q}}_1,\hat{\mathbf{q}}_2,\hat{\mathbf{q}}_3,\omega_1,\omega_2,\omega_3) \quad (4.41)$$

Then using time-dependent perturbation theory, detailed in appendix D, one can get the general expression for the third-order density response function obtained from the current,

$$\chi_{\rho\rho\rho\rho}(\hat{\mathbf{q}},\hat{\mathbf{q}}_1,\hat{\mathbf{q}}_2,\hat{\mathbf{q}}_3,\omega_1,\omega_2,\omega_3) = \frac{1}{V}\,\frac{1}{(\omega_1+\omega_2+\omega_3)\omega_1\omega_2\omega_3} \sum_{\mathbf{k}} \sum_{n,m,p,l} \\ \frac{\langle\phi_{n,\mathbf{k}}|\hat{\mathbf{q}}\hat{\mathbf{v}}|\phi_{m,\mathbf{k}}\rangle}{E_{n,\mathbf{k}}-E_{m,\mathbf{k}}+\omega_1+\omega_2+\omega_3+3i\eta}\,\langle\phi_{m,\mathbf{k}}|\hat{\mathbf{q}}_1\hat{\mathbf{v}}|\phi_{p,\mathbf{k}}\rangle\,\langle\phi_{p,\mathbf{k}}|\hat{\mathbf{q}}_2\hat{\mathbf{v}}|\phi_{l,\mathbf{k}}\rangle\,\langle\phi_{l,\mathbf{k}}|\hat{\mathbf{q}}_3\hat{\mathbf{v}}|\phi_{n,\mathbf{k}}\rangle \\ \times\left[\frac{1}{E_{n,\mathbf{k}}-E_{l,\mathbf{k}}+\omega_3+i\eta}\left(\frac{f_{n,\mathbf{k}}-f_{p,\mathbf{k}}}{E_{n,\mathbf{k}}-E_{p,\mathbf{k}}+\omega_2+\omega_3+2i\eta}+\frac{f_{p,\mathbf{k}}-f_{l,\mathbf{k}}}{E_{l,\mathbf{k}}-E_{p,\mathbf{k}}+\omega_2+i\eta}\right)\right. \\ \left.+\frac{1}{E_{p,\mathbf{k}}-E_{m,\mathbf{k}}+\omega_1+i\eta}\left(\frac{f_{l,\mathbf{k}}-f_{m,\mathbf{k}}}{E_{l,\mathbf{k}}-E_{m,\mathbf{k}}+\omega_2+\omega_1+2i\eta}+\frac{f_{p,\mathbf{k}}-f_{l,\mathbf{k}}}{E_{l,\mathbf{k}}-E_{p,\mathbf{k}}+\omega_2+i\eta}\right)\right] \\ +\big((\mathbf{q}_1,\omega_1)\leftrightarrow(\mathbf{q}_2,\omega_2)\leftrightarrow(\mathbf{q}_3,\omega_3)\big), \quad (4.42)$$

with $\mathbf{q}=\mathbf{q}_1+\mathbf{q}_2+\mathbf{q}_3$. The double commutator $[i\mathbf{q}_1\hat{\mathbf{r}},[i\mathbf{q}_2\hat{\mathbf{r}},\hat{V}_{nl}]]$ and triple commutator $[i\mathbf{q}_1\hat{\mathbf{r}},[i\mathbf{q}_2\hat{\mathbf{r}},[i\mathbf{q}_3\hat{\mathbf{r}},\hat{V}_{nl}]]]$ have already been neglected in the above formula but one should consider those terms if adding a scissor operator. The third order expression contains the permutation of the three fields that corresponds to six symmetric terms, displayed in Figure 4.8. Equation (4.42) presents a divergence in

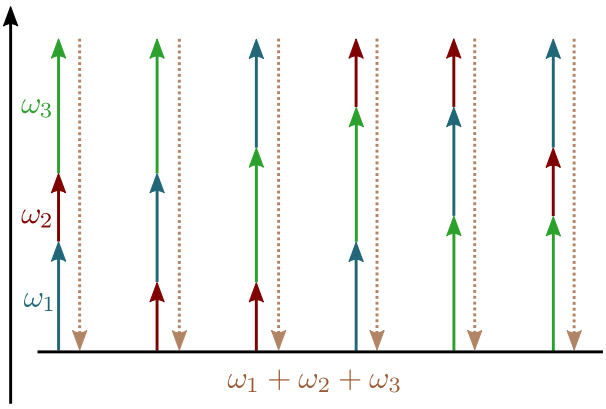

Figure 4.8: All scheme representing third order processes.

$(\omega_1+\omega_2+\omega_3)\omega_1\omega_2\omega_3$, which is not always physical and should not be there for phenomena such as

THG or EFISH, which are known to be finite when applied on semiconductors. One must then get rid of it by writing the formula in a different way to obtain the correct spectrum at low frequency, where this divergence occurs. In our formalism, it is not so obvious to remove the divergence in the general case, where all frequencies are different, which is why it has be done for specific cases.

Third harmonic generation

One of the simplest case for the third order would be the third harmonic generation (THG), obtained by setting $\omega_1 = \omega_2 = \omega_3$ in equation (4.42). The resulting expression then displays a divergence in ω^4, that occurs when $\omega \to 0$, which is taken care of by writing an expansion that follows the idea of Ghahramani and Sipe for the second harmonic in Ref. [44],

$$\frac{1}{E_{nm,\mathbf{k}}+3\tilde{\omega}}\left[\frac{1}{E_{nl,\mathbf{k}}+\tilde{\omega}}\left(\frac{f_{np}}{E_{np,\mathbf{k}}+2\tilde{\omega}}+\frac{f_{pl}}{E_{lp,\mathbf{k}}+\tilde{\omega}}\right)+\frac{1}{E_{pm,\mathbf{k}}+\tilde{\omega}}\left(\frac{f_{lm}}{E_{lm,\mathbf{k}}+2\tilde{\omega}}+\frac{f_{pl}}{E_{lp,\mathbf{k}}+\tilde{\omega}}\right)\right] = \mathcal{A}+\tilde{\omega}\mathcal{B}+\tilde{\omega}^2\mathcal{C}+\tilde{\omega}^3\mathcal{F}+\tilde{\omega}^4\mathcal{J}(\omega), \quad (4.43)$$

where the terms $\mathcal{A}$, $\mathcal{B}$ $\mathcal{C}$ and $\mathcal{F}$ must be zero to effectively remove all divergence. They are presented in appendix E. These kinds of terms have been shown to be zero for the first and second order in general, which is why we are confident that they should also vanish for the third order. The terms associated with $\mathcal{B}$ and $\mathcal{F}$ are easily canceled with their symmetric terms in the permutation using time-reversal symmetry. While the terms associated with $\mathcal{A}$ and $\mathcal{C}$ were not formally proven to be zero, the computation of those terms indicates that they are vanishing, in the limit of the accuracy of the numerical procedure, which will be later confirmed by the comparison between the divergent and divergence-free formula.

This development gives us a simple formula for THG, free of any divergences, that contains all the four-, three- and two-band terms but depends on the matrix elements of the velocity, which, unlike those of the position operator, are modified when applying a scissor.

$$\begin{aligned}\chi_0^{(3)}(\hat{\mathbf{q}},\hat{\mathbf{q}}_1,\hat{\mathbf{q}}_2,\hat{\mathbf{q}}_3,\omega,\omega,\omega) = \frac{1}{V}\sum_{\mathbf{k}}\sum_{n,m,p,l}\hat{\mathbf{v}}_{nm,\mathbf{k}}(\hat{\mathbf{q}})\,\hat{\mathbf{v}}_{mp,\mathbf{k}}(\hat{\mathbf{q}}_1)\,\hat{\mathbf{v}}_{pl,\mathbf{k}}(\hat{\mathbf{q}}_2)\,\hat{\mathbf{v}}_{ln,\mathbf{k}}(\hat{\mathbf{q}}_3)\\ \times\Bigg[-\frac{243 f_{nm}}{(E_{nm,\mathbf{k}}-3E_{nl,\mathbf{k}})(E_{nm,\mathbf{k}}-3E_{pm,\mathbf{k}})(E_{nm,\mathbf{k}}+3\tilde{\omega})(E_{nm,\mathbf{k}})^4}\\ -\frac{f_{nl}}{3(E_{nm,\mathbf{k}}-3E_{nl,\mathbf{k}})(E_{nl,\mathbf{k}}-E_{lp,\mathbf{k}})(E_{nl,\mathbf{k}}+\tilde{\omega})(E_{nl,\mathbf{k}})^4}\\ +\frac{64 f_{np}}{3(2E_{nl,\mathbf{k}}-E_{np,\mathbf{k}})(2E_{nm,\mathbf{k}}-3E_{np,\mathbf{k}})(E_{np,\mathbf{k}}+2\tilde{\omega})(E_{np,\mathbf{k}})^4}\\ -\frac{f_{pm}}{3(E_{nm,\mathbf{k}}-3E_{pm,\mathbf{k}})(E_{pm,\mathbf{k}}-E_{lp,\mathbf{k}})(E_{pm,\mathbf{k}}+\tilde{\omega})(E_{pm,\mathbf{k}})^4}\\ +\frac{64 f_{lm}}{3(2E_{pm,\mathbf{k}}-E_{lm,\mathbf{k}})(2E_{nm,\mathbf{k}}-3E_{lm,\mathbf{k}})(E_{lm,\mathbf{k}}+2\tilde{\omega})(E_{lm,\mathbf{k}})^4}\\ +\frac{f_{pl}}{3(E_{nl,\mathbf{k}}-E_{lp,\mathbf{k}})(E_{pm,\mathbf{k}}-E_{lp,\mathbf{k}})(E_{lp,\mathbf{k}}+\tilde{\omega})(E_{lp,\mathbf{k}})^4}\Bigg]+\left(\mathbf{q}_1\leftrightarrow\mathbf{q}_2\leftrightarrow\mathbf{q}_3\right)\end{aligned} \quad (4.44)$$

In their paper[13], Aversa and Sipe presented general compact formulae for the second and third order, which appear to be free of divergence in general. While the second-order expression presents a good agreement regarding the computation of the second harmonic, the third-order one is difficult to use in practice due to major convergence issue. Some of the terms may be plagued by internal divergence in the energy denominators that are not properly canceled. As a matter of fact, no actual spectra, computed from this formula, were presented.

The divergent and divergence-free formulae, that should be similar at high energies, are then compared, in Figure 4.9 for the linear response, second and third harmonic generation, in order to check the validity of the formula (4.44) for THG. For all orders, the divergence that was plaguing the formulae so far only seems to affect the spectra in the band-gap region and perfectly reproduces the correct spectrum at higher energies. Nonetheless this treatment was necessary to obtain the correct value for $\omega = 0$ to later compare with the EFISH response, since for the first and third order, the divergent curves act in a way that makes it difficult to evaluate the value at $\omega = 0$, while it could easily be extrapolated for the second harmonic. This could imply that the ω-divergence has a bigger effect on odd-order susceptibilities than it has on even-order ones. This may be explained by the fact that one could view odd-order response as the addition of different terms, and even-order ones as a subtraction of terms, which leads to its cancellation for centrosymmetric materials. And this subtraction of terms instead of addition would lead to a better cancellation of the effect of the divergence at $\omega \to 0$. However to confirm this trend, one would need to look at the effect on the fourth order.

- **Linear response (LR)**

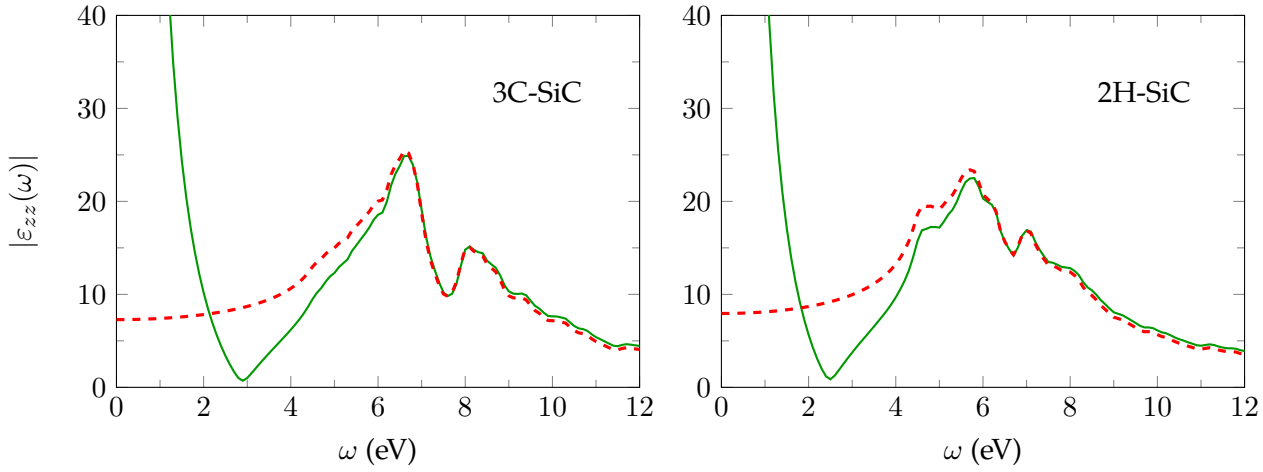

- **Second Harmonic Generation (SHG)**

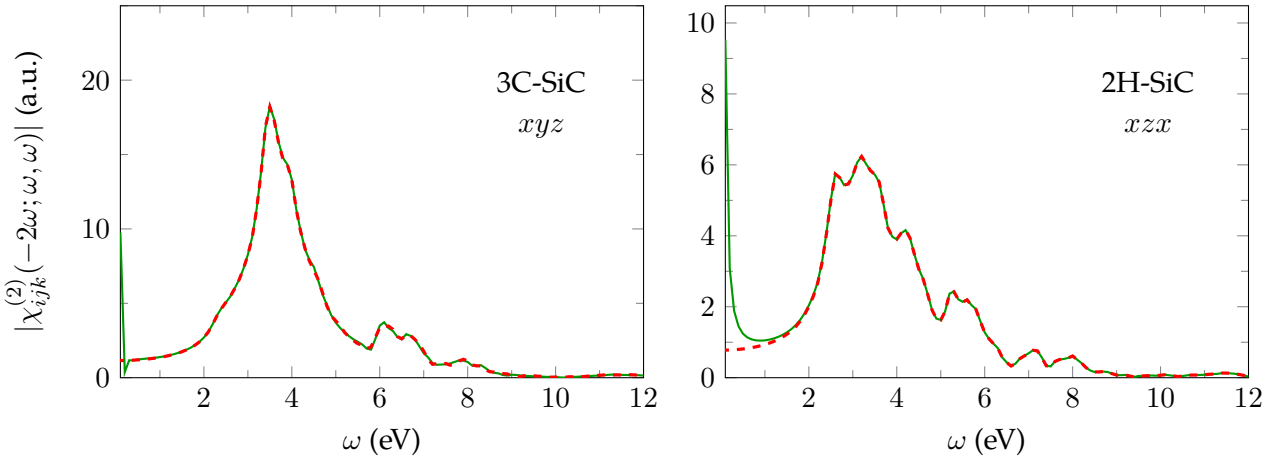

- **Third Harmonic Generation (THG)**

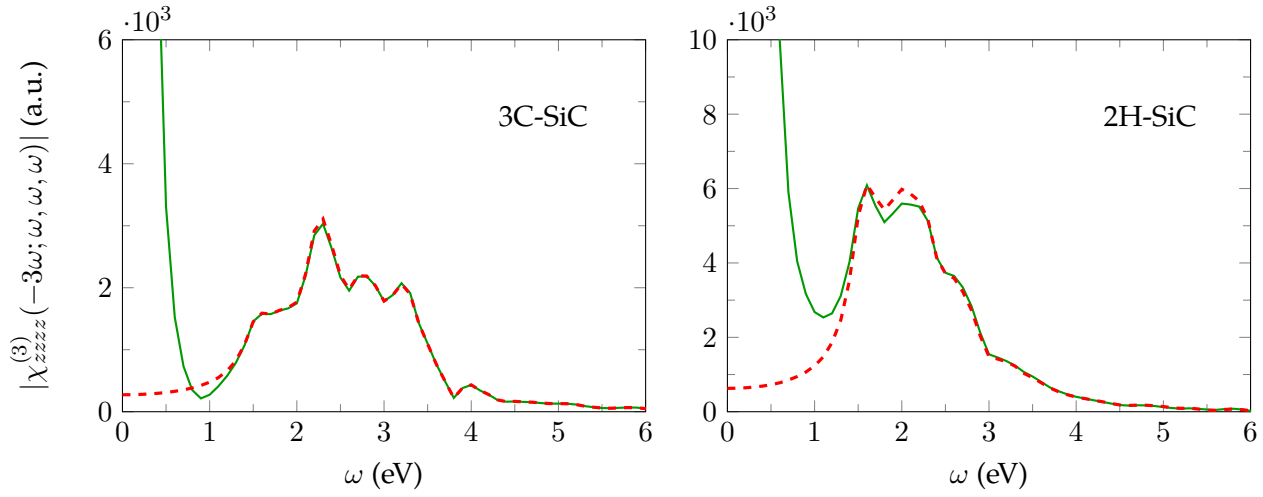

Figure 4.9: Spectra of cubic (3C-SiC) and hexagonal (2H-SiC) silicon carbide generated from the formula before (green curve) and after (red curve) getting rid of the divergence in ω for LR, SHG and THG.

Electric Field Induced Second Harmonic

The kind of development of equation 4.43 will not remove the divergences in the general case where all frequencies are different. In the case of EFISH, we partially loose the symmetry in frequency that we had for THG since one of the frequencies is different from the other two: we want to set $\omega_3 = 0$ and $\omega_1 = \omega_2 = \omega$. To do that, we first need to remove the divergence in ω_3. For that we come back to the definition of the time-dependent electric field,

$$E(t) = E_0 \left(e^{i\omega t} + e^{-i\omega t}\right). \tag{4.45}$$

The first term corresponds to the absorption while the second corresponds to the emission of a photon, as shown in Figure 4.10. When looking at the linear response, only the first term intervenes, since

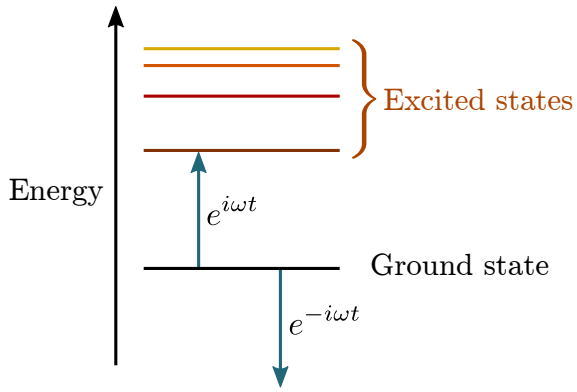

Figure 4.10: Absorption and emission of a photon from the ground state.

we only look at the absorption and not the emission from the ground state, for which the probability is zero. For the second order, when a single field is present, one would get three kinds of processes, displayed in Figure 4.11a, where only the first one corresponds to the second harmonic. The second one illustrates the optical rectification and the third one, while theoretically possible since only virtual states are involved, does not corresponds to SHG, which only describes the emission of a photon at 2ω and not the absorption. However, when considering a static field, both the absorption and emission becomes equivalent and should be accounted for. Therefore, regarding LEO, there would be four schemes, shown in Figure 4.11b, describing both the absorption and emission corresponding to the static field and only the absorption corresponding to the optical field, and includes the permutation of the two input fields. A similar sketch can be done for EFISH that would involve six different processes. This effect of the static field can be expressed by writing the following relation for the response function

$$\lim_{\omega_3 \to 0} \chi^{(3)}(\omega_1, \omega_2, \omega_3) = \lim_{\omega_3 \to 0} \frac{1}{2} \left[\chi^{(3)}(\omega_1, \omega_2, \omega_3) + \chi^{(3)}(\omega_1, \omega_2, -\omega_3)\right], \tag{4.46}$$

which gives us an expression no longer divergent in ω_3. Note that it makes no difference which frequency is set to zero since the expression contains all the permutations:

$$\begin{aligned}\chi_0^{(3)}(\hat{\mathbf{q}}, \hat{\mathbf{q}}_1, \hat{\mathbf{q}}_2, \hat{\mathbf{q}}_3, \omega, \omega, 0) = \frac{1}{V} \sum_{\mathbf{k}} \sum_{n,m,p,l} \frac{1}{\omega^4} \hat{\mathbf{v}}_{nm}(\hat{\mathbf{q}}) \left[\hat{\mathbf{v}}_{mp}(\hat{\mathbf{q}}_1)\hat{\mathbf{v}}_{pl}(\hat{\mathbf{q}}_2)\hat{\mathbf{v}}_{ln}(\hat{\mathbf{q}}_3)\ f_1(\omega, \omega, 0)\right. \\ \left. + \hat{\mathbf{v}}_{mp}(\hat{\mathbf{q}}_3)\hat{\mathbf{v}}_{pl}(\hat{\mathbf{q}}_2)\hat{\mathbf{v}}_{ln}(\hat{\mathbf{q}}_1)\ f_2(0, \omega, \omega) + \hat{\mathbf{v}}_{mp}(\hat{\mathbf{q}}_1)\hat{\mathbf{v}}_{pl}(\hat{\mathbf{q}}_3)\hat{\mathbf{v}}_{ln}(\hat{\mathbf{q}}_2)\ f_3(\omega, 0, \omega)\right] \\ + \left(\mathbf{q}_1 \leftrightarrow \mathbf{q}_2\right)\end{aligned} \tag{4.47}$$

The second term f_2 corresponds to the permutation $(\mathbf{q}_2, \omega_2) \leftrightarrow (\mathbf{q}_3, \omega_3)$ and the third term f_3 corresponds to the permutation in the first term of $(\mathbf{q}_1, \omega_1) \leftrightarrow (\mathbf{q}_3, \omega_3)$. The first and third permutations f_1

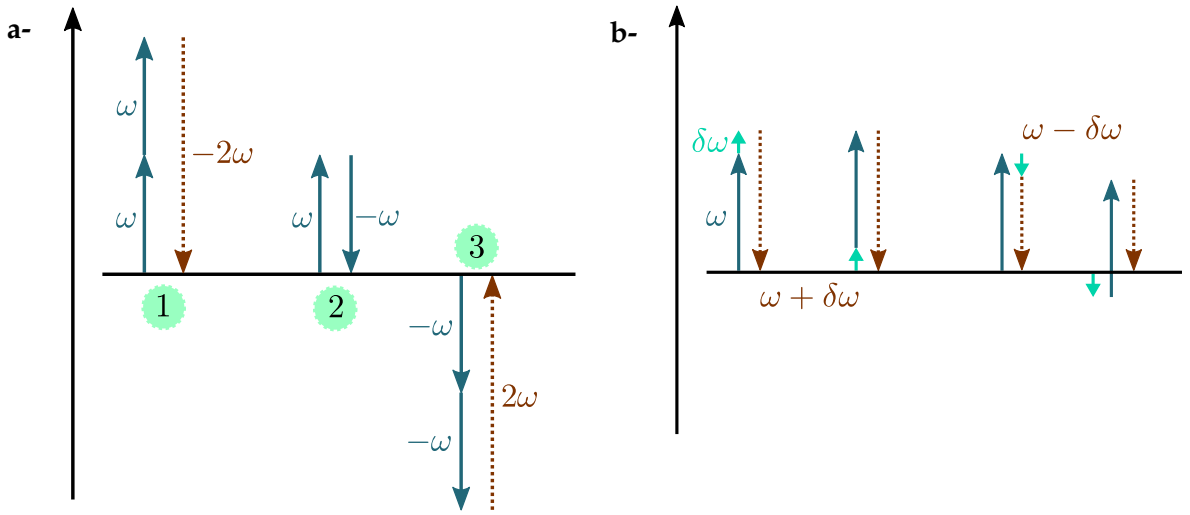

Figure 4.11: Scheme of optical second-order processes. Panel a shows the different second-order phenomena corresponding to one input field at ω, while panel b describes all the LEO scheme with $\delta\omega \to 0$.

and f_3 are symmetric in $+\omega/-\omega$, while the second permuation f_2 is symmetric with itself. We can then set $\omega_3 = 0$ in the expression and obtain a formula that only depends on ω. However a special treatment must be granted for the case $E_{nl,\mathbf{k}} = 0$ in f_1 and $E_{pm,\mathbf{k}} = 0$ in f_3, since each term contained respectively $(E_{nl,\mathbf{k}} + \omega_3)$ and $(E_{pm,\mathbf{k}} + \omega_3)$ at the denominator. Indeed setting $\omega_3 = 0$ in the following term (f_1) does not pose any problem,

$$\frac{1}{E_{nl,\mathbf{k}} + \tilde{\omega}_3}\left(\frac{f_{np}}{E_{np,\mathbf{k}} + \tilde{\omega}_2 + \tilde{\omega}_3} + \frac{f_{pl}}{E_{lp,\mathbf{k}} + \tilde{\omega}_2}\right), \tag{4.48}$$

since this term is canceled when $E_{n,\mathbf{k}} = E_{l,\mathbf{k}}$. However applying equation (4.46) on it will make a square appear for $(E_{np,\mathbf{k}} + \tilde{\omega}_2)$ and not for $(E_{lp,\mathbf{k}} + \tilde{\omega}_2)$. Therefore it will no longer cancels when $E_{n,\mathbf{k}} = E_{l,\mathbf{k}}$, creating a new divergence. To avoid that, these two cases need to be treated separately from the rest, for which $E_{n,\mathbf{k}} = E_{l,\mathbf{k}}$ is set directly in equation (4.42) before using equation (4.46). Doing that, we obtain the following ω-divergent EFISH formula

$$\begin{aligned}
\chi_0^{(3)}(\hat{\mathbf{q}}, \hat{\mathbf{q}}_1, \hat{\mathbf{q}}_2, \hat{\mathbf{q}}_3, \omega, \omega, 0) = \frac{1}{V}\sum_{\mathbf{k}}\sum_{n,m,p,l} \{\hat{\mathbf{v}}_{nm,\mathbf{k}}(\hat{\mathbf{q}})\hat{\mathbf{v}}_{mp,\mathbf{k}}(\hat{\mathbf{q}}_1)\hat{\mathbf{v}}_{pl,\mathbf{k}}(\hat{\mathbf{q}}_2)\hat{\mathbf{v}}_{ln,\mathbf{k}}(\hat{\mathbf{q}}_3) \\
\times\Bigg[-\frac{\sigma_{nl}}{2\omega^3(E_{nm,\mathbf{k}}+2\tilde{\omega})E_{nl,\mathbf{k}}}\left(\frac{f_{np}}{(E_{nm,\mathbf{k}}+2\tilde{\omega})(E_{np,\mathbf{k}}+\tilde{\omega})} + \frac{f_{np}}{(E_{np,\mathbf{k}}+\tilde{\omega})^2} + \frac{f_{np}}{(E_{np,\mathbf{k}}+\tilde{\omega})E_{nl,\mathbf{k}}}\right. \\
\left. + \frac{f_{pl}}{(E_{nm,\mathbf{k}}+2\tilde{\omega})(E_{lp,\mathbf{k}}+\tilde{\omega})} + \frac{f_{pl}}{(E_{lp,\mathbf{k}}+\tilde{\omega})E_{nl,\mathbf{k}}}\right) - \frac{\sigma_{nl}}{4\omega^4(E_{nm,\mathbf{k}}+2\tilde{\omega})E_{nl,\mathbf{k}}}\left(\frac{f_{np}}{(E_{np,\mathbf{k}}+\tilde{\omega})}\right. \\
\left. + \frac{f_{pl}}{(E_{lp,\mathbf{k}}+\tilde{\omega})}\right) - \frac{1}{2\omega^3(E_{nm,\mathbf{k}}+2\tilde{\omega})^2(E_{pm,\mathbf{k}}+\tilde{\omega})}\left(\frac{f_{lm}}{E_{lm,\mathbf{k}}+2\tilde{\omega}} + \frac{f_{pl}}{E_{lp,\mathbf{k}}+\tilde{\omega}}\right) \\
- \frac{1}{4\omega^4(E_{nm,\mathbf{k}}+2\tilde{\omega})(E_{pm,\mathbf{k}}+\tilde{\omega})}\left(\frac{f_{lm}}{E_{lm,\mathbf{k}}+2\tilde{\omega}} + \frac{f_{pl}}{E_{lp,\mathbf{k}}+\tilde{\omega}}\right) \\
+\frac{\delta_{nl}}{2\omega^3(E_{nm,\mathbf{k}}+2\tilde{\omega})(E_{np,\mathbf{k}}+\tilde{\omega})^2}\left(\frac{f_{np}}{(E_{nm,\mathbf{k}}+2\tilde{\omega})} + \frac{f_{np}}{(E_{np,\mathbf{k}}+\tilde{\omega})}\right) + \frac{\delta_{nl}}{4\omega^4}\frac{f_{np}}{(E_{nm,\mathbf{k}}+2\tilde{\omega})(E_{np,\mathbf{k}}+\tilde{\omega})^2}\Bigg] \\
+ \hat{\mathbf{v}}_{nm,\mathbf{k}}(\hat{\mathbf{q}})\,\hat{\mathbf{v}}_{mp,\mathbf{k}}(\hat{\mathbf{q}}_1)\,\hat{\mathbf{v}}_{pl,\mathbf{k}}(\hat{\mathbf{q}}_3)\,\hat{\mathbf{v}}_{ln,\mathbf{k}}(\hat{\mathbf{q}}_2)\left[-\frac{1}{2\omega^3(E_{nm,\mathbf{k}}+2\tilde{\omega})(E_{nl,\mathbf{k}}+\tilde{\omega})}\right.
\end{aligned}$$

$$\times\left(\frac{f_{np}}{(E_{nm,\mathbf{k}}+2\tilde{\omega})(E_{np,\mathbf{k}}+\tilde{\omega})}+\frac{f_{np}}{(E_{np,\mathbf{k}}+\tilde{\omega})^2}+\frac{f_{pl}}{(E_{nm,\mathbf{k}}+2\tilde{\omega})E_{lp,\mathbf{k}}}+\frac{f_{pl}}{E_{lp,\mathbf{k}}^2}\right)$$
$$-\frac{1}{4\omega^4(E_{nm,\mathbf{k}}+2\tilde{\omega})(E_{nl,\mathbf{k}}+\tilde{\omega})}\left(\frac{f_{np}}{(E_{np,\mathbf{k}}+\tilde{\omega})}+\frac{f_{pl}}{E_{lp,\mathbf{k}}}\right)$$
$$-\frac{1}{2\omega^3(E_{nm,\mathbf{k}}+2\tilde{\omega})(E_{pm,\mathbf{k}}+\tilde{\omega})}\left(\frac{f_{lm}}{(E_{nm,\mathbf{k}}+2\tilde{\omega})(E_{lm,\mathbf{k}}+\tilde{\omega})}+\frac{f_{lm}}{(E_{lm,\mathbf{k}}+\tilde{\omega})^2}\right.$$
$$\left.+\frac{f_{pl}}{(E_{nm,\mathbf{k}}+2\tilde{\omega})E_{lp,\mathbf{k}}}+\frac{f_{pl}}{E_{lp,\mathbf{k}}^2}\right)-\frac{1}{4\omega^4(E_{nm,\mathbf{k}}+2\tilde{\omega})(E_{pm,\mathbf{k}}+\tilde{\omega})}\left(\frac{f_{lm}}{(E_{lm,\mathbf{k}}+\tilde{\omega})}+\frac{f_{pl}}{E_{lp,\mathbf{k}}}\right)\Bigg]$$
$$+\hat{\mathbf{v}}_{nm,\mathbf{k}}(\hat{\mathbf{q}})\,\hat{\mathbf{v}}_{mp,\mathbf{k}}(\hat{\mathbf{q}}_3)\,\hat{\mathbf{v}}_{pl,\mathbf{k}}(\hat{\mathbf{q}}_2)\,\hat{\mathbf{v}}_{ln,\mathbf{k}}(\hat{\mathbf{q}}_1)\left[-\frac{\sigma_{pm}}{2\omega^3(E_{nm,\mathbf{k}}+2\tilde{\omega})^2(E_{nl,\mathbf{k}}+\tilde{\omega})}\left(\frac{f_{np}}{(E_{np,\mathbf{k}}+2\tilde{\omega})}\right.\right.$$
$$\left.+\frac{f_{pl}}{(E_{lp,\mathbf{k}}+\tilde{\omega})}\right)-\frac{\sigma_{pm}}{4\omega^4(E_{nm,\mathbf{k}}+2\tilde{\omega})(E_{nl,\mathbf{k}}+\tilde{\omega})}\left(\frac{f_{np}}{(E_{np,\mathbf{k}}+2\tilde{\omega})}+\frac{f_{pl}}{(E_{lp,\mathbf{k}}+\tilde{\omega})}\right)$$
$$-\frac{1}{2\omega^3(E_{nm,\mathbf{k}}+2\tilde{\omega})E_{pm,\mathbf{k}}}\left(\frac{f_{lm}}{(E_{nm,\mathbf{k}}+2\tilde{\omega})(E_{lm,\mathbf{k}}+\tilde{\omega})}+\frac{f_{lm}}{(E_{lm,\mathbf{k}}+\tilde{\omega})^2}+\frac{f_{lm}}{(E_{lm,\mathbf{k}}+\tilde{\omega})E_{pm,\mathbf{k}}}\right.$$
$$\left.+\frac{f_{pl}}{(E_{nm,\mathbf{k}}+2\tilde{\omega})(E_{lp,\mathbf{k}}+\tilde{\omega})}+\frac{f_{pl}}{(E_{lp,\mathbf{k}}+\tilde{\omega})E_{pm,\mathbf{k}}}\right)-\frac{1}{4\omega^4(E_{nm,\mathbf{k}}+2\tilde{\omega})E_{pm,\mathbf{k}}}\left(\frac{f_{lm}}{E_{lm,\mathbf{k}}+\tilde{\omega}}\right.$$
$$\left.+\frac{f_{pl}}{E_{lp,\mathbf{k}}+\tilde{\omega}}\right)+\frac{\delta_{pm}}{2\omega^3}\left(\frac{f_{lm}}{(E_{nm,\mathbf{k}}+2\tilde{\omega})^2(E_{lm,\mathbf{k}}+\tilde{\omega})^2}+\frac{f_{lm}}{(E_{nm,\mathbf{k}}+2\tilde{\omega})(E_{lm,\mathbf{k}}+\tilde{\omega})^3}\right)$$
$$\left.+\frac{\delta_{pm}}{4\omega^4}\frac{f_{lm}}{(E_{nm,\mathbf{k}}+2\tilde{\omega})(E_{lm,\mathbf{k}}+\tilde{\omega})^2}\right]\Bigg\}+(\mathbf{q}_1\leftrightarrow\mathbf{q}_2)\quad(4.49)$$

where σ_{nl} is zero when $n=l$ and 1 otherwise. The remaining divergence in ω^4 is taken care of by writing a similar expansion to equation 4.43,

$$f_1(\omega,\omega,0)=\mathcal{A}_1+\omega\mathcal{B}_1+\omega^2\mathcal{C}_1+\omega^3\mathcal{F}_1+\omega^4\mathcal{J}_1(\omega),\quad(4.50)$$

where the terms associated with $\mathcal{A}$, $\mathcal{B}$ $\mathcal{C}$ and $\mathcal{F}$ are all zero. After some algebra, we obtain the final formula for EFISH, which is fully displayed in appendix F. Since it is quite a large formula, I only present here part of the four-band term:

$$\chi_0^{(3),4bnd}(\hat{\mathbf{q}},\hat{\mathbf{q}}_1,\hat{\mathbf{q}}_2,\hat{\mathbf{q}}_3,\omega,\omega,0)=\frac{1}{V}\sum_{\mathbf{k}}\sum_{n,m,p,l}\Big[\hat{\mathbf{r}}_{nm,\mathbf{k}}(\hat{\mathbf{q}})\,\hat{\mathbf{r}}_{mp,\mathbf{k}}(\hat{\mathbf{q}}_1)\,\hat{\mathbf{r}}_{pl,\mathbf{k}}(\hat{\mathbf{q}}_2)\,\hat{\mathbf{r}}_{ln,\mathbf{k}}(\hat{\mathbf{q}}_3)$$
$$\times\left(-\frac{f_{nl}}{(E_{nm,\mathbf{k}}+2\tilde{\omega})(E_{np,\mathbf{k}}+\tilde{\omega})E_{nl,\mathbf{k}}}-\frac{f_{pl}}{(E_{nm,\mathbf{k}}+2\tilde{\omega})(E_{np,\mathbf{k}}+\tilde{\omega})(E_{lp,\mathbf{k}}+\tilde{\omega})}\right.$$
$$-\frac{f_{lm}}{(E_{nm,\mathbf{k}}+2\tilde{\omega})(E_{pm,\mathbf{k}}+\tilde{\omega})(E_{lm,\mathbf{k}}+2\tilde{\omega})}-\frac{f_{pl}}{(E_{nm,\mathbf{k}}+2\tilde{\omega})(E_{pm,\mathbf{k}}+\tilde{\omega})(E_{lp,\mathbf{k}}+\tilde{\omega})}$$
$$\left.-\frac{f_{np}(E_{nm,\mathbf{k}}+E_{np,\mathbf{k}})}{2(E_{np,\mathbf{k}}+\tilde{\omega})E_{nl,\mathbf{k}}(E_{np,\mathbf{k}})^2}-\frac{f_{pl}(E_{nm,\mathbf{k}}+E_{lp,\mathbf{k}})}{2(E_{lp,\mathbf{k}}+\tilde{\omega})E_{nl,\mathbf{k}}(E_{lp,\mathbf{k}})^2}+\dots\right)$$
$$+\hat{\mathbf{r}}_{nm,\mathbf{k}}(\hat{\mathbf{q}})\,\hat{\mathbf{r}}_{mp,\mathbf{k}}(\hat{\mathbf{q}}_1)\,\hat{\mathbf{r}}_{ln,\mathbf{k}}(\hat{\mathbf{q}}_2)\,\hat{\mathbf{r}}_{pl,\mathbf{k}}(\hat{\mathbf{q}}_3)\left(-\frac{f_{np}}{(E_{nm,\mathbf{k}}+2\tilde{\omega})(E_{nl,\mathbf{k}}+\tilde{\omega})(E_{np,\mathbf{k}}+\tilde{\omega})}\right.$$
$$-\frac{f_{pl}}{(E_{nm,\mathbf{k}}+2\tilde{\omega})(E_{nl,\mathbf{k}}+\tilde{\omega})E_{lp,\mathbf{k}}}-\frac{f_{pl}}{(E_{nm,\mathbf{k}}+2\tilde{\omega})(E_{pm,\mathbf{k}}+\tilde{\omega})E_{lp,\mathbf{k}}}$$
$$-\frac{f_{lm}}{(E_{nm,\mathbf{k}}+2\tilde{\omega})(E_{pm,\mathbf{k}}+\tilde{\omega})(E_{lm,\mathbf{k}}+\tilde{\omega})}+\frac{f_{np}}{(E_{pm,\mathbf{k}}+\tilde{\omega})(E_{np,\mathbf{k}}+\tilde{\omega})^2}$$
$$\left.-\frac{f_{nm}}{(E_{nm,\mathbf{k}}+2\tilde{\omega})^2(E_{pm,\mathbf{k}}+\tilde{\omega})}+\dots\right)$$
$$+\hat{\mathbf{r}}_{nm,\mathbf{k}}(\hat{\mathbf{q}})\,\hat{\mathbf{r}}_{ln,\mathbf{k}}(\hat{\mathbf{q}}_1)\,\hat{\mathbf{r}}_{pl,\mathbf{k}}(\hat{\mathbf{q}}_2)\,\hat{\mathbf{r}}_{mp,\mathbf{k}}(\hat{\mathbf{q}}_3)\left(-\frac{f_{np}}{(E_{nm,\mathbf{k}}+2\tilde{\omega})(E_{nl,\mathbf{k}}+\tilde{\omega})(E_{np,\mathbf{k}}+2\tilde{\omega})}\right.$$

$$- \frac{f_{pm}}{(E_{nm,\mathbf{k}} + 2\tilde{\omega})(E_{lm,\mathbf{k}} + \tilde{\omega})E_{pm,\mathbf{k}}} - \frac{f_{pl}}{(E_{nm,\mathbf{k}} + 2\tilde{\omega})(E_{nl,\mathbf{k}} + \tilde{\omega})(E_{lp,\mathbf{k}} + \tilde{\omega})}$$
$$- \frac{f_{pl}}{(E_{nm,\mathbf{k}} + 2\tilde{\omega})(E_{lp,\mathbf{k}} + \tilde{\omega})(E_{lm,\mathbf{k}} + \tilde{\omega})} - \frac{f_{lm}(E_{nm,\mathbf{k}} + E_{lm,\mathbf{k}})}{2(E_{lm,\mathbf{k}} + \tilde{\omega})E_{pm,\mathbf{k}}E^2_{lm,\mathbf{k}}}$$
$$- \frac{f_{pl}(E_{nm,\mathbf{k}} + E_{lp,\mathbf{k}})}{2(E_{lp,\mathbf{k}} + \tilde{\omega})E_{pm,\mathbf{k}}E^2_{lp,\mathbf{k}}} + \dots \Bigg)\Bigg] + \dots + (\mathbf{q}_1 \leftrightarrow \mathbf{q}_2) \quad (4.51)$$

For the third order, the computation seems a lot more sensitive to the way the formula is written than for the second or first order. While removing the divergence in frequency ω that occurs at $\omega \to 0$, we added new divergences in the energy terms of the type $E_{nn',\mathbf{k}}$ when $E_{n,\mathbf{k}} = E_{n',\mathbf{k}}$ that occurs for every frequency, corresponding to the cyan terms in equation (4.51). Usually for the previous order, the difference in the occupation numbers f_{nm} matched the difference in energies $E_{nm,\mathbf{k}}$ at the denominators, meaning that, in this term, $E_{nm,\mathbf{k}}$ was always greater than the gap. For the third order however, there are energy differences, colored in purple in equation (4.51), that don't match the occupation numbers. In that case, when the divergence occurs, it should be canceled by another term, like for the last two terms of equation (4.51), colored in cyan, which are both separately divergent when $E_{pm,\mathbf{k}} = 0$ but together compensate. This means that the expression should be written so that this kind of terms are all compensated around each divergence.

It is not possible for EFISH to write a shorter formula, containing all the four-, three- and two-band terms together, like for THG in equation (4.44) since, here, this kind of expression would be divergent in energy. We then need to develop each term and treat the four-, three- and two-band terms separately. The first four terms, colored in red, in each of the permutations of equation (4.51) corresponds to what is referred to as the interband transitions in Ref. [42; 9], while the rest corresponds to the intraband contribution. The same color code was used for the LEO formula in equation (4.33).

Like for the other responses, we plot the comparison between the divergent formula (4.49) and the final expression (4.51) in Figure 4.12, which shows a good agreement between the two formulae. Using the divergent-free fromulae, it is then possible to compare the value at $\omega = 0$ of THG and

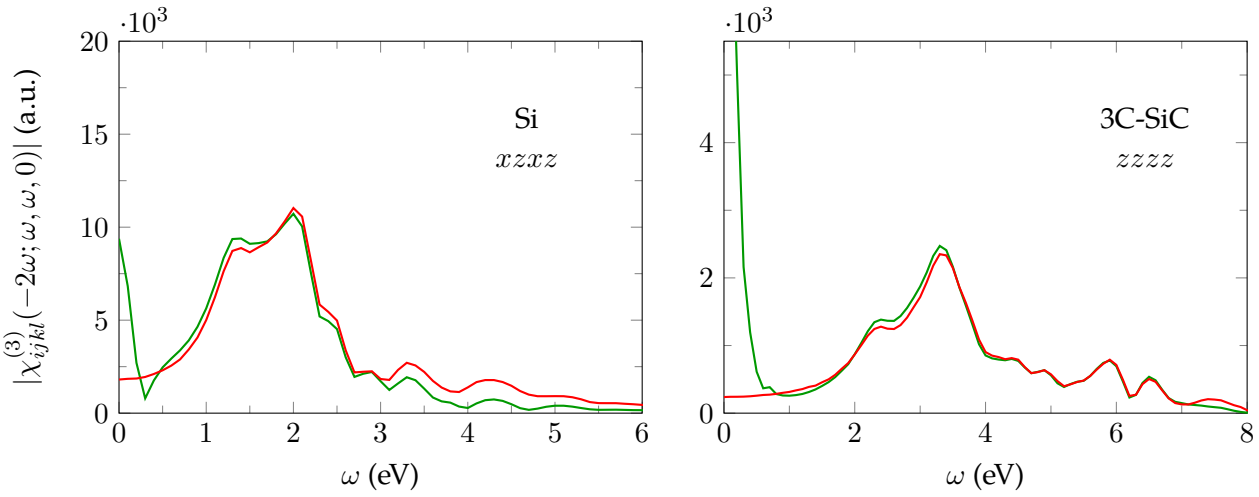

Figure 4.12: EFISH spectrum of cubic silicon and silicon carbide (3C-SiC) generated from both the ω-divergent (green curve) and divergent-free formula (red curve).

EFISH, displayed in Figure (4.13), which should be the same (see equation (1.16)). This results in a good agreement between the two susceptibilities with a value of $2 \cdot 10^2$ a.u. at $\omega = 0$ for cubic silicon carbide, which again validate the final expression (4.51) calculated for EFISH.

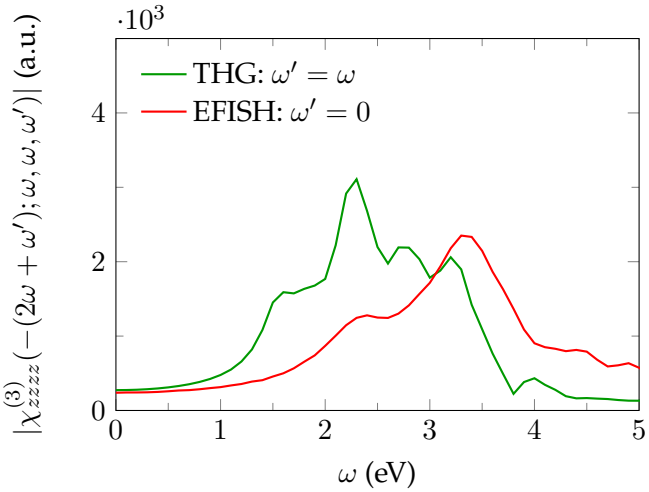

Figure 4.13: Comparison between the THG and EFISH curves for cubic silicon carbide (3C-SiC).

Chapter 5

Applications

In this chapter, I will show numerical results based on the formalism introduced in the previous chapters for the linear electro-optic effect and the electric-field induced second harmonic. The interest for both is to study the intensity of the response for a reasonable static field to determine their importance in comparison to other effects.

5.1 Linear Electro-Optic effect

The susceptibilities calculated in this thesis were first tested on simple semiconductors such as silicon and silicon carbide, and then on more complex materials such as Si/Ge superlattices and strained materials. I present in this section the application on this different systems. All the results contain a scissor unless stated otherwise. The spectrum of silicon is not plotted for LEO since it is zero due to the centrosymmetry of the system.

The non-vanishing components of the $\chi^{(2)}$ for the symmetry of interest in this section are reported in Table 5.1.

Symmetry class	International notation	Schoenflies notation	Nonvanishing tensor components		Compounds
Cubic	$\bar{4}3m$	T_d	$xyz = xzy = yzx = yxz = zxy = zyx$	(1)	3C-SiC, GaAs
Hexagonal	$6mm$	C_{6v}	$xzx = yzy,\ xxz = yyz,\ zxx = zyy,\ zzz$	(4)	2H-SiC
Tetragonal	$\bar{4}2m$	D_{2d}	$xyz = yxz,\ xzy = yzx,\ zxy = zyx$	(3)	Si/Ge
	$4mm$	C_{4v}	$xzx = yzy,\ xxz = yyz,\ zxx = zyy,\ zzz$	(4)	strained Si

Table 5.1: List of non-zero components of $\chi^{(2)}(\omega_1, \omega_2)$ for some symmetry class.

5.1.1 Silicon carbide

Silicon carbide is a compound that exists in many different crystalline forms. Its most symmetric one is 3C-SiC, also referred to as β-SiC, which displays a Zinc blende crystal structure, illustrated in Figure 5.1, that corresponds to a cubic symmetry $\bar{4}3m$. Since the system is isotropic in this symmetry, the

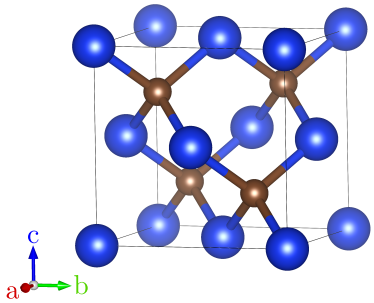

Figure 5.1: Unit cell of cubic silicon carbide 3C-SiC that displays a Zinc blende structure. The blue atoms corresponds to silicon and the brown ones to carbon.

dielectric tensor is diagonal and we have $\varepsilon^{lr} = \varepsilon_{xx} = \varepsilon_{yy} = \varepsilon_{zz}$,

$$\overleftrightarrow{\varepsilon}_M(\omega) = \begin{pmatrix} \varepsilon^{lr}(\omega) & 0 & 0 \\ 0 & \varepsilon^{lr}(\omega) & 0 \\ 0 & 0 & \varepsilon^{lr}(\omega) \end{pmatrix}, \qquad lr = \text{linear response} \tag{5.1}$$

If a static field is then added to the system, electro-optic effects are induced and appear in the dielctric tensor in the form of off-diagonal matrix element $\varepsilon^{leo}(\omega)$. If this field is chosen to be along the z-direction for example, this off-diagonal term is expressed as $\varepsilon^{leo}(\omega) = 8\pi\chi^{(2)}_{xyz}(-\omega;\omega,0)\mathcal{E}_z$, and the dielectric tensor becomes

$$\overleftrightarrow{\varepsilon}^{(\mathcal{E}_z)}_M(\omega) = \begin{pmatrix} \varepsilon^{lr}(\omega) & \varepsilon^{leo}(\omega) & 0 \\ \varepsilon^{leo}(\omega) & \varepsilon^{lr}(\omega) & 0 \\ 0 & 0 & \varepsilon^{lr}(\omega) \end{pmatrix} \tag{5.2}$$

with $\varepsilon^{leo} = \varepsilon^{(\mathcal{E}_z)}_{xy} = \varepsilon^{(\mathcal{E}_z)}_{yx}$. All the extra-diagonal terms are equal since all the non-vanishing $\chi^{(2)}$ components are equivalent in this symmetry (see the first row of Table 5.1). Here the quadratic electro-optic effect and beyond are neglected. This symmetry is also represented by GaAs, GaP, etc.

I present here the real and imaginary part of these two components for 3C-SiC in Figure 5.2. The

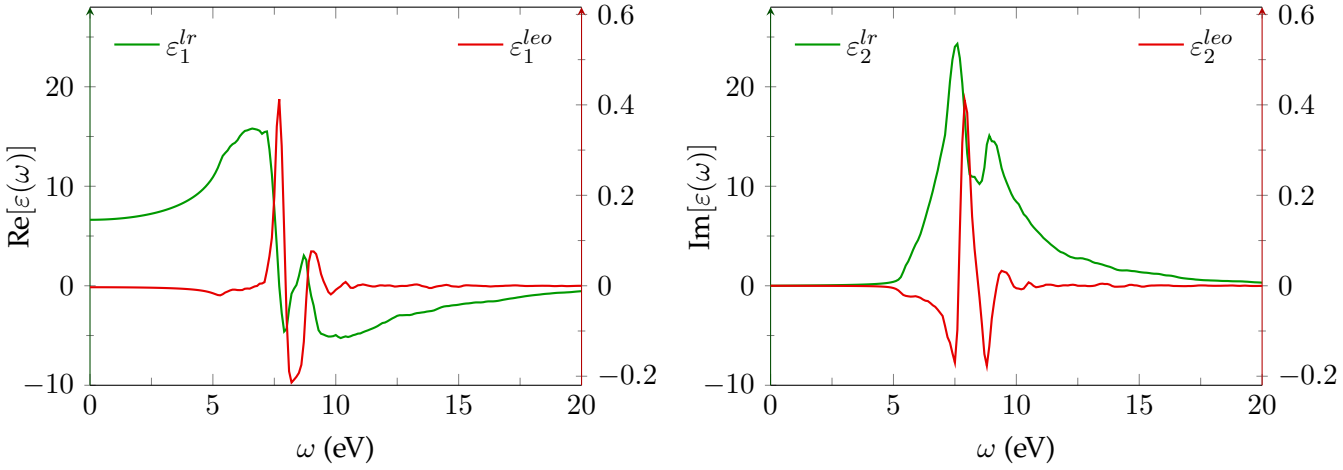

Figure 5.2: Components of the dielectric tensor already present (green curve, intensity scaled on the left side) or induced by a static field (red curve, intensity scaled on the right side) of $7 \cdot 10^5$ V.cm^{-1} for cubic silicon carbide with a scissor of $\Delta = 0.84$ eV.

field-induced component ε^{leo} represents the extra-diagonal part of the tensor, for which its imaginary

part, unlike the diagonal element, does not have to be greater than zero. A strong static field was chosen here, but still weak enough in order not to destroy the material through an electrical breakdown (see Appendix G). Since the intensity of the component ε^{leo} is considerably lower than the one of the diagonal component ε^{lr}, the two are here displayed on different scales. Indeed if the two components were plotted on the same scale, the off-diagonal one would not be visible.

From the $\chi^{(2)}_{xyz}(-\omega;\omega,0)$, one can also extract the electro-optic coefficient $r_{xyz}(\omega)$ using equation (1.10), that is plotted in Figure 5.3. The experimental value of this coefficient was reported at 2 eV for

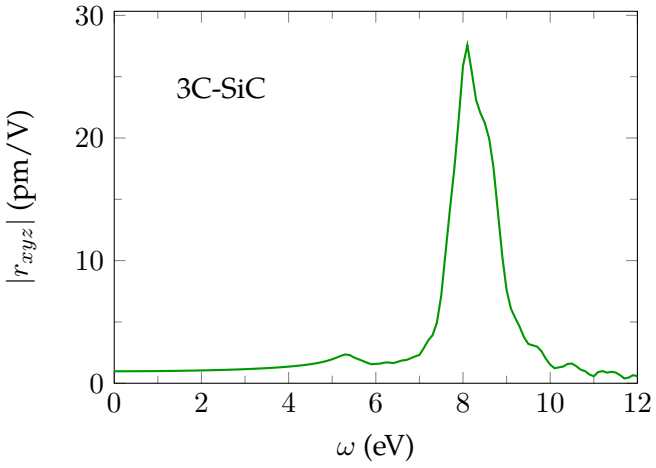

Figure 5.3: Electro-optic coefficient of cubic silicon carbide.

3C-SiC in Ref.[45] to be 2.7 $\pm$ 0.5 pm/V. In our calculation however, we find it to be around 1 pm/V. However, this calculation does not include local field and excitonic effects. The influence of these two contributions has not been investigated so far for LEO but it has been for both the linear response and the second harmonic. We know that it has little effect on the value of ε at 2 eV[46] that stays around 7, while it has a larger effect on the second harmonic. Indeed, for SHG, the local fields tend to decrease the intensity, while the α-kernel acts in the opposite way and increases it[9]. Around the resonant peak, the resulting effect is an increase in intensity but the value of α in the long-range kernel is chosen to reproduce correctly the resonant peak and is know to overestimate the static value. This problem is due to the static approximation made in the α kernel that is not frequency-dependent. Nonetheless, looking at the value for the second harmonic at 2 eV, the $\chi^{(2)}$ goes from 38 pm/V for IPA, to 33 pm/V for RPA (with local fields) and finally reaches 74 pm/V for the excitonic calculation using the α kernel, leading to a factor 2 between the independent-particle approximation and the final calculation of $\chi^{(2)}$. A similar trend is expected for LEO which, with the 10% difference on ε, would explain the difference between the experimental measurement and this theoretical value.

Another polytype of silicon carbide, 2H-SiC, was studied. It is arranged in a wurtzite structure, displayed in Figure 5.4 that corresponds to an hexagonal symmetry $6mm$. This new system is anisotropic, meaning that the dielectric tensor will present different diagonal components,

$$\overleftrightarrow{\varepsilon}_M(\omega) = \begin{pmatrix} \varepsilon^{lr}_{xx}(\omega) & 0 & 0 \\ 0 & \varepsilon^{lr}_{xx}(\omega) & 0 \\ 0 & 0 & \varepsilon^{lr}_{zz}(\omega) \end{pmatrix}. \tag{5.3}$$

Now, applying a dc-field, this tensor becomes

$$\overleftrightarrow{\varepsilon}^{(\boldsymbol{\mathcal{E}})}_M(\omega) = \begin{pmatrix} \varepsilon^{lr}_{xx}(\omega) + \varepsilon^{leo}_{xx}(\omega) & 0 & \varepsilon^{leo}_{xz}(\omega) \\ 0 & \varepsilon^{lr}_{xx}(\omega) + \varepsilon^{leo}_{xx}(\omega) & \varepsilon^{leo}_{xz}(\omega) \\ \varepsilon^{leo}_{zx}(\omega) & \varepsilon^{leo}_{zx}(\omega) & \varepsilon^{lr}_{zz}(\omega) + \varepsilon^{leo}_{zz}(\omega) \end{pmatrix} \tag{5.4}$$

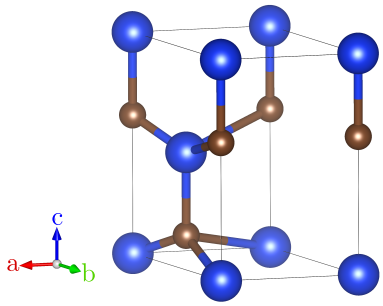

Figure 5.4: Representation of the wurtzite crystal structure of hexagonal silicon carbide 2H-SiC. The blue atoms corresponds to silicon and the brown ones to carbon.

Again QEO effects are not included here, otherwise the whole matrix would be filled. Different components are plotted in Figure 5.5, where the blue and green curves depend on the strength of static field. The two part of $\varepsilon_{xx}^{(\boldsymbol{\mathcal{E}})}$ are shown separately.

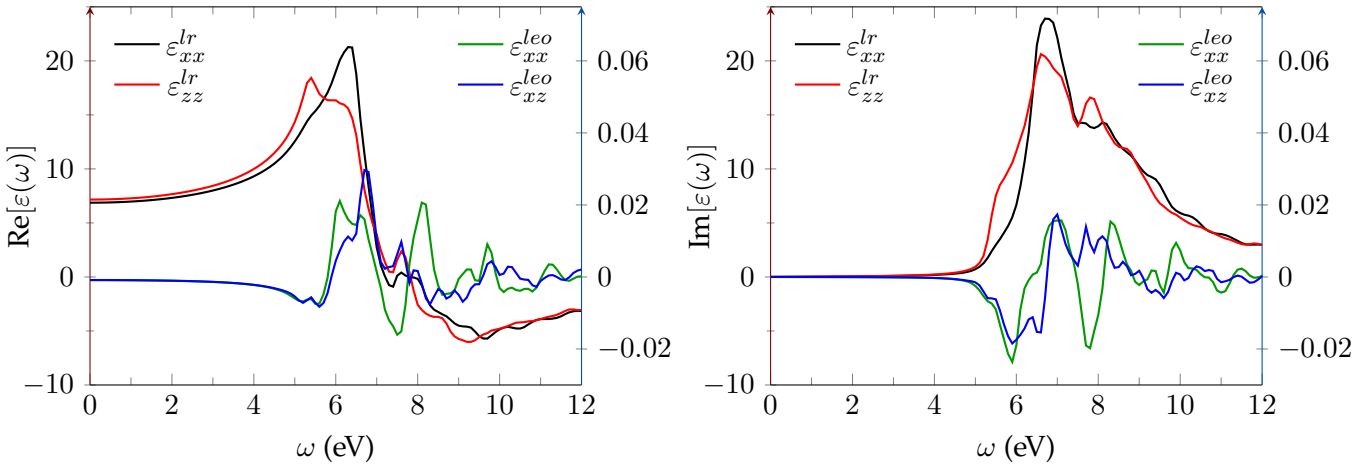

Figure 5.5: Real and imaginary parts of the components of the dielectric tensor already present (black and red curves, intensity scaled on the left side) or induced by a static field (green and blue curves, intensity scaled on the right side) of $3 \cdot 10^5$ V.cm^{-1} for 2H-SiC with a scissor of $\Delta = 0.8$ eV.

As previously stated, a strong dc-field was chosen but not intense enough to destroy the material (see Appendix G) and the two field-induced components are also plotted on a different scale since they are very small and would not be seen otherwise. Therefore adding the extra part on the diagonal component (green curve, intensity scaled on the right side) would have no visible effect on the spectrum (black curve, intensity scaled on the left side). One can notice that the imaginary part of ε_{xx}^{leo} is not positive, but only the total component $\varepsilon_{xx}^{(\boldsymbol{\mathcal{E}})} = \varepsilon_{xx}^{lr} + \varepsilon_{xx}^{leo}$ needs to be. Moreover, it is important to note that, while the dc-field chosen here is only half of the one used for the cubic polytype, the intensity of the LEO response is one order of magnitude smaller, meaning that the linear electro-optic effect has a bigger influence on the cubic polytype than on the hexagonal one.

5.1.2 Gallium arsenide

Bandstructures and LEO spectra were already calculated by Sipe in the 90's for GaAs and GaP, using the second order formula shown in Ref. [13]. The results were displayed in Ref. [7] only below the band-gap and included a scissor. However, it was later shown in 2005[43] by the same authors that

the scissor was, at that time, not correctly introduced and that it really affected the SHG spectrum, including the value at $\omega = 0$, which is the same for LEO (see equation (1.3)). This would indicate that the second-order results presented in that article for both SHG and LEO are not correct, despite the fact that there was a good agreement with the LEO experiments.

I report here the different experimental and theoretical results obtained for GaAs in Figure 5.6. The experimental results are given in the form of electro-optic coefficients $r_{xyz}(\omega)$ and converted into a second-order susceptibility $\chi^{(2)}(-\omega;\omega,0)$ by the relation (1.10).

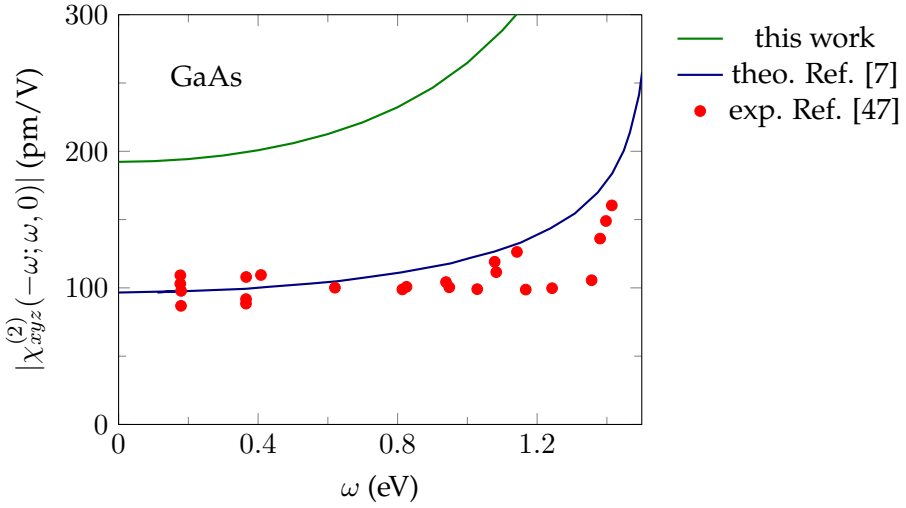

Figure 5.6: Comparison between the LEO spectrum of GaAs calculated in this work (green curve) and the one displayed in Ref. [7] (blue curve) along with the experimental results compiled in Ref. [47] (red dots).

As previously stated, despite the fact that the theoretical calculations from Ref. [7] seem to match the experiments, we now know them to be wrong. And unlike what we discussed in the case of silicon carbide, the excitonic effects described by the α-kernel, and absent in our calculation, will not, here, get us closer to the experimental values. In fact, the trend will most likely be an increase in intensity, taking us even farther away from the measurements.

We know that, in the band-gap region, the SHG susceptibility of GaAs is higher in intensity than the one of 3C-SiC, which is confirmed by experimental results. This would mean that the LEO susceptibilities, which are the same as the SHG ones at $\omega = 0$, should have the same trend, which is what is actually observed in our calculations. But, the experimental results indicate that the 3C-SiC linear electro-optic coefficient are higher than the one of GaAs[45].

This disagreement could have many origins. One of the explanation may be that the phonons, which are more important in GaAs than in SiC, play here a larger role and have a greater influence on the experimental results. Another will be that GaAs, as any III-V semiconductors of zinc-blende structure, is a piezoelectric material[48] and that the dc-field applied for the LEO measurement changed the volume of the cell, which altered the results. The effect of such a change in volume is shown in Figure 5.7, which displays a huge impact on the spectrum. One could note that the decrease in volume of 9%, shown in Figure 5.7, is significantly larger than the difference between the theoretical and experimental volume of the unit-cell (only 1%), meaning that the disagreement between experiments and theory is not due to a wrong value taken for the volume. But this kind of change in volume would only occur if the static field was applied similarly in every direction.

A more realistic effect of the piezoelectricity would be that the static field, applied in one direction, could have induced a displacement of atoms, thus creating stress inside the material. This would then

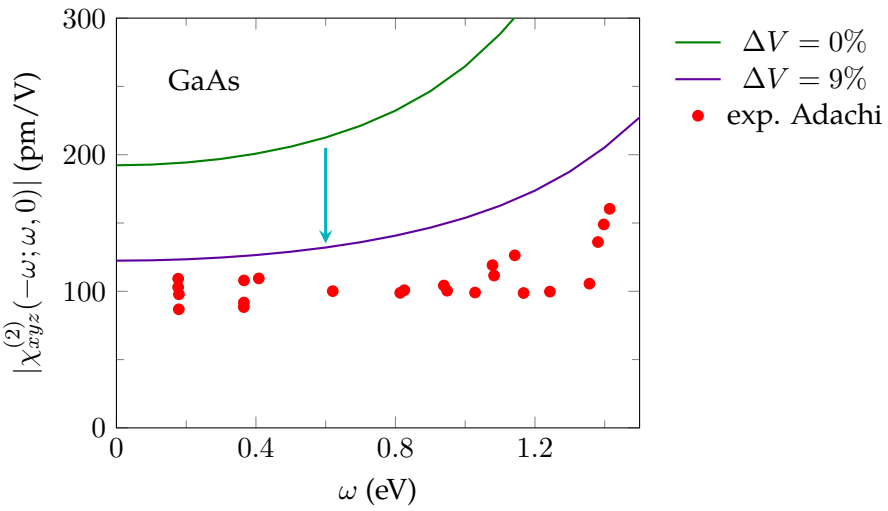

Figure 5.7: Effect of the variation of the volume on the theoretical LEO spectrum of GaAs: (i) no change in volume (green curve), (ii) 9% decrease in the unit-cell volume (purple curve) and (iii) the experimental results from Ref. [47] (red dots).

generate new components in the $\chi^{(2)}$ tensor, that were previously zero, due to the symmetry of the system, and possibility change the already existing one. Therefore, if such a displacement occurred, the experimental linear electro-optic coefficient r_{xyz} would have been wrongly defined and include other components, that are no longer vanishing due to the strain. And the different components may have had destructive interferences with each other, thus reducing the experimental value. The effect this would have on the susceptibility could be determined by performing calculation on strained GaAs, as it is done for Si in section 5.1.4, which were not done here by lack of time.

5.1.3 Si/Ge interfaces

A previous study on Si/Ge superlattices was realized in Ref. [49] for the second harmonic using the same formalism. The same optimized cells were used here to investigate the linear electro-optic response generated in this kind of layered materials.

Nowadays, microelectronic components are based on silicon. But it presents a lot of limitations, which is why a lot of researches have been centered around developing Si-compatible photonics to be integrated onto silicon chips, that can overcome these limitations. For instance, some of those shortcomings have been dealt with by introducing SiGe alloys and strained Si. But one of the main issue of Si or SiGe alloys is the fact that their fundamental band-gap is indirect in nature. To that effect, short-period Si/Ge superlattices have been widely studied in the 90's due to the possibility to engineer the band-gap to fit one's criteria due to quantum confinement, by varying the number of Si and Ge layers, which can lead to interesting electronic and optical properties. They are also an interesting type of materials to study for us since they display multiple interfaces that can effectively create an electrostatic field inside the material. Moreover, some results are already available for the second harmonic both experimental[50;51;52;53] and theoretical[54;44]. Some experimental work was also realized for LEO[55] but it was focused around the excitonic peak, whose effect is missing in this calculation.

Si_n/Ge_n superlattices are created from the structure of bulk silicon, illustrated in Figure 5.8. The

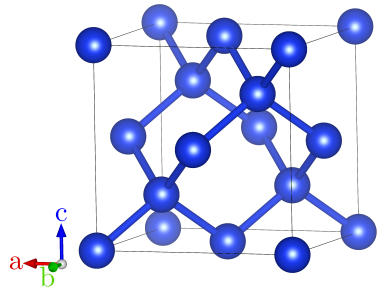

Figure 5.8: Bulk silicon unit cell corresponding to the diamond structure.

system then undergoes a $\pi/4$ rotation of the axis a and b in the plane (x,y),

$$\begin{cases} \mathbf{a}' = & \frac{1}{2}(\mathbf{a}+\mathbf{b}) \\ \mathbf{b}' = & \frac{1}{2}(-\mathbf{a}+\mathbf{b}) \\ \mathbf{c}' = & \tilde{n}\mathbf{c} \end{cases}, \tag{5.5}$$

which can be viewed as a rotation of $-\pi/4$ around the z-axis on the atom coordinates,

$$r' = \begin{pmatrix} x' = & \frac{1}{\sqrt{2}}(x+y) \\ y' = & \frac{1}{\sqrt{2}}(-x+y) \\ z' = & z \end{pmatrix}; \qquad a' = \frac{a}{\sqrt{2}}; \quad c' = \tilde{n}a, \tag{5.6}$$

where $\tilde{n} = n$ if the index n is odd, and $\tilde{n} = n/2$ if n is even. The silicon atoms are then partially replaced by germanium atoms so that the number of alternated layers of each corresponds to the index n. For an odd number n of layers, the tetragonal unit cell contains 2 set of layers of each, as shown in Figure 5.9, while it can be reduced to one set for an even number n (see Figure 5.10). It

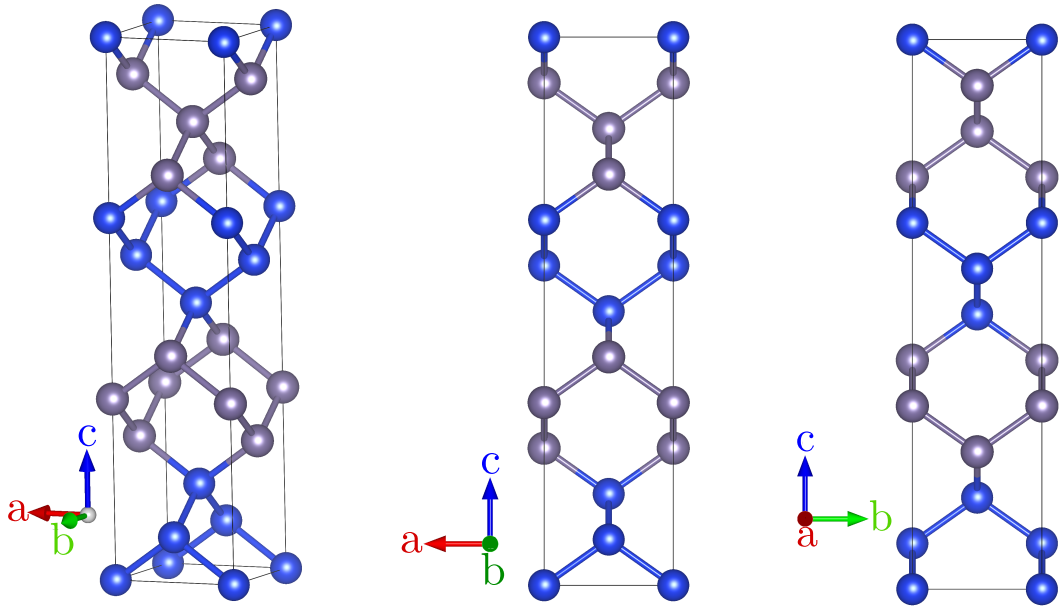

Figure 5.9: Different views of the Si_3/Ge_3 tetragonal unit cell in the basis $(\mathbf{a}', \mathbf{b}', \mathbf{c}')$. Blue spheres represents Si atoms and gray spheres Ge atoms.

means that the tetragonal unit cell contains 12 atoms for Si_3/Ge_3, 8 atoms for Si_4/Ge_4, 20 for Si_5/Ge_5, etc. A way to reduce those numbers, for an odd number of layers, would be to consider a triclinic cell

with the same basis ($\mathbf{a}'$,$\mathbf{b}'$) and change the remaining axis as $\mathbf{c}'' = (\mathbf{a}' + \mathbf{b}' + \mathbf{c}')/2 = (\mathbf{b} + n\mathbf{c})/2$. Doing that decreases the symmetries of the unit cell, but, considering that those symmetries are not explicitly taken into account when calculating the nonlinear response, it doesn't matter. And the symmetries of the $\chi^{(2)}$ would still correspond to those of a tetragonal system. The cells were then relaxed following Ref. [54]: the in-plane lattice parameter a' was kept fixed and was taken to be 5.389Å, corresponding to the one of bulk silicon to simulate the growth of this superlattice on top of a Si(001) substrate and the lattice parameter c' was relaxed.

Note that unrelaxed cells with an even number n of layers, illustrated in Figure 5.10, are centrosymmetric and, as such, do not generate a dipole second-order response. But when they are relaxed, the symmetry of the system is broken and a small $\chi^{(2)}$ response can arise. However, SHG calculations showed that it was very small for the even Si_4/Ge_4 compared to the signal obtained for Si_3/Ge_3 and Si_5/Ge_5 [54].

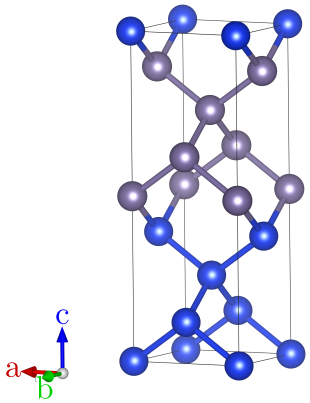

Figure 5.10: Si_4/Ge_4 tetragonal unit cell.

The LEO spectrum of relaxed Si_3/Ge_3 is displayed in Figure 5.11. From that spectrum and LEO

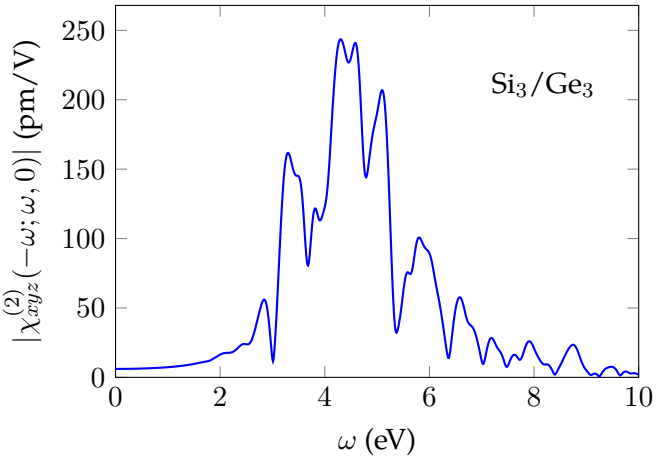

Figure 5.11: LEO susceptibility of the relaxed Si_3/Ge_3 superlattice with a scissor operator of $\Delta = 1.1$ eV.

measurements, one could extrapolate the value of the static field created at the interfaces.

In the LEO experiments in Ref. [55], the value provided corresponds to the variation of the refractive index at 0.8 eV, below the excitonic peak, which is of about $n = 10^{-3}$ for a static field of $9 \cdot 10^4$ V.cm^{-1}. But the refractive index is only defined when $\overleftrightarrow{\varepsilon}_M$ is diagonal, which is no longer the case with the LEO correction. This means that, to observe the change in the refractive index, we first need

to diagonalize this matrix:

$$\overleftrightarrow{\varepsilon}^{(\boldsymbol{\mathcal{E}})}_{M}(\omega) = \begin{pmatrix} \varepsilon^{lr}_{xx}(\omega) & \varepsilon^{leo}_{xy}(\omega) & \varepsilon^{leo}_{xz}(\omega) \\ \varepsilon^{leo}_{xy}(\omega) & \varepsilon^{lr}_{xx}(\omega) & \varepsilon^{leo}_{xz}(\omega) \\ \varepsilon^{leo}_{zx}(\omega) & \varepsilon^{leo}_{zx}(\omega) & \varepsilon^{lr}_{zz}(\omega) \end{pmatrix} \rightarrow \begin{pmatrix} \varepsilon^{(\boldsymbol{\mathcal{E}})}_{x'x'}(\omega) & 0 & 0 \\ 0 & \varepsilon^{(\boldsymbol{\mathcal{E}})}_{y'y'}(\omega) & 0 \\ 0 & 0 & \varepsilon^{(\boldsymbol{\mathcal{E}})}_{z'z'}(\omega) \end{pmatrix}, \tag{5.7}$$

which amounts to redefining the optical axes of the system. The index variation is then displayed in Figure 5.12 in the band-gap region, where the matrix in equation (5.7) is real and therefore diagonalizable. To find an index variation of about 10^{-3}, we need a field around 10^7 V.cm^{-1}, which is two

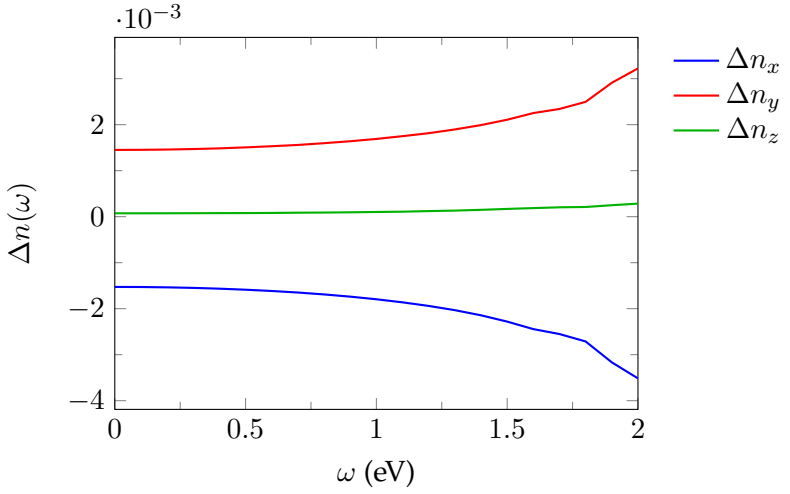

Figure 5.12: Refractive index variation for a dc-field of $9 \cdot 10^6$ V/cm.

orders of magnitude higher than what is found experimentally in Ref. [55]. The difference can be explained by the fact that the system are not the same, which can influence the susceptibility. Also their measurement is done near the excitonic peak, which cannot be reproduced here since the excitonic effects are not included at this level of approximation. And finally, the value of the static field given was the one applied on the material, which do not account for the electric field already present at the interfaces of the material. Therefore the total field may have been higher.

5.1.4 Strained silicon

Silicon, shown in Figure 5.8, is a centrosymmetric material, meaning that the dipole contribution of the $\chi^{(2)}$ is zero for the bulk. Therefore, the only non-vanishing term comes from the surface. In order to generate a response from the bulk, one needs to break the symmetries of the system. This can be done either by creating a static field inside the material (EFISH), which will be discussed in the next section or it could be achieved by applying a strain on the system. This was already thoroughly investigated for the second harmonic[56;57] and I now wish to present some results for LEO.

In this simulation, the strain is applied inside the unit cell and is represented by an atom displacement, which is done in a way that no stress is created at the boundary of the cell, that is then repeated in space. This corresponds to a periodic microscopic stress, which is different from the macroscopic stress applied on the material in experiments[58]. Nonetheless, one can still observe some general tendencies. Different kinds of strain were applied on Si, either along an axis (1D), or applied on a plane (2D) effectively creating a shear stress inside the material.

The strain is applied on bulk Si, for which we switch from the diamond-like unit cell (see Figure 5.8) to the tetragonal cell introduced in the previous section for the Si/Ge superlattice (see Figure 5.9),

using the same transformation of equations (5.5) and (5.6) with $\tilde{n} = 2$, leading to a 8-atom unit cell. The strain is then generated by moving atoms, initially in their bulk positions, leading to an increase or decrease of the bonds lengths, thus creating a tensile or compressive strain, respectively. In practice, it is atom 7 in Figure 5.13 that is moved along the z-axis for the uniaxial strain and in the (y',z) plane for the biaxial strain, thus creating the elongation or shortening of the bond 6-7 and 7-8. Atom 8 is also

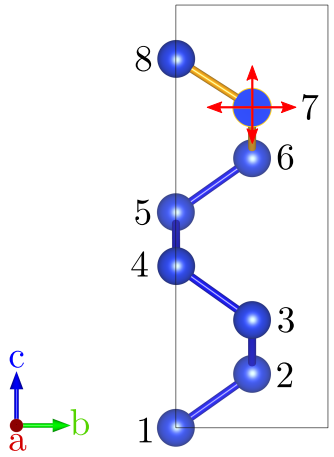

Figure 5.13: Scheme of the strain applied inside the tetragonal unit cell: atom 7 is moved creating a compressive or tensile strain on the yellow bonds between atoms 6-7 and 7-8.

moved along the z-axis to have a more precise control over the compressive or tensile strain applied on the yellow bonds in Figure 5.13. The lattice parameter c' is then slightly increased or decreased, following the motion of atom 8 to preserve the boundary conditions by keeping the same distance between two neighboring cells in z, meaning conserving the bond length between atom 8 and atom 1 of the next cell.

The different structures are designated as in Ref. [57], where C and T refer to a compressive or tensile strain, respectively, with a percentage of elongation or compression of the bond compared to the bulk value. For instance, the structure $C_{1.8}$-$T_{3.0}$ refers to a compressive bond of 1.8% between atoms 6-7 and a tensile bond of 3.0% between atoms 7-8. If the strain is the same in the two bonds, for instance $C_{3.0}$-$C_{3.0}$ then the system is still centrosymmetric, despite the strain applied, and the second-order susceptibility remains zero. However the pressure inside the material is not zero. Now, if the strain in the two bonds is opposite, for instance $C_{3.0}$-$T_{3.0}$, then the pressure is compensated inside the material but $\chi^{(2)}$ is non-zero. The spectra for different uniaxial strains are shown in Figure 5.14. The band-gaps of the different systems are situated around 1 eV. Therefore the peak observed at this energy in each spectrum corresponds to the transition in the gap, which is induced by the strain, while the second one around 4 eV corresponds to the absorption peak in the linear response for bulk Si. For the second peak, the highest intensities are reached by the systems that are the farther away from the centrosymmetry with the lowest pressures of the type CT or TC, while a compressive strain seems to be what is more effective to generate the first peak, which is smaller in general.

The spectra for the biaxial strained system are displayed in Figure 5.15. The letter Y is added to the denomination of the different systems for the biaxial stress to indicate an additional strain along the y-axis. The component $\chi^{(2)}_{zzz}$ (in Figure 5.15) displays similar characteristics with the same component shown for the uniaxial strain in Figure 5.14, while the new non-zero component $\chi^{(2)}_{yyy}$, induced by the additional strain along Y, shows an increase in intensity for the first peak around 1 eV. From that, one can conclude that a biaxial strain is more effective to generate a high intensity response in the band-gap region, whereas a uniaxial stress is enough if one is interested in the peak around 4.2 eV,

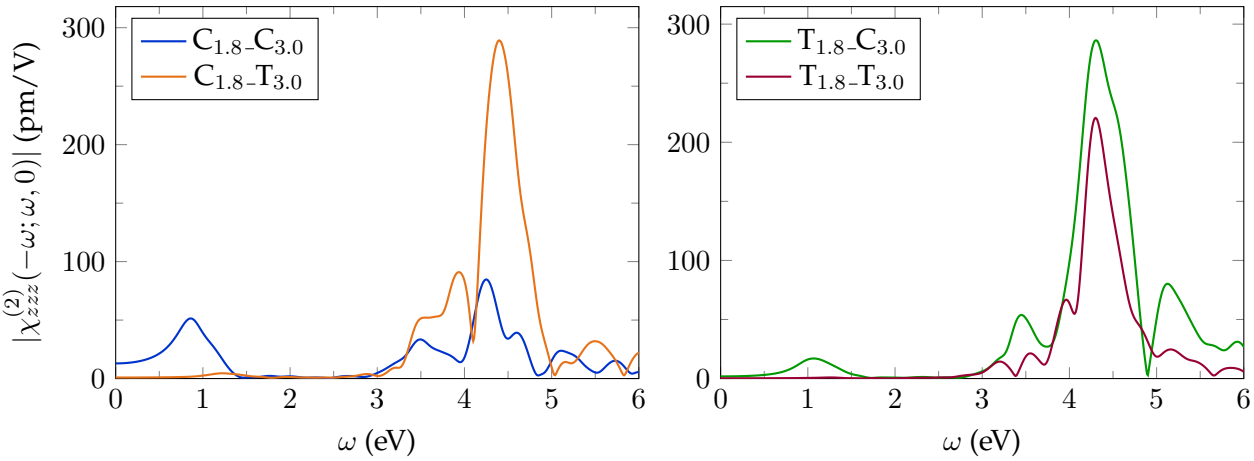

Figure 5.14: Linear electro-optic spectra for uniaxial strained silicon with a scissor $\Delta = 0.6$ eV.

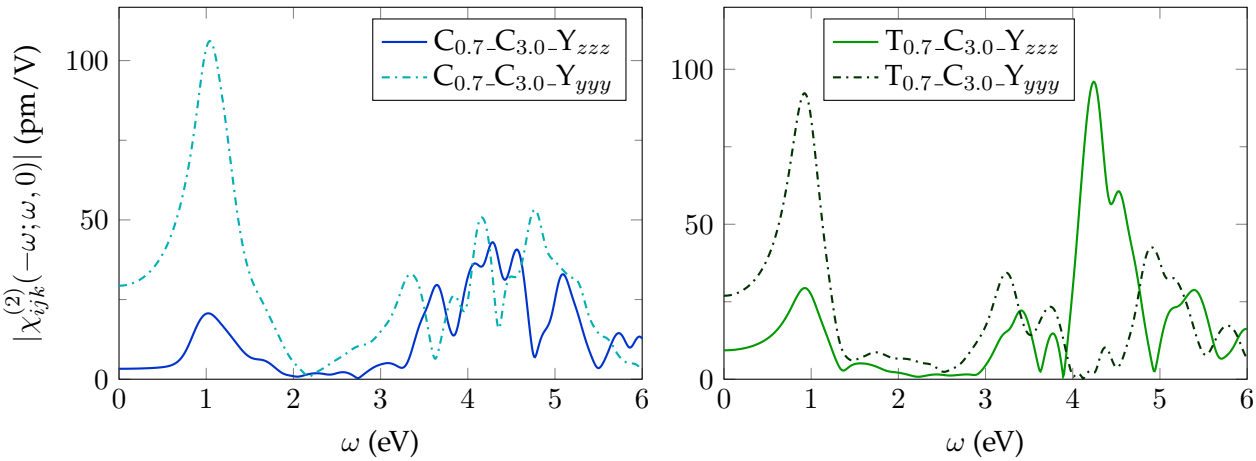

Figure 5.15: Linear electro-optic spectra for biaxial strained Si with a scissor $\Delta = 0.6$ eV. Solid line: component zzz, dotted-dashed line: component yyy.

corresponding to the position of the peak in the linear response spectrum of unstrained silicon.

Although the way to apply the strain on the material is different, we can still have a general comparison with the LEO experiments in Ref. [58], where a compressive strain is applied by a straining layer deposited on top of silicon. They found an induced coefficient of 15 pm.V^{-1} at 0.8 eV, which can then be enhanced by the experimental setup, like for example guiding the light in a photonic crystal waveguide. The order of magnitude corresponds here to what is found for the $C_{0.7}$-$C_{3.0}$-Y system, which is at 11 pm.V^{-1}.

5.2 Third-order response

In this section, I present some results for the $\chi^{(3)}$, calculated at the IPA level without a scissor. The non-vanishing components of the third-order susceptibility for the symmetry classes of interest are reported in Table 5.2.

Symmetry class	International notation	Schoenflies notation	Nonvanishing tensor components	
Cubic	$\bar{4}3m$	T_d	$xxxx = yyyy = zzzz,$ $yyzz = zzyy = zzxx = xxzz = xxyy = yyxx,$ $yzyz = zyzy = xyxy = yxyx = xzxz = zxzx,$ $xzzx = zxxz = yzzy = zyyz = xyyx = yxxy$	(4)
Hexagonal	$6mm$	C_{6v}	$zzzz,\ xxxx = yyyy,\ xxyy = yyxx,$ $xyyx = yxxy,\ xyxy = yxyx,\ yyzz = xxzz,$ $zzyy = zzxx,\ zyyz = zxxz,\ yzzy = xzzx,$ $yzyz = xzxz,\ zyzy = zxzx$	(11)

Table 5.2: List of non-zero components of $\chi^{(3)}(\omega_1, \omega_2, \omega_3)$ for some symmetry class.

5.2.1 Third Harmonic Generation

Since the third harmonic was not really the focus of this thesis, it was not applied on advance materials or really analyzed. Nonetheless, I present here, in Figure 5.16, the comparison between the formalism introduced in the previous chapter and another developped by C. Attaccalite and M. Grüning in Ref. [14; 15], based on real-time propagation of the equations of motion, where the $\chi^{(3)}$ is extracted from the total polarization, as defined in equation (1.1). The peaks appear to be positioned at the same

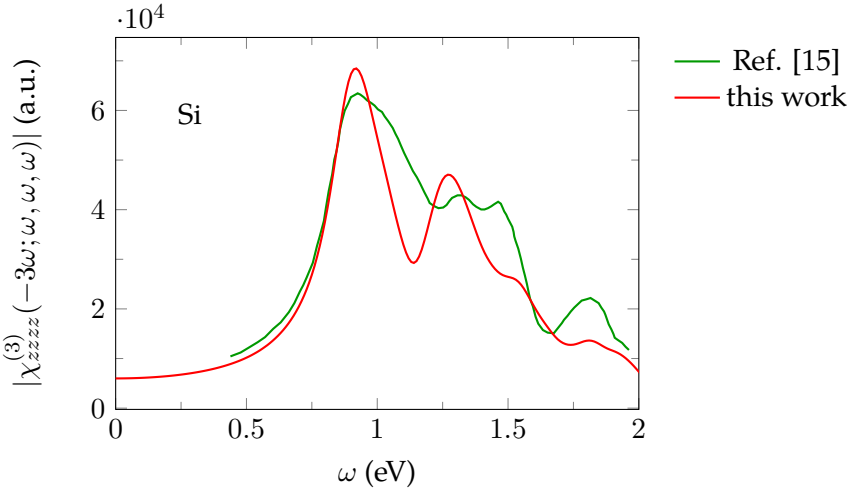

Figure 5.16: Comparison of THG for bulk Si within IPA between equation (4.44) with $\eta = 0.07$ eV (red curve) and Ref. [15] (green curve).

energies. The general agreement between the two curves is relatively good, although not as good as the agreement reached between the two formalisms for the second harmonic. The difference between the intensity of the peaks could come from the broadening, which is not introduced in the same way in the two method. Indeed, it is known to affect the intensity of the peaks and may have a larger influence on higher order.

5.2.2 Electric-Field Induced Second Harmonic

EFISH can be used as a way to generate a "second harmonic" response in centrosymmetric material, for which $\chi^{(2)}$ is zero in the dipole approximation. But it can also be used as a probe to determine the

magnitude of the dc-field created at the interfaces of a material. There are a few experimental works focusing on the measurement of EFISH inside Si/SiO_2 interface[59;60;61;62], for which the strength of the response is known to be quite important compared to other materials.

Since it is a third order response, it is expected to be a lot smaller than the $\chi^{(2)}$. And it would take an intense static field for it to become of the same magnitude. However, for centrosymmetric material, the second-order response only comes from the surface and is usually smaller since there is far less surface than bulk. We are not discussing here about nanoparticles, for which the ratio surface/volume is very high. In that case, the EFISH response from the bulk could be one of the main contributions.

When considering the cubic symmetry of silicon and silicon carbide (see Figures 5.8 and 5.1), the $\chi^{(2)}$ tensor without a static field is

$$\overset{\leftrightarrow}{\chi}^{(2)}(\omega,\omega) = \left(\begin{array}{ccc:cc:cc:cc} 0 & 0 & 0 & \chi^{(2)}_{xyz} & \chi^{(2)}_{xzy} & 0 & 0 & 0 & 0 \\ 0 & 0 & 0 & 0 & 0 & \chi^{(2)}_{yzx} & \chi^{(2)}_{yxz} & 0 & 0 \\ 0 & 0 & 0 & 0 & 0 & 0 & 0 & \chi^{(2)}_{zxy} & \chi^{(2)}_{zyx} \end{array}\right), \tag{5.8}$$

which is here written in its more convenient 9×3 matrix form instead of the $3 \times 3 \times 3$ tensor, where the 9 columns correspond to xx, yy, zz, yz, zy, zx, xz, xy, yx, respectively. In this symmetry, all the non-vanishing components of the tensor are equal, meaning that there is only one independent component.

Then adding a static field along the z-direction, new components of the tensor are created through equation (1.14),

$$\overset{\leftrightarrow}{\chi}^{(2)\mathcal{E}_z}(\omega,\omega) = \left(\begin{array}{ccc:cc:cc:cc} 0 & 0 & 0 & \chi^{(2)}_{xyz} & \chi^{(2)}_{xzy} & \chi^{(2)\mathcal{E}_z}_{xzx} & \chi^{(2)\mathcal{E}_z}_{xxz} & 0 & 0 \\ 0 & 0 & 0 & \chi^{(2)\mathcal{E}_z}_{yyz} & \chi^{(2)\mathcal{E}_z}_{yzy} & \chi^{(2)}_{yzx} & \chi^{(2)}_{yxz} & 0 & 0 \\ \chi^{(2)\mathcal{E}_z}_{zxx} & \chi^{(2)\mathcal{E}_z}_{zyy} & \chi^{(2)\mathcal{E}_z}_{zzz} & 0 & 0 & 0 & 0 & \chi^{(2)}_{zxy} & \chi^{(2)}_{zyx} \end{array}\right), \tag{5.9}$$

filling part of the tensor of equation (5.8) that was previously zero with three independent components:

$$\begin{cases} \chi^{(2)\mathcal{E}_z}_{zzz}(\omega,\omega) = 3\chi^{(3)}_{zzzz}(\omega,\omega,0)\ \mathcal{E}_z \\ \chi^{(2)\mathcal{E}_z}_{xzx}(\omega,\omega) = 3\chi^{(3)}_{xzxz}(\omega,\omega,0)\ \mathcal{E}_z \\ \chi^{(2)\mathcal{E}_z}_{zxx}(\omega,\omega) = 3\chi^{(3)}_{zxxz}(\omega,\omega,0)\ \mathcal{E}_z \end{cases}, \tag{5.10}$$

shown for silicon and silicon carbide in Figure 5.17. Note that there is no additional contribution due to EFISH for the $\chi^{(2)}_{xyz}$ component. One can see that the two components $\chi^{(3)}_{xzxz}$ and $\chi^{(3)}_{zxxz}$ are the same for silicon, which was expected at $\omega = 0$ due to Kleinman symmetry[63], but not at higher energies. Indeed, only the indices j and k are interchangeable in the EFISH susceptibility $\chi^{(2)}_{ijkl}(-2\omega;\omega,\omega,0)$, in addition to the natural symmetries of the system shown in Table 5.2 (1st row). The equality between these two components in silicon comes from the fact that the material presents an inversion symmetry. For silicon carbide, which is not centrosymmetric, these two components cease to be equal beyond 2.3 eV where the first resonance start at half the value of the band gap. Moreover, in the two materials, the $\chi^{(3)}_{xzxz}$ component shows an intensity of half the one of the $\chi^{(3)}_{zzzz}$.

In order to compare the intensity of SHG and EFISH, I looked at a non-centrosymmetric material: silicon carbide, for which I plotted the only non-vanishing $\chi^{(2)}$ component with the field-induced $\widetilde{\chi}^{(2)}_{zzz}$ in Figure 5.18. The strength of the static field was chosen here at the same value as for LEO in Figure 5.2. And, in that case, we can actually compare the SHG and EFSIH components on the same scale, unlike what was done for LEO. This means that the field-induced component, while smaller than the other one, is far from being negligible.

Finally, I compare the EFISH intensity of the $\chi^{(3)}_{zzzz}$ component in Si and 3C-SiC, shown in Figure 5.19 , which displays a factor 10 difference between the two, clearly showing that the EFISH response

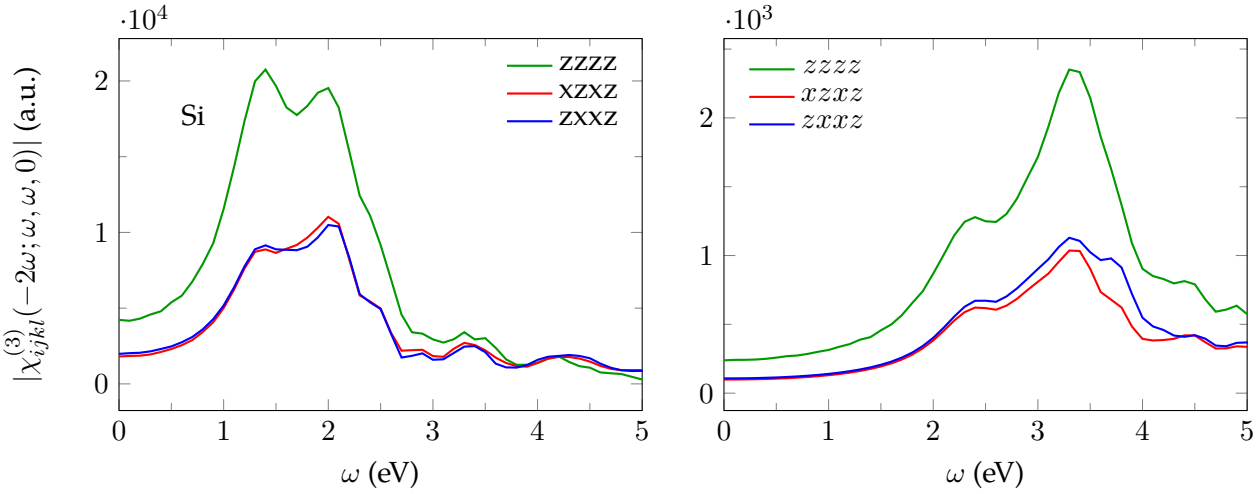

Figure 5.17: Different components of the EFISH susceptibility of bulk silicon and cubic silicon carbide.

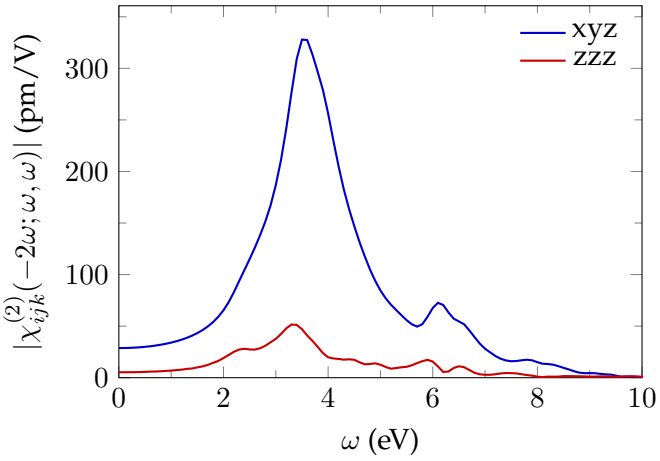

Figure 5.18: Comparison for SiC between the two $\chi^{(2)}$ component xyz coming from SHG (blue curve) and zzz coming from EFISH (red curve) with a static field of $\mathcal{E}_z = 7 \cdot 10^5$ V/cm

in silicon is larger. In fact, using the same strength for the static field as in Figure 5.18, the field-induced $\widetilde{\chi}^{(2)}_{zzz}$ thus generated would be even larger than the $\chi^{(2)}_{xyz}$ of SiC.

Finally, using a static field seems to be a more effective way to generate a non-vanishing dipolar contribution for the second-harmonic than to apply a strain on the material, although both those contributions depend on an external parameter, which is the strength of the dc-field for EFISH and the pressure inside the system for strained Si, making the comparison somewhat arbitrary. For a hydrostatic pressure of about 2 GPa, the second-order susceptibility reaches a value of 30 pm.V^{-1} [57], while it will reach 140 pm.V^{-1} for a field of $5 \cdot 10^5$ pm.V^{-1}.

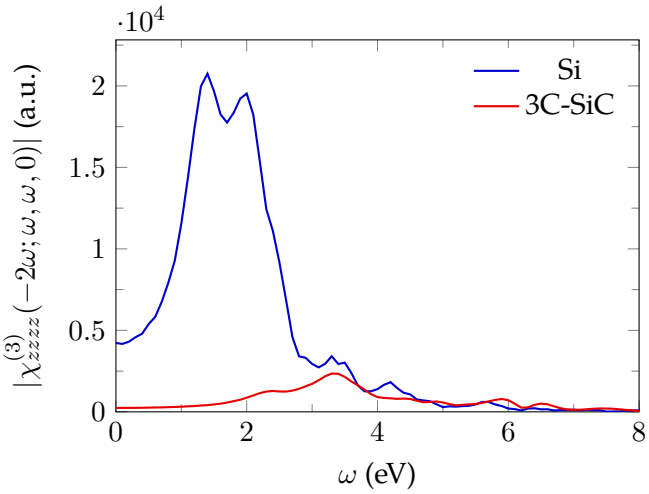

Figure 5.19: Comparison of the EFISH response between Si and 3C-SiC for the $zzzz$ component.

Chapter 6

Conclusion

This thesis aimed to describe nonlinear optical responses induced by an electrostatic field, in particular the linear electro-optic response and the electric-field induced second harmonic. The main result is the independent-particle description of this two phenomena. The first approach presented to describe these processes was to include the static field at the ground-state level, which seemed a priori easier since a polarized-second-order response would give us the EFISH correction instead of having to calculate a third-order susceptibility. However, it proved to not be so easy and was, *in fine*, not successful due to the problem of correctly defining the Hamiltonian in periodic conditions with Bloch functions, and then for the susceptibility generated from this Hamiltonian to behave accordingly with the symmetries of the system.

The second approach was then to describe each of these phenomena with their respective susceptibility. Having already done it for SHG, the density calculation was quite straightforward for LEO, since there were little more difficulties than for SHG. The same calculation for the third-order was however not so managable, which is why it was performed through the current density. But this led to new problems on how to write the formula so that it is free of any unphysical divergences that may occur. Indeed removing the divergence in ω, naturally present in the current density calculation, created new divergences in energy terms, which did not happen for the second order. And extra-care was required to make sure that all these divergences were compensated and did not appear on the final spectrum. As a result, the final expression showed good agreement with the ω-divergent spectra after the band-gap region, proving the validity of the formula.

Still part of the many-body effects are missing from this description. However, we know that regarding bulk materials, the effect of local fields will most likely be negligible. Therefore the main focus should be to solve the problem of including excitonic effects. This should be relatively easy for LEO since it was already done for the second harmonic through the second-order Dyson-like equation,

$$\chi^{(2)} = \chi_0^{(2)} + \chi_0^{(2)}(v + f_{xc})\,\chi^{(1)} + \chi_0^{(1)}\frac{\partial f_{xc}}{\partial \rho}\,\chi^{(1)}\chi^{(1)} + \chi_0^{(1)}(v + f_{xc})\,\chi^{(2)}, \tag{6.1}$$

here written in a simple notation. Therefore, it should not be too difficult to reproduce this calculation but for two different frequencies. It will however be a lot more complicated for the third order considering that we first need to determine the third-order Dyson-like equation that will depend on

both the first and second-order susceptibilities,

$$\chi^{(3)} = \chi_0^{(3)} + \chi_0^{(3)}(v + f_{xc})\,\chi^{(1)} + \chi_0^{(2)}\frac{\partial f_{xc}}{\partial \rho}\,\chi^{(1)}\chi^{(1)} + \chi_0^{(2)}(v + f_{xc})\,\chi^{(2)} + \chi_0^{(2)}\frac{\partial f_{xc}}{\partial \rho}\,\chi^{(1)}\chi^{(1)} + \chi_0^{(1)}\frac{\partial^2 f_{xc}}{\partial \rho^2}\,\chi^{(1)}\chi^{(1)}\chi^{(1)} + \chi_0^{(1)}\frac{\partial f_{xc}}{\partial \rho}\,\chi^{(2)}\chi^{(1)} + \chi_0^{(1)}\frac{\partial f_{xc}}{\partial \rho}\,\chi^{(1)}\chi^{(2)} + \chi_0^{(2)}(v + f_{xc})\,\chi^{(2)} + \chi_0^{(1)}\frac{\partial f_{xc}}{\partial \rho}\,\chi^{(1)}\chi^{(2)} + \chi_0^{(1)}(v + f_{xc})\,\chi^{(3)}, \quad (6.2)$$

also written in simplify notation.

Although these effects were not included in this thesis, it is still possible to get the general tendencies with the IPA response alone. And one of the main results is the first principles calculation of the EFISH spectrum for silicon, which appears to be very intense compared to other materials like silicon carbide and could be, if the dc-field applied is intense enough, one of the main contribution in second harmonic experiments. However this remark needs to be dampened by the fact that we did not assume here any inhomogeneities in the dc-field. But if the static field was, for instance, induced by an accumulation of charges at an interface then this field would only be located at the interface. This means that the field-induced response, such as EFISH, would only be induced around this interface and it would not come from the whole bulk, which would, in that case, diminish the intensity given here to the EFISH susceptibility.

Part III

Appendices

Appendix A

Prefactor for the susceptibility

A.1 Second order

For the second harmonic, there is only one input field, which is the same as for the linear response. The total field can be written as

$$E(t) = E_0 \left(e^{-i\omega t} + e^{i\omega t}\right) \tag{A.1}$$

The second-order susceptibility $\chi^{(2)}$ which is responsible for the nonlinear optical effects relates the polarization to the total field. The second-order polarization is quadratically dependent on the total field E(t) and can be expressed as

$$P^{(2)} = \chi^{(2)} EE = \chi^{(2)} E_0^2 \left(e^{-2i\omega t} + e^{2i\omega t}\right) + 2\chi^{(2)} E_0^2 \tag{A.2}$$

The first term corresponds to the second harmonic generation (SHG) and the second term to the optical rectification (OR). For the general second-order, there are two input electric fields:

$$\begin{cases} E_1(t) = E_{0,1} \left(e^{-i\omega_1 t} + e^{i\omega_1 t}\right) \\ E_2(t) = E_{0,2} \left(e^{-i\omega_2 t} + e^{i\omega_2 t}\right) \end{cases} \tag{A.3}$$

The total incident field is the sum of all the fields,

$$E(t) = E_{0,1} \left(e^{-i\omega_1 t} + e^{i\omega_1 t}\right) + E_{0,2} \left(e^{-i\omega_2 t} + e^{i\omega_2 t}\right) \tag{A.4}$$

We then calculate the second-order polarization and obtain

$$\begin{aligned} P^{(2)} = {} & \chi^{(2)} E_{0,1}^2 \left(e^{-2i\omega_1 t} + e^{2i\omega_1 t}\right) + \chi^{(2)} E_{0,2}^2 \left(e^{-2i\omega_2 t} + e^{2i\omega_2 t}\right) + 2\chi^{(2)} E_{0,1}^2 + 2\chi^{(2)} E_{0,2}^2 \\ & + 2\chi^{(2)} E_{0,1} E_{0,2} \left(e^{-i(\omega_1+\omega_2)t} + e^{i(\omega_1+\omega_2)t}\right) + 2\chi^{(2)} E_{0,1} E_{0,2} \left(e^{-i(\omega_1-\omega_2)t} + e^{i(\omega_1-\omega_2)t}\right) \end{aligned} \tag{A.5}$$

where the last two terms corresponds respectively to the sum frequency generation (SFG) and the difference frequency generation (DFG). Written in term of its frequency components we obtain:

$$P^{(2)} = P^{shg}_{(2\omega_1)} + P^{shg}_{(2\omega_2)} + P^{or}_{(0)} + P^{sfg}_{(\omega_1+\omega_2)} + P^{dfg}_{(\omega_1-\omega_2)} \tag{A.6}$$

For the linear electro-optic effect (LEO), the total field is

$$E(t) = E_0 \left(e^{-i\omega_1 t} + e^{i\omega_1 t}\right) + E_{dc} \tag{A.7}$$

where $E_{dc} = \lim_{\omega \to 0} E_2(t) = 2E_{0,2}$. The polarization is then

$$P^{(2)} = \chi^{(2)} E_0^2 \left(e^{-2i\omega_1 t} + e^{2i\omega_1 t}\right) + 2\chi^{(2)} E_{dc}^2 + 2\chi^{(2)} E_0^2 \quad + 2\chi^{(2)} E_0 E_{dc} \left(e^{-i\omega_1 t} + e^{i\omega_1 t}\right) \tag{A.8}$$

The last term corresponds to linear electro-optic effect.

$$P^{(2)} = P^{shg}_{(2\omega_1)} + P^{shg}_{(0)} + P^{or}_{(0)} + P^{leo}_{(\omega_1)} \tag{A.9}$$

One can generalize the expression while accounting for the factor 2 that appears for SFG and DFG,

$$P^{(2)}(\omega_3) = K\chi^{(2)}E(\omega_1)E(\omega_2) \tag{A.10}$$

where K is the factor that depends on the frequencies ω_1 and ω_2 of interest. It is equal to 1 when the frequencies are the same for both input fields and 2 when they are different.

A.2 Third order

For the third harmonic, the total field is the same as for SHG or the linear case (see equation (A.1)). The third-order polarization has a cubic dependence on the total field and is expressed as followed

$$P^{(3)} = \chi^{(3)}EEE = \chi^{(3)}E_0^3\left(e^{-3i\omega t} + e^{3i\omega t}\right) + 3\chi^{(3)}E_0^3\left(e^{-i\omega t} + e^{i\omega t}\right), \tag{A.11}$$

where the first term corresponds to the third harmonic generation (THG) and the second to degenerate four-wave mixing (DFWM), the imaginary part of the latter corresponding to the two-photon absorption (TPA).

In the EFISH case, there are two input fields, therefore the total field is

$$E(t) = E_0\left(e^{-i\omega t} + e^{i\omega t}\right) + E_{dc} \tag{A.12}$$

The polarization is then

$$\begin{aligned} P^{(3)} = \chi^3 E_{dc}\left(E_{dc}^2 + 6E_0^2\right) + \chi^3 E_0^3\left(e^{-3i\omega t} + e^{3i\omega t}\right) + 3\chi^3 E_0^3\left(e^{-i\omega t} + e^{i\omega t}\right) \\ + 3\chi^3 E_{dc}^2 E_0\left(e^{-i\omega t} + e^{i\omega t}\right) + 3\chi^3 E_{dc}E_0^2\left(e^{-2i\omega t} + e^{2i\omega t}\right) \end{aligned} \tag{A.13}$$

The last two term corresponds to the quadratic electro-optic effect (QEO or static-Kerr effect) and the electric field induced second harmonic (EFISH).

$$P^{(3)} = P_{(0)} + P^{thg}_{(3\omega)} + P^{dfwm}_{(\omega)} + P^{qeo}_{(\omega)} + P^{efish}_{(2\omega)} \tag{A.14}$$

Appendix B

LEO: charge density calculation

The general formula for the second-order density response function obtained from the density is

$$\begin{aligned}\chi_{\rho\rho\rho}(\mathbf{q}+\mathbf{G},\mathbf{q}_1+\mathbf{G}_1,\mathbf{q}_2+\mathbf{G}_2,\omega_1,\omega_2) = \frac{1}{V}\sum_{\mathbf{k}}\sum_{n,m,p}\frac{\left\langle\phi_{n,\mathbf{k}}\middle|e^{-i(\mathbf{q}+\mathbf{G})\mathbf{r}}\middle|\phi_{m,\mathbf{k}+\mathbf{q}}\right\rangle}{E_{n,\mathbf{k}}-E_{m,\mathbf{k}+\mathbf{q}}+\omega_1+\omega_2+2i\eta}\\ \times\left\langle\phi_{m,\mathbf{k}+\mathbf{q}}\middle|e^{i(\mathbf{q}_1+\mathbf{G}_1)\mathbf{r}_1}\middle|\phi_{p,\mathbf{k}+\mathbf{q}_2}\right\rangle\left\langle\phi_{p,\mathbf{k}+\mathbf{q}_2}\middle|e^{i(\mathbf{q}_2+\mathbf{G}_2)\mathbf{r}_2}\middle|\phi_{n,\mathbf{k}}\right\rangle\\ \times\left(\frac{f_{n,\mathbf{k}}-f_{p,\mathbf{k}+\mathbf{q}_2}}{E_{n,\mathbf{k}}-E_{p,\mathbf{k}+\mathbf{q}_2}+\omega_2+i\eta}+\frac{f_{m,\mathbf{k}+\mathbf{q}}-f_{p,\mathbf{k}+\mathbf{q}_2}}{E_{p,\mathbf{k}+\mathbf{q}_2}-E_{m,\mathbf{k}+\mathbf{q}}+\omega_1+i\eta}\right)\\ +\big((\mathbf{q}_1,\omega_1)\leftrightarrow(\mathbf{q}_2,\omega_2)\big)\end{aligned} \tag{B.1}$$

In the independent particle approximation (IPA), the local fields are neglected and all vectors $\mathbf{G}$, $\mathbf{G}_1$, $\mathbf{G}_2$ are set to zero. There is no dependence in $\mathbf{k}$-points for the occupation numbers in the case of cold semiconductors. This calculation is done using the dipole approximation, for which the development of the limit $\mathbf{q}\to 0$ stops to the first non-vanishing order. This should corresponds to the third order contribution $T^{(3)}$, since they are three matrix elements, in order for $\chi_{\rho\rho\rho}$ to be proportional to the norm of $\mathbf{q}$, $\mathbf{q}_1$ and $\mathbf{q}_2$. The response function is then expressed as a sum of four terms,

$$\chi_{\rho\rho\rho} = \frac{1}{V}\sum_{\mathbf{k}}\sum_{n,m,p}\left(T^{(0)}+T^{(1)}+T^{(2)}+T^{(3)}\right), \tag{B.2}$$

where the three first contributions in terms of $\mathbf{q}$, $\mathbf{q}_1$ and $\mathbf{q}_2$ should be zero. The matrix elements elements, calculated in the optical limit, are developed to the third order following equation (4.27):

$$\begin{cases}\left\langle\phi_{n,\mathbf{k}}\middle|e^{-i\mathbf{q}\hat{\mathbf{r}}}\middle|\phi_{m,\mathbf{k}+\mathbf{q}}\right\rangle = \delta_{n,m}+a'_{n,m}(\mathbf{q})+a''_{n,m}(\mathbf{q})+a'''_{n,m}(\mathbf{q})\\ \left\langle\phi_{m,\mathbf{k}+\mathbf{q}}\middle|e^{i\mathbf{q}_2\mathbf{r}_2}\middle|\phi_{p,\mathbf{k}+\mathbf{q}_1}\right\rangle = \delta_{m,p}+b'_{m,p}(\mathbf{q},\mathbf{q}_2,\mathbf{q}_1)+b''_{m,p}(\mathbf{q},\mathbf{q}_2,\mathbf{q}_1)+b'''_{m,p}(\mathbf{q},\mathbf{q}_2,\mathbf{q}_1)\\ \left\langle\phi_{p,\mathbf{k}+\mathbf{q}_1}\middle|e^{i\mathbf{q}_1\mathbf{r}_1}\middle|\phi_{n,\mathbf{k}}\right\rangle = \delta_{p,n}+c'_{p,n}(\mathbf{q}_1)+c''_{p,n}(\mathbf{q}_1)+c'''_{p,n}(\mathbf{q}_1)\end{cases} \tag{B.3}$$

We first verify that the zeroth, first and second-order contributions $T^{(0)}$, $T^{(1)}$ and $T^{(2)}$ are zero. It is straightforward to show that any combination containing two δ of equation (B.3) is canceled with the occupation numbers, meaning that $T^{(0)}$ and $T^{(1)}$ are zero and we only need to develop the energy denominator to the first order:

$$\frac{1}{E_{n,\mathbf{k}}-E_{p,\mathbf{k}+\mathbf{q}_2}+\omega_2+i\eta} = \frac{1}{(E_{n,\mathbf{k}}-E_{p,\mathbf{k}}+\omega_2+i\eta)}+\frac{\mathbf{q}_2E^{(1)}_{p,\mathbf{k}}}{(E_{n,\mathbf{k}}-E_{p,\mathbf{k}}+\omega_2+i\eta)^2} \tag{B.4}$$

As a consequence, any combination in $T^{(3)}$ containing the third order matrix elements a''', b''' or c''' will also be zero. The second-order contribution is

$$\begin{aligned}
T_2(\mathbf{q},\mathbf{q}_1,\mathbf{q}_2,\omega_1,\omega_2) = (f_n - f_p)\,\frac{b'_{n,p}(\mathbf{q},\mathbf{q}_2,\mathbf{q}_1)\,c'_{p,n}(\mathbf{q}_1)}{(\omega_1+\omega_2+2i\eta)(E_{n,\mathbf{k}}-E_{p,\mathbf{k}}+\omega_1+i\eta)} \\
+ (f_n - f_m)\,\frac{a'_{n,m}(\mathbf{q})\,c'_{m,n}(\mathbf{q}_1)}{(E_{n,\mathbf{k}}-E_{m,\mathbf{k}}+\omega_1+\omega_2+2i\eta)(E_{n,\mathbf{k}}-E_{m,\mathbf{k}}+\omega_1+i\eta)} \\
+ (f_n - f_p)\,\frac{b'_{n,p}(\mathbf{q},\mathbf{q}_2,\mathbf{q}_1)\,c'_{p,n}(\mathbf{q}_1)}{(\omega_1+\omega_2+2i\eta)(E_{p,\mathbf{k}}-E_{n,\mathbf{k}}+\omega_2+i\eta)} \\
+ (f_m - f_n)\,\frac{a'_{n,m}(\mathbf{q})\,b'_{m,n}(\mathbf{q},\mathbf{q}_2,\mathbf{q}_1)}{(E_{n,\mathbf{k}}-E_{m,\mathbf{k}}+\omega_1+\omega_2+2i\eta)(E_{n,\mathbf{k}}-E_{m,\mathbf{k}}+\omega_2+i\eta)} \\
+ \big((\mathbf{q}_1,\omega_1)\leftrightarrow(\mathbf{q}_2,\omega_2)\big) \qquad \text{(B.5)}
\end{aligned}$$

From equation (4.30), obtained using perturbation theory, we have

$$\begin{aligned}
a'_{n,m}(\mathbf{q}) &= \langle\phi_{n,\mathbf{k}}|-i\mathbf{q}\hat{\mathbf{r}}|\phi_{m,\mathbf{k}}\rangle \\
b'_{m,p}(\mathbf{q},\mathbf{q}_2,\mathbf{q}_1) &= \langle\phi_{m,\mathbf{k}}|i(\mathbf{q}-\mathbf{q}_1)\hat{\mathbf{r}}|\phi_{p,\mathbf{k}}\rangle \\
c'_{p,n}(\mathbf{q}_1) &= \langle\phi_{p,\mathbf{k}}|i\mathbf{q}_1\hat{\mathbf{r}}|\phi_{n,\mathbf{k}}\rangle
\end{aligned} \qquad \text{(B.6)}$$

Since $\mathbf{q}=\mathbf{q}_1+\mathbf{q}_2$, we can replace $b'_{m,p}(\mathbf{q},\mathbf{q}_2,\mathbf{q}_1)$ by $c'_{m,p}(\mathbf{q}_2)$. By exchanging $(\mathbf{q}_1,\omega_1)\leftrightarrow(\mathbf{q}_2,\omega_2)$ in the last two terms and $(n\leftrightarrow p)$ in the third one, we get

$$\begin{aligned}
T_2(\mathbf{q},\mathbf{q}_1,\mathbf{q}_2,\omega_1,\omega_2) = (f_n - f_p)\,\frac{c'_{n,p}(\mathbf{q}_2)\,c'_{p,n}(\mathbf{q}_1)}{(\omega_1+\omega_2+2i\eta)(E_{n,\mathbf{k}}-E_{p,\mathbf{k}}+\omega_1+i\eta)} \\
+ (f_n - f_m)\,\frac{a'_{n,m}(\mathbf{q})\left\{c'_{m,n}(\mathbf{q}_1)-c'_{m,n}(\mathbf{q}_1)\right\}}{(E_{n,\mathbf{k}}-E_{m,\mathbf{k}}+\omega_1+\omega_2+2i\eta)(E_{n,\mathbf{k}}-E_{m,\mathbf{k}}+\omega_1+i\eta)} \\
- (f_n - f_p)\,\frac{c'_{p,n}(\mathbf{q}_1)\,c'_{n,p}(\mathbf{q}_2)}{(\omega_1+\omega_2+2i\eta)(E_{n,\mathbf{k}}-E_{p,\mathbf{k}}+\omega_1+i\eta)} \\
+ \big((\mathbf{q}_1,\omega_1)\leftrightarrow(\mathbf{q}_2,\omega_2)\big), \qquad \text{(B.7)}
\end{aligned}$$

which is zero. Therefore, the only remaining contributions is $T^{(3)}$, which we separate in different terms:

$$T^{(3)} = T^{3bnd}_{inter} + T^{3bnd}_{intra} + T^{2bnd}_{intra} + T^{2bnd}_{ene}, \qquad \text{(B.8)}$$

where T_{inter} and T_{intra} contains respectively the interband and intraband contribution and T_{ene} is similar to $T^{(2)}$ but with the first order energy correction of equation (B.4).

B.1 Three-band term

The interband term is

$$\begin{aligned}
T^{3bnd}_{inter}(\mathbf{q},\mathbf{q}_1,\mathbf{q}_2,\omega_1,\omega_2) = (f_n - f_p)\,\frac{a'_{n,m}(\mathbf{q})\,b'_{m,p}(\mathbf{q},\mathbf{q}_2,\mathbf{q}_1)\,c'_{p,n}(\mathbf{q}_1)}{(E_{n,\mathbf{k}}-E_{m,\mathbf{k}}+\omega_1+\omega_2+2i\eta)(E_{n,\mathbf{k}}-E_{p,\mathbf{k}}+\omega_1+i\eta)} \\
+ (f_m - f_p)\,\frac{a'_{n,m}(\mathbf{q})\,b'_{m,p}(\mathbf{q},\mathbf{q}_2,\mathbf{q}_1)\,c'_{p,n}(\mathbf{q}_1)}{(E_{n,\mathbf{k}}-E_{m,\mathbf{k}}+\omega_1+\omega_2+2i\eta)(E_{p,\mathbf{k}}-E_{m,\mathbf{k}}+\omega_2+i\eta)} \\
+ \big((\mathbf{q}_1,\omega_1)\leftrightarrow(\mathbf{q}_2,\omega_2)\big), \qquad \text{(B.9)}
\end{aligned}$$

which gives for LEO, using equation (B.6),

$$
\begin{aligned}
T^{3bnd}_{inter}(\hat{\mathbf{q}},\hat{\mathbf{q}}_1,\hat{\mathbf{q}}_2,\omega,0) = &-(f_n-f_p)\,\frac{\langle\phi_{n,\mathbf{k}}|i\mathbf{q}\hat{\mathbf{r}}|\phi_{m,\mathbf{k}}\rangle\,\langle\phi_{m,\mathbf{k}}|i\hat{\mathbf{q}}_2\hat{\mathbf{r}}|\phi_{p,\mathbf{k}}\rangle\,\langle\phi_{p,\mathbf{k}}|i\hat{\mathbf{q}}_1\hat{\mathbf{r}}|\phi_{n,\mathbf{k}}\rangle}{(E_{n,\mathbf{k}}-E_{m,\mathbf{k}}+\omega+i\eta)(E_{n,\mathbf{k}}-E_{p,\mathbf{k}}+\omega+i\eta)}\\
&-(f_m-f_p)\,\frac{\langle\phi_{n,\mathbf{k}}|i\mathbf{q}\hat{\mathbf{r}}|\phi_{m,\mathbf{k}}\rangle\,\langle\phi_{m,\mathbf{k}}|i\hat{\mathbf{q}}_2\hat{\mathbf{r}}|\phi_{p,\mathbf{k}}\rangle\,\langle\phi_{p,\mathbf{k}}|i\hat{\mathbf{q}}_1\hat{\mathbf{r}}|\phi_{n,\mathbf{k}}\rangle}{(E_{n,\mathbf{k}}-E_{m,\mathbf{k}}+\omega+i\eta)(E_{p,\mathbf{k}}-E_{m,\mathbf{k}})}\\
&-(f_n-f_p)\,\frac{\langle\phi_{n,\mathbf{k}}|i\mathbf{q}\hat{\mathbf{r}}|\phi_{m,\mathbf{k}}\rangle\,\langle\phi_{m,\mathbf{k}}|i\hat{\mathbf{q}}_1\hat{\mathbf{r}}|\phi_{p,\mathbf{k}}\rangle\,\langle\phi_{p,\mathbf{k}}|i\hat{\mathbf{q}}_2\hat{\mathbf{r}}|\phi_{n,\mathbf{k}}\rangle}{(E_{n,\mathbf{k}}-E_{m,\mathbf{k}}+\omega+i\eta)(E_{n,\mathbf{k}}-E_{p,\mathbf{k}})}\\
&-(f_m-f_p)\,\frac{\langle\phi_{n,\mathbf{k}}|i\mathbf{q}\hat{\mathbf{r}}|\phi_{m,\mathbf{k}}\rangle\,\langle\phi_{m,\mathbf{k}}|i\hat{\mathbf{q}}_1\hat{\mathbf{r}}|\phi_{p,\mathbf{k}}\rangle\,\langle\phi_{p,\mathbf{k}}|i\hat{\mathbf{q}}_2\hat{\mathbf{r}}|\phi_{n,\mathbf{k}}\rangle}{(E_{n,\mathbf{k}}-E_{m,\mathbf{k}}+\omega+i\eta)(E_{p,\mathbf{k}}-E_{m,\mathbf{k}}+\omega+i\eta)}
\end{aligned}
\tag{B.10}
$$

This term is the easiest to obtain since it is equivalent to replacing the matrix elements containing the exponential $e^{i\mathbf{q}_i\mathbf{r}_i}$, in equation (B.1), by its first order expansion and it is directly proportional to $\mathbf{q}\,\mathbf{q}_1\mathbf{q}_2$. The intraband contribution contains the remaining three-band term,

$$
\begin{aligned}
T^{3bnd}_{intra}(\mathbf{q},\mathbf{q}_1,\mathbf{q}_2,\omega_1,\omega_2) = &(f_n-f_p)\,\frac{\left\{b'_{n,p}(\mathbf{q},\mathbf{q}_2,\mathbf{q}_1)\,\gamma''_{p,n}(\mathbf{q}_1)+\beta''_{n,p}(\mathbf{q},\mathbf{q}_2,\mathbf{q}_1)\,c'_{p,n}(\mathbf{q}_1)\right\}}{(\omega_1+\omega_2+2i\eta)(E_{n,\mathbf{k}}-E_{p,\mathbf{k}}+\omega_1+i\eta)}\\
&+(f_n-f_m)\,\frac{\left\{a'_{n,m}(\mathbf{q})\,\gamma''_{m,n}(\mathbf{q}_1)+a''_{n,m}(\mathbf{q})\,c'_{m,n}(\mathbf{q}_1)\right\}}{(E_{n,\mathbf{k}}-E_{m,\mathbf{k}}+\omega_1+\omega_2+2i\eta)(E_{n,\mathbf{k}}-E_{m,\mathbf{k}}+\omega_1+i\eta)}\\
&+(f_n-f_p)\,\frac{\left\{b'_{n,p}(\mathbf{q},\mathbf{q}_2,\mathbf{q}_1)\,\gamma''_{p,n}(\mathbf{q}_1)+\beta''_{n,p}(\mathbf{q},\mathbf{q}_2,\mathbf{q}_1)\,c'_{p,n}(\mathbf{q}_1)\right\}}{(\omega_1+\omega_2+2i\eta)(E_{p,\mathbf{k}}-E_{n,\mathbf{k}}+\omega_2+i\eta)}\\
&+(f_m-f_n)\,\frac{\left\{a'_{n,m}(\mathbf{q})\,\beta''_{m,n}(\mathbf{q},\mathbf{q}_2,\mathbf{q}_1)+a''_{n,m}(\mathbf{q})\,b'_{m,n}(\mathbf{q},\mathbf{q}_2,\mathbf{q}_1)\right\}}{(E_{n,\mathbf{k}}-E_{m,\mathbf{k}}+\omega_1+\omega_2+2i\eta)(E_{n,\mathbf{k}}-E_{m,\mathbf{k}}+\omega_2+i\eta)}\\
&+\big((\mathbf{q}_1,\omega_1)\leftrightarrow(\mathbf{q}_2,\omega_2)\big),
\end{aligned}
\tag{B.11}
$$

where β'' and γ'' are the three-band part of b'' and c'' respectively. We replace b' elements by c' and exchange $(\mathbf{q}_1,\omega_1)\leftrightarrow(\mathbf{q}_2,\omega_2)$ in the last two terms,

$$
\begin{aligned}
T^{3bnd}_{intra}(\mathbf{q},\mathbf{q}_1,\mathbf{q}_2,\omega_1,\omega_2) = &(f_n-f_p)\,\frac{\left\{c'_{n,p}(\mathbf{q}_2)\,\gamma''_{p,n}(\mathbf{q}_1)+\beta''_{n,p}(\mathbf{q},\mathbf{q}_2,\mathbf{q}_1)\,c'_{p,n}(\mathbf{q}_1)\right\}}{(\omega_1+\omega_2+2i\eta)(E_{n,\mathbf{k}}-E_{p,\mathbf{k}}+\omega_1+i\eta)}\\
&+(f_n-f_m)\,\frac{a'_{n,m}(\mathbf{q})\left\{\gamma''_{m,n}(\mathbf{q}_1)-\beta''_{m,n}(\mathbf{q},\mathbf{q}_1,\mathbf{q}_2)\right\}}{(E_{n,\mathbf{k}}-E_{m,\mathbf{k}}+\omega_1+\omega_2+2i\eta)(E_{n,\mathbf{k}}-E_{m,\mathbf{k}}+\omega_1+i\eta)}\\
&+(f_n-f_p)\,\frac{\left\{c'_{n,p}(\mathbf{q}_1)\,\gamma''_{p,n}(\mathbf{q}_2)+\beta''_{n,p}(\mathbf{q},\mathbf{q}_1,\mathbf{q}_2)\,c'_{p,n}(\mathbf{q}_2)\right\}}{(\omega_1+\omega_2+2i\eta)(E_{p,\mathbf{k}}-E_{n,\mathbf{k}}+\omega_1+i\eta)}\\
&+\big((\mathbf{q}_1,\omega_1)\leftrightarrow(\mathbf{q}_2,\omega_2)\big).
\end{aligned}
\tag{B.12}
$$

Using equation (4.31), from perturbation theory, we get

$$
\begin{aligned}
\beta''_{m,p}(\mathbf{q},\mathbf{q}_2,\mathbf{q}_1) = &\sum_{n\notin D_p}\frac{\langle\phi_{m,\mathbf{k}}|\mathbf{q}_1\hat{\mathbf{v}}|\phi_{n,\mathbf{k}}\rangle\,\langle\phi_{n,\mathbf{k}}|\mathbf{q}_1\hat{\mathbf{v}}|\phi_{p,\mathbf{k}}\rangle}{(E_{p,\mathbf{k}}-E_{n,\mathbf{k}})(E_{p,\mathbf{k}}-E_{m,\mathbf{k}})}+\sum_{n\notin D_m}\frac{\langle\phi_{n,\mathbf{k}}|\mathbf{q}\hat{\mathbf{v}}|\phi_{p,\mathbf{k}}\rangle\,\langle\phi_{m,\mathbf{k}}|\mathbf{q}\hat{\mathbf{v}}|\phi_{n,\mathbf{k}}\rangle}{(E_{m,\mathbf{k}}-E_{n,\mathbf{k}})(E_{m,\mathbf{k}}-E_{p,\mathbf{k}})}\\
&+\sum_{n\notin D_{p,m}}\frac{\langle\phi_{n,\mathbf{k}}|\mathbf{q}_1\hat{\mathbf{v}}|\phi_{p,\mathbf{k}}\rangle}{E_{p,\mathbf{k}}-E_{n,\mathbf{k}}}\,\frac{\langle\phi_{m,\mathbf{k}}|\mathbf{q}\hat{\mathbf{v}}|\phi_{n,\mathbf{k}}\rangle}{E_{m,\mathbf{k}}-E_{n,\mathbf{k}}}\\
\gamma''_{p,n}(\mathbf{q}_1) = &\sum_{m\notin D_p}\frac{\langle\phi_{m,\mathbf{k}}|\mathbf{q}_1\hat{\mathbf{v}}|\phi_{n,\mathbf{k}}\rangle\,\langle\phi_{p,\mathbf{k}}|\mathbf{q}_1\hat{\mathbf{v}}|\phi_{m,\mathbf{k}}\rangle}{(E_{p,\mathbf{k}}-E_{m,\mathbf{k}})(E_{p,\mathbf{k}}-E_{n,\mathbf{k}})}
\end{aligned}
\tag{B.13}
$$

After some lengthy calculation and having obtained an expression proportional to $\mathbf{q}\,\mathbf{q}_1\mathbf{q}_2$, we can write for LEO,

$$
\begin{aligned}
T^{3bnd}_{intra}(\hat{\mathbf{q}},\hat{\mathbf{q}}_1,\hat{\mathbf{q}}_2,\omega,0) &= \langle\phi_{n,\mathbf{k}}|i\mathbf{q}\hat{\mathbf{r}}|\phi_{m,\mathbf{k}}\rangle\,\langle\phi_{m,\mathbf{k}}|i\hat{\mathbf{q}}_2\hat{\mathbf{r}}|\phi_{p,\mathbf{k}}\rangle\,\langle\phi_{p,\mathbf{k}}|i\hat{\mathbf{q}}_1\hat{\mathbf{r}}|\phi_{n,\mathbf{k}}\rangle \\
&\times\Bigg[\frac{(f_n-f_m)(E_{n,\mathbf{k}}-E_{p,\mathbf{k}})}{(E_{n,\mathbf{k}}-E_{m,\mathbf{k}}+\omega+i\eta)^2(E_{n,\mathbf{k}}-E_{m,\mathbf{k}})}-\frac{(f_n-f_m)(E_{p,\mathbf{k}}-E_{m,\mathbf{k}})}{(E_{n,\mathbf{k}}-E_{m,\mathbf{k}}+\omega+i\eta)(E_{n,\mathbf{k}}-E_{m,\mathbf{k}})^2} \\
&-\frac{(f_n-f_p)(E_{m,\mathbf{k}}-E_{p,\mathbf{k}})}{(E_{n,\mathbf{k}}-E_{p,\mathbf{k}}+\omega+i\eta)(E_{n,\mathbf{k}}-E_{p,\mathbf{k}})^2}+\frac{(f_n-f_p)(E_{n,\mathbf{k}}-E_{m,\mathbf{k}})}{(E_{p,\mathbf{k}}-E_{n,\mathbf{k}}+\omega+i\eta)(E_{n,\mathbf{k}}-E_{p,\mathbf{k}})^2} \\
&-\frac{(f_n-f_m)(E_{n,\mathbf{k}}-E_{p,\mathbf{k}})}{(E_{m,\mathbf{k}}-E_{n,\mathbf{k}}+\omega+i\eta)(E_{n,\mathbf{k}}-E_{m,\mathbf{k}})^2}\Bigg] \\
&+\langle\phi_{n,\mathbf{k}}|i\mathbf{q}\hat{\mathbf{r}}|\phi_{m,\mathbf{k}}\rangle\,\langle\phi_{m,\mathbf{k}}|i\hat{\mathbf{q}}_1\hat{\mathbf{r}}|\phi_{p,\mathbf{k}}\rangle\,\langle\phi_{p,\mathbf{k}}|i\hat{\mathbf{q}}_2\hat{\mathbf{r}}|\phi_{n,\mathbf{k}}\rangle\Bigg[-\frac{(f_n-f_m)(E_{p,\mathbf{k}}-E_{m,\mathbf{k}})}{(E_{n,\mathbf{k}}-E_{m,\mathbf{k}}+\omega+i\eta)^2(E_{n,\mathbf{k}}-E_{m,\mathbf{k}})} \\
&+\frac{(f_n-f_m)(E_{n,\mathbf{k}}-E_{p,\mathbf{k}})}{(E_{n,\mathbf{k}}-E_{m,\mathbf{k}}+\omega+i\eta)(E_{n,\mathbf{k}}-E_{m,\mathbf{k}})^2}+\frac{(f_n-f_p)(E_{m,\mathbf{k}}-E_{p,\mathbf{k}})}{(E_{p,\mathbf{k}}-E_{n,\mathbf{k}}+\omega+i\eta)(E_{n,\mathbf{k}}-E_{p,\mathbf{k}})^2} \\
&-\frac{(f_n-f_p)(E_{n,\mathbf{k}}-E_{m,\mathbf{k}})}{(E_{n,\mathbf{k}}-E_{p,\mathbf{k}}+\omega+i\eta)(E_{n,\mathbf{k}}-E_{p,\mathbf{k}})^2}+\frac{(f_n-f_m)(E_{n,\mathbf{k}}-E_{p,\mathbf{k}})}{(E_{n,\mathbf{k}}-E_{m,\mathbf{k}}+\omega+i\eta)(E_{n,\mathbf{k}}-E_{m,\mathbf{k}})^2}\Bigg] \qquad \text{(B.14)}
\end{aligned}
$$

B.2 Two-band term

Let us now consider the two-band contribution of the intra term,

$$
\begin{aligned}
T^{2bnd}_{intra}(\mathbf{q},\mathbf{q}_1,\mathbf{q}_2,\omega_1,\omega_2) &= (f_n-f_m)\,\frac{\left\{b'_{n,m}(\mathbf{q},\mathbf{q}_2,\mathbf{q}_1)c''_{m,n}(\mathbf{q}_1)+b''_{n,m}(\mathbf{q},\mathbf{q}_2,\mathbf{q}_1)\,c'_{m,n}(\mathbf{q}_1)\right\}}{(\omega_1+\omega_2+2i\eta)(E_{n,\mathbf{k}}-E_{m,\mathbf{k}}+\omega_1+i\eta)} \\
&+(f_n-f_m)\,\frac{a'_{n,m}(\mathbf{q})\left\{c''_{m,n}(\mathbf{q}_1)-b''_{m,n}(\mathbf{q},\mathbf{q}_1,\mathbf{q}_2)\right\}}{(E_{n,\mathbf{k}}-E_{m,\mathbf{k}}+\omega_1+\omega_2+2i\eta)(E_{n,\mathbf{k}}-E_{m,\mathbf{k}}+\omega_1+i\eta)} \\
&+(f_n-f_m)\,\frac{\left\{b'_{n,m}(\mathbf{q},\mathbf{q}_2,\mathbf{q}_1)\,c''_{m,n}(\mathbf{q}_1)+b''_{n,m}(\mathbf{q},\mathbf{q}_2,\mathbf{q}_1)\,c'_{m,n}(\mathbf{q}_1)\right\}}{(\omega_1+\omega_2+2i\eta)(E_{m,\mathbf{k}}-E_{n,\mathbf{k}}+\omega_2+i\eta)} \\
&+\big((\mathbf{q}_1,\omega_1)\leftrightarrow(\mathbf{q}_2,\omega_2)\big), \qquad \text{(B.15)}
\end{aligned}
$$

where, here, b'' and c'' only contain the two-band part:

$$
\begin{aligned}
c''_{m,n}(\mathbf{q}_1) &= \mathbf{q}_1\Delta_{nm,\mathbf{k}}\,\frac{\langle\phi_{m,\mathbf{k}}|\mathbf{q}_1\hat{\mathbf{v}}|\phi_{n,\mathbf{k}}\rangle}{(E_{m,\mathbf{k}}-E_{n,\mathbf{k}})^2}+\frac{\left\langle\phi_{m,\mathbf{k}}\right|-\frac{i}{2}\left[\mathbf{q}_1\hat{\mathbf{r}},\mathbf{q}_1\hat{\mathbf{v}}\right]\left|\phi_{n,\mathbf{k}}\right\rangle}{E_{m,\mathbf{k}}-E_{n,\mathbf{k}}}-\frac{1}{2}\sum_{m\notin D_m}\frac{\left|\langle\phi_{m,\mathbf{k}}|\mathbf{q}_1\hat{\mathbf{v}}|\phi_{m,\mathbf{k}}\rangle\right|^2}{(E_{m,\mathbf{k}}-E_{m,\mathbf{k}})^2}\,\delta_{mn} \\
b''_{m,n}(\mathbf{q},\mathbf{q}_1,\mathbf{q}_2) &= \mathbf{q}_2\Delta_{m,n,\mathbf{k}}\frac{\langle\phi_{m,\mathbf{k}}|\mathbf{q}_2\hat{\mathbf{v}}|\phi_{n,\mathbf{k}}\rangle}{(E_{n,\mathbf{k}}-E_{m,\mathbf{k}})^2}+\frac{\left\langle\phi_{m,\mathbf{k}}\right|-\frac{i}{2}\left[\mathbf{q}_2\hat{\mathbf{r}},\mathbf{q}_2\hat{\mathbf{v}}\right]\left|\phi_{n,\mathbf{k}}\right\rangle}{E_{n,\mathbf{k}}-E_{m,\mathbf{k}}}+\mathbf{q}\Delta_{nm,\mathbf{k}}\frac{\langle\phi_{m,\mathbf{k}}|\mathbf{q}\hat{\mathbf{v}}|\phi_{n,\mathbf{k}}\rangle}{(E_{m,\mathbf{k}}-E_{n,\mathbf{k}})^2} \\
&+\frac{\left\langle\phi_{m,\mathbf{k}}\right|-\frac{i}{2}\left[\mathbf{q}\hat{\mathbf{r}},\mathbf{q}\hat{\mathbf{v}}\right]\left|\phi_{n,\mathbf{k}}\right\rangle}{E_{m,\mathbf{k}}-E_{n,\mathbf{k}}}-\frac{1}{2}\sum_{m\notin D_m}\frac{\left|\langle\phi_{m,\mathbf{k}}|\mathbf{q}_2\hat{\mathbf{v}}|\phi_{n,\mathbf{k}}\rangle\right|^2}{(E_{n,\mathbf{k}}-E_{m,\mathbf{k}})^2}\,\delta_{mn}-\frac{1}{2}\sum_{m\notin D_m}\frac{\left|\langle\phi_{m,\mathbf{k}}|\mathbf{q}\hat{\mathbf{v}}|\phi_{m,\mathbf{k}}\rangle\right|^2}{(E_{m,\mathbf{k}}-E_{m,\mathbf{k}})^2}\,\delta_{mn}
\end{aligned} \qquad \text{(B.16)}
$$

with $\Delta_{nm,\mathbf{k}}=\langle\phi_{n,\mathbf{k}}|\hat{\mathbf{v}}|\phi_{n,\mathbf{k}}\rangle-\langle\phi_{m,\mathbf{k}}|\hat{\mathbf{v}}|\phi_{m,\mathbf{k}}\rangle$. These terms contain the commutator $[\hat{\mathbf{r}},\hat{\mathbf{v}}]$ that will give extra-contributions if a scissor is present. The expression for LEO is

$$
\begin{aligned}
&T^{2bnd}_{intra}(\hat{\mathbf{q}},\hat{\mathbf{q}}_1,\hat{\mathbf{q}}_2,\omega,0) = \\
&-\frac{\hat{\mathbf{q}}_1\Delta_{nm,\mathbf{k}}\,\langle\phi_{n,\mathbf{k}}|i\hat{\mathbf{q}}\hat{\mathbf{r}}|\phi_{m,\mathbf{k}}\rangle\,\langle\phi_{m,\mathbf{k}}|i\hat{\mathbf{q}}_2\hat{\mathbf{r}}|\phi_{n,\mathbf{k}}\rangle}{(E_{n,\mathbf{k}}-E_{m,\mathbf{k}}+\omega+i\eta)(E_{n,\mathbf{k}}-E_{m,\mathbf{k}})}\left[\frac{(f_n-f_m)}{(E_{n,\mathbf{k}}-E_{m,\mathbf{k}}+\omega+i\eta)}+\frac{2(f_n-f_m)}{(E_{n,\mathbf{k}}-E_{m,\mathbf{k}})}\right] \\
&-\frac{\hat{\mathbf{q}}_2\Delta_{nm,\mathbf{k}}\,\langle\phi_{n,\mathbf{k}}|i\hat{\mathbf{q}}\hat{\mathbf{r}}|\phi_{m,\mathbf{k}}\rangle\,\langle\phi_{m,\mathbf{k}}|i\hat{\mathbf{q}}_1\hat{\mathbf{r}}|\phi_{n,\mathbf{k}}\rangle}{(E_{n,\mathbf{k}}-E_{m,\mathbf{k}}+\omega+i\eta)(E_{n,\mathbf{k}}-E_{m,\mathbf{k}})}\left[\frac{(f_n-f_m)}{(E_{n,\mathbf{k}}-E_{m,\mathbf{k}}+\omega+i\eta)}+\frac{2(f_n-f_m)}{(E_{n,\mathbf{k}}-E_{m,\mathbf{k}})}\right], \qquad \text{(B.17)}
\end{aligned}
$$

which is symmetric in $(\mathbf{q}_1, \mathbf{q}_2)$. We now consider the term with the energy correction,

$$
\begin{aligned}
T^{2bnd}_{ene}(\mathbf{q},\mathbf{q}_1,\mathbf{q}_2,\omega_1,\omega_2) = (f_n - f_p)\,\frac{b'_{n,p}(\mathbf{q},\mathbf{q}_2,\mathbf{q}_1)\,c'_{p,n}(\mathbf{q}_1)\,\mathbf{q}E^{(1)}_{n,\mathbf{k}}}{(\omega_1+\omega_2+2i\eta)^2(E_{n,\mathbf{k}}-E_{p,\mathbf{k}}+\omega_1+i\eta)} \\
+ (f_n - f_p)\,\frac{b'_{n,p}(\mathbf{q},\mathbf{q}_2,\mathbf{q}_1)\,c'_{p,n}(\mathbf{q}_1)\,\mathbf{q}_1E^{(1)}_{p,\mathbf{k}}}{(\omega_1+\omega_2+2i\eta)(E_{n,\mathbf{k}}-E_{p,\mathbf{k}}+\omega_1+i\eta)^2} \\
+ \frac{(f_n - f_m)\,a'_{n,m}(\mathbf{q})\,c'_{m,n}(\mathbf{q}_1)\,\mathbf{q}E^{(1)}_{m,\mathbf{k}}}{(E_{n,\mathbf{k}}-E_{m,\mathbf{k}}+\omega_1+\omega_2+2i\eta)^2(E_{n,\mathbf{k}}-E_{m,\mathbf{k}}+\omega_1+i\eta)} \\
+ \frac{(f_n - f_m)\,a'_{n,m}(\mathbf{q})\,c'_{m,n}(\mathbf{q}_1)\,\mathbf{q}_1E^{(1)}_{m,\mathbf{k}}}{(E_{n,\mathbf{k}}-E_{m,\mathbf{k}}+\omega_1+\omega_2+2i\eta)(E_{n,\mathbf{k}}-E_{m,\mathbf{k}}+\omega_1+i\eta)^2} \\
+ \frac{(f_n - f_p)\,b'_{n,p}(\mathbf{q},\mathbf{q}_2,\mathbf{q}_1)\,c'_{p,n}(\mathbf{q}_1)\,\mathbf{q}E^{(1)}_{n,\mathbf{k}}}{(\omega_1+\omega_2+2i\eta)^2(E_{p,\mathbf{k}}-E_{n,\mathbf{k}}+\omega_2+i\eta)} \\
+ \frac{(f_n - f_p)\,b'_{n,p}(\mathbf{q},\mathbf{q}_2,\mathbf{q}_1)\,c'_{p,n}(\mathbf{q}_1)\left(\mathbf{q}\,E^{(1)}_{n,\mathbf{k}}-\mathbf{q}_1E^{(1)}_{p,\mathbf{k}}\right)}{(\omega_1+\omega_2+2i\eta)(E_{p,\mathbf{k}}-E_{n,\mathbf{k}}+\omega_2+i\eta)^2} \\
+ \frac{(f_m - f_n)\,a'_{n,m}(\mathbf{q})\,b'_{m,n}(\mathbf{q},\mathbf{q}_2,\mathbf{q}_1)\,\mathbf{q}E^{(1)}_{m,\mathbf{k}}}{(E_{n,\mathbf{k}}-E_{m,\mathbf{k}}+\omega_1+\omega_2+2i\eta)^2(E_{n,\mathbf{k}}-E_{m,\mathbf{k}}+\omega_2+i\eta)} \\
+ \frac{(f_m - f_n)\,a'_{n,m}(\mathbf{q})\,b'_{m,n}(\mathbf{q},\mathbf{q}_2,\mathbf{q}_1)\left(\mathbf{q}\,E^{(1)}_{m,\mathbf{k}}-\mathbf{q}_1E^{(1)}_{n,\mathbf{k}}\right)}{(E_{n,\mathbf{k}}-E_{m,\mathbf{k}}+\omega_1+\omega_2+2i\eta)(E_{n,\mathbf{k}}-E_{m,\mathbf{k}}+\omega_2+i\eta)^2} \\
+ \big((\mathbf{q}_1,\omega_1)\leftrightarrow(\mathbf{q}_2,\omega_2)\big), \qquad \text{(B.18)}
\end{aligned}
$$

with $\mathbf{q}E^{(1)}_{n,\mathbf{k}} = \langle\phi_{n,\mathbf{k}}|\mathbf{q}\hat{\mathbf{v}}|\phi_{n,\mathbf{k}}\rangle$. After some algebra, we get, for LEO,

$$
\begin{aligned}
T^{2bnd}_{ene}(\hat{\mathbf{q}},\hat{\mathbf{q}}_1,\hat{\mathbf{q}}_2,\omega,0) = (f_n - f_m)\,\frac{\hat{\mathbf{q}}\Delta_{nm,\mathbf{k}}\,\langle\phi_{n,\mathbf{k}}|i\hat{\mathbf{q}}_2\hat{\mathbf{r}}|\phi_{m,\mathbf{k}}\rangle\,\langle\phi_{m,\mathbf{k}}|i\hat{\mathbf{q}}_1\hat{\mathbf{r}}|\phi_{n,\mathbf{k}}\rangle}{(E_{n,\mathbf{k}}-E_{m,\mathbf{k}}+\omega+i\eta)(E_{n,\mathbf{k}}-E_{m,\mathbf{k}})^2} \\
- \hat{\mathbf{q}}_2\Delta_{nm,\mathbf{k}}\frac{\langle\phi_{n,\mathbf{k}}|i\hat{\mathbf{q}}\hat{\mathbf{r}}|\phi_{m,\mathbf{k}}\rangle\,\langle\phi_{m,\mathbf{k}}|i\hat{\mathbf{q}}_1\hat{\mathbf{r}}|\phi_{n,\mathbf{k}}\rangle}{(E_{n,\mathbf{k}}-E_{m,\mathbf{k}}+\omega+i\eta)}\left[\frac{(f_n - f_m)}{(E_{n,\mathbf{k}}-E_{m,\mathbf{k}})^2}\right. \\
\left.+\frac{(f_n - f_m)}{(E_{n,\mathbf{k}}-E_{m,\mathbf{k}}+\omega+i\eta)(E_{n,\mathbf{k}}-E_{m,\mathbf{k}})} + \frac{(f_n - f_m)}{(E_{n,\mathbf{k}}-E_{m,\mathbf{k}}+\omega+i\eta)^2}\right] \\
- (f_n - f_m)\,\frac{\hat{\mathbf{q}}_1\Delta_{nm,\mathbf{k}}\,\langle\phi_{n,\mathbf{k}}|i\hat{\mathbf{q}}\hat{\mathbf{r}}|\phi_{m,\mathbf{k}}\rangle\,\langle\phi_{m,\mathbf{k}}|i\hat{\mathbf{q}}_2\hat{\mathbf{r}}|\phi_{n,\mathbf{k}}\rangle}{(E_{n,\mathbf{k}}-E_{m,\mathbf{k}}+\omega+i\eta)(E_{n,\mathbf{k}}-E_{m,\mathbf{k}})^2} \qquad \text{(B.19)}
\end{aligned}
$$

The two-band terms containing a square or cube in the denominator of the type $(E_{n,\mathbf{k}}-E_{m,\mathbf{k}}+\omega+i\eta)^2$ are recast using equation (4.32). For instance, let us consider the following term

$$
I^a = (f_n - f_m)\,\frac{\mathbf{q}_2\Delta_{nm,\mathbf{k}}\,\langle\phi_{n,\mathbf{k}}|\mathbf{q}\hat{\mathbf{v}}|\phi_{m,\mathbf{k}}\rangle\,\langle\phi_{m,\mathbf{k}}|\mathbf{q}_1\hat{\mathbf{v}}|\phi_{n,\mathbf{k}}\rangle}{(E_{n,\mathbf{k}}-E_{m,\mathbf{k}}+\omega+i\eta)^2(E_{n,\mathbf{k}}-E_{m,\mathbf{k}})^3}. \qquad \text{(B.20)}
$$

Using equation (4.32) and the relation on the derivative $fg' = [fg]' - f'g$, we get

$$
\begin{aligned}
I^a = -\mathbf{q}_2\frac{\partial}{\partial\mathbf{k}}(f_n - f_m)\,\frac{\langle\phi_{n,\mathbf{k}}|\mathbf{q}\hat{\mathbf{v}}|\phi_{m,\mathbf{k}}\rangle\,\langle\phi_{m,\mathbf{k}}|\mathbf{q}_1\hat{\mathbf{v}}|\phi_{n,\mathbf{k}}\rangle}{(E_{n,\mathbf{k}}-E_{m,\mathbf{k}}+\omega+i\eta)(E_{n,\mathbf{k}}-E_{m,\mathbf{k}})^3} \\
+ \frac{1}{(E_{n,\mathbf{k}}-E_{m,\mathbf{k}}+\omega+i\eta)}\mathbf{q}_2\frac{\partial}{\partial\mathbf{k}}(f_n - f_m)\,\frac{\langle\phi_{n,\mathbf{k}}|\mathbf{q}\hat{\mathbf{v}}|\phi_{m,\mathbf{k}}\rangle\,\langle\phi_{m,\mathbf{k}}|\mathbf{q}_1\hat{\mathbf{v}}|\phi_{n,\mathbf{k}}\rangle}{(E_{n,\mathbf{k}}-E_{m,\mathbf{k}})^3} \qquad \text{(B.21)}
\end{aligned}
$$

The first term of (B.21) corresponds to the gradient of a function periodic throughout the BZ. Therefore the sum over $\mathbf{k}$ of this term is zero. From the $\mathbf{k}\cdot\mathbf{p}$ perturbation theory, we know the derivative of the

velocity operator to be

$$\mathbf{q}\frac{\partial}{\partial \mathbf{k}}\langle\phi_{n,\mathbf{k}}|\mathbf{q}_1\hat{\mathbf{v}}|\phi_{m,\mathbf{k}}\rangle = -\langle\phi_{n,\mathbf{k}}|[i\mathbf{q}\hat{\mathbf{r}},\mathbf{q}_1\hat{\mathbf{v}}]|\phi_{m,\mathbf{k}}\rangle - \frac{\mathbf{q}_1\Delta_{nm,\mathbf{k}}\langle\phi_{n,\mathbf{k}}|\mathbf{q}\hat{\mathbf{v}}|\phi_{m,\mathbf{k}}\rangle}{E_{n,\mathbf{k}}-E_{m,\mathbf{k}}} + \sum_{p\notin D_n,D_m}\left[\frac{\langle\phi_{n,\mathbf{k}}|\mathbf{q}_1\hat{\mathbf{v}}|\phi_{p,\mathbf{k}}\rangle\langle\phi_{p,\mathbf{k}}|\mathbf{q}\hat{\mathbf{v}}|\phi_{m,\mathbf{k}}\rangle}{E_{m,\mathbf{k}}-E_{p,\mathbf{k}}} + \frac{\langle\phi_{n,\mathbf{k}}|\mathbf{q}\hat{\mathbf{v}}|\phi_{p,\mathbf{k}}\rangle\langle\phi_{p,\mathbf{k}}|\mathbf{q}_1\hat{\mathbf{v}}|\phi_{m,\mathbf{k}}\rangle}{E_{n,\mathbf{k}}-E_{p,\mathbf{k}}}\right], \quad \text{(B.22)}$$

which contains the commutator $[\hat{\mathbf{r}},\hat{\mathbf{v}}]$ that will also give extra-contributions when applying a scissor operator on the Hamiltonian. From equation (B.21) and (B.22), we obtain a new two-band term

$$\begin{aligned} I^{a,2bnd} = 3(f_n-f_m)&\frac{\mathbf{q}_2\Delta_{nm,\mathbf{k}}\langle\phi_{n,\mathbf{k}}|i\mathbf{q}\hat{\mathbf{r}}|\phi_{m,\mathbf{k}}\rangle\langle\phi_{m,\mathbf{k}}|i\mathbf{q}_1\hat{\mathbf{r}}|\phi_{n,\mathbf{k}}\rangle}{(E_{n,\mathbf{k}}-E_{m,\mathbf{k}}+\omega+i\eta)(E_{n,\mathbf{k}}-E_{m,\mathbf{k}})^2} \\ &+(f_n-f_m)\frac{\mathbf{q}\Delta_{nm,\mathbf{k}}\langle\phi_{n,\mathbf{k}}|i\mathbf{q}_2\hat{\mathbf{r}}|\phi_{m,\mathbf{k}}\rangle\langle\phi_{m,\mathbf{k}}|i\mathbf{q}_1\hat{\mathbf{r}}|\phi_{n,\mathbf{k}}\rangle}{(E_{n,\mathbf{k}}-E_{m,\mathbf{k}}+\omega+i\eta)(E_{n,\mathbf{k}}-E_{m,\mathbf{k}})^2} \\ &+(f_n-f_m)\frac{\mathbf{q}_1\Delta_{nm,\mathbf{k}}\langle\phi_{n,\mathbf{k}}|i\mathbf{q}\hat{\mathbf{r}}|\phi_{m,\mathbf{k}}\rangle\langle\phi_{m,\mathbf{k}}|i\mathbf{q}_2\hat{\mathbf{r}}|\phi_{n,\mathbf{k}}\rangle}{(E_{n,\mathbf{k}}-E_{m,\mathbf{k}}+\omega+i\eta)(E_{n,\mathbf{k}}-E_{m,\mathbf{k}})^2}, \end{aligned} \quad \text{(B.23)}$$

and a new three-band contribution

$$\begin{aligned} I^{a,3bnd} = &(f_n-f_p)\frac{\langle\phi_{n,\mathbf{k}}|i\mathbf{q}\hat{\mathbf{r}}|\phi_{m,\mathbf{k}}\rangle\langle\phi_{m,\mathbf{k}}|i\mathbf{q}_2\hat{\mathbf{r}}|\phi_{p,\mathbf{k}}\rangle\langle\phi_{p,\mathbf{k}}|i\mathbf{q}_1\hat{\mathbf{r}}|\phi_{n,\mathbf{k}}\rangle(E_{n,\mathbf{k}}-E_{m,\mathbf{k}})}{(E_{n,\mathbf{k}}-E_{p,\mathbf{k}}+\omega+i\eta)(E_{n,\mathbf{k}}-E_{p,\mathbf{k}})^2} \\ &-(f_p-f_m)\frac{\langle\phi_{n,\mathbf{k}}|i\mathbf{q}\hat{\mathbf{r}}|\phi_{m,\mathbf{k}}\rangle\langle\phi_{m,\mathbf{k}}|i\mathbf{q}_1\hat{\mathbf{r}}|\phi_{p,\mathbf{k}}\rangle\langle\phi_{p,\mathbf{k}}|i\mathbf{q}_2\hat{\mathbf{r}}|\phi_{n,\mathbf{k}}\rangle(E_{n,\mathbf{k}}-E_{m,\mathbf{k}})}{(E_{p,\mathbf{k}}-E_{m,\mathbf{k}}+\omega+i\eta)(E_{p,\mathbf{k}}-E_{m,\mathbf{k}})^2} \\ &+(f_n-f_m)\frac{\langle\phi_{n,\mathbf{k}}|i\mathbf{q}\hat{\mathbf{r}}|\phi_{m,\mathbf{k}}\rangle\langle\phi_{m,\mathbf{k}}|i\mathbf{q}_1\hat{\mathbf{r}}|\phi_{p,\mathbf{k}}\rangle\langle\phi_{p,\mathbf{k}}|i\mathbf{q}_2\hat{\mathbf{r}}|\phi_{n,\mathbf{k}}\rangle(E_{p,\mathbf{k}}-E_{m,\mathbf{k}})}{(E_{n,\mathbf{k}}-E_{m,\mathbf{k}}+\omega+i\eta)(E_{n,\mathbf{k}}-E_{m,\mathbf{k}})^2} \\ &-(f_n-f_m)\frac{\langle\phi_{n,\mathbf{k}}|i\mathbf{q}\hat{\mathbf{r}}|\phi_{m,\mathbf{k}}\rangle\langle\phi_{m,\mathbf{k}}|i\mathbf{q}_2\hat{\mathbf{r}}|\phi_{p,\mathbf{k}}\rangle\langle\phi_{p,\mathbf{k}}|i\mathbf{q}_1\hat{\mathbf{r}}|\phi_{n,\mathbf{k}}\rangle(E_{n,\mathbf{k}}-E_{p,\mathbf{k}})}{(E_{n,\mathbf{k}}-E_{m,\mathbf{k}}+\omega+i\eta)(E_{n,\mathbf{k}}-E_{m,\mathbf{k}})^2} \end{aligned} \quad \text{(B.24)}$$

At this point, assembling all the terms will give us the same expression as the one obtained in the calculation carried out using the current density, in equation (C.18). Continuing this development for all the problematic two-band terms will lead to equation (4.33).

B.3 Scissor

The addition of a scissor means that we need to reconsider all the terms that contained the commutator $[\hat{\mathbf{r}},\hat{\mathbf{v}}]$ and were, so far, neglected. For the second-order calculation, it means looking at the commutator terms in b'' and c'' that intervened in T^{2bnd}_{intra} and the one appearing in the derivative of the matrix elements, shown in equation (B.22). For the remaining part of the formula, the energies are replaced by scissored energies and there is no change in the matrix elements since only the ones of the position operator and the diagonal ones of the velocity operator appeared in the final form of the expression.

To express the scissored commutator, we use the equivalence in the matrix elements of $\hat{\mathbf{r}}$, written in equation (4.36), which leads to an equivalence in its derivative:

$$\mathbf{q}_1\frac{\partial}{\partial\mathbf{k}}\langle\phi_{n,\mathbf{k}}|i\mathbf{q}_2\hat{\mathbf{r}}|\phi_{m,\mathbf{k}}\rangle = \mathbf{q}_1\frac{\partial}{\partial\mathbf{k}}\frac{\langle\phi_{n,\mathbf{k}}|\mathbf{q}_2\hat{\mathbf{v}}^{\Sigma}|\phi_{m,\mathbf{k}}\rangle}{E^{\Sigma}_{n,\mathbf{k}}-E^{\Sigma}_{m,\mathbf{k}}} = \mathbf{q}_1\frac{\partial}{\partial\mathbf{k}}\frac{\langle\phi_{n,\mathbf{k}}|\mathbf{q}_2\hat{\mathbf{v}}|\phi_{m,\mathbf{k}}\rangle}{E_{n,\mathbf{k}}-E_{m,\mathbf{k}}}, \quad \text{(B.25)}$$

with

$$\mathbf{q}_1 \frac{\partial}{\partial \mathbf{k}} \frac{\langle \phi_{n,\mathbf{k}} | \mathbf{q}_2 \hat{\mathbf{v}}^{\Sigma} | \phi_{m,\mathbf{k}} \rangle}{E^{\Sigma}_{n,\mathbf{k}} - E^{\Sigma}_{m,\mathbf{k}}} = -\mathbf{q}_1 \Delta_{nm,\mathbf{k}} \frac{\langle \phi_{n,\mathbf{k}} | i\mathbf{q}_2 \hat{\mathbf{r}} | \phi_{m,\mathbf{k}} \rangle}{E^{\Sigma}_{n,\mathbf{k}} - E^{\Sigma}_{m,\mathbf{k}}} - \mathbf{q}_2 \Delta_{nm,\mathbf{k}} \frac{\langle \phi_{n,\mathbf{k}} | i\mathbf{q}_1 \hat{\mathbf{r}} | \phi_{m,\mathbf{k}} \rangle}{E^{\Sigma}_{n,\mathbf{k}} - E^{\Sigma}_{m,\mathbf{k}}}$$
$$- \frac{\langle \phi_{n,\mathbf{k}} | \left[i\mathbf{q}_1 \hat{\mathbf{r}}, \mathbf{q}_2 \hat{\mathbf{v}}^{\Sigma} \right] | \phi_{m,\mathbf{k}} \rangle}{E^{\Sigma}_{n,\mathbf{k}} - E^{\Sigma}_{m,\mathbf{k}}} - \sum_{p \notin D_n, D_m} \langle \phi_{n,\mathbf{k}} | i\mathbf{q}_2 \hat{\mathbf{r}} | \phi_{p,\mathbf{k}} \rangle \langle \phi_{p,\mathbf{k}} | i\mathbf{q}_1 \hat{\mathbf{r}} | \phi_{m,\mathbf{k}} \rangle \frac{E^{\Sigma}_{n,\mathbf{k}} - E^{\Sigma}_{p,\mathbf{k}}}{E^{\Sigma}_{n,\mathbf{k}} - E^{\Sigma}_{m,\mathbf{k}}}$$
$$+ \sum_{p \notin D_n, D_m} \langle \phi_{n,\mathbf{k}} | i\mathbf{q}_1 \hat{\mathbf{r}} | \phi_{p,\mathbf{k}} \rangle \langle \phi_{p,\mathbf{k}} | i\mathbf{q}_2 \hat{\mathbf{r}} | \phi_{m,\mathbf{k}} \rangle \frac{E^{\Sigma}_{p,\mathbf{k}} - E^{\Sigma}_{m,\mathbf{k}}}{E^{\Sigma}_{n,\mathbf{k}} - E^{\Sigma}_{m,\mathbf{k}}} \quad \text{(B.26)}$$

From equation (B.25) and (B.26), we get an expression for the scissored commutator that only depends on elements of $\hat{\mathbf{r}}$ that we know how to evaluate and not of $\hat{\mathbf{v}}^{\Sigma}$,

$$\langle \phi_{n,\mathbf{k}} | \left[i\mathbf{q}_1 \hat{\mathbf{r}}, \mathbf{q}_2 \hat{\mathbf{v}}^{\Sigma} \right] | \phi_{m,\mathbf{k}} \rangle = -\mathbf{q}_1 \Delta_{nm,\mathbf{k}} \langle \phi_{n,\mathbf{k}} | i\mathbf{q}_2 \hat{\mathbf{r}} | \phi_{m,\mathbf{k}} \rangle - \mathbf{q}_2 \Delta_{nm,\mathbf{k}} \langle \phi_{n,\mathbf{k}} | i\mathbf{q}_1 \hat{\mathbf{r}} | \phi_{m,\mathbf{k}} \rangle$$
$$- \sum_{p \notin D_n, D_m} \langle \phi_{n,\mathbf{k}} | i\mathbf{q}_2 \hat{\mathbf{r}} | \phi_{p,\mathbf{k}} \rangle \langle \phi_{p,\mathbf{k}} | i\mathbf{q}_1 \hat{\mathbf{r}} | \phi_{m,\mathbf{k}} \rangle (E^{\Sigma}_{n,\mathbf{k}} - E^{\Sigma}_{p,\mathbf{k}})$$
$$+ \sum_{p \notin D_n, D_m} \langle \phi_{n,\mathbf{k}} | i\mathbf{q}_1 \hat{\mathbf{r}} | \phi_{p,\mathbf{k}} \rangle \langle \phi_{p,\mathbf{k}} | i\mathbf{q}_2 \hat{\mathbf{r}} | \phi_{m,\mathbf{k}} \rangle (E^{\Sigma}_{p,\mathbf{k}} - E^{\Sigma}_{m,\mathbf{k}})$$
$$+ \mathbf{q}_1 \Delta_{nm,\mathbf{k}} \langle \phi_{n,\mathbf{k}} | i\mathbf{q}_2 \hat{\mathbf{r}} | \phi_{m,\mathbf{k}} \rangle \frac{E^{\Sigma}_{n,\mathbf{k}} - E^{\Sigma}_{m,\mathbf{k}}}{E_{n,\mathbf{k}} - E_{m,\mathbf{k}}} + \mathbf{q}_2 \Delta_{nm,\mathbf{k}} \langle \phi_{n,\mathbf{k}} | i\mathbf{q}_1 \hat{\mathbf{r}} | \phi_{m,\mathbf{k}} \rangle \frac{E^{\Sigma}_{n,\mathbf{k}} - E^{\Sigma}_{m,\mathbf{k}}}{E_{n,\mathbf{k}} - E_{m,\mathbf{k}}}$$
$$+ \delta_{nm} \frac{E^{\Sigma}_{n,\mathbf{k}} - E^{\Sigma}_{m,\mathbf{k}}}{E_{n,\mathbf{k}} - E_{m,\mathbf{k}}} + \sum_{p \notin D_n, D_m} \langle \phi_{n,\mathbf{k}} | i\mathbf{q}_2 \hat{\mathbf{r}} | \phi_{p,\mathbf{k}} \rangle \langle \phi_{p,\mathbf{k}} | i\mathbf{q}_1 \hat{\mathbf{r}} | \phi_{m,\mathbf{k}} \rangle \frac{(E^{\Sigma}_{n,\mathbf{k}} - E^{\Sigma}_{m,\mathbf{k}})(E_{n,\mathbf{k}} - E_{p,\mathbf{k}})}{E_{n,\mathbf{k}} - E_{m,\mathbf{k}}}$$
$$- \sum_{p \notin D_n, D_m} \langle \phi_{n,\mathbf{k}} | i\mathbf{q}_1 \hat{\mathbf{r}} | \phi_{p,\mathbf{k}} \rangle \langle \phi_{p,\mathbf{k}} | i\mathbf{q}_2 \hat{\mathbf{r}} | \phi_{m,\mathbf{k}} \rangle \frac{(E^{\Sigma}_{n,\mathbf{k}} - E^{\Sigma}_{m,\mathbf{k}})(E_{p,\mathbf{k}} - E_{m,\mathbf{k}})}{E_{n,\mathbf{k}} - E_{m,\mathbf{k}}} \quad \text{(B.27)}$$

Using equation (B.27) to replace all the mentioned commutators and, after some algebra, we obtain the final equation (4.39) and (4.38) for the three- and two-band term.

Appendix C

LEO: current density calculation

The general formula for the second-order density response function obtained from the current is

$$\begin{aligned}
\chi_{\rho\rho\rho}(\mathbf{q},\mathbf{q}_1,\mathbf{q}_2,\omega_1,\omega_2) &= \frac{1}{V}\sum_{\mathbf{k}}\sum_{n,m,p}\frac{1}{\omega\omega_1\omega_2}\frac{\langle\phi_{n,\mathbf{k}}|\mathbf{q}\hat{\mathbf{v}}|\phi_{m,\mathbf{k}}\rangle}{E_{n,\mathbf{k}}-E_{m,\mathbf{k}}+\omega_1+\omega_2+2i\eta}\\
&\times\Bigg[\langle\phi_{m,\mathbf{k}}|\mathbf{q}_1\hat{\mathbf{v}}|\phi_{p,\mathbf{k}}\rangle\langle\phi_{p,\mathbf{k}}|\mathbf{q}_2\hat{\mathbf{v}}|\phi_{n,\mathbf{k}}\rangle\left(\frac{f_{n,\mathbf{k}}-f_{p,\mathbf{k}}}{E_{n,\mathbf{k}}-E_{p,\mathbf{k}}+\omega_2+i\eta}+\frac{f_{m,\mathbf{k}}-f_{p,\mathbf{k}}}{E_{p,\mathbf{k}}-E_{m,\mathbf{k}}+\omega_1+i\eta}\right)\\
&+\langle\phi_{m,\mathbf{k}}|\mathbf{q}_2\hat{\mathbf{v}}|\phi_{p,\mathbf{k}}\rangle\langle\phi_{p,\mathbf{k}}|\mathbf{q}_1\hat{\mathbf{v}}|\phi_{n,\mathbf{k}}\rangle\left(\frac{f_{n,\mathbf{k}}-f_{p,\mathbf{k}}}{E_{n,\mathbf{k}}-E_{p,\mathbf{k}}+\omega_1+i\eta}+\frac{f_{m,\mathbf{k}}-f_{p,\mathbf{k}}}{E_{p,\mathbf{k}}-E_{m,\mathbf{k}}+\omega_2+i\eta}\right)\Bigg]\\
&-\frac{1}{2V}\frac{1}{\omega\omega_1\omega_2}\sum_{\mathbf{k}}\sum_{n,m}(f_{n,\mathbf{k}}-f_{m,\mathbf{k}})\frac{\langle\phi_{n,\mathbf{k}}|\mathbf{q}\hat{\mathbf{v}}|\phi_{m,\mathbf{k}}\rangle}{E_{n,\mathbf{k}}-E_{m,\mathbf{k}}+\omega_1+\omega_2+2i\eta}\\
&\times\Big(\langle\phi_{m,\mathbf{k}}|[i\mathbf{q}_1\hat{\mathbf{r}},\mathbf{q}_2\hat{\mathbf{v}}]|\phi_{n,\mathbf{k}}\rangle+\langle\phi_{m,\mathbf{k}}|[i\mathbf{q}_2\hat{\mathbf{r}},\mathbf{q}_1\hat{\mathbf{v}}]|\phi_{n,\mathbf{k}}\rangle\Big)\\
&-\frac{1}{V}\frac{1}{\omega\omega_1\omega_2}\sum_{\mathbf{k}}\sum_{n,m}(f_{n,\mathbf{k}}-f_{m,\mathbf{k}})\Bigg[\frac{\langle\phi_{m,\mathbf{k}}|\mathbf{q}_1\hat{\mathbf{v}}|\phi_{n,\mathbf{k}}\rangle\langle\phi_{n,\mathbf{k}}|[i\mathbf{q}\hat{\mathbf{r}},\mathbf{q}_2\hat{\mathbf{v}}]|\phi_{m,\mathbf{k}}\rangle}{E_{n,\mathbf{k}}-E_{m,\mathbf{k}}+\omega_1+i\eta}\\
&+\frac{\langle\phi_{m,\mathbf{k}}|\mathbf{q}_2\hat{\mathbf{v}}|\phi_{n,\mathbf{k}}\rangle\langle\phi_{n,\mathbf{k}}|[i\mathbf{q}\hat{\mathbf{r}},\mathbf{q}_1\hat{\mathbf{v}}]|\phi_{m,\mathbf{k}}\rangle}{E_{n,\mathbf{k}}-E_{m,\mathbf{k}}+\omega_2+i\eta}\Bigg]\\
&-\frac{1}{2V}\frac{1}{\omega\omega_1\omega_2}\sum_{\mathbf{k}}\sum_{n}f_{n,\mathbf{k}}\Big(\langle\phi_{n,\mathbf{k}}|[\mathbf{q}\hat{\mathbf{r}},[\mathbf{q}_1\hat{\mathbf{r}},\mathbf{q}_2\hat{\mathbf{v}}]]|\phi_{n,\mathbf{k}}\rangle+\langle\phi_{n,\mathbf{k}}|[\mathbf{q}\hat{\mathbf{r}},[\mathbf{q}_2\hat{\mathbf{r}},\mathbf{q}_1\hat{\mathbf{v}}]]|\phi_{n,\mathbf{k}}\rangle\Big)
\end{aligned}\tag{C.1}$$

Here the permutation $\big((\mathbf{q}_1,\omega_1)\leftrightarrow(\mathbf{q}_2,\omega_2)\big)$ is already included in the formula. If there is no scissor, we can neglect the terms containing commutator since we neglect the double commutators $[i\mathbf{q}_1\hat{\mathbf{r}},[i\hat{\mathbf{r}},\hat{V}_{nl}]]$ coming from the definition of the velocity operator $\hat{\mathbf{v}}=\hat{\mathbf{p}}-i[\hat{\mathbf{r}},\hat{V}_{nl}]$ and, for the momentum operator, we have the relation

$$\begin{cases}\langle\phi_{n,\mathbf{k}}|[i\mathbf{q}_1\hat{\mathbf{r}},\mathbf{q}_2\hat{\mathbf{p}}]|\phi_{m,\mathbf{k}}\rangle=-\mathbf{q}_2\mathbf{q}_1\delta_{nm}\\ \langle\phi_{n,\mathbf{k}}|[\mathbf{q}\hat{\mathbf{r}},[\mathbf{q}_1\hat{\mathbf{r}},\mathbf{q}_2\hat{\mathbf{p}}]]|\phi_{n,\mathbf{k}}\rangle=0\end{cases},\tag{C.2}$$

which is canceled with the difference in occupation numbers $(f_{n,\mathbf{k}}-f_{m,\mathbf{k}})$. The formula then becomes

$$\begin{aligned}
\chi_{\rho\rho\rho}(\mathbf{q},\mathbf{q}_1,\mathbf{q}_2,\omega_1,\omega_2) &= \frac{1}{V}\sum_{\mathbf{k}}\sum_{n,m,p}\frac{1}{\omega\omega_1\omega_2}\frac{\hat{\mathbf{v}}_{nm}(\mathbf{q})}{E_{nm,\mathbf{k}}+\tilde{\omega}_1+\tilde{\omega}_2}\\
\times\Bigg[\hat{\mathbf{v}}_{mp}(\mathbf{q}_1)\hat{\mathbf{v}}_{pn}(\mathbf{q}_2)&\left(\frac{f_{np,\mathbf{k}}}{E_{np,\mathbf{k}}+\tilde{\omega}_2}+\frac{f_{mp,\mathbf{k}}}{E_{pm,\mathbf{k}}+\tilde{\omega}_1}\right)+\hat{\mathbf{v}}_{mp}(\mathbf{q}_2)\hat{\mathbf{v}}_{pn}(\mathbf{q}_1)\left(\frac{f_{np,\mathbf{k}}}{E_{np,\mathbf{k}}+\tilde{\omega}_1}+\frac{f_{mp,\mathbf{k}}}{E_{pm,\mathbf{k}}+\tilde{\omega}_2}\right)\Bigg],
\end{aligned}\tag{C.3}$$

using the short notation of equation (4.34). For LEO, we want to set $\omega_2 = 0$, so we first need to remove the divergence in ω_2, which is done using the relation

$$\lim_{\omega_2 \to 0} \chi^{(3)}(\omega_1, \omega_2) = \lim_{\omega_2 \to 0} \frac{1}{2} \left[\chi^{(3)}(\omega_1, \omega_2) + \chi^{(3)}(\omega_1, -\omega_2) \right]. \tag{C.4}$$

We then obtain the following ω-divergent LEO expression:

$$\begin{aligned}
\chi_0^{2bnd}(\hat{\mathbf{q}}, \hat{\mathbf{q}}_1, \hat{\mathbf{q}}_2, \omega, 0) = \frac{1}{V} \sum_{\mathbf{k}} \sum_{n,m,p} \Bigg[& -\frac{1}{\omega^3} \hat{\mathbf{v}}_{nm,\mathbf{k}}(\hat{\mathbf{q}}) \hat{\mathbf{v}}_{mp,\mathbf{k}}(\hat{\mathbf{q}}_1) \hat{\mathbf{v}}_{pn,\mathbf{k}}(\hat{\mathbf{q}}_2) \Bigg(\frac{\omega f_{np}}{(E_{nm,\mathbf{k}} + \tilde{\omega})^2 E_{np,\mathbf{k}}} \\
& + \frac{\omega f_{np}}{(E_{nm,\mathbf{k}} + \tilde{\omega}) E_{np,\mathbf{k}}^2} + \frac{\omega f_{mp}}{(E_{nm,\mathbf{k}} + \tilde{\omega})^2 (E_{pm,\mathbf{k}} + \tilde{\omega})} + \frac{f_{np}}{(E_{nm,\mathbf{k}} + \tilde{\omega}) E_{np,\mathbf{k}}} \\
& + \frac{f_{mp}}{(E_{nm,\mathbf{k}} + \tilde{\omega})(E_{pm,\mathbf{k}} + \tilde{\omega})} \Bigg) \\
& - \frac{1}{\omega^3} \hat{\mathbf{v}}_{nm,\mathbf{k}}(\hat{\mathbf{q}}) \, \hat{\mathbf{v}}_{mp,\mathbf{k}}(\hat{\mathbf{q}}_2) \, \hat{\mathbf{v}}_{pn,\mathbf{k}}(\hat{\mathbf{q}}_1) \Bigg(\frac{\omega f_{np}}{(E_{nm,\mathbf{k}} + \tilde{\omega})^2 (E_{np,\mathbf{k}} + \tilde{\omega})} + \frac{\omega f_{mp}}{(E_{nm,\mathbf{k}} + \tilde{\omega})^2 E_{pm,\mathbf{k}}} \\
& + \frac{\omega f_{mp}}{(E_{nm,\mathbf{k}} + \tilde{\omega}) E_{pm,\mathbf{k}}^2} + \frac{f_{np}}{(E_{nm,\mathbf{k}} + \tilde{\omega})(E_{np,\mathbf{k}} + \tilde{\omega})} + \frac{f_{mp}}{(E_{nm,\mathbf{k}} + \tilde{\omega}) E_{pm,\mathbf{k}}} \Bigg) \Bigg]
\end{aligned} \tag{C.5}$$

The spectrum obtained from this ω-divergent formula is then compared (in Figure C.1) with the spectrum from the divergence-free formula in the density calculation since they should be similar at high energies. There is a perfect agreement above the band-gap region and the effect of the divergence is

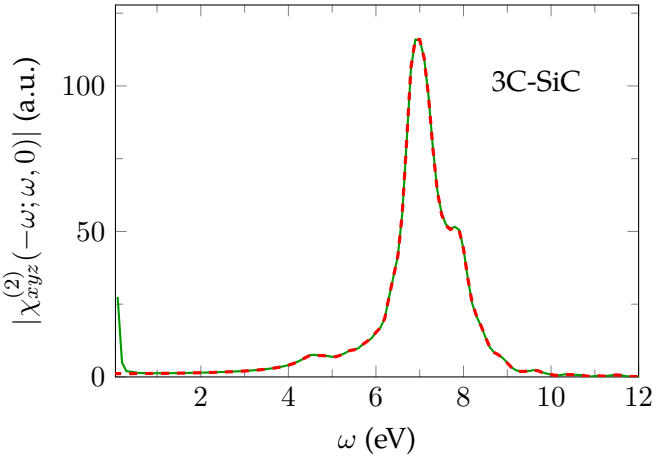

Figure C.1: LEO spectra of cubic silicon carbide (3C-SiC) generated from the ω-divergent formula (equation (C.5), green curve) and the divergence-free formula (equation (4.33), red dashed curve).

only visible at very small frequency in a similar fashion as SHG (see 2nd row of Figure 4.9).

To get rid of the remaining divergence, we decompose f_1 and f_2, defined as

$$\chi_0^{(2)}(\hat{\mathbf{q}}, \hat{\mathbf{q}}_1, \hat{\mathbf{q}}_2, \omega, 0) = \frac{1}{V} \sum_{\mathbf{k}} \sum_{n,m,p} \frac{1}{\omega^3} \hat{\mathbf{v}}_{nm}(\hat{\mathbf{q}}) \Big[\hat{\mathbf{v}}_{mp}(\hat{\mathbf{q}}_1) \hat{\mathbf{v}}_{pn}(\hat{\mathbf{q}}_2) f_1(\omega, 0) + \hat{\mathbf{v}}_{mp}(\hat{\mathbf{q}}_2) \hat{\mathbf{v}}_{pn}(\hat{\mathbf{q}}_1) f_2(0, \omega) \Big] \tag{C.6}$$

with

$$\begin{cases} f_1(\omega, 0) = \mathcal{A}_1 + \omega \mathcal{B}_1 + \omega^2 \mathcal{C}_1 + \omega^3 \mathcal{F}_1(\omega) \\ f_2(0, \omega) = \mathcal{A}_2 + \omega \mathcal{B}_2 + \omega^2 \mathcal{C}_2 + \omega^3 \mathcal{F}_2(\omega) \end{cases}, \tag{C.7}$$

where $\mathcal{A}$ corresponds to $f(0,0)$ and $\mathcal{B}$ and $\mathcal{C}$ are the first and second derivative of f with respect to ω, taken at $\omega = 0$:

$$\mathcal{A}_1 = -\frac{f_{np}}{E_{nm,\mathbf{k}}E_{np,\mathbf{k}}} - \frac{f_{mp}}{E_{nm,\mathbf{k}}E_{pm,\mathbf{k}}}; \qquad \mathcal{A}_2 = -\frac{f_{np}}{E_{nm,\mathbf{k}}E_{np,\mathbf{k}}} - \frac{f_{mp}}{E_{nm,\mathbf{k}}E_{pm,\mathbf{k}}} \tag{C.8a}$$

$$\mathcal{B}_1 = -\frac{f_{np}}{E_{nm,\mathbf{k}}E_{np,\mathbf{k}}^2} + \frac{f_{mp}}{E_{nm,\mathbf{k}}E_{pm,\mathbf{k}}^2}; \qquad \mathcal{B}_2 = \frac{f_{np}}{E_{nm,\mathbf{k}}E_{np,\mathbf{k}}^2} - \frac{f_{mp}}{E_{nm,\mathbf{k}}E_{pm,\mathbf{k}}^2} \tag{C.8b}$$

$$\begin{aligned}\mathcal{C}_1 &= \frac{f_{np}}{E_{nm,\mathbf{k}}E_{np,\mathbf{k}}}\left(\frac{1}{E_{nm,\mathbf{k}}E_{np,\mathbf{k}}} + \frac{1}{E_{nm,\mathbf{k}}^2}\right) + \frac{f_{mp}}{E_{nm,\mathbf{k}}E_{pm,\mathbf{k}}}\left(-\frac{1}{E_{pm,\mathbf{k}}^2} + \frac{1}{E_{nm,\mathbf{k}}^2}\right); \\ \mathcal{C}_2 &= \frac{f_{np}}{E_{nm,\mathbf{k}}E_{np,\mathbf{k}}}\left(-\frac{1}{E_{np,\mathbf{k}}^2} + \frac{1}{E_{nm,\mathbf{k}}^2}\right) + \frac{f_{mp}}{E_{nm,\mathbf{k}}E_{pm,\mathbf{k}}}\left(\frac{1}{E_{nm,\mathbf{k}}E_{pm,\mathbf{k}}} + \frac{1}{E_{nm,\mathbf{k}}^2}\right)\end{aligned} \tag{C.8c}$$

$$\begin{aligned}\mathcal{F}_1(\omega) = &-\frac{f_{nm}}{(E_{nm,\mathbf{k}}+\tilde{\omega})E_{nm,\mathbf{k}}^2E_{np,\mathbf{k}}}\left(\frac{1}{E_{np,\mathbf{k}}} + \frac{1}{E_{nm,\mathbf{k}}}\right) - \frac{f_{nm}}{(E_{nm,\mathbf{k}}+\tilde{\omega})^2E_{nm,\mathbf{k}}^2E_{np,\mathbf{k}}} \\ &+ \frac{f_{mp}}{(E_{pm,\mathbf{k}}+\tilde{\omega})E_{pm,\mathbf{k}}^2E_{np,\mathbf{k}}}\left(\frac{1}{E_{pm,\mathbf{k}}} - \frac{1}{E_{np,\mathbf{k}}}\right); \\ \mathcal{F}_2(\omega) = &\frac{f_{nm}}{(E_{nm,\mathbf{k}}+\tilde{\omega})E_{nm,\mathbf{k}}^2E_{pm,\mathbf{k}}}\left(\frac{1}{E_{nm,\mathbf{k}}} + \frac{1}{E_{pm,\mathbf{k}}}\right) + \frac{f_{nm}}{(E_{nm,\mathbf{k}}+\tilde{\omega})^2E_{nm,\mathbf{k}}^2E_{pm,\mathbf{k}}} \\ &+ \frac{f_{np}}{(E_{np,\mathbf{k}}+\tilde{\omega})E_{pm,\mathbf{k}}E_{np,\mathbf{k}}^2}\left(\frac{1}{E_{np,\mathbf{k}}} - \frac{1}{E_{pm,\mathbf{k}}}\right)\end{aligned} \tag{C.8d}$$

All $\mathcal{A}_i$, $\mathcal{B}_i$, $\mathcal{C}_i$ terms need to vanish for the divergence in ω^3 to be removed. The terms associated with $\mathcal{A}$ and $\mathcal{C}$ are canceled with the corresponding terms in the permutation due to time-reversal symmetry, in the same fashion as for SHG, detailed in Ref. [44]:

$$\begin{aligned}\chi_{\rho\rho\rho}^{\mathcal{A}_1} &= \sum_{\mathbf{k}}\sum_{n,m,p}\hat{\mathbf{v}}_{nm}(\hat{\mathbf{q}})\hat{\mathbf{v}}_{mp}(\hat{\mathbf{q}}_1)\hat{\mathbf{v}}_{pn}(\hat{\mathbf{q}}_2)\left[-\frac{f_{np}}{E_{nm,\mathbf{k}}E_{np,\mathbf{k}}} - \frac{f_{mp}}{E_{nm,\mathbf{k}}E_{pm,\mathbf{k}}}\right] = -\chi_{\rho\rho\rho}^{\mathcal{A}_2} \\ \chi_{\rho\rho\rho}^{\mathcal{C}_1} &= \sum_{\mathbf{k}}\sum_{n,m,p}\hat{\mathbf{v}}_{nm}(\hat{\mathbf{q}})\hat{\mathbf{v}}_{mp}(\hat{\mathbf{q}}_1)\hat{\mathbf{v}}_{pn}(\hat{\mathbf{q}}_2)\left[\frac{f_{np}}{E_{nm,\mathbf{k}}E_{np,\mathbf{k}}}\left(\frac{1}{E_{nm,\mathbf{k}}E_{np,\mathbf{k}}} + \frac{1}{E_{nm,\mathbf{k}}^2}\right)\right. \\ &\qquad \left. + \frac{f_{mp}}{E_{nm,\mathbf{k}}E_{pm,\mathbf{k}}}\left(-\frac{1}{E_{pm,\mathbf{k}}^2} + \frac{1}{E_{nm,\mathbf{k}}^2}\right)\right] = -\chi_{\rho\rho\rho}^{\mathcal{C}_2}\end{aligned} \tag{C.9}$$

The same treatment for the term associated with $\mathcal{B}$ does not lead to any cancellation:

$$\chi_{\rho\rho\rho}^{\mathcal{B}_1} = \int d\mathbf{k}\sum_{n,m,p}\hat{\mathbf{v}}_{nm,\mathbf{k}}(\mathbf{q})\hat{\mathbf{v}}_{mp,\mathbf{k}}(\mathbf{q}_1)\hat{\mathbf{v}}_{pn,\mathbf{k}}(\mathbf{q}_2)\left[\frac{f_{np}}{E_{nm,\mathbf{k}}E_{np,\mathbf{k}}^2} - \frac{f_{mp}}{E_{nm,\mathbf{k}}E_{pm,\mathbf{k}}^2}\right] = \chi_{\rho\rho\rho}^{\mathcal{B}_2} \tag{C.10}$$

We then need to prove that $\mathcal{B}$ is zero in a different way. The two- and three-band terms of $\mathcal{B}$ are explicitly written,

$$\begin{aligned}\chi_{\rho\rho\rho}^{\mathcal{B}_1} + \chi_{\rho\rho\rho}^{\mathcal{B}_2} = \int d\mathbf{k}\sum_{n,m,p}\hat{\mathbf{v}}_{nm,\mathbf{k}}(\mathbf{q})\Bigg[&\Delta_{mn,\mathbf{k}}(\mathbf{q}_1)\hat{\mathbf{v}}_{mn,\mathbf{k}}(\mathbf{q}_2)\frac{f_{nm}}{E_{nm,\mathbf{k}}^3} + \hat{\mathbf{v}}_{mn,\mathbf{k}}(\mathbf{q}_1)\Delta_{nm,\mathbf{k}}(\mathbf{q}_2)\frac{f_{nm}}{E_{nm,\mathbf{k}}^3} \\ &+\sigma_{nmp}\hat{\mathbf{v}}_{mp,\mathbf{k}}(\mathbf{q}_1)\hat{\mathbf{v}}_{pn,\mathbf{k}}(\mathbf{q}_2)\left(\frac{f_{np}}{E_{nm,\mathbf{k}}E_{np,\mathbf{k}}^2} - \frac{f_{mp}}{E_{nm,\mathbf{k}}E_{pm,\mathbf{k}}^2}\right) \\ &+\sigma_{nmp}\hat{\mathbf{v}}_{pn,\mathbf{k}}(\mathbf{q}_1)\hat{\mathbf{v}}_{mp,\mathbf{k}}(\mathbf{q}_2)\left(-\frac{f_{np}}{E_{nm,\mathbf{k}}E_{np,\mathbf{k}}^2} + \frac{f_{mp}}{E_{nm,\mathbf{k}}E_{pm,\mathbf{k}}^2}\right)\Bigg],\end{aligned} \tag{C.11}$$

where σ_{nmp} is 1 if n, m, p are different and zero otherwise.
We then consider the second-order tensor $\overleftrightarrow{T}$

$$\overleftrightarrow{T}(\mathbf{q}_1, \mathbf{q}_2) = \sum_{n,m} f_{nm} \, \frac{\hat{\mathbf{v}}_{nm,\mathbf{k}}(\mathbf{q}_1) \, \hat{\mathbf{v}}_{mn,\mathbf{k}}(\mathbf{q}_2)}{E^2_{nm,\mathbf{k}}}. \tag{C.12}$$

From the $\mathbf{k} \cdot \mathbf{p}$ perturbation theory, we know the derivative of the velocity operator to be

$$\mathbf{q} \, \frac{\partial}{\partial \mathbf{k}} \hat{\mathbf{v}}_{nm,\mathbf{k}}(\mathbf{q}_1) = \mathbf{q}\mathbf{q}_1 \delta_{nm} - \frac{\hat{\mathbf{v}}_{nm,\mathbf{k}}(\mathbf{q}) \Delta_{nm,\mathbf{k}}(\mathbf{q}_1)}{E_{nm,\mathbf{k}}} + \sum_{p \notin D_n, D_m} \left[\frac{\hat{\mathbf{v}}_{np,\mathbf{k}}(\mathbf{q}_1) \hat{\mathbf{v}}_{pm,\mathbf{k}}(\mathbf{q})}{E_{mp,\mathbf{k}}} + \frac{\hat{\mathbf{v}}_{np,\mathbf{k}}(\mathbf{q}) \hat{\mathbf{v}}_{pm,\mathbf{k}}(\mathbf{q}_1)}{E_{np,\mathbf{k}}} \right] \tag{C.13}$$

Using equation (C.12) and (C.13), we can write the derivative with respect to $\mathbf{k}$ of the tensor T,

$$\begin{aligned} \mathbf{q} \frac{\partial}{\partial \mathbf{k}} T(\mathbf{q}_1, \mathbf{q}_2) = \sum_{n,m,p} \sigma_{nmp} \Bigg[& -f_{mp} \, \frac{\hat{\mathbf{v}}_{nm,\mathbf{k}}(\mathbf{q}) \hat{\mathbf{v}}_{mp,\mathbf{k}}(\mathbf{q}_2) \hat{\mathbf{v}}_{pn,\mathbf{k}}(\mathbf{q}_1)}{E_{nm,\mathbf{k}} E^2_{pm,\mathbf{k}}} - f_{np} \, \frac{\hat{\mathbf{v}}_{nm,\mathbf{k}}(\mathbf{q}) \hat{\mathbf{v}}_{mp,\mathbf{k}}(\mathbf{q}_1) \hat{\mathbf{v}}_{pn,\mathbf{k}}(\mathbf{q}_2)}{E_{nm,\mathbf{k}} E^2_{np,\mathbf{k}}} \\ & + f_{nm} \, \frac{\hat{\mathbf{v}}_{nm,\mathbf{k}}(\mathbf{q}) \Delta_{nm,\mathbf{k}}(\mathbf{q}_1) \hat{\mathbf{v}}_{mn,\mathbf{k}}(\mathbf{q}_2)}{E^3_{nm,\mathbf{k}}} + f_{np} \, \frac{\hat{\mathbf{v}}_{nm,\mathbf{k}}(\mathbf{q}) \hat{\mathbf{v}}_{mp,\mathbf{k}}(\mathbf{q}_2) \hat{\mathbf{v}}_{pn,\mathbf{k}}(\mathbf{q}_1)}{E_{nm,\mathbf{k}} E^2_{np,\mathbf{k}}} \\ & + f_{mp} \, \frac{\hat{\mathbf{v}}_{nm,\mathbf{k}}(\mathbf{q}) \hat{\mathbf{v}}_{mp,\mathbf{k}}(\mathbf{q}_1) \hat{\mathbf{v}}_{pn,\mathbf{k}}(\mathbf{q}_2)}{E_{nm,\mathbf{k}} E^2_{pm,\mathbf{k}}} - f_{nm} \, \frac{\hat{\mathbf{v}}_{nm,\mathbf{k}}(\mathbf{q}) \hat{\mathbf{v}}_{mn,\mathbf{k}}(\mathbf{q}_1) \, \Delta_{nm,\mathbf{k}}(\mathbf{q}_2)}{E^3_{nm,\mathbf{k}}} \\ & - 2 f_{nm} \, \frac{\Delta_{nm,\mathbf{k}}(\mathbf{q}) \hat{\mathbf{v}}_{nm,\mathbf{k}}(\mathbf{q}_1) \hat{\mathbf{v}}_{mn,\mathbf{k}}(\mathbf{q}_2)}{E^3_{nm,\mathbf{k}}} \Bigg] \end{aligned} \tag{C.14}$$

This leads us to the relation

$$\begin{aligned} \chi^{\mathcal{B}_1}_{\rho\rho\rho} + \chi^{\mathcal{B}_2}_{\rho\rho\rho} = \frac{1}{2} \int d\mathbf{k} \Bigg[& \mathbf{q} \frac{\partial}{\partial \mathbf{k}} \Big(T(\mathbf{q}_1, \mathbf{q}_2) - T(\mathbf{q}_2, \mathbf{q}_1) \Big) - \sum_{n,m} 2 f_{nm} \, \frac{\Delta_{nm,\mathbf{k}}(\mathbf{q})}{E^3_{nm,\mathbf{k}}} \\ & \times \Big(\hat{\mathbf{v}}_{mn,\mathbf{k}}(\mathbf{q}_1) \hat{\mathbf{v}}_{nm,\mathbf{k}}(\mathbf{q}_2) + \hat{\mathbf{v}}_{nm,\mathbf{k}}(\mathbf{q}_1) \hat{\mathbf{v}}_{mn,\mathbf{k}}(\mathbf{q}_2) \Big) \Bigg] \end{aligned} \tag{C.15}$$

The second term vanishes from time-reversal symmetry. As for the first term, since $\overleftrightarrow{T}$ is a periodic function over the BZ, its gradient vanishes when integrated over the BZ, as explained in Ref. [44]. Therefore the term associated with $\mathcal{B}$ is also zero. As a consequence, equation (C.6) becomes

$$\chi^{(2)}_0(\hat{\mathbf{q}}, \hat{\mathbf{q}}_1, \hat{\mathbf{q}}_2, \omega, 0) = \frac{1}{V} \sum_{\mathbf{k}} \sum_{n,m,p} \hat{\mathbf{v}}_{nm}(\hat{\mathbf{q}}) \Big[\hat{\mathbf{v}}_{mp}(\hat{\mathbf{q}}_1) \hat{\mathbf{v}}_{pn}(\hat{\mathbf{q}}_2) \, \mathcal{F}_1(\omega) + \hat{\mathbf{v}}_{mp}(\hat{\mathbf{q}}_2) \hat{\mathbf{v}}_{pn}(\hat{\mathbf{q}}_1) \, \mathcal{F}_2(\omega) \Big] \tag{C.16}$$

We separate the two- and three-band contributions and replace the matrix elements of the velocity by those of the position operator, defined as

$$\hat{\mathbf{r}}_{nm}(\mathbf{q}) = \langle \phi_{n,\mathbf{k}} | i \mathbf{q} \hat{\mathbf{r}} | \phi_{m,\mathbf{k}} \rangle = \frac{\langle \phi_{n,\mathbf{k}} | \mathbf{q} \hat{\mathbf{v}} | \phi_{m,\mathbf{k}} \rangle}{E_{nm,\mathbf{k}}} = \hat{\mathbf{v}}_{nm}(\mathbf{q}), \tag{C.17}$$

which give us

$$\chi_{\rho\rho\rho}(\hat{\mathbf{q}},\hat{\mathbf{q}}_1,\hat{\mathbf{q}}_2,\omega,0)=\frac{1}{V}\sum_{\mathbf{k}}\sum_{n,m,p}\sigma_{nmp}\Bigg[\hat{\mathbf{r}}_{nm,\mathbf{k}}(\hat{\mathbf{q}})\,\hat{\mathbf{r}}_{mp,\mathbf{k}}(\hat{\mathbf{q}}_1)\,\hat{\mathbf{r}}_{pn,\mathbf{k}}(\hat{\mathbf{q}}_2)\left(-\frac{f_{np}}{(E_{nm,\mathbf{k}}+\tilde{\omega})E_{np,\mathbf{k}}}\right.$$
$$-\frac{f_{mp}}{(E_{nm,\mathbf{k}}+\tilde{\omega})(E_{pm,\mathbf{k}}+\tilde{\omega})}+\frac{f_{nm}E_{np,\mathbf{k}}}{(E_{nm,\mathbf{k}}+\tilde{\omega})E_{nm,\mathbf{k}}^2}-\frac{f_{nm}E_{pm,\mathbf{k}}}{(E_{nm,\mathbf{k}}+\tilde{\omega})^2E_{nm,\mathbf{k}}}+\frac{f_{mp}E_{nm,\mathbf{k}}}{(E_{pm,\mathbf{k}}+\tilde{\omega})E_{pm,\mathbf{k}}^2}$$
$$\left.-\frac{f_{mp}}{(E_{pm,\mathbf{k}}+\tilde{\omega})E_{pm,\mathbf{k}}}\right)+\hat{\mathbf{r}}_{nm,\mathbf{k}}(\hat{\mathbf{q}})\,\hat{\mathbf{r}}_{pn,\mathbf{k}}(\hat{\mathbf{q}}_1)\,\hat{\mathbf{r}}_{mp,\mathbf{k}}(\hat{\mathbf{q}}_2)\left(\frac{f_{np}E_{nm,\mathbf{k}}}{(E_{np,\mathbf{k}}+\tilde{\omega})E_{np,\mathbf{k}}^2}-\frac{f_{np}}{(E_{np,\mathbf{k}}+\tilde{\omega})E_{np,\mathbf{k}}}\right.$$
$$\left.-\frac{f_{np}}{(E_{nm,\mathbf{k}}+\tilde{\omega})(E_{np,\mathbf{k}}+\tilde{\omega})}-\frac{f_{nm}E_{pm,\mathbf{k}}}{(E_{nm,\mathbf{k}}+\tilde{\omega})E_{nm,\mathbf{k}}^2}+\frac{f_{nm}E_{np,\mathbf{k}}}{(E_{nm,\mathbf{k}}+\tilde{\omega})^2E_{nm,\mathbf{k}}}-\frac{f_{mp}}{(E_{nm,\mathbf{k}}+\tilde{\omega})E_{pm,\mathbf{k}}}\right)$$
$$-\hat{\mathbf{r}}_{nm,\mathbf{k}}(\hat{\mathbf{q}})\,\Delta_{nm,\mathbf{k}}(\hat{\mathbf{q}}_1)\,\hat{\mathbf{r}}_{mn,\mathbf{k}}(\hat{\mathbf{q}}_2)\left(\frac{2f_{nm}}{(E_{nm,\mathbf{k}}+\tilde{\omega})E_{nm,\mathbf{k}}^2}+\frac{f_{nm}}{(E_{nm,\mathbf{k}}+\tilde{\omega})^2E_{nm,\mathbf{k}}}\right)$$
$$-\hat{\mathbf{r}}_{nm,\mathbf{k}}(\hat{\mathbf{q}})\,\hat{\mathbf{r}}_{mn,\mathbf{k}}(\hat{\mathbf{q}}_1)\,\Delta_{nm,\mathbf{k}}(\hat{\mathbf{q}}_2)\left(\frac{f_{nm}}{(E_{nm,\mathbf{k}}+\tilde{\omega})^2E_{nm,\mathbf{k}}}+\frac{f_{nm}}{(E_{nm,\mathbf{k}}+\tilde{\omega})^3}\right)$$
$$+\Delta_{nm,\mathbf{k}}(\hat{\mathbf{q}})\,\hat{\mathbf{r}}_{mn,\mathbf{k}}(\hat{\mathbf{q}}_1)\,\hat{\mathbf{r}}_{nm,\mathbf{k}}(\hat{\mathbf{q}}_2)\,\frac{2f_{nm}}{(E_{nm,\mathbf{k}}+\tilde{\omega})E_{nm,\mathbf{k}}^2}\Bigg] \quad \text{(C.18)}$$

The two-band term containing a square term in the denominator of the type $(E_{nm,\mathbf{k}}+\tilde{\omega})^2$ are known to be harder to converge than the rest. To avoid this issue those terms are recast as sum of two- and three-band term, using the fact that

$$\mathbf{q}\,\frac{\partial}{\partial\mathbf{k}}\,\frac{1}{(E_{nm,\mathbf{k}}+\tilde{\omega})}=-\frac{\Delta_{nm,\mathbf{k}}(\mathbf{q})}{(E_{nm,\mathbf{k}}+\tilde{\omega})^2};\qquad \mathbf{q}\,\frac{\partial}{\partial\mathbf{k}}\,\frac{1}{(E_{nm,\mathbf{k}}+\tilde{\omega})^2}=-2\frac{\Delta_{nm,\mathbf{k}}(\mathbf{q})}{(E_{nm,\mathbf{k}}+\tilde{\omega})^3} \quad \text{(C.19)}$$

and following the same procedure described in section B.2, which leads to the final expression (4.33).

Appendix D

Perturbation theory to the third order: current density calculation

The general definition of the induced current density, obtain through the continuity equation, is

$$\mathbf{j}_{ind}(\mathbf{r},t) = \frac{-i}{2}\sum_i f_i \left(\phi_i^*(\mathbf{r},t)\left[\hat{\mathbf{r}},H\right]\phi_i(\mathbf{r},t) - \phi_i(\mathbf{r},t)\left[\hat{\mathbf{r}},H\right]\phi_i^*(\mathbf{r},t)\right) \tag{D.1}$$

Under a perturbation $H_I^{(1)} + H_I^{(2)} + H_I^{(3)}$, the wavefunctions ϕ_i becomes $\phi_i + \delta\phi_i$, where

$$\delta\phi_i(\mathbf{r},t) = \sum_j \left(c_j^{(1)}(t) + c_j^{(2)}(t) + d_j^{(2)}(t) + c_j^{(3)}(t) + d_j^{(3)}(t) + e_j^{(3)}(t)\right)\phi_j(\mathbf{r},t) \tag{D.2}$$

and

$$c_j^{(1)}(t) = -i\int dt'\,\theta(t-t')\left\langle\phi_j(t')\middle|H_I^{(1)}(t')\middle|\phi_i(t')\right\rangle \tag{D.3a}$$

$$c_j^{(2)}(t) = -\sum_k \int dt'\theta(t-t')\int dt''\theta(t'-t'')\left\langle\phi_j(t')\middle|H_I^{(1)}(t')\middle|\phi_k(t')\right\rangle\left\langle\phi_k(t'')\middle|H_I^{(1)}(t'')\middle|\phi_i(t'')\right\rangle \tag{D.3b}$$

$$d_j^{(2)}(t) = -i\int dt'\theta(t-t')\left\langle\phi_j(t')\middle|H_I^{(2)}(t')\middle|\phi_i(t')\right\rangle \tag{D.3c}$$

$$c_j^{(3)}(t) = i\sum_k\sum_l \int dt'\,\theta(t-t')\int dt''\,\theta(t'-t'')\int dt'''\,\theta(t''-t''')\left\langle\phi_j(t')\middle|H_I^{(1)}(t')\middle|\phi_k(t')\right\rangle \left\langle\phi_k(t'')\middle|H_I^{(1)}(t'')\middle|\phi_l(t'')\right\rangle\left\langle\phi_l(t''')\middle|H_I^{(1)}(t''')\middle|\phi_i(t''')\right\rangle \tag{D.3d}$$

$$d_j^{(3)}(t) = -\sum_k \int dt'\theta(t-t')\int dt''\theta(t'-t'')\left[\left\langle\phi_j(t')\middle|H_I^{(1)}(t')\middle|\phi_k(t')\right\rangle\left\langle\phi_k(t'')\middle|H_I^{(2)}(t'')\middle|\phi_i(t'')\right\rangle + \left\langle\phi_j(t')\middle|H_I^{(2)}(t')\middle|\phi_k(t')\right\rangle\left\langle\phi_k(t'')\middle|H_I^{(2)}(t'')\middle|\phi_i(t'')\right\rangle\right] \tag{D.3e}$$

$$e_j^{(3)}(t) = -i\int dt'\,\theta(t-t')\left\langle\phi_j(t')\middle|H_I^{(3)}(t')\middle|\phi_i(t')\right\rangle \tag{D.3f}$$

The third-order current density is

$$\mathbf{j}_{ind}^{(3)}(\mathbf{r},t) = \mathbf{j}_{\mathcal{Z}}^{(3)}(\mathbf{r},t) + \mathbf{j}_{\mathcal{O}}^{(3)}(\mathbf{r},t) + \mathbf{j}_{\mathcal{D}}^{(3)}(\mathbf{r},t) + \mathbf{j}_{\mathcal{T}}^{(3)}(\mathbf{r},t) \tag{D.4}$$

where

$$\begin{aligned}\mathbf{j}^{(3)}_{\mathcal{Z}}(\mathbf{r},t) = \frac{-i}{2}\sum_i f_i \Big[&\phi_i^*(\mathbf{r},t)\left[\hat{\mathbf{r}},H_I^{(0)}\right]\delta\phi_i^{(3)}(\mathbf{r},t) - \phi_i(\mathbf{r},t)\left[\hat{\mathbf{r}},H_I^{(0)}\right]\delta\phi_i^{(3)\,*}(\mathbf{r},t)\\ &+\delta\phi_i^{(3)\,*}(\mathbf{r},t)\left[\hat{\mathbf{r}},H_I^{(0)}\right]\phi_i(\mathbf{r},t) - \delta\phi_i^{(3)}(\mathbf{r},t)\left[\hat{\mathbf{r}},H_I^{(0)}\right]\phi_i^*(\mathbf{r},t)\\ &+\delta\phi_i^{(1)\,*}(\mathbf{r},t)\left[\hat{\mathbf{r}},H_I^{(0)}\right]\delta\phi_i^{(2)}(\mathbf{r},t) - \delta\phi_i^{(1)}(\mathbf{r},t)\left[\hat{\mathbf{r}},H_I^{(0)}\right]\delta\phi_i^{(2)\,*}(\mathbf{r},t)\\ &+\delta\phi_i^{(2)\,*}(\mathbf{r},t)\left[\hat{\mathbf{r}},H_I^{(0)}\right]\delta\phi_i^{(1)}(\mathbf{r},t) - \delta\phi_i^{(2)}(\mathbf{r},t)\left[\hat{\mathbf{r}},H_I^{(0)}\right]\delta\phi_i^{(1)\,*}(\mathbf{r},t)\Big]\end{aligned} \tag{D.5a}$$

$$\begin{aligned}\mathbf{j}^{(3)}_{\mathcal{O}}(\mathbf{r},t) = \frac{-i}{2}\sum_i f_i \Big[&\phi_i^*(\mathbf{r},t)\left[\hat{\mathbf{r}},H_I^{(1)}\right]\delta\phi_i^{(2)}(\mathbf{r},t) - \phi_i(\mathbf{r},t)\left[\hat{\mathbf{r}},H_I^{(1)}\right]\delta\phi_i^{(2)\,*}(\mathbf{r},t)\\ &+\delta\phi_i^{(2)\,*}(\mathbf{r},t)\left[\hat{\mathbf{r}},H_I^{(1)}\right]\phi_i(\mathbf{r},t) - \delta\phi_i^{(2)}(\mathbf{r},t)\left[\hat{\mathbf{r}},H_I^{(1)}\right]\phi_i^*(\mathbf{r},t)\\ &+\delta\phi_i^{(1)\,*}(\mathbf{r},t)\left[\hat{\mathbf{r}},H_I^{(1)}\right]\delta\phi_i^{(1)}(\mathbf{r},t) - \delta\phi_i^{(1)}(\mathbf{r},t)\left[\hat{\mathbf{r}},H_I^{(1)}\right]\delta\phi_i^{(1)\,*}(\mathbf{r},t)\Big]\end{aligned} \tag{D.5b}$$

$$\begin{aligned}\mathbf{j}^{(3)}_{\mathcal{D}}(\mathbf{r},t) = \frac{-i}{2}\sum_i f_i \Big[&\phi_i^*(\mathbf{r},t)\left[\hat{\mathbf{r}},H_I^{(2)}\right]\delta\phi_i^{(1)}(\mathbf{r},t) - \phi_i(\mathbf{r},t)\left[\hat{\mathbf{r}},H_I^{(2)}\right]\delta\phi_i^{(1)\,*}(\mathbf{r},t)\\ &+\delta\phi_i^{(1)\,*}(\mathbf{r},t)\left[\hat{\mathbf{r}},H_I^{(2)}\right]\phi_i(\mathbf{r},t) - \delta\phi_i^{(1)}(\mathbf{r},t)\left[\hat{\mathbf{r}},H_I^{(2)}\right]\phi_i^*(\mathbf{r},t)\Big]\end{aligned} \tag{D.5c}$$

$$\mathbf{j}^{(3)}_{\mathcal{T}}(\mathbf{r},t) = \frac{-i}{2}\sum_i f_i\left[\phi_i^*(\mathbf{r},t)\left[\hat{\mathbf{r}},H^{(3)}\right]\phi_i(\mathbf{r},t) - \phi_i(\mathbf{r},t)\left[\hat{\mathbf{r}},H^{(3)}\right]\phi_i^*(\mathbf{r},t)\right] \tag{D.5d}$$

Calculation of $\mathbf{j}^{(3)}_{\mathcal{T}}$

Using equation 3.35 and with $\phi_i(\mathbf{r},t) = e^{-iE_it}\phi_i(\mathbf{r})$, one gets, in the frequency domain,

$$\begin{aligned}\mathbf{j}^{(3)}_{\mathcal{T}}(\mathbf{r},\omega) = -\frac{i}{6c^3}\int d\omega'\int d\omega''\int d\omega'''\sum_i f_i\,\phi_i^*(\mathbf{r})\left[\hat{\mathbf{r}},\left[\mathbf{A}(\mathbf{r},\omega')\hat{\mathbf{r}},\left[\mathbf{A}(\mathbf{r},\omega'')\hat{\mathbf{r}},\mathbf{A}(\mathbf{r},\omega''')\mathbf{v}\right]\right]\right]\phi_i(\mathbf{r})\\ \times\,\delta(\omega-\omega'-\omega''-\omega''')\end{aligned} \tag{D.6}$$

In the gauge $\varphi^P = 0$, we have, in the reciprocal space,

$$\mathbf{E}^P(\mathbf{k},\omega) = \frac{i\omega}{c}\,\mathbf{A}^P(\mathbf{k},\omega), \tag{D.7}$$

that gives

$$\begin{aligned}\mathbf{j}^{(3)}_{\mathcal{T}}(\mathbf{k},\omega) = \frac{1}{V}\sum_{\mathbf{k}',\mathbf{k}'',\mathbf{k}'''}\frac{1}{6}\int d\omega'\int d\omega''\int d\omega'''\,\delta(\omega-\omega'-\omega''-\omega''')\,\frac{1}{\omega'\omega''\omega'''}\sum_i f_i\\ \left\langle\phi_i\middle|e^{-i\mathbf{k}\mathbf{r}}\left[\hat{\mathbf{r}},\left[e^{i\mathbf{k}'\mathbf{r}}\mathbf{E}^P(\mathbf{k}',\omega')\hat{\mathbf{r}},\left[e^{i\mathbf{k}''\mathbf{r}}\mathbf{E}^P(\mathbf{k}'',\omega'')\hat{\mathbf{r}},e^{i\mathbf{k}'''\mathbf{r}}\mathbf{E}^P(\mathbf{k}''',\omega''')\mathbf{v}\right]\right]\right]\middle|\phi_i\right\rangle\end{aligned} \tag{D.8}$$

Calculation of $\mathbf{j}^{(3)}_{\mathcal{D}}$

$$\begin{aligned}\mathbf{j}^{(3)}_{\mathcal{D}}(\mathbf{r},t) = \frac{-i}{2}\sum_{ijk} f_i\Big(&c_j^{(1)}(t)\,\phi_i^*(\mathbf{r},t)\left[\mathbf{r},H_I^{(2)}(\mathbf{r},t)\right]\phi_j(\mathbf{r},t) - c_j^{(1)\,*}(t)\,\phi_i(\mathbf{r},t)\left[\mathbf{r},H_I^{(2)}(\mathbf{r},t)\right]\phi_j^*(\mathbf{r},t)\\ &+c_j^{(1)\,*}(t)\,\phi_j^*(\mathbf{r},t)\left[\mathbf{r},H_I^{(2)}(\mathbf{r},t)\right]\phi_i(\mathbf{r},t) - c_j^{(1)}(t)\,\phi_j(\mathbf{r},t)\left[\mathbf{r},H_I^{(2)}(\mathbf{r},t)\right]\phi_i^*(\mathbf{r},t)\Big)\end{aligned} \tag{D.9}$$

Using equation (D.3a) and (3.35), one gets, in the frequency domain,

$$\mathbf{j}^{(3)}_{\mathcal{D}}(\mathbf{r},\omega) = \lim_{\eta\to 0}\ \frac{1}{2c^3}\sum_{ijk}\int d\mathbf{r}'\int d\omega'\int d\omega''\ \delta(\omega-\omega'-\omega''-\omega''')\ \frac{f_i-f_j}{E_i-E_j+\omega'+i\eta}$$
$$\times\ \phi_j^*(\mathbf{r}')\ \mathbf{A}^P(\mathbf{r}',\omega')\hat{\mathbf{v}}\ \phi_i(\mathbf{r}')\phi_i^*(\mathbf{r})\left[\hat{\mathbf{r}},\left[\mathbf{A}^P(\mathbf{r},\omega'')\hat{\mathbf{r}},\mathbf{A}^P(\mathbf{r},\omega''')\hat{\mathbf{v}}\right]\right]\phi_j(\mathbf{r}) \quad \text{(D.10)}$$

After a Fourier transform in the reciprocal space and using equation (D.7), we obtain

$$\mathbf{j}^{(3)}_{\mathcal{D}}(\mathbf{k},\omega) = \frac{1}{V}\sum_{\mathbf{k}',\mathbf{k}'',\mathbf{k}'''}\ \lim_{\eta\to 0}\ \frac{i}{2}\sum_{ijk}\int d\omega'\int d\omega''\ \delta(\omega-\omega'-\omega''-\omega''')\ \frac{f_i-f_j}{\omega'\omega''\omega'''(E_i-E_j+\omega'+i\eta)}$$
$$\left\langle\phi_i\middle|e^{-i\mathbf{k}\mathbf{r}}\left[\hat{\mathbf{r}},\left[e^{i\mathbf{k}''\mathbf{r}}\mathbf{E}^P(\mathbf{k}'',\omega'')\hat{\mathbf{r}},e^{i\mathbf{k}'''\mathbf{r}}\mathbf{E}^P(\mathbf{k}''',\omega''')\hat{\mathbf{v}}\right]\right]\middle|\phi_j\right\rangle\ \left\langle\phi_j\middle|e^{i\mathbf{k}'\mathbf{r}'}\mathbf{E}^P(\mathbf{k}',\omega')\hat{\mathbf{v}}\middle|\phi_i\right\rangle \quad \text{(D.11)}$$

Calculation of $\mathbf{j}^{(3)}_{\mathcal{O}}$

$$\begin{aligned}\mathbf{j}^{(3)}_{\mathcal{O}}(\mathbf{r},t) = \frac{-i}{2}\sum_{ijk}\ & f_i\left(\phi_i^*(\mathbf{r},t)\left[\mathbf{r},H_I^{(1)}(\mathbf{r},t)\right]\left(c_j^{(2)}(t)+d_j^{(2)}(t)\right)\phi_j(\mathbf{r},t)\right.\\
&-\phi_i(\mathbf{r},t)\left[\mathbf{r},H_I^{(1)}(\mathbf{r},t)\right]\left(c_j^{(2)\,*}(t)+d_j^{(2)\,*}(t)\right)\phi_j^*(\mathbf{r},t)\\
&+\left(c_j^{(2)\,*}(t)+d_j^{(2)\,*}(t)\right)\phi_j^*(\mathbf{r},t)\left[\mathbf{r},H_I^{(1)}(\mathbf{r},t)\right]\phi_i(\mathbf{r},t)\\
&-\left(c_j^{(2)}(t)+d_j^{(2)}(t)\right)\phi_j(\mathbf{r},t)\left[\mathbf{r},H_I^{(1)}(\mathbf{r},t)\right]\phi_i^*(\mathbf{r},t)\\
&+c_j^{(1)\,*}(t)\ \phi_j^*(\mathbf{r},t)\left[\mathbf{r},H_I^{(1)}(\mathbf{r},t)\right]c_k^{(1)}(t)\ \phi_k(\mathbf{r},t)\\
&\left.-c_j^{(1)}(t)\ \phi_j(\mathbf{r},t)\left[\mathbf{r},H_I^{(1)}(\mathbf{r},t)\right]c_k^{(1)\,*}(t)\ \phi_k^*(\mathbf{r},t)\right) \quad \text{(D.12)}\end{aligned}$$

Using equation (D.3) and (3.35), one gets

$$\mathbf{j}^{(3)}_{\mathcal{O}}(\mathbf{r},\omega) = \lim_{\eta\to 0}\ \frac{1}{c^3}\sum_{ijk}\int d\mathbf{r}'\int d\mathbf{r}''\int d\omega'\int d\omega''\int d\omega'''\ \delta(\omega-\omega'-\omega''-\omega''')$$
$$\times\left[i\ \frac{\phi_i^*(\mathbf{r})\left[\hat{\mathbf{r}},\mathbf{A}^P(\mathbf{r},\omega''')\hat{\mathbf{v}}\right]\phi_j(\mathbf{r})}{E_i-E_j+\omega'+\omega''+2i\eta}\left((f_i-f_k)\ \frac{\phi_k^*(\mathbf{r}')\ \mathbf{A}^P(\mathbf{r}',\omega')\hat{\mathbf{v}}\ \phi_i(\mathbf{r}')\ \phi_j^*(\mathbf{r}'')\ \mathbf{A}^P(\mathbf{r}'',\omega'')\hat{\mathbf{v}}\ \phi_k(\mathbf{r}'')}{(E_i-E_k+\omega'+i\eta)}\right.$$
$$\left.+(f_j-f_k)\ \frac{\phi_k^*(\mathbf{r}')\ \mathbf{A}^P(\mathbf{r}',\omega')\hat{\mathbf{v}}\ \phi_i(\mathbf{r}')\ \phi_j^*(\mathbf{r}'')\ \mathbf{A}^P(\mathbf{r}'',\omega'')\hat{\mathbf{v}}\ \phi_k(\mathbf{r}'')}{(E_k-E_j+\omega''+i\eta)}\right)$$
$$+\frac{1}{2}\ (f_i-f_j)\ \frac{\phi_i^*(\mathbf{r})\left[\mathbf{r},\mathbf{A}^P(\mathbf{r},\omega'')\hat{\mathbf{v}}\right]\phi_j(\mathbf{r})\ \phi_j^*(\mathbf{r}')\left[\mathbf{A}^P(\mathbf{r}',\omega''')\hat{\mathbf{r}},\mathbf{A}^P(\mathbf{r}',\omega')\hat{\mathbf{v}}\right]\phi_i(\mathbf{r}')}{E_i-E_j+\omega'+\omega'''+i\eta}\Bigg] \quad \text{(D.13)}$$

$$\mathbf{j}^{(3)}_{\mathcal{O}}(\mathbf{k},\omega) = \frac{1}{V}\sum_{\mathbf{k}',\mathbf{k}'',\mathbf{k}'''}\lim_{\eta\to 0}\sum_{ijk}\int d\omega'\int d\omega''\int d\omega'''\,\delta(\omega-\omega'-\omega''-\omega''')\,\frac{1}{\omega'\omega''\omega'''}$$
$$\left[-\frac{\left\langle\phi_i\middle|e^{-i\mathbf{kr}}\left[\hat{\mathbf{r}},e^{i\mathbf{k}'''\mathbf{r}}\mathbf{E}^P(\mathbf{k}''',\omega''')\hat{\mathbf{v}}\right]\middle|\phi_j\right\rangle}{E_i-E_j+\omega'+\omega''+2i\eta}\right.$$
$$\left((f_i-f_k)\,\frac{\left\langle\phi_k\middle|e^{i\mathbf{k}'\mathbf{r}'}\mathbf{E}^P(\mathbf{k}',\omega')\hat{\mathbf{v}}\middle|\phi_i\right\rangle\left\langle\phi_j\middle|e^{i\mathbf{k}''\mathbf{r}''}\mathbf{E}^P(\mathbf{k}'',\omega'')\hat{\mathbf{v}}\middle|\phi_k\right\rangle}{(E_i-E_k+\omega'+i\eta)}\right.$$
$$\left.+(f_j-f_k)\,\frac{\left\langle\phi_k\middle|e^{i\mathbf{k}'\mathbf{r}'}\mathbf{E}^P(\mathbf{k}',\omega')\hat{\mathbf{v}}\middle|\phi_i\right\rangle\left\langle\phi_j\middle|e^{i\mathbf{k}''\mathbf{r}''}\mathbf{E}^P(\mathbf{k}'',\omega'')\hat{\mathbf{v}}\middle|\phi_k\right\rangle}{(E_k-E_j+\omega''+i\eta)}\right)$$
$$\left.+\frac{i}{2}\,(f_i-f_j)\,\frac{\left\langle\phi_i\middle|e^{-i\mathbf{kr}}\left[\mathbf{r},e^{i\mathbf{k}''\mathbf{r}}\mathbf{E}^P(\mathbf{k}'',\omega'')\hat{\mathbf{v}}\right]\middle|\phi_j\right\rangle\left\langle\phi_j\middle|\left[e^{i\mathbf{k}'''\mathbf{r}'}\mathbf{E}^P(\mathbf{k}''',\omega''')\hat{\mathbf{r}},e^{i\mathbf{k}'\mathbf{r}'}\mathbf{E}^P(\mathbf{k}',\omega')\hat{\mathbf{v}}\right]\middle|\phi_i\right\rangle}{E_i-E_j+\omega'+\omega'''+i\eta}\right] \tag{D.14}$$

Calculation of $\mathbf{j}^{(3)}_{\mathcal{Z}}$

$$\mathbf{j}^{(3)}_{\mathcal{Z}}(\mathbf{r},t) = \frac{1}{2}\sum_{ijk} f_i\left[\left(c_j^{(3)}(t)+d_j^{(3)}(t)+e_j^{(3)}(t)\right)\phi_i^*(\mathbf{r},t)\,\mathbf{v}\,\phi_j(\mathbf{r},t)\right.$$
$$+\left(c_j^{(3)\,*}(t)+d_j^{(3)\,*}(t)+e_j^{(3)\,*}(t)\right)\phi_i(\mathbf{r},t)\,(\mathbf{v}\phi_j(\mathbf{r},t))^*$$
$$+\left(c_j^{(3)\,*}(t)+d_j^{(3)\,*}(t)+e_j^{(3)\,*}(t)\right)\phi_j^*(\mathbf{r},t)\,\mathbf{v}\phi_i(\mathbf{r},t)$$
$$+\left(c_j^{(3)}(t)+d_j^{(3)}(t)+e_j^{(3)}(t)\right)\phi_j(\mathbf{r},t)\,(\mathbf{v}\phi_i(\mathbf{r},t))^*$$
$$+c_j^{(1)\,*}(t)\left(c_k^{(2)}(t)+d_k^{(2)}(t)\right)\phi_j^*(\mathbf{r},t)\,\mathbf{v}\phi_k(\mathbf{r},t)$$
$$+c_j^{(1)}(t)\left(c_k^{(2)\,*}(t)+d_k^{(2)\,*}(t)\right)\phi_j(\mathbf{r},t)\,(\mathbf{v}\phi_k(\mathbf{r},t))^*$$
$$+\left(c_j^{(2)\,*}(t)+d_j^{(2)\,*}(t)\right)c_k^{(1)}(t)\,\phi_j^*(\mathbf{r},t)\,\mathbf{v}\phi_k(\mathbf{r},t)$$
$$\left.+\left(c_j^{(2)}(t)+d_j^{(2)}(t)\right)c_k^{(1)\,*}(t)\,\phi_j(\mathbf{r},t)\,(\mathbf{v}\phi_k(\mathbf{r},t))^*\right] \tag{D.15}$$

$$\mathbf{j}^{(3)}_{\mathcal{Z}}(\mathbf{r},\omega) = -\lim_{\eta\to 0}\frac{1}{2c^3}\sum_{ijkl}\int d\mathbf{r}'\,d\mathbf{r}''\,d\mathbf{r}'''\int d\omega'\int d\omega''\int d\omega'''\,\delta(\omega-\omega'-\omega''-\omega''')$$
$$\times\,\frac{\phi_i^*(\mathbf{r})\,\mathbf{v}\phi_j(\mathbf{r})+\phi_j(\mathbf{r})\,(\mathbf{v}\phi_i(\mathbf{r}))^*}{E_i-E_j+\omega'+\omega''+\omega'''+3i\eta}$$
$$\left[(f_i-f_k)\,\frac{\phi_j^*(\mathbf{r}')\,\mathbf{A}^P(\mathbf{r}',\omega')\mathbf{v}\,\phi_k(\mathbf{r}')\,\phi_k^*(\mathbf{r}'')\,\mathbf{A}^P(\mathbf{r}'',\omega'')\mathbf{v}\,\phi_l(\mathbf{r}'')\,\phi_l^*(\mathbf{r}''')\,\mathbf{A}^P(\mathbf{r}''',\omega''')\mathbf{v}\,\phi_i(\mathbf{r}''')}{(E_i-E_k+\omega''+\omega'''+2i\eta)(E_i-E_l+\omega'''+i\eta)}\right.$$
$$+(f_k-f_j)\,\frac{\phi_j^*(\mathbf{r}''')\,\mathbf{A}^P(\mathbf{r}''',\omega''')\mathbf{v}\,\phi_l(\mathbf{r}''')\,\phi_l^*(\mathbf{r}'')\,\mathbf{A}^P(\mathbf{r}'',\omega'')\mathbf{v}\,\phi_k(\mathbf{r}'')\,\phi_k^*(\mathbf{r}')\,\mathbf{A}^P(\mathbf{r}',\omega')\mathbf{v}\,\phi_i(\mathbf{r}')}{(E_k-E_j+\omega''+\omega'''+2i\eta)(E_l-E_j+\omega'''+i\eta)}$$
$$+(f_k-f_l)\,\frac{\phi_l^*(\mathbf{r}''')\,\mathbf{A}^P(\mathbf{r}''',\omega''')\mathbf{v}\,\phi_i(\mathbf{r}''')\,\phi_j^*(\mathbf{r}')\,\mathbf{A}^P(\mathbf{r}',\omega')\mathbf{v}\,\phi_k(\mathbf{r}')\,\phi_k^*(\mathbf{r}'')\,\mathbf{A}^P(\mathbf{r}'',\omega'')\mathbf{v}\,\phi_l(\mathbf{r}'')}{(E_i-E_l+\omega'''+i\eta)(E_l-E_k+\omega''+i\eta)}$$
$$\left.+(f_l-f_k)\,\frac{\phi_j^*(\mathbf{r}''')\,\mathbf{A}^P(\mathbf{r}''',\omega''')\mathbf{v}\,\phi_l(\mathbf{r}''')\,\phi_l^*(\mathbf{r}'')\,\mathbf{A}^P(\mathbf{r}'',\omega'')\mathbf{v}\,\phi_k(\mathbf{r}'')\,\phi_k^*(\mathbf{r}')\,\mathbf{A}^P(\mathbf{r}',\omega')\mathbf{v}\,\phi_i(\mathbf{r}')}{(E_l-E_j+\omega'''+i\eta)(E_k-E_l+\omega''+i\eta)}\right]$$

$$
+\lim_{\eta\to 0}\ \frac{i}{4c^3}\ \sum_{ijk}\int d\mathbf{r}'\,d\mathbf{r}''\int d\omega'\ \int d\omega''\int d\omega'''\ \delta(\omega-\omega'-\omega''-\omega''')\ \frac{\phi_i^*(\mathbf{r})\ \mathbf{v}\phi_j(\mathbf{r})+\phi_j(\mathbf{r})\ (\mathbf{v}\phi_i(\mathbf{r}))^*}{E_i-E_j+\omega'+\omega''+\omega'''+2i\eta}
$$
$$
\Bigg[(f_i-f_k)\ \frac{\phi_j^*(\mathbf{r}')\ \mathbf{A}^P(\mathbf{r}',\omega')\mathbf{v}\ \phi_k(\mathbf{r}')\ \phi_k^*(\mathbf{r}'')\left[\mathbf{A}^P(\mathbf{r}'',\omega''')\hat{\mathbf{r}},\mathbf{A}^P(\mathbf{r}'',\omega'')\hat{\mathbf{v}}\right]\phi_i(\mathbf{r}'')}{E_i-E_k+\omega''+\omega'''+i\eta}
$$
$$
+(f_i-f_k)\ \frac{\phi_j^*(\mathbf{r}')\left[\mathbf{A}^P(\mathbf{r}',\omega''')\hat{\mathbf{r}},\mathbf{A}^P(\mathbf{r}',\omega')\hat{\mathbf{v}}\right]\phi_k(\mathbf{r}')\ \phi_k^*(\mathbf{r}'')\ \mathbf{A}^P(\mathbf{r}'',\omega'')\mathbf{v}\ \phi_i(\mathbf{r}'')}{E_i-E_k+\omega''+i\eta}
$$
$$
+(f_j-f_k)\ \frac{\phi_j^*(\mathbf{r}'')\left[\mathbf{A}^P(\mathbf{r}'',\omega''')\hat{\mathbf{r}},\mathbf{A}^P(\mathbf{r}'',\omega'')\hat{\mathbf{v}}\right]\phi_k(\mathbf{r}'')\ \phi_k^*(\mathbf{r}')\ \mathbf{A}^P(\mathbf{r}',\omega')\mathbf{v}\ \phi_i(\mathbf{r}')}{E_k-E_j+\omega''+\omega'''+i\eta}
$$
$$
+(f_j-f_k)\ \frac{\phi_j^*(\mathbf{r}'')\ \mathbf{A}^P(\mathbf{r}'',\omega'')\mathbf{v}\ \phi_k(\mathbf{r}'')\ \phi_k^*(\mathbf{r}')\left[\mathbf{A}^P(\mathbf{r}',\omega''')\hat{\mathbf{r}},\mathbf{A}^P(\mathbf{r}',\omega')\hat{\mathbf{v}}\right]\phi_i(\mathbf{r}')}{E_k-E_j+\omega''+i\eta}\Bigg] \tag{D.16}
$$

$$
\mathbf{j}_z^{(3)}(\mathbf{k},\omega)=-\frac{1}{V}\ \lim_{\eta\to 0}\sum_{ijkl}\int d\omega'\int d\omega''\int d\omega'''\ \delta(\omega-\omega'-\omega''-\omega''')\ \frac{i}{\omega'\omega''\omega'''}\sum_{\mathbf{k}',\mathbf{k}'',\mathbf{k}'''}
$$
$$
\times\Bigg[\frac{\left\langle\phi_i\right|e^{-i\mathbf{k}\mathbf{r}}\ \mathbf{v}\left|\phi_j\right\rangle}{E_i-E_j+\omega'+\omega''+\omega'''+3i\eta}
$$
$$
\Bigg((f_i-f_k)\ \frac{\left\langle\phi_j\right|e^{i\mathbf{k}'\mathbf{r}'}\mathbf{E}^P(\mathbf{k}',\omega')\mathbf{v}\left|\phi_k\right\rangle\left\langle\phi_k\right|e^{i\mathbf{k}''\mathbf{r}''}\mathbf{E}^P(\mathbf{k}'',\omega'')\mathbf{v}\left|\phi_l\right\rangle\left\langle\phi_l\right|e^{i\mathbf{k}'''\mathbf{r}'''}\mathbf{E}^P(\mathbf{k}''',\omega''')\mathbf{v}\left|\phi_i\right\rangle}{(E_i-E_k+\omega''+\omega'''+2i\eta)(E_i-E_l+\omega'''+i\eta)}
$$
$$
+(f_k-f_j)\ \frac{\left\langle\phi_j\right|e^{i\mathbf{k}'''\mathbf{r}'''}\mathbf{E}^P(\mathbf{k}''',\omega''')\mathbf{v}\left|\phi_l\right\rangle\left\langle\phi_l\right|e^{i\mathbf{k}''\mathbf{r}''}\mathbf{E}^P(\mathbf{k}'',\omega'')\mathbf{v}\left|\phi_k\right\rangle\left\langle\phi_k\right|e^{i\mathbf{k}'\mathbf{r}'}\mathbf{E}^P(\mathbf{k}',\omega')\mathbf{v}\left|\phi_i\right\rangle}{(E_k-E_j+\omega''+\omega'''+2i\eta)(E_l-E_j+\omega'''+i\eta)}
$$
$$
+(f_k-f_l)\ \frac{\left\langle\phi_l\right|e^{i\mathbf{k}'''\mathbf{r}'''}\mathbf{E}^P(\mathbf{k}''',\omega''')\mathbf{v}\left|\phi_i\right\rangle\left\langle\phi_j\right|e^{i\mathbf{k}'\mathbf{r}'}\mathbf{E}^P(\mathbf{k}',\omega')\mathbf{v}\left|\phi_k\right\rangle\left\langle\phi_k\right|e^{i\mathbf{k}''\mathbf{r}''}\mathbf{E}^P(\mathbf{k}'',\omega'')\mathbf{v}\left|\phi_l\right\rangle}{(E_i-E_l+\omega'''+i\eta)(E_l-E_k+\omega''+i\eta)}
$$
$$
+(f_l-f_k)\ \frac{\left\langle\phi_j\right|e^{i\mathbf{k}'''\mathbf{r}'''}\mathbf{E}^P(\mathbf{k}''',\omega''')\mathbf{v}\left|\phi_l\right\rangle\left\langle\phi_l\right|e^{i\mathbf{k}''\mathbf{r}''}\mathbf{E}^P(\mathbf{k}'',\omega'')\mathbf{v}\left|\phi_k\right\rangle\left\langle\phi_k\right|e^{i\mathbf{k}'\mathbf{r}'}\mathbf{E}^P(\mathbf{k}',\omega')\mathbf{v}\left|\phi_i\right\rangle}{(E_l-E_j+\omega'''+i\eta)(E_k-E_l+\omega''+i\eta)}\Bigg)
$$
$$
+\frac{i}{2}\ \frac{\left\langle\phi_i\right|e^{-i\mathbf{k}\mathbf{r}}\ \mathbf{v}\left|\phi_j\right\rangle}{E_i-E_j+\omega'+\omega''+\omega'''+2i\eta}
$$
$$
\Bigg((f_i-f_k)\ \frac{\left\langle\phi_j\right|e^{i\mathbf{k}'\mathbf{r}'}\mathbf{E}^P(\mathbf{k}',\omega')\mathbf{v}\left|\phi_k\right\rangle\left\langle\phi_k\right|\left[e^{i\mathbf{k}'''\mathbf{r}''}\mathbf{E}^P(\mathbf{k}''',\omega''')\hat{\mathbf{r}},e^{i\mathbf{k}''\mathbf{r}''}\mathbf{E}^P(\mathbf{k}'',\omega'')\hat{\mathbf{v}}\right]\left|\phi_i\right\rangle}{E_i-E_k+\omega''+\omega'''+i\eta}
$$
$$
+(f_i-f_k)\ \frac{\left\langle\phi_j\right|\left[e^{i\mathbf{r}'\mathbf{k}'''}\mathbf{E}^P(\mathbf{k}''',\omega''')\hat{\mathbf{r}},e^{i\mathbf{k}'\mathbf{r}'}\mathbf{E}^P(\mathbf{k}',\omega')\hat{\mathbf{v}}\right]\left|\phi_k\right\rangle\left\langle\phi_k\right|e^{i\mathbf{k}''\mathbf{r}''}\mathbf{E}^P(\mathbf{k}'',\omega'')\mathbf{v}\left|\phi_i\right\rangle}{E_i-E_k+\omega''+i\eta}
$$
$$
+(f_j-f_k)\ \frac{\left\langle\phi_j\right|\left[e^{i\mathbf{k}'''\mathbf{r}''}\mathbf{E}^P(\mathbf{k}''',\omega''')\hat{\mathbf{r}},e^{i\mathbf{k}''\mathbf{r}''}\mathbf{E}^P(\mathbf{k}'',\omega'')\hat{\mathbf{v}}\right]\left|\phi_k\right\rangle\left\langle\phi_k\right|e^{i\mathbf{k}'\mathbf{r}'}\mathbf{E}^P(\mathbf{k}',\omega')\mathbf{v}\left|\phi_i\right\rangle}{E_k-E_j+\omega''+\omega'''+i\eta}
$$
$$
+(f_j-f_k)\ \frac{\left\langle\phi_j\right|e^{i\mathbf{k}''\mathbf{r}''}\mathbf{E}^P(\mathbf{k}'',\omega'')\mathbf{v}\left|\phi_k\right\rangle\left\langle\phi_k\right|\left[e^{i\mathbf{k}'''\mathbf{r}'}\mathbf{E}^P(\mathbf{k}''',\omega''')\hat{\mathbf{r}},e^{i\mathbf{k}'\mathbf{r}'}\mathbf{E}^P(\mathbf{k}',\omega')\hat{\mathbf{v}}\right]\left|\phi_i\right\rangle}{E_k-E_j+\omega''+i\eta}\Bigg)\Bigg] \tag{D.17}
$$

Calculation of $\mathbf{j}^{(3)}_{ind}(\mathbf{r},\omega)$

We now assemble all the terms,

$$\mathbf{j}^{(3)}_{ind}(\mathbf{k},\omega) = \frac{1}{6V}\lim_{\eta\to 0}\sum_{ijkl}\int d\omega'\int d\omega''\int d\omega'''\,\delta(\omega-\omega'-\omega''-\omega''')\,\frac{1}{\omega'\omega''\omega'''}\sum_{\mathbf{k}',\mathbf{k}'',\mathbf{k}'''}$$

$$\times\left[-i\,\frac{\langle\phi_i|e^{-i\mathbf{kr}}\,\mathbf{v}|\phi_j\rangle}{E_i-E_j+\omega'+\omega''+\omega'''+3i\eta}\right.$$

$$\times\left(\left(f_i-f_k\right)\frac{\left\langle\phi_j\middle|e^{i\mathbf{k}'\mathbf{r}'}\mathbf{E}^P(\mathbf{k}',\omega')\mathbf{v}\middle|\phi_k\right\rangle\left\langle\phi_k\middle|e^{i\mathbf{k}''\mathbf{r}''}\mathbf{E}^P(\mathbf{k}'',\omega'')\mathbf{v}\middle|\phi_l\right\rangle\left\langle\phi_l\middle|e^{i\mathbf{k}'''\mathbf{r}'''}\mathbf{E}^P(\mathbf{k}''',\omega''')\mathbf{v}\middle|\phi_i\right\rangle}{(E_i-E_k+\omega''+\omega'''+2i\eta)(E_i-E_l+\omega'''+i\eta)}\right.$$

$$+\left(f_k-f_j\right)\frac{\left\langle\phi_j\middle|e^{i\mathbf{k}'''\mathbf{r}'''}\mathbf{E}^P(\mathbf{k}''',\omega''')\mathbf{v}\middle|\phi_l\right\rangle\left\langle\phi_l\middle|e^{i\mathbf{k}''\mathbf{r}''}\mathbf{E}^P(\mathbf{k}'',\omega'')\mathbf{v}\middle|\phi_k\right\rangle\left\langle\phi_k\middle|e^{i\mathbf{k}'\mathbf{r}'}\mathbf{E}^P(\mathbf{k}',\omega')\mathbf{v}\middle|\phi_i\right\rangle}{(E_k-E_j+\omega''+\omega'''+2i\eta)(E_l-E_j+\omega'''+i\eta)}$$

$$+\left(f_k-f_l\right)\frac{\left\langle\phi_l\middle|e^{i\mathbf{k}'''\mathbf{r}'''}\mathbf{E}^P(\mathbf{k}''',\omega''')\mathbf{v}\middle|\phi_i\right\rangle\left\langle\phi_j\middle|e^{i\mathbf{k}'\mathbf{r}'}\mathbf{E}^P(\mathbf{k}',\omega')\mathbf{v}\middle|\phi_k\right\rangle\left\langle\phi_k\middle|e^{i\mathbf{k}''\mathbf{r}''}\mathbf{E}^P(\mathbf{k}'',\omega'')\mathbf{v}\middle|\phi_l\right\rangle}{(E_i-E_l+\omega'''+i\eta)(E_l-E_k+\omega''+i\eta)}$$

$$\left.+(f_l-f_k)\frac{\left\langle\phi_j\middle|e^{i\mathbf{k}'''\mathbf{r}'''}\mathbf{E}^P(\mathbf{k}''',\omega''')\mathbf{v}\middle|\phi_l\right\rangle\left\langle\phi_l\middle|e^{i\mathbf{k}''\mathbf{r}''}\mathbf{E}^P(\mathbf{k}'',\omega'')\mathbf{v}\middle|\phi_k\right\rangle\left\langle\phi_k\middle|e^{i\mathbf{k}'\mathbf{r}'}\mathbf{E}^P(\mathbf{k}',\omega')\mathbf{v}\middle|\phi_i\right\rangle}{(E_l-E_j+\omega'''+i\eta)(E_k-E_l+\omega''+i\eta)}\right)$$

$$+\frac{1}{2}\,\frac{\langle\phi_i|e^{-i\mathbf{kr}}\,\mathbf{v}|\phi_j\rangle}{E_i-E_j+\omega'+\omega''+\omega'''+2i\eta}$$

$$\times\left(\left(f_i-f_k\right)\frac{\left\langle\phi_j\middle|e^{i\mathbf{k}'\mathbf{r}'}\mathbf{E}^P(\mathbf{k}',\omega')\mathbf{v}\middle|\phi_k\right\rangle\left\langle\phi_k\middle|\left[e^{i\mathbf{k}'''\mathbf{r}''}\mathbf{E}^P(\mathbf{k}''',\omega''')\hat{\mathbf{r}},e^{i\mathbf{k}''\mathbf{r}''}\mathbf{E}^P(\mathbf{k}'',\omega'')\hat{\mathbf{v}}\right]\middle|\phi_i\right\rangle}{E_i-E_k+\omega''+\omega'''+i\eta}\right.$$

$$+\left(f_i-f_k\right)\frac{\left\langle\phi_j\middle|\left[e^{i\mathbf{r}'\mathbf{k}'''}\mathbf{E}^P(\mathbf{k}''',\omega''')\hat{\mathbf{r}},e^{i\mathbf{k}'\mathbf{r}'}\mathbf{E}^P(\mathbf{k}',\omega')\hat{\mathbf{v}}\right]\middle|\phi_k\right\rangle\left\langle\phi_k\middle|e^{i\mathbf{k}''\mathbf{r}''}\mathbf{E}^P(\mathbf{k}'',\omega'')\mathbf{v}\middle|\phi_i\right\rangle}{E_i-E_k+\omega''+i\eta}$$

$$+\left(f_j-f_k\right)\frac{\left\langle\phi_j\middle|\left[e^{i\mathbf{k}'''\mathbf{r}''}\mathbf{E}^P(\mathbf{k}''',\omega''')\hat{\mathbf{r}},e^{i\mathbf{k}''\mathbf{r}''}\mathbf{E}^P(\mathbf{k}'',\omega'')\hat{\mathbf{v}}\right]\middle|\phi_k\right\rangle\left\langle\phi_k\middle|e^{i\mathbf{k}'\mathbf{r}'}\mathbf{E}^P(\mathbf{k}',\omega')\mathbf{v}\middle|\phi_i\right\rangle}{E_k-E_j+\omega''+\omega'''+i\eta}$$

$$\left.+(f_j-f_k)\frac{\left\langle\phi_j\middle|e^{i\mathbf{k}''\mathbf{r}''}\mathbf{E}^P(\mathbf{k}'',\omega'')\mathbf{v}\middle|\phi_k\right\rangle\left\langle\phi_k\middle|\left[e^{i\mathbf{k}'''\mathbf{r}'}\mathbf{E}^P(\mathbf{k}''',\omega''')\hat{\mathbf{r}},e^{i\mathbf{k}'\mathbf{r}'}\mathbf{E}^P(\mathbf{k}',\omega')\hat{\mathbf{v}}\right]\middle|\phi_i\right\rangle}{E_k-E_j+\omega''+i\eta}\right)$$

$$-\frac{\left\langle\phi_i\middle|e^{-i\mathbf{kr}}\left[\hat{\mathbf{r}},e^{i\mathbf{k}'''\mathbf{r}}\mathbf{E}^P(\mathbf{k}''',\omega''')\hat{\mathbf{v}}\right]\middle|\phi_j\right\rangle}{E_i-E_j+\omega'+\omega''+2i\eta}$$

$$\times\left(\left(f_i-f_k\right)\frac{\left\langle\phi_k\middle|e^{i\mathbf{k}'\mathbf{r}'}\mathbf{E}^P(\mathbf{k}',\omega')\hat{\mathbf{v}}\middle|\phi_i\right\rangle\left\langle\phi_j\middle|e^{i\mathbf{k}''\mathbf{r}''}\mathbf{E}^P(\mathbf{k}'',\omega'')\hat{\mathbf{v}}\middle|\phi_k\right\rangle}{(E_i-E_k+\omega'+i\eta)}\right.$$

$$\left.+(f_j-f_k)\frac{\left\langle\phi_k\middle|e^{i\mathbf{k}'\mathbf{r}'}\mathbf{E}^P(\mathbf{k}',\omega')\hat{\mathbf{v}}\middle|\phi_i\right\rangle\left\langle\phi_j\middle|e^{i\mathbf{k}''\mathbf{r}''}\mathbf{E}^P(\mathbf{k}'',\omega'')\hat{\mathbf{v}}\middle|\phi_k\right\rangle}{(E_k-E_j+\omega''+i\eta)}\right)$$

$$+\frac{i}{2}\,(f_i-f_j)\,\frac{\left\langle\phi_i\middle|e^{-i\mathbf{kr}}\left[\mathbf{r},e^{i\mathbf{k}''\mathbf{r}}\mathbf{E}^P(\mathbf{k}'',\omega'')\hat{\mathbf{v}}\right]\middle|\phi_j\right\rangle\left\langle\phi_j\middle|\left[e^{i\mathbf{k}'''\mathbf{r}'}\mathbf{E}^P(\mathbf{k}''',\omega''')\hat{\mathbf{r}},e^{i\mathbf{k}'\mathbf{r}'}\mathbf{E}^P(\mathbf{k}',\omega')\hat{\mathbf{v}}\right]\middle|\phi_i\right\rangle}{E_i-E_j+\omega'+\omega'''+i\eta}$$

$$-\frac{i}{2}\,(f_j-f_i)\,\frac{\left\langle\phi_i\middle|e^{-i\mathbf{kr}}\left[\hat{\mathbf{r}},\left[e^{i\mathbf{k}''\mathbf{r}}\mathbf{E}^P(\mathbf{k}'',\omega'')\hat{\mathbf{r}},e^{i\mathbf{k}'''\mathbf{r}}\mathbf{E}^P(\mathbf{k}''',\omega''')\hat{\mathbf{v}}\right]\right]\middle|\phi_j\right\rangle\left\langle\phi_j\middle|e^{i\mathbf{k}'\mathbf{r}'}\mathbf{E}^P(\mathbf{k}',\omega')\hat{\mathbf{v}}\middle|\phi_i\right\rangle}{E_i-E_j+\omega'+i\eta}$$

$$+\frac{1}{6}\,f_i\left\langle\phi_i\middle|e^{-i\mathbf{kr}}\left[\hat{\mathbf{r}},\left[e^{i\mathbf{k}'\mathbf{r}}\mathbf{E}^P(\mathbf{k}',\omega')\hat{\mathbf{r}},\left[e^{i\mathbf{k}''\mathbf{r}}\mathbf{E}^P(\mathbf{k}'',\omega'')\hat{\mathbf{r}},e^{i\mathbf{k}'''\mathbf{r}}\mathbf{E}^P(\mathbf{k}''',\omega''')\mathbf{v}\right]\right]\right]\middle|\phi_i\right\rangle\Bigg]$$

$$+Sym\big((\mathbf{q}',\omega'),(\mathbf{q}'',\omega''),(\mathbf{q}''',\omega''')\big) \quad \text{(D.18)}$$

Using the following relation, obtained from the continuity equation,

$$\mathbf{j}^{(3)}_{ind}(\mathbf{k},\omega) = -\frac{i}{6}\int d\omega' \int d\omega'' \int d\omega''' \, \delta(\omega-\omega'-\omega''-\omega''') \sum_{\mathbf{k}',\mathbf{k}'',\mathbf{k}'''} \frac{\omega}{\mathbf{k}\mathbf{k}'\mathbf{k}''\mathbf{k}'''} \, \mathbf{E}^P(\mathbf{k}',\omega') \\ \mathbf{E}^P(\mathbf{k}'',\omega'') \, \mathbf{E}^P(\mathbf{k}''',\omega''') \, \chi_{\rho\rho\rho\rho}(\mathbf{k},\mathbf{k}',\mathbf{k}'',\mathbf{k}''',\omega',\omega'',\omega'''), \quad \text{(D.19)}$$

one can extract the third-order density response function $\chi_{\rho\rho\rho\rho}$. In the reciprocal space, the vector $\mathbf{k}$ can be written as sum $\mathbf{q}+\mathbf{G}$, where $\mathbf{q}$ is a vector inside the BZ and $\mathbf{G}$ a reciprocal lattice vector. However in the independent-particle approximation all vectors $\mathbf{G}$ are considered equal to zero. The indices i,j,k run over both the bands and k-points and can therefore be separated into two indices, one that runs over the bands and the other over the k-point. The $\chi_{\rho\rho\rho\rho}$ thus extracted is written in equation (E.1).

Appendix E

THG: current density calculation

The general formula for the third-order density response function obtained from the current is

$$\chi_{\rho\rho\rho\rho}(\mathbf{q},\mathbf{q}_1,\mathbf{q}_2,\mathbf{q}_3,\omega_1,\omega_2,\omega_3) = \frac{1}{V}\sum_{\mathbf{k}}\sum_{n,m,p,l}\frac{1}{(\omega_1+\omega_2+\omega_3)\omega_1\omega_2\omega_3}$$
$$\times\Bigg\{\frac{\langle\phi_{n,\mathbf{k}}|\mathbf{q}\hat{\mathbf{v}}|\phi_{m,\mathbf{k}}\rangle}{E_{n,\mathbf{k}}-E_{m,\mathbf{k}}+\omega_1+\omega_2+\omega_3+3i\eta}\Big[\langle\phi_{m,\mathbf{k}}|\mathbf{q}_1\hat{\mathbf{v}}|\phi_{p,\mathbf{k}}\rangle\langle\phi_{p,\mathbf{k}}|\mathbf{q}_2\hat{\mathbf{v}}|\phi_{l,\mathbf{k}}\rangle\langle\phi_{l,\mathbf{k}}|\mathbf{q}_3\hat{\mathbf{v}}|\phi_{n,\mathbf{k}}\rangle$$
$$\times\Bigg(\frac{1}{(E_{n,\mathbf{k}}-E_{l,\mathbf{k}}+\omega_3+i\eta)}\left[\frac{f_{n,\mathbf{k}}-f_{p,\mathbf{k}}}{(E_{n,\mathbf{k}}-E_{p,\mathbf{k}}+\omega_2+\omega_3+2i\eta)}+\frac{f_{p,\mathbf{k}}-f_{l,\mathbf{k}}}{(E_{l,\mathbf{k}}-E_{p,\mathbf{k}}+\omega_2+i\eta)}\right]$$
$$+\frac{1}{(E_{p,\mathbf{k}}-E_{m,\mathbf{k}}+\omega_1+i\eta)}\left[\frac{f_{l,\mathbf{k}}-f_{m,\mathbf{k}}}{(E_{l,\mathbf{k}}-E_{m,\mathbf{k}}+\omega_1+\omega_2+2i\eta)}+\frac{f_{p,\mathbf{k}}-f_{l,\mathbf{k}}}{(E_{l,\mathbf{k}}-E_{p,\mathbf{k}}+\omega_2+i\eta)}\right]\Bigg)$$
$$+\langle\phi_{m,\mathbf{k}}|\mathbf{q}_1\hat{\mathbf{v}}|\phi_{p,\mathbf{k}}\rangle\langle\phi_{p,\mathbf{k}}|[i\mathbf{q}_3\hat{\mathbf{r}},\mathbf{q}_2\hat{\mathbf{v}}]|\phi_{n,\mathbf{k}}\rangle\Bigg(\frac{f_{n,\mathbf{k}}-f_{p,\mathbf{k}}}{2(E_{n,\mathbf{k}}-E_{p,\mathbf{k}}+\omega_2+\omega_3+2i\eta)}$$
$$+\frac{f_{m,\mathbf{k}}-f_{p,\mathbf{k}}}{2(E_{p,\mathbf{k}}-E_{m,\mathbf{k}}+\omega_1+i\eta)}\Bigg)+\langle\phi_{m,\mathbf{k}}|[i\mathbf{q}_3\hat{\mathbf{r}},\mathbf{q}_2\hat{\mathbf{v}}]|\phi_{p,\mathbf{k}}\rangle\langle\phi_{p,\mathbf{k}}|\mathbf{q}_1\hat{\mathbf{v}}|\phi_{n,\mathbf{k}}\rangle$$
$$\times\left(\frac{f_{n,\mathbf{k}}-f_{p,\mathbf{k}}}{2(E_{n,\mathbf{k}}-E_{p,\mathbf{k}}+\omega_1+i\eta)}+\frac{f_{m,\mathbf{k}}-f_{p,\mathbf{k}}}{2(E_{p,\mathbf{k}}-E_{m,\mathbf{k}}+\omega_2+\omega_3+2i\eta)}\right)\Big]$$
$$-\frac{\langle\phi_{n,\mathbf{k}}|[i\mathbf{q}\hat{\mathbf{r}},\mathbf{q}_3\hat{\mathbf{v}}]|\phi_{m,\mathbf{k}}\rangle}{E_{n,\mathbf{k}}-E_{m,\mathbf{k}}+\omega_1+\omega_2+2i\eta}\langle\phi_{p,\mathbf{k}}|\mathbf{q}_1\hat{\mathbf{v}}|\phi_{n,\mathbf{k}}\rangle\langle\phi_{m,\mathbf{k}}|\mathbf{q}_2\hat{\mathbf{v}}|\phi_{p,\mathbf{k}}\rangle\left(\frac{f_{n,\mathbf{k}}-f_{p,\mathbf{k}}}{(E_{n,\mathbf{k}}-E_{p,\mathbf{k}}+\omega_1+i\eta)}\right.$$
$$\left.+\frac{f_{m,\mathbf{k}}-f_{p,\mathbf{k}}}{(E_{p,\mathbf{k}}-E_{m,\mathbf{k}}+\omega_2+i\eta)}\right)+\frac{1}{2}\left(f_{n,\mathbf{k}}-f_{m,\mathbf{k}}\right)\frac{\langle\phi_{n,\mathbf{k}}|[i\mathbf{q}\hat{\mathbf{r}},\mathbf{q}_3\hat{\mathbf{v}}]|\phi_{m,\mathbf{k}}\rangle\langle\phi_{m,\mathbf{k}}|[i\mathbf{q}_2\hat{\mathbf{r}},\mathbf{q}_1\hat{\mathbf{v}}]|\phi_{n,\mathbf{k}}\rangle}{E_{n,\mathbf{k}}-E_{m,\mathbf{k}}+\omega_1+\omega_2+2i\eta}$$
$$-\frac{1}{2}\left(f_{m,\mathbf{k}}-f_{n,\mathbf{k}}\right)\frac{\langle\phi_{n,\mathbf{k}}|[i\mathbf{q}\hat{\mathbf{r}},[i\mathbf{q}_2\hat{\mathbf{r}},\mathbf{q}_3\hat{\mathbf{v}}]]|\phi_{m,\mathbf{k}}\rangle\ \langle\phi_{m,\mathbf{k}}|\mathbf{q}_1\hat{\mathbf{v}}|\phi_{n,\mathbf{k}}\rangle}{E_{n,\mathbf{k}}-E_{m,\mathbf{k}}+\omega_1+i\eta}$$
$$-\frac{1}{6}f_{n,\mathbf{k}}\langle\phi_{n,\mathbf{k}}|[i\mathbf{q}\hat{\mathbf{r}},[i\mathbf{q}_1\hat{\mathbf{r}},[i\mathbf{q}_2\hat{\mathbf{r}},\mathbf{q}_3\hat{\mathbf{v}}]]]|\phi_{n,\mathbf{k}}\rangle\Bigg\}+\big((\mathbf{q}_1,\omega_1)\leftrightarrow(\mathbf{q}_2,\omega_2)\leftrightarrow(\mathbf{q}_3,\omega_3)\big) \quad \text{(E.1)}$$

As previously mentioned, we neglect the double and triple commutator involving the nonlocal potential in the velocity operator and using equation (C.2), we arrive to the general expression (4.42), when there is no scissor, which lead for the third harmonic to

$$\chi_{\rho\rho\rho\rho}(\mathbf{q},\mathbf{q}_1,\mathbf{q}_2,\mathbf{q}_3,\omega,\omega,\omega) = \frac{1}{V}\frac{1}{3\omega^4}\sum_{\mathbf{k}}\sum_{n,m,p,l}\frac{\hat{\mathbf{v}}_{nm}(\mathbf{q})\hat{\mathbf{v}}_{mp}(\mathbf{q}_1)\hat{\mathbf{v}}_{pl}(\mathbf{q}_2)\hat{\mathbf{v}}_{ln}(\mathbf{q}_3)}{E_{nm,\mathbf{k}}+3\tilde{\omega}}$$
$$\times\left[\frac{1}{E_{nl,\mathbf{k}}+\tilde{\omega}}\left(\frac{f_{np,\mathbf{k}}}{E_{np,\mathbf{k}}+2\tilde{\omega}}+\frac{f_{pl,\mathbf{k}}}{E_{lp,\mathbf{k}}+\tilde{\omega}}\right)+\frac{1}{E_{pm,\mathbf{k}}+\tilde{\omega}}\left(\frac{f_{lm,\mathbf{k}}}{E_{lm,\mathbf{k}}+2\tilde{\omega}}+\frac{f_{pl,\mathbf{k}}}{E_{lp,\mathbf{k}}+\tilde{\omega}}\right)\right]$$
$$+\big(\mathbf{q}_1\leftrightarrow\mathbf{q}_2\leftrightarrow\mathbf{q}_3\big), \quad \text{(E.2)}$$

Following the development of equation (4.43) to get rid of ω^4 in the denominator, we derive the terms $\mathcal{A}$, $\mathcal{B}$, $\mathcal{C}$ and $\mathcal{F}$ that need to be proven zero, in the same fashion as in appendix C.

$$\mathcal{A} = \frac{f_{np,\mathbf{k}}}{E_{nm,\mathbf{k}}E_{nl,\mathbf{k}}E_{np,\mathbf{k}}} + \frac{f_{pl,\mathbf{k}}}{E_{nm,\mathbf{k}}E_{nl,\mathbf{k}}E_{lp,\mathbf{k}}} + \frac{f_{lm,\mathbf{k}}}{E_{nm,\mathbf{k}}E_{pm,\mathbf{k}}E_{lm,\mathbf{k}}} + \frac{f_{pl,\mathbf{k}}}{E_{nm,\mathbf{k}}E_{pm,\mathbf{k}}E_{lp,\mathbf{k}}} \tag{E.3a}$$

$$\begin{aligned}\mathcal{B} = &-\frac{f_{np,\mathbf{k}}}{E_{nm,\mathbf{k}}E_{nl,\mathbf{k}}E_{np,\mathbf{k}}}\left[\frac{1}{E_{nl,\mathbf{k}}} + \frac{3}{E_{nm,\mathbf{k}}} + \frac{2}{E_{np,\mathbf{k}}}\right] - \frac{f_{pl,\mathbf{k}}}{E_{nm,\mathbf{k}}E_{nl,\mathbf{k}}E_{lp,\mathbf{k}}}\left[\frac{1}{E_{nl,\mathbf{k}}} + \frac{3}{E_{nm,\mathbf{k}}} + \frac{1}{E_{lp,\mathbf{k}}}\right] \\ &- \frac{f_{lm,\mathbf{k}}}{E_{nm,\mathbf{k}}E_{pm,\mathbf{k}}E_{lm,\mathbf{k}}}\left[\frac{3}{E_{nm,\mathbf{k}}} + \frac{1}{E_{pm,\mathbf{k}}} + \frac{2}{E_{lm,\mathbf{k}}}\right] - \frac{f_{pl,\mathbf{k}}}{E_{nm,\mathbf{k}}E_{pm,\mathbf{k}}E_{lp,\mathbf{k}}}\left[\frac{3}{E_{nm,\mathbf{k}}} + \frac{1}{E_{pm,\mathbf{k}}} + \frac{1}{E_{lp,\mathbf{k}}}\right]\end{aligned} \tag{E.3b}$$

$$\begin{aligned}\mathcal{C} = &\frac{f_{np,\mathbf{k}}}{E_{nm,\mathbf{k}}E_{nl,\mathbf{k}}E_{np,\mathbf{k}}}\left[\frac{3}{E_{nm,\mathbf{k}}E_{nl,\mathbf{k}}} + \frac{2}{E_{nl,\mathbf{k}}E_{np,\mathbf{k}}} + \frac{6}{E_{nm,\mathbf{k}}E_{np,\mathbf{k}}} + \frac{1}{E_{nl,\mathbf{k}}^2} + \frac{9}{E_{nm,\mathbf{k}}^2} + \frac{4}{E_{np,\mathbf{k}}^2}\right] \\ &+ \frac{f_{pl,\mathbf{k}}}{E_{nm,\mathbf{k}}E_{nl,\mathbf{k}}E_{lp,\mathbf{k}}}\left[\frac{3}{E_{nm,\mathbf{k}}E_{nl,\mathbf{k}}} + \frac{1}{E_{nl,\mathbf{k}}E_{lp,\mathbf{k}}} + \frac{3}{E_{nm,\mathbf{k}}E_{lp,\mathbf{k}}} + \frac{1}{E_{nl,\mathbf{k}}^2} + \frac{9}{E_{nm,\mathbf{k}}^2} + \frac{1}{E_{lp,\mathbf{k}}^2}\right] \\ &+ \frac{f_{lm,\mathbf{k}}}{E_{nm,\mathbf{k}}E_{pm,\mathbf{k}}E_{lm,\mathbf{k}}}\left[\frac{9}{E_{nm,\mathbf{k}}^2} + \frac{3}{E_{nm,\mathbf{k}}E_{pm,\mathbf{k}}} + \frac{6}{E_{nm,\mathbf{k}}E_{lm,\mathbf{k}}} + \frac{1}{E_{pm,\mathbf{k}}^2} + \frac{2}{E_{pm,\mathbf{k}}E_{lm,\mathbf{k}}} + \frac{4}{E_{lm,\mathbf{k}}^2}\right] \\ &+ \frac{f_{pl,\mathbf{k}}}{E_{nm,\mathbf{k}}E_{pm,\mathbf{k}}E_{lp,\mathbf{k}}}\left[\frac{9}{E_{nm,\mathbf{k}}^2} + \frac{3}{E_{nm,\mathbf{k}}E_{pm,\mathbf{k}}} + \frac{3}{E_{nm,\mathbf{k}}E_{lp,\mathbf{k}}} + \frac{1}{E_{pm,\mathbf{k}}^2} + \frac{1}{E_{pm,\mathbf{k}}E_{lp,\mathbf{k}}} + \frac{1}{E_{lp,\mathbf{k}}^2}\right]\end{aligned} \tag{E.3c}$$

$$\begin{aligned}\mathcal{F} = &-\frac{f_{np,\mathbf{k}}}{E_{nm,\mathbf{k}}E_{nl,\mathbf{k}}E_{np,\mathbf{k}}}\left[\frac{6}{E_{nm,\mathbf{k}}E_{nl,\mathbf{k}}E_{np,\mathbf{k}}} + \frac{3}{E_{nm,\mathbf{k}}E_{nl,\mathbf{k}}^2} + \frac{2}{E_{nl,\mathbf{k}}^2E_{np,\mathbf{k}}} + \frac{9}{E_{nm,\mathbf{k}}^2E_{nl,\mathbf{k}}}\right. \\ &\left. + \frac{18}{E_{nm,\mathbf{k}}^2E_{np,\mathbf{k}}} + \frac{4}{E_{nl,\mathbf{k}}E_{np,\mathbf{k}}^2} + \frac{12}{E_{nm,\mathbf{k}}E_{np,\mathbf{k}}^2} + \frac{1}{E_{nl,\mathbf{k}}^3} + \frac{27}{E_{nm,\mathbf{k}}^3} + \frac{8}{E_{np,\mathbf{k}}^3}\right] \\ &- \frac{f_{pl\mathbf{k}}}{E_{nm,\mathbf{k}}E_{nl,\mathbf{k}}E_{lp\mathbf{k}}}\left[\frac{3}{E_{nm,\mathbf{k}}E_{nl,\mathbf{k}}E_{lp\mathbf{k}}} + \frac{3}{E_{nm,\mathbf{k}}E_{nl,\mathbf{k}}^2} + \frac{9}{E_{nm,\mathbf{k}}^2E_{nl,\mathbf{k}}} + \frac{9}{E_{nm,\mathbf{k}}^2E_{lp\mathbf{k}}}\right. \\ &\left. + \frac{1}{E_{nl,\mathbf{k}}E_{lp\mathbf{k}}^2} + \frac{3}{E_{nm,\mathbf{k}}E_{lp\mathbf{k}}^2} + \frac{1}{E_{nl,\mathbf{k}}^3} + \frac{27}{E_{nm,\mathbf{k}}^3} + \frac{1}{E_{nl,\mathbf{k}}^2E_{lp\mathbf{k}}} + \frac{1}{E_{lp\mathbf{k}}^3}\right] \\ &- \frac{f_{lm\mathbf{k}}}{E_{nm,\mathbf{k}}E_{pm\mathbf{k}}E_{lm\mathbf{k}}}\left[\frac{27}{E_{nm,\mathbf{k}}^3} + \frac{9}{E_{nm,\mathbf{k}}^2E_{pm\mathbf{k}}} + \frac{18}{E_{nm,\mathbf{k}}^2E_{lm\mathbf{k}}} + \frac{3}{E_{nm,\mathbf{k}}E_{pm\mathbf{k}}^2}\right. \\ &\left. + \frac{6}{E_{nm,\mathbf{k}}E_{pm\mathbf{k}}E_{lm\mathbf{k}}} + \frac{12}{E_{nm,\mathbf{k}}E_{lm\mathbf{k}}^2} + \frac{1}{E_{pm\mathbf{k}}^3} + \frac{2}{E_{pm\mathbf{k}}^2E_{lm\mathbf{k}}} + \frac{4}{E_{pm\mathbf{k}}E_{lm\mathbf{k}}^2} + \frac{8}{E_{lm\mathbf{k}}^3}\right] \\ &- \frac{f_{pl\mathbf{k}}}{E_{nm,\mathbf{k}}E_{pm\mathbf{k}}E_{lp\mathbf{k}}}\left[\frac{27}{E_{nm,\mathbf{k}}^3} + \frac{9}{E_{nm,\mathbf{k}}^2E_{pm\mathbf{k}}} + \frac{9}{E_{nm,\mathbf{k}}^2E_{lp\mathbf{k}}} + \frac{3}{E_{nm,\mathbf{k}}E_{pm\mathbf{k}}^2} + \frac{3}{E_{nm,\mathbf{k}}E_{lp\mathbf{k}}^2}\right. \\ &\left. + \frac{1}{E_{pm\mathbf{k}}^3} + \frac{1}{E_{pm\mathbf{k}}^2E_{lp\mathbf{k}}} + \frac{1}{E_{pm\mathbf{k}}E_{lp\mathbf{k}}^2} + \frac{3}{E_{nm,\mathbf{k}}E_{pm\mathbf{k}}E_{lp\mathbf{k}}} + \frac{1}{E_{lp\mathbf{k}}^3}\right]\end{aligned} \tag{E.3d}$$

The terms associated with $\mathcal{B}$ and $\mathcal{F}$ are canceled by interchanging indices $(n \leftrightarrow m)$ and $(p \leftrightarrow l)$ and by summing over $-\mathbf{k}$ instead of $\mathbf{k}$, which leads to $\chi^{\mathcal{B}}_{\rho\rho\rho\rho} = -\chi^{\mathcal{B}}_{\rho\rho\rho\rho}$ and $\chi^{\mathcal{F}}_{\rho\rho\rho\rho} = -\chi^{\mathcal{F}}_{\rho\rho\rho\rho}$.

I thought about proving the terms $\mathcal{A}$ and $\mathcal{C}$ to vanish in the same fashion as for the term $\mathcal{B}$ for the second order (see section C for LEO), by writing it as the derivative over $\mathbf{k}$ of a function periodic throughout the BZ. However, this demonstration was not finished. Nonetheless, I present here the tensor $\overset{\leftrightarrow}{T}$ that was introduced to prove the term $\mathcal{A}$ zero.

$$\overset{\leftrightarrow}{T}(\mathbf{q}, \mathbf{q}_1, \mathbf{q}_2) = \sum_{n,m,p} \hat{\mathbf{v}}_{nm,\mathbf{k}}(\mathbf{q})\hat{\mathbf{v}}_{mp,\mathbf{k}}(\mathbf{q}_1)\hat{\mathbf{v}}_{pn}(\mathbf{q}_2)\left[\frac{f_{np}}{E_{nm,\mathbf{k}}E_{np,\mathbf{k}}} + \frac{f_{mp}}{E_{nm,\mathbf{k}}E_{pm,\mathbf{k}}}\right] \tag{E.4}$$

Also the terms $\mathcal{A}$ and $\mathcal{C}$ were not formally proven to be zero, we know that all these terms vanishes for the first and third order. Moreover, when plotting the initial formula containing the divergence in ω with the one for which these terms were subtracted, shown in Figure E.1, we find a good agreement after the gap-region further suggesting that these terms are indeed zero.

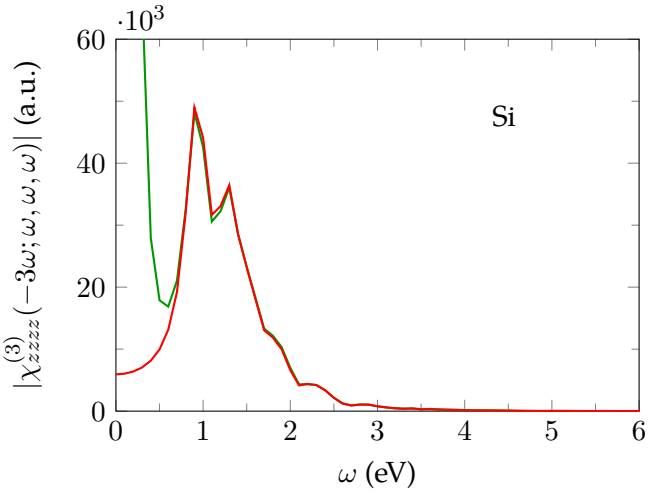

Figure E.1: Comparison between the ω-divergent and final THG formula for silicon.

Appendix F

EFISH formula

The calculation of the EFISH response starts from the general third-order formula (E.1), for which the double and triple commutator $[i\hat{\mathbf{r}}, \dots [i\hat{\mathbf{r}}, \hat{V}_{nl}]]$, that we know to be very small, are neglected. As a results, all the terms containing a commutator are either canceled with their occupation numbers or with other terms, leading us to the following formula:

$$\chi_{\rho\rho\rho\rho}(\hat{\mathbf{q}}, \hat{\mathbf{q}}_1, \hat{\mathbf{q}}_2, \hat{\mathbf{q}}_3, \omega_1, \omega_2, \omega_3) = \frac{1}{V} \frac{1}{(\omega_1+\omega_2+\omega_3)\omega_1\omega_2\omega_3} \sum_{\mathbf{k}} \sum_{n,m,p,l} \frac{\hat{\mathbf{v}}_{nm}(\hat{\mathbf{q}})\hat{\mathbf{v}}_{mp}(\hat{\mathbf{q}}_1)\hat{\mathbf{v}}_{pl}(\hat{\mathbf{q}}_2)\hat{\mathbf{v}}_{ln}(\hat{\mathbf{q}}_3)}{E_{nm,\mathbf{k}}+\tilde{\omega}_1+\tilde{\omega}_2+\tilde{\omega}_3}$$
$$\times \left[\frac{1}{E_{nl,\mathbf{k}}+\tilde{\omega}_3}\left(\frac{f_{np,\mathbf{k}}}{E_{np,\mathbf{k}}+\tilde{\omega}_2+\tilde{\omega}_3}+\frac{f_{pl,\mathbf{k}}}{E_{lp,\mathbf{k}}+\tilde{\omega}_2}\right)+\frac{1}{E_{pm,\mathbf{k}}+\tilde{\omega}_1}\left(\frac{f_{lm,\mathbf{k}}}{E_{lm,\mathbf{k}}+\tilde{\omega}_1+\tilde{\omega}_2}+\frac{f_{pl,\mathbf{k}}}{E_{lp,\mathbf{k}}+\tilde{\omega}_2}\right)\right]$$
$$+ \big((\mathbf{q}_1,\omega_1) \leftrightarrow (\mathbf{q}_2,\omega_2) \leftrightarrow (\mathbf{q}_3,\omega_3)\big), \quad \text{(F.1)}$$

This expression contains all the permutations in $\mathbf{q}$ and ω that are then treated separately, except for the one $(\mathbf{q}', \omega') \leftrightarrow (\mathbf{q}'', \omega'')$, since, in fine, ω_1 and ω_2 will be equal.

After getting rid of the divergence in ω''' following equation (4.46), and setting $\omega_1 = \omega_2$ and $\omega_3 = 0$, we reach equation (4.49). From there, a development in ω, shown in equation (4.50), is done for each of the permutation to remove the remaining divergence.

We then also separate the four-, three- and two-band terms.

$$\chi_0^{(3)} = \chi_{0,1}^{(3),4bnd} + \chi_{0,2}^{(3),4bnd} + \chi_{0,3}^{(3),4bnd} + \chi_{0,1}^{(3),3bnd} + \chi_{0,2}^{(3),3bnd} + \chi_{0,3}^{(3),3bnd} + \chi_0^{(3),2bnd} \quad \text{(F.2)}$$

The contribution $\chi_{0,1}^{(3),4bnd}$ corresponds to the permutation displayed in equation (F.1) and $\chi_{0,2}^{(3),4bnd}$ and $\chi_{0,3}^{(3),4bnd}$ corresponds to the permutation $(\mathbf{q}'', \omega'') \leftrightarrow (\mathbf{q}''', \omega''')$ and $(\mathbf{q}', \omega') \leftrightarrow (\mathbf{q}''', \omega''')$, respectively. For the three-band contribution, all the permutations are mixed together and it is separated depending on the position of $\Delta_{n,n',\mathbf{k}}$, either in $\mathbf{q}$, $\mathbf{q}'$ or $\mathbf{q}'''$.

After a lengthy calculation, the four-band terms obtained is, for the first permutation,

$$\chi_{0,1}^{(3),4bnd}(\hat{\mathbf{q}}, \hat{\mathbf{q}}_1, \hat{\mathbf{q}}_2, \hat{\mathbf{q}}_3, \omega, \omega, 0) = \frac{1}{V} \sum_{nmpl} \hat{\mathbf{r}}_{nm,\mathbf{k}}(\hat{\mathbf{q}})\, \hat{\mathbf{r}}_{mp,\mathbf{k}}(\hat{\mathbf{q}}_1)\, \hat{\mathbf{r}}_{pl,\mathbf{k}}(\hat{\mathbf{q}}_2)\, \hat{\mathbf{r}}_{ln,\mathbf{k}}(\hat{\mathbf{q}}_3)$$
$$\times \Bigg[-\frac{f_{nl}}{(E_{nm,\mathbf{k}}+2\tilde{\omega})(E_{np,\mathbf{k}}+\tilde{\omega})E_{nl,\mathbf{k}}} - \frac{f_{pl}}{(E_{nm,\mathbf{k}}+2\tilde{\omega})(E_{np,\mathbf{k}}+\tilde{\omega})(E_{lp,\mathbf{k}}+\tilde{\omega})}$$
$$- \frac{f_{lm}}{(E_{nm,\mathbf{k}}+2\tilde{\omega})(E_{pm,\mathbf{k}}+\tilde{\omega})(E_{lm,\mathbf{k}}+2\tilde{\omega})} - \frac{f_{pl}}{(E_{nm,\mathbf{k}}+2\tilde{\omega})(E_{pm,\mathbf{k}}+\tilde{\omega})(E_{lp,\mathbf{k}}+\tilde{\omega})}$$
$$- \frac{5f_{np}E_{pm,\mathbf{k}}E_{lp,\mathbf{k}}}{4(E_{np,\mathbf{k}}+\tilde{\omega})(E_{np,\mathbf{k}})^4} + \frac{f_{np}(E_{nm,\mathbf{k}}+E_{nl,\mathbf{k}}-3E_{lp,\mathbf{k}})}{2(E_{np,\mathbf{k}}+\tilde{\omega})(E_{np,\mathbf{k}})^3} - \frac{f_{np}(E_{nm,\mathbf{k}}+E_{np,\mathbf{k}})E_{lp,\mathbf{k}}}{2(E_{np,\mathbf{k}}+\tilde{\omega})^2(E_{np,\mathbf{k}})^3}$$
$$- \frac{f_{np}(E_{nm,\mathbf{k}}+E_{np,\mathbf{k}})}{2(E_{np,\mathbf{k}}+\tilde{\omega})E_{nl,\mathbf{k}}(E_{np,\mathbf{k}})^2} - \frac{f_{np}E_{lp,\mathbf{k}}}{(E_{pm,\mathbf{k}}+\tilde{\omega})(E_{np,\mathbf{k}}+\tilde{\omega})^2E_{np,\mathbf{k}}} - \frac{f_{np}E_{lp,\mathbf{k}}}{2(E_{pm,\mathbf{k}}+\tilde{\omega})(E_{np,\mathbf{k}}+\tilde{\omega})(E_{np,\mathbf{k}})^2}$$

$$
\begin{aligned}
&- \frac{f_{np}E_{lp,\mathbf{k}}}{2(E_{pm,\mathbf{k}}+\tilde{\omega})E_{nm,\mathbf{k}}(E_{np,\mathbf{k}})^2} - \frac{f_{np}E_{lp,\mathbf{k}}}{2(E_{nm,\mathbf{k}}+2\tilde{\omega})(E_{np,\mathbf{k}}+\tilde{\omega})(E_{np,\mathbf{k}})^2} - \frac{f_{np}E_{lp,\mathbf{k}}}{(E_{nm,\mathbf{k}}+2\tilde{\omega})E_{pm,\mathbf{k}}(E_{np,\mathbf{k}})^2} \\
&+ \frac{f_{np}}{(E_{pm,\mathbf{k}}+\tilde{\omega})(E_{np,\mathbf{k}}+\tilde{\omega})E_{np,\mathbf{k}}} + \frac{f_{np}}{(E_{pm,\mathbf{k}}+\tilde{\omega})E_{nm,\mathbf{k}}E_{np,\mathbf{k}}} + \frac{4f_{lm}E_{nl,\mathbf{k}}E_{lp,\mathbf{k}}}{(E_{lm,\mathbf{k}}+2\tilde{\omega})(E_{lm,\mathbf{k}})^4} \\
&- \frac{2f_{lm}E_{nl,\mathbf{k}}}{(E_{lm,\mathbf{k}}+2\tilde{\omega})(E_{lm,\mathbf{k}})^3} + \frac{2f_{lm}(E_{lm,\mathbf{k}}-2E_{lp,\mathbf{k}})}{(E_{lm,\mathbf{k}}+2\tilde{\omega})E_{nl,\mathbf{k}}(E_{lm,\mathbf{k}})^2} + \frac{f_{lm}}{(E_{lm,\mathbf{k}}+2\tilde{\omega})(E_{lp,\mathbf{k}}+\tilde{\omega})E_{lm,\mathbf{k}}} \\
&- \frac{f_{lm}}{2(E_{lp,\mathbf{k}}+\tilde{\omega})E_{pm,\mathbf{k}}E_{lm,\mathbf{k}}} + \frac{f_{lm}E_{nm,\mathbf{k}}}{(E_{pm,\mathbf{k}}+\tilde{\omega})(E_{lm,\mathbf{k}}+2\tilde{\omega})(E_{lm,\mathbf{k}})^2} - \frac{f_{lm}E_{nm,\mathbf{k}}}{2(E_{pm,\mathbf{k}}+\tilde{\omega})(E_{lm,\mathbf{k}})^2E_{lp,\mathbf{k}}} \\
&+ \frac{f_{pl}E_{nm,\mathbf{k}}}{4(E_{lp,\mathbf{k}}+\tilde{\omega})(E_{lp,\mathbf{k}})^3} - \frac{f_{pl}(E_{nm,\mathbf{k}}+E_{lp,\mathbf{k}})}{2(E_{lp,\mathbf{k}}+\tilde{\omega})E_{nl,\mathbf{k}}(E_{lp,\mathbf{k}})^2} - \frac{f_{pl}}{2(E_{lp,\mathbf{k}}+\tilde{\omega})E_{pm,\mathbf{k}}E_{lp,\mathbf{k}}} \\
&+ \frac{f_{pl}E_{nm,\mathbf{k}}}{4(E_{pm,\mathbf{k}}+\tilde{\omega})(E_{lp,\mathbf{k}}+\tilde{\omega})(E_{lp,\mathbf{k}})^2} + \frac{f_{pl}E_{nm,\mathbf{k}}}{4(E_{pm,\mathbf{k}}+\tilde{\omega})E_{lm,\mathbf{k}}(E_{lp,\mathbf{k}})^2} + \frac{f_{pm}(E_{nl,\mathbf{k}}-E_{pm,\mathbf{k}})}{4(E_{pm,\mathbf{k}}+\tilde{\omega})E_{pm,\mathbf{k}}^3} \\
&+ \frac{f_{pm}E_{lp,\mathbf{k}}}{2(E_{nm,\mathbf{k}}+2\tilde{\omega})(E_{pm,\mathbf{k}}+\tilde{\omega})E_{pm,\mathbf{k}}^2} - \frac{f_{pm}E_{lp,\mathbf{k}}}{2(E_{pm,\mathbf{k}}+\tilde{\omega})E_{nm,\mathbf{k}}E_{pm,\mathbf{k}}^2} + \frac{f_{pm}E_{lp,\mathbf{k}}}{(E_{nm,\mathbf{k}}+2\tilde{\omega})E_{pm,\mathbf{k}}^2E_{np,\mathbf{k}}} \\
&- \frac{f_{pm}}{(E_{pm,\mathbf{k}}+\tilde{\omega})E_{nm,\mathbf{k}}E_{pm,\mathbf{k}}} - \frac{f_{pm}}{2(E_{pm,\mathbf{k}}+\tilde{\omega})(E_{lp,\mathbf{k}}+\tilde{\omega})E_{pm,\mathbf{k}}} + \frac{f_{pm}E_{nm,\mathbf{k}}}{2(E_{pm,\mathbf{k}}+\tilde{\omega})E_{pm,\mathbf{k}}^2E_{lp,\mathbf{k}}} \\
&- \frac{f_{pm}E_{nm,\mathbf{k}}}{4(E_{pm,\mathbf{k}}+\tilde{\omega})E_{pm,\mathbf{k}}^2E_{lm,\mathbf{k}}} + \frac{4f_{nm}E_{lp,\mathbf{k}}}{(E_{nm,\mathbf{k}}+2\tilde{\omega})^2E_{nm,\mathbf{k}}^2} + \frac{8f_{nm}E_{lp,\mathbf{k}}}{(E_{nm,\mathbf{k}}+2\tilde{\omega})E_{nm,\mathbf{k}}^3} \\
&+ \frac{2f_{nm}E_{lp,\mathbf{k}}}{(E_{nm,\mathbf{k}}+2\tilde{\omega})^2(E_{pm,\mathbf{k}}+\tilde{\omega})E_{nm,\mathbf{k}}} + \frac{f_{nm}E_{lp,\mathbf{k}}}{(E_{nm,\mathbf{k}}+2\tilde{\omega})E_{nm,\mathbf{k}}^2E_{pm,\mathbf{k}}} - \frac{f_{nm}E_{lp,\mathbf{k}}}{(E_{nm,\mathbf{k}}+2\tilde{\omega})E_{nm,\mathbf{k}}^2E_{np,\mathbf{k}}} \\
&- \frac{2f_{nm}}{(E_{nm,\mathbf{k}}+2\tilde{\omega})(E_{pm,\mathbf{k}}+\tilde{\omega})E_{nm,\mathbf{k}}} - \frac{2f_{nm}(E_{nm,\mathbf{k}}-2E_{lp,\mathbf{k}})}{(E_{nm,\mathbf{k}}+2\tilde{\omega})E_{nm,\mathbf{k}}^2E_{nl,\mathbf{k}}}\Bigg] \qquad \text{(F.3)}
\end{aligned}
$$

for the second permutation,

$$
\begin{aligned}
\chi_{0,2}^{(3),4bnd}(\hat{\mathbf{q}},\hat{\mathbf{q}}_1,\hat{\mathbf{q}}_2,\hat{\mathbf{q}}_3,\omega,\omega,0) &= \frac{1}{V}\sum_{n,m,p,l}\hat{\mathbf{r}}_{nm,\mathbf{k}}(\hat{\mathbf{q}})\,\hat{\mathbf{r}}_{mp,\mathbf{k}}(\hat{\mathbf{q}}_1)\,\hat{\mathbf{r}}_{ln,\mathbf{k}}(\hat{\mathbf{q}}_2)\,\hat{\mathbf{r}}_{pl,\mathbf{k}}(\hat{\mathbf{q}}_3) \\
&\times\Bigg[-\frac{f_{np}}{(E_{nm,\mathbf{k}}+2\tilde{\omega})(E_{nl,\mathbf{k}}+\tilde{\omega})(E_{np,\mathbf{k}}+\tilde{\omega})} - \frac{f_{pl,\mathbf{k}}}{(E_{nm,\mathbf{k}}+2\tilde{\omega})(E_{nl,\mathbf{k}}+\tilde{\omega})E_{lp,\mathbf{k}}} \\
&- \frac{f_{pl,\mathbf{k}}}{(E_{nm,\mathbf{k}}+2\tilde{\omega})(E_{pm,\mathbf{k}}+\tilde{\omega})E_{lp,\mathbf{k}}} - \frac{f_{lm,\mathbf{k}}}{(E_{nm,\mathbf{k}}+2\tilde{\omega})(E_{pm,\mathbf{k}}+\tilde{\omega})(E_{lm,\mathbf{k}}+\tilde{\omega})} + \frac{5f_{np}E_{pm,\mathbf{k}}E_{nl,\mathbf{k}}}{4(E_{np,\mathbf{k}}+\tilde{\omega})E_{np,\mathbf{k}}^4} \\
&+ \frac{f_{np}(2E_{nl,\mathbf{k}}-E_{lm,\mathbf{k}}-E_{lp,\mathbf{k}})}{2(E_{np,\mathbf{k}}+\tilde{\omega})E_{np,\mathbf{k}}^3} + \frac{f_{np}(E_{nm,\mathbf{k}}+E_{np,\mathbf{k}})E_{nl,\mathbf{k}}}{2(E_{np,\mathbf{k}}+\tilde{\omega})^2E_{np,\mathbf{k}}^3} + \frac{f_{np}}{(E_{pm,\mathbf{k}}+\tilde{\omega})(E_{np,\mathbf{k}}+\tilde{\omega})^2} \\
&- \frac{f_{np}E_{lp,\mathbf{k}}}{(E_{pm,\mathbf{k}}+\tilde{\omega})(E_{np,\mathbf{k}}+\tilde{\omega})^2E_{np,\mathbf{k}}} - \frac{f_{np}E_{lp,\mathbf{k}}}{2(E_{np,\mathbf{k}}+\tilde{\omega})(E_{pm,\mathbf{k}}+\tilde{\omega})E_{np,\mathbf{k}}^2} - \frac{f_{np}E_{lp,\mathbf{k}}}{2(E_{pm,\mathbf{k}}+\tilde{\omega})E_{nm,\mathbf{k}}E_{np,\mathbf{k}}^2} \\
&- \frac{f_{np}E_{lp,\mathbf{k}}}{2(E_{nm,\mathbf{k}}+2\tilde{\omega})(E_{np,\mathbf{k}}+\tilde{\omega})E_{np,\mathbf{k}}^2} - \frac{f_{np}E_{lp,\mathbf{k}}}{(E_{nm,\mathbf{k}}+2\tilde{\omega})E_{pm,\mathbf{k}}E_{np,\mathbf{k}}^2} + \frac{f_{np}E_{pm,\mathbf{k}}}{2(E_{np,\mathbf{k}}+\tilde{\omega})E_{np,\mathbf{k}}^2E_{lp,\mathbf{k}}} \\
&+ \frac{f_{np}}{(E_{np,\mathbf{k}}+\tilde{\omega})E_{np,\mathbf{k}}E_{lp,\mathbf{k}}} + \frac{f_{nl}E_{pm,\mathbf{k}}}{4(E_{nl,\mathbf{k}}+\tilde{\omega})E_{nl,\mathbf{k}}^3} - \frac{f_{nl}E_{lp,\mathbf{k}}}{2(E_{nl,\mathbf{k}}+\tilde{\omega})E_{nm,\mathbf{k}}E_{nl,\mathbf{k}}^2} \\
&+ \frac{f_{nl}E_{lp,\mathbf{k}}}{2(E_{nm,\mathbf{k}}+2\tilde{\omega})(E_{nl,\mathbf{k}}+\tilde{\omega})E_{nl,\mathbf{k}}^2} + \frac{f_{nl}E_{lp,\mathbf{k}}}{(E_{nm,\mathbf{k}}+2\tilde{\omega})E_{lm,\mathbf{k}}E_{nl,\mathbf{k}}^2} - \frac{f_{nl}E_{pm,\mathbf{k}}}{2(E_{nl,\mathbf{k}}+\tilde{\omega})E_{nl,\mathbf{k}}^2E_{lp,\mathbf{k}}} \\
&- \frac{f_{nl}}{(E_{nl,\mathbf{k}}+\tilde{\omega})E_{nl,\mathbf{k}}E_{lp,\mathbf{k}}} + \frac{5f_{lm}E_{pm,\mathbf{k}}E_{nl,\mathbf{k}}}{4(E_{lm,\mathbf{k}}+\tilde{\omega})E_{lm,\mathbf{k}}^4} + \frac{f_{lm}(2E_{pm,\mathbf{k}}-E_{np,\mathbf{k}}-E_{lp,\mathbf{k}})}{2(E_{lm,\mathbf{k}}+\tilde{\omega})E_{lm,\mathbf{k}}^3} \\
&+ \frac{f_{lm}E_{pm,\mathbf{k}}(E_{nm,\mathbf{k}}+E_{lm,\mathbf{k}})}{2(E_{lm,\mathbf{k}}+\tilde{\omega})^2E_{lm,\mathbf{k}}^3} + \frac{f_{lm}}{(E_{nl,\mathbf{k}}+\tilde{\omega})(E_{lm,\mathbf{k}}+\tilde{\omega})^2} - \frac{f_{lm}E_{lp,\mathbf{k}}}{(E_{nl,\mathbf{k}}+\tilde{\omega})(E_{lm,\mathbf{k}}+\tilde{\omega})^2E_{lm,\mathbf{k}}}
\end{aligned}
$$

$$
\begin{aligned}
&- \frac{f_{lm}E_{lp,\mathbf{k}}}{2(E_{lm,\mathbf{k}}+\tilde{\omega})(E_{nl,\mathbf{k}}+\tilde{\omega})E_{lm,\mathbf{k}}^2} - \frac{f_{lm}E_{lp,\mathbf{k}}}{2(E_{nl,\mathbf{k}}+\tilde{\omega})E_{nm,\mathbf{k}}E_{lm,\mathbf{k}}^2} - \frac{f_{lm}E_{lp,\mathbf{k}}}{2(E_{nm,\mathbf{k}}+2\tilde{\omega})(E_{lm,\mathbf{k}}+\tilde{\omega})E_{lm,\mathbf{k}}^2} \\
&- \frac{f_{lm}E_{lp,\mathbf{k}}}{(E_{nm,\mathbf{k}}+2\tilde{\omega})E_{nl,\mathbf{k}}E_{lm,\mathbf{k}}^2} + \frac{f_{lm}E_{nl,\mathbf{k}}}{2(E_{lm,\mathbf{k}}+\tilde{\omega})E_{lm,\mathbf{k}}^2E_{lp,\mathbf{k}}} + \frac{f_{lm}}{(E_{lm,\mathbf{k}}+\tilde{\omega})E_{lm,\mathbf{k}}E_{lp,\mathbf{k}}} \\
&+ \frac{f_{pm}E_{nl,\mathbf{k}}}{4(E_{pm,\mathbf{k}}+\tilde{\omega})E_{pm,\mathbf{k}}^3} - \frac{f_{pm}E_{lp,\mathbf{k}}}{2(E_{pm,\mathbf{k}}+\tilde{\omega})E_{nm,\mathbf{k}}E_{pm,\mathbf{k}}^2} + \frac{f_{pm}E_{lp,\mathbf{k}}}{2(E_{nm,\mathbf{k}}+2\tilde{\omega})(E_{pm,\mathbf{k}}+\tilde{\omega})E_{pm,\mathbf{k}}^2} \\
&+ \frac{f_{pm}E_{lp,\mathbf{k}}}{(E_{nm,\mathbf{k}}+2\tilde{\omega})E_{np,\mathbf{k}}E_{pm,\mathbf{k}}^2} - \frac{f_{pm}E_{nl,\mathbf{k}}}{2(E_{pm,\mathbf{k}}+\tilde{\omega})E_{pm,\mathbf{k}}^2E_{lp,\mathbf{k}}} - \frac{f_{pm}}{(E_{pm,\mathbf{k}}+\tilde{\omega})E_{pm,\mathbf{k}}E_{lp,\mathbf{k}}} \\
&+ \frac{4f_{nm}E_{lp,\mathbf{k}}}{(E_{nm,\mathbf{k}}+2\tilde{\omega})^2E_{nm,\mathbf{k}}^2} + \frac{8f_{nm}E_{lp,\mathbf{k}}}{(E_{nm,\mathbf{k}}+2\tilde{\omega})E_{nm,\mathbf{k}}^3} - \frac{f_{nm}}{(E_{nm,\mathbf{k}}+2\tilde{\omega})^2(E_{pm,\mathbf{k}}+\tilde{\omega})} \\
&- \frac{f_{nm}}{(E_{nm,\mathbf{k}}+2\tilde{\omega})^2(E_{nl,\mathbf{k}}+\tilde{\omega})} + \frac{2f_{nm}E_{lp,\mathbf{k}}}{(E_{nm,\mathbf{k}}+2\tilde{\omega})^2(E_{pm,\mathbf{k}}+\tilde{\omega})E_{nm,\mathbf{k}}} \\
&+ \frac{2f_{nm}E_{lp,\mathbf{k}}}{(E_{nm,\mathbf{k}}+2\tilde{\omega})^2(E_{nl,\mathbf{k}}+\tilde{\omega})E_{nm,\mathbf{k}}} + \frac{f_{nm}E_{lp,\mathbf{k}}}{(E_{nm,\mathbf{k}}+2\tilde{\omega})E_{nm,\mathbf{k}}^2E_{pm,\mathbf{k}}} - \frac{f_{nm}E_{lp,\mathbf{k}}}{(E_{nm,\mathbf{k}}+2\tilde{\omega})E_{nm,\mathbf{k}}^2E_{np,\mathbf{k}}} \\
&- \frac{f_{nm}E_{lp,\mathbf{k}}}{(E_{nm,\mathbf{k}}+2\tilde{\omega})E_{nm,\mathbf{k}}^2E_{lm,\mathbf{k}}} + \frac{f_{nm}E_{lp,\mathbf{k}}}{(E_{nm,\mathbf{k}}+2\tilde{\omega})E_{nm,\mathbf{k}}^2E_{nl,\mathbf{k}}}\Bigg] \qquad \text{(F.4)}
\end{aligned}
$$

for the third permutation,

$$
\begin{aligned}
\chi_{0,3}^{(3),4bnd}(\hat{\mathbf{q}},\hat{\mathbf{q}}_1,\hat{\mathbf{q}}_2,\hat{\mathbf{q}}_3,\omega,\omega,0) &= \frac{1}{V}\sum_{n,m,p,l}\hat{\mathbf{r}}_{nm,\mathbf{k}}(\hat{\mathbf{q}})\,\hat{\mathbf{r}}_{ln,\mathbf{k}}(\hat{\mathbf{q}}_1)\,\hat{\mathbf{r}}_{pl,\mathbf{k}}(\hat{\mathbf{q}}_2)\,\hat{\mathbf{r}}_{mp,\mathbf{k}}(\hat{\mathbf{q}}_3) \\
&\times\Bigg[-\frac{f_{np,\mathbf{k}}}{(E_{nm,\mathbf{k}}+2\tilde{\omega})(E_{nl,\mathbf{k}}+\tilde{\omega})(E_{np,\mathbf{k}}+2\tilde{\omega})} - \frac{f_{pm,\mathbf{k}}}{(E_{nm,\mathbf{k}}+2\tilde{\omega})(E_{lm,\mathbf{k}}+\tilde{\omega})E_{pm,\mathbf{k}}} \\
&- \frac{f_{pl,\mathbf{k}}}{(E_{nm,\mathbf{k}}+2\tilde{\omega})(E_{nl,\mathbf{k}}+\tilde{\omega})(E_{lp,\mathbf{k}}+\tilde{\omega})} - \frac{f_{pl,\mathbf{k}}}{(E_{nm,\mathbf{k}}+2\tilde{\omega})(E_{lp,\mathbf{k}}+\tilde{\omega})(E_{lm,\mathbf{k}}+\tilde{\omega})} \\
&+ \frac{4f_{np,\mathbf{k}}E_{nm,\mathbf{k}}E_{lp,\mathbf{k}}}{(E_{np,\mathbf{k}}+2\tilde{\omega})E_{np,\mathbf{k}}^4} - \frac{2f_{np,\mathbf{k}}(E_{lm,\mathbf{k}}+E_{lp,\mathbf{k}})}{(E_{np,\mathbf{k}}+2\tilde{\omega})E_{np,\mathbf{k}}^3} + \frac{2f_{np,\mathbf{k}}(E_{np,\mathbf{k}}-2E_{lp,\mathbf{k}})}{(E_{np,\mathbf{k}}+2\tilde{\omega})E_{pm,\mathbf{k}}E_{np,\mathbf{k}}^2} \\
&+ \frac{f_{np,\mathbf{k}}E_{nm,\mathbf{k}}}{(E_{nl,\mathbf{k}}+\tilde{\omega})(E_{np,\mathbf{k}}+2\tilde{\omega})E_{np,\mathbf{k}}^2} - \frac{f_{np,\mathbf{k}}E_{nm,\mathbf{k}}}{2(E_{nl,\mathbf{k}}+\tilde{\omega})E_{np,\mathbf{k}}^2E_{lp,\mathbf{k}}} + \frac{f_{np,\mathbf{k}}}{(E_{np,\mathbf{k}}+2\tilde{\omega})(E_{lp,\mathbf{k}}+\tilde{\omega})E_{np,\mathbf{k}}} \\
&- \frac{f_{np,\mathbf{k}}}{2(E_{lp,\mathbf{k}}+\tilde{\omega})E_{nl,\mathbf{k}}E_{np,\mathbf{k}}} - \frac{5f_{lm,\mathbf{k}}E_{lp,\mathbf{k}}E_{nl,\mathbf{k}}}{4(E_{lm,\mathbf{k}}+\tilde{\omega})E_{lm,\mathbf{k}}^4} + \frac{f_{lm,\mathbf{k}}(E_{nm,\mathbf{k}}+E_{pm,\mathbf{k}}-3E_{lp,\mathbf{k}})}{2(E_{lm,\mathbf{k}}+\tilde{\omega})E_{lm,\mathbf{k}}^3} \\
&- \frac{f_{lm,\mathbf{k}}E_{lp,\mathbf{k}}(E_{nm,\mathbf{k}}+E_{lm,\mathbf{k}})}{2(E_{lm,\mathbf{k}}+\tilde{\omega})^2E_{lm,\mathbf{k}}^3} - \frac{f_{lm,\mathbf{k}}(E_{nm,\mathbf{k}}+E_{lm,\mathbf{k}})}{2(E_{lm,\mathbf{k}}+\tilde{\omega})E_{pm,\mathbf{k}}E_{lm,\mathbf{k}}^2} - \frac{f_{lm,\mathbf{k}}E_{lp,\mathbf{k}}}{(E_{nl,\mathbf{k}}+\tilde{\omega})(E_{lm,\mathbf{k}}+\tilde{\omega})^2E_{lm,\mathbf{k}}} \\
&- \frac{f_{lm,\mathbf{k}}E_{lp,\mathbf{k}}}{2(E_{nl,\mathbf{k}}+\tilde{\omega})(E_{lm,\mathbf{k}}+\tilde{\omega})E_{lm,\mathbf{k}}^2} - \frac{f_{lm,\mathbf{k}}E_{lp,\mathbf{k}}}{2(E_{nl,\mathbf{k}}+\tilde{\omega})E_{nm,\mathbf{k}}E_{lm,\mathbf{k}}^2} - \frac{f_{lm,\mathbf{k}}E_{lp,\mathbf{k}}}{2(E_{nm,\mathbf{k}}+2\tilde{\omega})(E_{lm,\mathbf{k}}+\tilde{\omega})E_{lm,\mathbf{k}}^2} \\
&- \frac{f_{lm,\mathbf{k}}E_{lp,\mathbf{k}}}{(E_{nm,\mathbf{k}}+2\tilde{\omega})E_{nl,\mathbf{k}}E_{lm,\mathbf{k}}^2} + \frac{f_{lm,\mathbf{k}}}{(E_{nl,\mathbf{k}}+\tilde{\omega})(E_{lm,\mathbf{k}}+\tilde{\omega})E_{lm,\mathbf{k}}} + \frac{f_{lm,\mathbf{k}}}{(E_{nl,\mathbf{k}}+\tilde{\omega})E_{nm,\mathbf{k}}E_{lm,\mathbf{k}}} \\
&+ \frac{f_{pl,\mathbf{k}}E_{nm,\mathbf{k}}}{4(E_{lp,\mathbf{k}}+\tilde{\omega})E_{lp,\mathbf{k}}^3} - \frac{f_{pl,\mathbf{k}}(E_{nm,\mathbf{k}}+E_{lp,\mathbf{k}})}{2(E_{lp,\mathbf{k}}+\tilde{\omega})E_{pm,\mathbf{k}}E_{lp,\mathbf{k}}^2} + \frac{f_{pl,\mathbf{k}}E_{nm,\mathbf{k}}}{4(E_{nl,\mathbf{k}}+\tilde{\omega})(E_{lp,\mathbf{k}}+\tilde{\omega})E_{lp,\mathbf{k}}^2} \\
&+ \frac{f_{pl,\mathbf{k}}E_{nm,\mathbf{k}}}{4(E_{nl,\mathbf{k}}+\tilde{\omega})E_{np,\mathbf{k}}E_{lp,\mathbf{k}}^2} - \frac{f_{pl,\mathbf{k}}}{2(E_{lp,\mathbf{k}}+\tilde{\omega})E_{nl,\mathbf{k}}E_{lp,\mathbf{k}}} + \frac{f_{nl,\mathbf{k}}(E_{lm,\mathbf{k}}-E_{np,\mathbf{k}})}{4(E_{nl,\mathbf{k}}+\tilde{\omega})E_{nl,\mathbf{k}}^3} \\
&- \frac{f_{nl,\mathbf{k}}}{(E_{nl,\mathbf{k}}+\tilde{\omega})E_{nm,\mathbf{k}}E_{nl,\mathbf{k}}} - \frac{f_{nl,\mathbf{k}}E_{lp,\mathbf{k}}}{2(E_{nl,\mathbf{k}}+\tilde{\omega})E_{nm,\mathbf{k}}E_{nl,\mathbf{k}}^2} + \frac{f_{nl,\mathbf{k}}E_{lp,\mathbf{k}}}{2(E_{nm,\mathbf{k}}+2\tilde{\omega})(E_{nl,\mathbf{k}}+\tilde{\omega})E_{nl,\mathbf{k}}^2} \\
&+ \frac{f_{nl,\mathbf{k}}E_{lp,\mathbf{k}}}{(E_{nm,\mathbf{k}}+2\tilde{\omega})E_{nl,\mathbf{k}}^2E_{lm,\mathbf{k}}} - \frac{f_{nl,\mathbf{k}}E_{nm,\mathbf{k}}}{4(E_{nl,\mathbf{k}}+\tilde{\omega})E_{nl,\mathbf{k}}^2E_{np,\mathbf{k}}} + \frac{f_{nl,\mathbf{k}}E_{nm,\mathbf{k}}}{2(E_{nl,\mathbf{k}}+\tilde{\omega})E_{nl,\mathbf{k}}^2E_{lp,\mathbf{k}}}
\end{aligned}
$$

$$
- \frac{f_{nl,\mathbf{k}}}{2(E_{nl,\mathbf{k}}+\tilde{\omega})(E_{lp,\mathbf{k}}+\tilde{\omega})E_{nl,\mathbf{k}}} + \frac{8f_{nm,\mathbf{k}}E_{lp,\mathbf{k}}}{(E_{nm,\mathbf{k}}+2\tilde{\omega})E^3_{nm,\mathbf{k}}} + \frac{4f_{nm,\mathbf{k}}E_{lp,\mathbf{k}}}{(E_{nm,\mathbf{k}}+2\tilde{\omega})^2E^2_{nm,\mathbf{k}}}
$$
$$
- \frac{2f_{nm,\mathbf{k}}(E_{nm,\mathbf{k}}-2E_{lp,\mathbf{k}})}{(E_{nm,\mathbf{k}}+2\tilde{\omega})E^2_{nm,\mathbf{k}}E_{pm,\mathbf{k}}} + \frac{2f_{nm,\mathbf{k}}E_{lp,\mathbf{k}}}{(E_{nm,\mathbf{k}}+2\tilde{\omega})^2(E_{nl,\mathbf{k}}+\tilde{\omega})E_{nm,\mathbf{k}}} - \frac{f_{nm,\mathbf{k}}E_{lp,\mathbf{k}}}{(E_{nm,\mathbf{k}}+2\tilde{\omega})E^2_{nm,\mathbf{k}}E_{lm,\mathbf{k}}}
$$
$$
+ \frac{f_{nm,\mathbf{k}}E_{lp,\mathbf{k}}}{(E_{nm,\mathbf{k}}+2\tilde{\omega})E^2_{nm,\mathbf{k}}E_{nl,\mathbf{k}}} - \frac{2f_{nm,\mathbf{k}}}{(E_{nm,\mathbf{k}}+2\tilde{\omega})(E_{nl,\mathbf{k}}+\tilde{\omega})E_{nm,\mathbf{k}}}\Bigg] \tag{F.5}
$$

The third-band term is

$$
\chi^{(3),3bnd}_{0,1}(\hat{\mathbf{q}},\hat{\mathbf{q}}_1,\hat{\mathbf{q}}_2,\hat{\mathbf{q}}_3,\omega,\omega,0) = \Delta_{np,\mathbf{k}}(\hat{\mathbf{q}})\,\hat{\mathbf{r}}_{pn,\mathbf{k}}(\hat{\mathbf{q}}_1)\,\hat{\mathbf{r}}_{mp,\mathbf{k}}(\hat{\mathbf{q}}_2)\,\hat{\mathbf{r}}_{nm,\mathbf{k}}(\hat{\mathbf{q}}_3)\Bigg[\frac{f_{np,\mathbf{k}}(E_{nm,\mathbf{k}}-2E_{mp,\mathbf{k}})}{4(E_{np,\mathbf{k}}+\tilde{\omega})E^4_{np,\mathbf{k}}}
$$
$$
- \frac{f_{np,\mathbf{k}}E_{mp,\mathbf{k}}}{4(E_{np,\mathbf{k}}+\tilde{\omega})^2E^3_{np,\mathbf{k}}} - \frac{f_{np,\mathbf{k}}}{4(E_{np,\mathbf{k}}+\tilde{\omega})E^2_{np,\mathbf{k}}E_{nm,\mathbf{k}}} - \frac{f_{np,\mathbf{k}}E_{nm,\mathbf{k}}}{4(E_{np,\mathbf{k}}-\tilde{\omega})E^4_{np,\mathbf{k}}} - \frac{f_{pm,\mathbf{k}}E_{np,\mathbf{k}}}{4(E_{pm,\mathbf{k}}-\tilde{\omega})E^4_{pm,\mathbf{k}}}
$$
$$
+ \frac{f_{pm,\mathbf{k}}}{4(E_{pm,\mathbf{k}}-\tilde{\omega})E_{nm,\mathbf{k}}E^2_{pm,\mathbf{k}}}\Bigg] + \Delta_{nm,\mathbf{k}}(\hat{\mathbf{q}})\,\hat{\mathbf{r}}_{mp,\mathbf{k}}(\hat{\mathbf{q}}_1)\,\hat{\mathbf{r}}_{pn,\mathbf{k}}(\hat{\mathbf{q}}_2)\,\hat{\mathbf{r}}_{nm,\mathbf{k}}(\hat{\mathbf{q}}_3)\Bigg[-\frac{4f_{nm,\mathbf{k}}(E_{np,\mathbf{k}}-E_{pm,\mathbf{k}})}{(E_{nm,\mathbf{k}}+2\tilde{\omega})E^4_{nm,\mathbf{k}}}
$$
$$
- \frac{2f_{nm,\mathbf{k}}}{(E_{nm,\mathbf{k}}+2\tilde{\omega})(E_{pm,\mathbf{k}}+\tilde{\omega})E^2_{nm,\mathbf{k}}} + \frac{f_{nm,\mathbf{k}}}{(E_{pm,\mathbf{k}}+\tilde{\omega})E^2_{nm,\mathbf{k}}E_{np,\mathbf{k}}} - \frac{f_{pm,\mathbf{k}}}{4(E_{pm,\mathbf{k}}+\tilde{\omega})E^3_{pm,\mathbf{k}}}
$$
$$
- \frac{f_{pm,\mathbf{k}}}{(E_{pm,\mathbf{k}}+\tilde{\omega})E^2_{pm,\mathbf{k}}E_{np,\mathbf{k}}} + \frac{f_{pm,\mathbf{k}}}{2(E_{pm,\mathbf{k}}+\tilde{\omega})E_{nm,\mathbf{k}}E^2_{pm,\mathbf{k}}} + \frac{f_{np,\mathbf{k}}E_{nm,\mathbf{k}}}{4(E_{np,\mathbf{k}}+\tilde{\omega})E^4_{np,\mathbf{k}}}
$$
$$
+ \frac{f_{np,\mathbf{k}}}{2(E_{pm,\mathbf{k}}+\tilde{\omega})(E_{np,\mathbf{k}}+\tilde{\omega})E^2_{np,\mathbf{k}}} + \frac{f_{np,\mathbf{k}}}{2(E_{pm,\mathbf{k}}+\tilde{\omega})E_{nm,\mathbf{k}}E^2_{np,\mathbf{k}}}\Bigg]
$$
$$
+ \Delta_{pm,\mathbf{k}}(\hat{\mathbf{q}})\,\hat{\mathbf{r}}_{mp,\mathbf{k}}(\hat{\mathbf{q}}_1)\,\hat{\mathbf{r}}_{pn,\mathbf{k}}(\hat{\mathbf{q}}_2)\,\hat{\mathbf{r}}_{nm,\mathbf{k}}(\hat{\mathbf{q}}_3)\Bigg[-\frac{3f_{pm,\mathbf{k}}E_{np,\mathbf{k}}}{4(E_{pm,\mathbf{k}}+\tilde{\omega})E^4_{pm,\mathbf{k}}} + \frac{f_{pm,\mathbf{k}}}{4(E_{pm,\mathbf{k}}+\tilde{\omega})E_{nm,\mathbf{k}}E^2_{pm,\mathbf{k}}}
$$
$$
- \frac{f_{pm,\mathbf{k}}}{4(E_{pm,\mathbf{k}}+\tilde{\omega})E^3_{pm,\mathbf{k}}} - \frac{f_{pm,\mathbf{k}}E_{np,\mathbf{k}}}{4(E_{pm,\mathbf{k}}+\tilde{\omega})^2E^3_{pm,\mathbf{k}}} + \frac{f_{pm,\mathbf{k}}}{4(E_{pm,\mathbf{k}}-\tilde{\omega})E^3_{pm,\mathbf{k}}} - \frac{f_{np,\mathbf{k}}}{4(E_{np,\mathbf{k}}-\tilde{\omega})E_{nm,\mathbf{k}}E^2_{np,\mathbf{k}}}\Bigg] \tag{F.6}
$$

$$
\chi^{(3),3bnd}_{0,2}(\hat{\mathbf{q}},\hat{\mathbf{q}}_1,\hat{\mathbf{q}}_2,\hat{\mathbf{q}}_3,\omega,\omega,0) = \hat{\mathbf{r}}_{nm,\mathbf{k}}(\hat{\mathbf{q}})\,\Delta_{nm,\mathbf{k}}(\hat{\mathbf{q}}_1)\,\hat{\mathbf{r}}_{mp,\mathbf{k}}(\hat{\mathbf{q}}_2)\,\hat{\mathbf{r}}_{pn,\mathbf{k}}(\hat{\mathbf{q}}_3)\Bigg[-\frac{8f_{nm,\mathbf{k}}(2E_{pm,\mathbf{k}}-E_{np,\mathbf{k}})}{(E_{nm,\mathbf{k}}+2\tilde{\omega})E^4_{nm,\mathbf{k}}}
$$
$$
- \frac{f_{nm,\mathbf{k}}(2E_{np,\mathbf{k}}-5E_{pm,\mathbf{k}})}{4(E_{nm,\mathbf{k}}+\tilde{\omega})E^4_{nm,\mathbf{k}}} + \frac{f_{nm,\mathbf{k}}}{2(E_{nm,\mathbf{k}}+\tilde{\omega})E^2_{nm,\mathbf{k}}E_{np,\mathbf{k}}} - \frac{8f_{nm,\mathbf{k}}E_{pm,\mathbf{k}}}{(E_{nm,\mathbf{k}}+2\tilde{\omega})^2E^3_{nm,\mathbf{k}}}
$$
$$
+ \frac{f_{nm,\mathbf{k}}E_{pm,\mathbf{k}}}{2(E_{nm,\mathbf{k}}+\tilde{\omega})^2E^3_{nm,\mathbf{k}}} - \frac{f_{pm,\mathbf{k}}}{4(E_{pm,\mathbf{k}}+\tilde{\omega})E^3_{pm,\mathbf{k}}} - \frac{f_{pm,\mathbf{k}}}{2(E_{pm,\mathbf{k}}+\tilde{\omega})E^2_{pm,\mathbf{k}}E_{np,\mathbf{k}}}\Bigg]
$$
$$
+ \hat{\mathbf{r}}_{nm,\mathbf{k}}(\hat{\mathbf{q}})\,\Delta_{mp,\mathbf{k}}(\hat{\mathbf{q}}_1)\,\hat{\mathbf{r}}_{mp,\mathbf{k}}(\hat{\mathbf{q}}_2)\,\hat{\mathbf{r}}_{pn,\mathbf{k}}(\hat{\mathbf{q}}_3)\Bigg[\frac{8f_{nm,\mathbf{k}}}{(E_{nm,\mathbf{k}}+2\tilde{\omega})E^2_{nm,\mathbf{k}}E_{np,\mathbf{k}}} + \frac{8f_{pm,\mathbf{k}}E_{np,\mathbf{k}}}{(E_{pm,\mathbf{k}}+2\tilde{\omega})E^4_{pm,\mathbf{k}}}
$$
$$
- \frac{f_{pm,\mathbf{k}}E_{np,\mathbf{k}}}{4(E_{pm,\mathbf{k}}+\tilde{\omega})E^4_{pm,\mathbf{k}}} - \frac{8f_{pm,\mathbf{k}}}{(E_{pm,\mathbf{k}}+2\tilde{\omega})E^2_{pm,\mathbf{k}}E_{np,\mathbf{k}}}\Bigg]
$$
$$
+ \hat{\mathbf{r}}_{nm,\mathbf{k}}(\hat{\mathbf{q}})\,\Delta_{np,\mathbf{k}}(\hat{\mathbf{q}}_1)\,\hat{\mathbf{r}}_{mp,\mathbf{k}}(\hat{\mathbf{q}}_2)\,\hat{\mathbf{r}}_{pn,\mathbf{k}}(\hat{\mathbf{q}}_3)\Bigg[\frac{4f_{nm,\mathbf{k}}}{(E_{nm,\mathbf{k}}+2\tilde{\omega})^2E^2_{nm,\mathbf{k}}} + \frac{8f_{nm,\mathbf{k}}}{(E_{nm,\mathbf{k}}+2\tilde{\omega})E^3_{nm,\mathbf{k}}}
$$
$$
+ \frac{2f_{nm,\mathbf{k}}}{(E_{nm,\mathbf{k}}+2\tilde{\omega})^2(E_{pm,\mathbf{k}}+\tilde{\omega})E_{nm,\mathbf{k}}} + \frac{3f_{nm,\mathbf{k}}}{(E_{nm,\mathbf{k}}+2\tilde{\omega})E^2_{nm,\mathbf{k}}E_{pm,\mathbf{k}}} - \frac{3f_{nm,\mathbf{k}}}{(E_{nm,\mathbf{k}}+2\tilde{\omega})E^2_{nm,\mathbf{k}}E_{np,\mathbf{k}}}
$$
$$
- \frac{f_{np,\mathbf{k}}(7E_{nm,\mathbf{k}}+5E_{np,\mathbf{k}})}{4(E_{np,\mathbf{k}}+\tilde{\omega})E^4_{np,\mathbf{k}}} - \frac{f_{np,\mathbf{k}}}{(E_{pm,\mathbf{k}}+\tilde{\omega})(E_{np,\mathbf{k}}+\tilde{\omega})^2E_{np,\mathbf{k}}} - \frac{f_{np,\mathbf{k}}}{2(E_{pm,\mathbf{k}}+\tilde{\omega})(E_{np,\mathbf{k}}+\tilde{\omega})E^2_{np,\mathbf{k}}}
$$

$$
\begin{aligned}
&- \frac{f_{np,\mathbf{k}}}{2(E_{pm,\mathbf{k}}+\tilde{\omega})E_{nm,\mathbf{k}}E_{np,\mathbf{k}}^2} - \frac{f_{np,\mathbf{k}}(E_{nm,\mathbf{k}}+E_{np,\mathbf{k}})}{2(E_{np,\mathbf{k}}+\tilde{\omega})^2E_{np,\mathbf{k}}^3} - \frac{3f_{np,\mathbf{k}}}{2(E_{nm,\mathbf{k}}+2\tilde{\omega})(E_{np,\mathbf{k}}+\tilde{\omega})E_{np,\mathbf{k}}^2} \\
&- \frac{3f_{np,\mathbf{k}}}{(E_{nm,\mathbf{k}}+2\tilde{\omega})E_{pm,\mathbf{k}}E_{np,\mathbf{k}}^2} - \frac{f_{pm,\mathbf{k}}}{2(E_{pm,\mathbf{k}}+\tilde{\omega})E_{nm,\mathbf{k}}E_{pm,\mathbf{k}}^2} + \frac{3f_{pm,\mathbf{k}}}{2(E_{nm,\mathbf{k}}+2\tilde{\omega})(E_{pm,\mathbf{k}}+\tilde{\omega})E_{pm,\mathbf{k}}^2} \\
&+ \frac{3f_{pm,\mathbf{k}}}{(E_{nm,\mathbf{k}}+2\tilde{\omega})E_{pm,\mathbf{k}}^2E_{np,\mathbf{k}}}\Bigg] \\
&+ \hat{\mathbf{r}}_{nm,\mathbf{k}}(\hat{\mathbf{q}})\,\Delta_{nm,\mathbf{k}}(\hat{\mathbf{q}}_1)\,\hat{\mathbf{r}}_{pn,\mathbf{k}}(\hat{\mathbf{q}}_2)\,\hat{\mathbf{r}}_{mp,\mathbf{k}}(\hat{\mathbf{q}}_3)\Bigg[-\frac{8f_{nm,\mathbf{k}}(2E_{pm,\mathbf{k}}-E_{np,\mathbf{k}})}{(E_{nm,\mathbf{k}}+2\tilde{\omega})E_{nm,\mathbf{k}}^4} - \frac{f_{nm,\mathbf{k}}(5E_{np,\mathbf{k}}-2E_{pm,\mathbf{k}})}{4(E_{nm,\mathbf{k}}+\tilde{\omega})E_{nm,\mathbf{k}}^4} \\
&- \frac{f_{nm,\mathbf{k}}}{2(E_{nm,\mathbf{k}}+\tilde{\omega})E_{nm,\mathbf{k}}^2E_{pm,\mathbf{k}}} + \frac{8f_{nm,\mathbf{k}}E_{np,\mathbf{k}}}{(E_{nm,\mathbf{k}}+2\tilde{\omega})^2E_{nm,\mathbf{k}}^3} - \frac{f_{nm,\mathbf{k}}E_{np,\mathbf{k}}}{2(E_{nm,\mathbf{k}}+\tilde{\omega})^2E_{nm,\mathbf{k}}^3} \\
&+ \frac{f_{np,\mathbf{k}}}{4(E_{np,\mathbf{k}}+\tilde{\omega})E_{np,\mathbf{k}}^3} + \frac{f_{np,\mathbf{k}}}{2(E_{np,\mathbf{k}}+\tilde{\omega})E_{pm,\mathbf{k}}E_{np,\mathbf{k}}^2}\Bigg] \\
&+ \hat{\mathbf{r}}_{nm,\mathbf{k}}(\hat{\mathbf{q}})\,\Delta_{mp,\mathbf{k}}(\hat{\mathbf{q}}_1)\,\hat{\mathbf{r}}_{pn,\mathbf{k}}(\hat{\mathbf{q}}_2)\,\hat{\mathbf{r}}_{mp,\mathbf{k}}(\hat{\mathbf{q}}_3)\Bigg[\frac{4f_{nm,\mathbf{k}}}{(E_{nm,\mathbf{k}}+2\tilde{\omega})^2E_{nm,\mathbf{k}}^2} + \frac{2f_{nm,\mathbf{k}}}{(E_{nm,\mathbf{k}}+2\tilde{\omega})^2(E_{np,\mathbf{k}}+\tilde{\omega})E_{nm,\mathbf{k}}} \\
&- \frac{3f_{nm,\mathbf{k}}}{(E_{nm,\mathbf{k}}+2\tilde{\omega})E_{nm,\mathbf{k}}^2E_{pm,\mathbf{k}}} + \frac{3f_{nm,\mathbf{k}}}{(E_{nm,\mathbf{k}}+2\tilde{\omega})E_{nm,\mathbf{k}}^2E_{np,\mathbf{k}}} - \frac{f_{np,\mathbf{k}}}{2(E_{np,\mathbf{k}}+\tilde{\omega})E_{nm,\mathbf{k}}E_{np,\mathbf{k}}^2} \\
&+ \frac{3f_{np,\mathbf{k}}}{2(E_{nm,\mathbf{k}}+2\tilde{\omega})(E_{np,\mathbf{k}}+\tilde{\omega})E_{np,\mathbf{k}}^2} + \frac{3f_{np,\mathbf{k}}}{(E_{nm,\mathbf{k}}+2\tilde{\omega})E_{pm,\mathbf{k}}E_{np,\mathbf{k}}^2} - \frac{f_{pm,\mathbf{k}}(7E_{nm,\mathbf{k}}+5E_{pm,\mathbf{k}})}{4(E_{pm,\mathbf{k}}+\tilde{\omega})E_{pm,\mathbf{k}}^4} \\
&- \frac{f_{pm,\mathbf{k}}(E_{nm,\mathbf{k}}+E_{pm,\mathbf{k}})}{2(E_{pm,\mathbf{k}}+\tilde{\omega})^2E_{pm,\mathbf{k}}^3} - \frac{f_{pm,\mathbf{k}}}{(E_{np,\mathbf{k}}+\tilde{\omega})(E_{pm,\mathbf{k}}+\tilde{\omega})^2E_{pm,\mathbf{k}}} - \frac{f_{pm,\mathbf{k}}}{2(E_{pm,\mathbf{k}}+\tilde{\omega})(E_{np,\mathbf{k}}+\tilde{\omega})E_{pm,\mathbf{k}}^2} \\
&- \frac{f_{pm,\mathbf{k}}}{2(E_{np,\mathbf{k}}+\tilde{\omega})E_{nm,\mathbf{k}}E_{pm,\mathbf{k}}^2} - \frac{3f_{pm,\mathbf{k}}}{2(E_{nm,\mathbf{k}}+2\tilde{\omega})(E_{pm,\mathbf{k}}+\tilde{\omega})E_{pm,\mathbf{k}}^2} - \frac{3f_{pm,\mathbf{k}}}{(E_{nm,\mathbf{k}}+2\tilde{\omega})E_{np,\mathbf{k}}E_{pm,\mathbf{k}}^2}\Bigg] \\
&+ \hat{\mathbf{r}}_{nm,\mathbf{k}}(\hat{\mathbf{q}})\,\Delta_{np,\mathbf{k}}(\hat{\mathbf{q}}_1)\,\hat{\mathbf{r}}_{pn,\mathbf{k}}(\hat{\mathbf{q}}_2)\,\hat{\mathbf{r}}_{mp,\mathbf{k}}(\hat{\mathbf{q}}_3)\Bigg[\frac{8f_{nm,\mathbf{k}}}{(E_{nm,\mathbf{k}}+2\tilde{\omega})E_{nm,\mathbf{k}}^2E_{pm,\mathbf{k}}} + \frac{8f_{nm,\mathbf{k}}}{(E_{nm,\mathbf{k}}+2\tilde{\omega})E_{nm,\mathbf{k}}^3} \\
&+ \frac{8f_{np,\mathbf{k}}E_{pm,\mathbf{k}}}{(E_{np,\mathbf{k}}+2\tilde{\omega})E_{np,\mathbf{k}}^4} - \frac{8f_{np,\mathbf{k}}}{(E_{np,\mathbf{k}}+2\tilde{\omega})E_{pm,\mathbf{k}}E_{np,\mathbf{k}}^2} - \frac{f_{np,\mathbf{k}}E_{pm,\mathbf{k}}}{4(E_{np,\mathbf{k}}+\tilde{\omega})E_{np,\mathbf{k}}^4}\Bigg] \qquad \text{(F.7)}
\end{aligned}
$$

$$
\begin{aligned}
&\chi_{0,3}^{(3),3bnd}(\hat{\mathbf{q}},\hat{\mathbf{q}}_1,\hat{\mathbf{q}}_2,\hat{\mathbf{q}}_3,\omega,\omega,0) = \hat{\mathbf{r}}_{nm,\mathbf{k}}(\hat{\mathbf{q}})\,\hat{\mathbf{r}}_{mp,\mathbf{k}}(\hat{\mathbf{q}}_1)\,\hat{\mathbf{r}}_{pn,\mathbf{k}}(\hat{\mathbf{q}}_2)\,\Delta_{np,\mathbf{k}}(\hat{\mathbf{q}}_3)\Bigg[\frac{8f_{nm,\mathbf{k}}E_{np,\mathbf{k}}}{(E_{nm,\mathbf{k}}+2\tilde{\omega})E_{nm,\mathbf{k}}^4} \\
&+ \frac{4f_{nm,\mathbf{k}}E_{np,\mathbf{k}}}{(E_{nm,\mathbf{k}}+2\tilde{\omega})^2E_{nm,\mathbf{k}}^3} - \frac{f_{np,\mathbf{k}}(8E_{nm,\mathbf{k}}+3E_{np,\mathbf{k}})}{4(E_{np,\mathbf{k}}+\tilde{\omega})E_{np,\mathbf{k}}^4} - \frac{f_{np,\mathbf{k}}(5E_{nm,\mathbf{k}}+3E_{np,\mathbf{k}})}{4(E_{np,\mathbf{k}}+\tilde{\omega})^2E_{np,\mathbf{k}}^3} \\
&- \frac{f_{np,\mathbf{k}}(E_{nm,\mathbf{k}}+E_{np,\mathbf{k}})}{2(E_{np,\mathbf{k}}+\tilde{\omega})^3E_{np,\mathbf{k}}^2} - \frac{f_{pm,\mathbf{k}}}{4(E_{pm,\mathbf{k}}+\tilde{\omega})E_{pm,\mathbf{k}}^3}\Bigg] \\
&+ \hat{\mathbf{r}}_{nm,\mathbf{k}}(\hat{\mathbf{q}})\,\hat{\mathbf{r}}_{mp,\mathbf{k}}(\hat{\mathbf{q}}_1)\,\hat{\mathbf{r}}_{pn,\mathbf{k}}(\hat{\mathbf{q}}_2)\,\Delta_{nm,\mathbf{k}}(\hat{\mathbf{q}}_3)\Bigg[\frac{2f_{nm,\mathbf{k}}(E_{np,\mathbf{k}}-E_{pm,\mathbf{k}})}{(E_{nm,\mathbf{k}}+2\tilde{\omega})^2E_{nm,\mathbf{k}}^3} + \frac{f_{nm,\mathbf{k}}}{(E_{nm,\mathbf{k}}+2\tilde{\omega})^3(E_{pm,\mathbf{k}}+\tilde{\omega})} \\
&+ \frac{2f_{nm,\mathbf{k}}}{(E_{nm,\mathbf{k}}+2\tilde{\omega})^2(E_{pm,\mathbf{k}}+\tilde{\omega})E_{nm,\mathbf{k}}} + \frac{2f_{nm,\mathbf{k}}(E_{np,\mathbf{k}}-E_{pm,\mathbf{k}})}{(E_{nm,\mathbf{k}}+2\tilde{\omega})^3E_{nm,\mathbf{k}}^2} - \frac{f_{nm,\mathbf{k}}}{2(E_{nm,\mathbf{k}}+2\tilde{\omega})E_{nm,\mathbf{k}}^2E_{np,\mathbf{k}}} \\
&+ \frac{f_{nm,\mathbf{k}}}{2(E_{nm,\mathbf{k}}+2\tilde{\omega})E_{nm,\mathbf{k}}^2E_{pm,\mathbf{k}}} - \frac{f_{pm,\mathbf{k}}}{2(E_{pm,\mathbf{k}}+\tilde{\omega})E_{nm,\mathbf{k}}E_{pm,\mathbf{k}}^2} + \frac{f_{pm,\mathbf{k}}}{4(E_{nm,\mathbf{k}}+2\tilde{\omega})(E_{pm,\mathbf{k}}+\tilde{\omega})E_{pm,\mathbf{k}}^2} \\
&+ \frac{f_{pm,\mathbf{k}}}{2(E_{nm,\mathbf{k}}+2\tilde{\omega})E_{np,\mathbf{k}}E_{pm,\mathbf{k}}^2} - \frac{f_{np,\mathbf{k}}}{(E_{pm,\mathbf{k}}+\tilde{\omega})(E_{np,\mathbf{k}}+\tilde{\omega})^3} - \frac{f_{np,\mathbf{k}}}{(E_{pm,\mathbf{k}}+\tilde{\omega})(E_{np,\mathbf{k}}+\tilde{\omega})^2E_{np,\mathbf{k}}}
\end{aligned}
$$

$$
\begin{aligned}
&- \frac{f_{np,\mathbf{k}}}{2(E_{pm,\mathbf{k}}+\tilde{\omega})(E_{np,\mathbf{k}}+\tilde{\omega})E_{np,\mathbf{k}}^2} - \frac{f_{np,\mathbf{k}}}{2(E_{pm,\mathbf{k}}+\tilde{\omega})E_{nm,\mathbf{k}}E_{np,\mathbf{k}}^2} - \frac{f_{np,\mathbf{k}}}{4(E_{nm,\mathbf{k}}+2\tilde{\omega})(E_{np,\mathbf{k}}+\tilde{\omega})E_{np,\mathbf{k}}^2} \\
&\qquad - \frac{f_{np,\mathbf{k}}}{2(E_{nm,\mathbf{k}}+2\tilde{\omega})E_{pm,\mathbf{k}}E_{np,\mathbf{k}}^2}\Bigg] \\
&+ \hat{\mathbf{r}}_{nm,\mathbf{k}}(\hat{\mathbf{q}})\,\hat{\mathbf{r}}_{mp,\mathbf{k}}(\hat{\mathbf{q}}_1)\,\hat{\mathbf{r}}_{pn,\mathbf{k}}(\hat{\mathbf{q}}_2)\,\Delta_{pm,\mathbf{k}}(\hat{\mathbf{q}}_3)\Bigg[-\frac{8f_{nm,\mathbf{k}}E_{pm,\mathbf{k}}}{(E_{nm,\mathbf{k}}+2\tilde{\omega})E_{nm,\mathbf{k}}^4} - \frac{4f_{nm,\mathbf{k}}E_{pm,\mathbf{k}}}{(E_{nm,\mathbf{k}}+2\tilde{\omega})^2E_{nm,\mathbf{k}}^3} \\
&\quad - \frac{f_{nm,\mathbf{k}}}{(E_{nm,\mathbf{k}}+2\tilde{\omega})^2(E_{pm,\mathbf{k}}+\tilde{\omega})(E_{np,\mathbf{k}}+\tilde{\omega})} - \frac{2f_{nm,\mathbf{k}}}{(E_{nm,\mathbf{k}}+2\tilde{\omega})(E_{pm,\mathbf{k}}+\tilde{\omega})(E_{np,\mathbf{k}}+\tilde{\omega})E_{nm,\mathbf{k}}} \\
&\qquad + \frac{f_{np,\mathbf{k}}}{4(E_{np,\mathbf{k}}+\tilde{\omega})E_{np,\mathbf{k}}^3} + \frac{f_{np,\mathbf{k}}}{(E_{pm,\mathbf{k}}+\tilde{\omega})(E_{np,\mathbf{k}}+\tilde{\omega})^3} + \frac{f_{np,\mathbf{k}}}{(E_{np,\mathbf{k}}+\tilde{\omega})E_{nm,\mathbf{k}}E_{np,\mathbf{k}}^2} \\
&+ \frac{f_{np,\mathbf{k}}}{(E_{pm,\mathbf{k}}+\tilde{\omega})(E_{np,\mathbf{k}}+\tilde{\omega})^2E_{np,\mathbf{k}}} + \frac{f_{np,\mathbf{k}}}{(E_{pm,\mathbf{k}}+\tilde{\omega})(E_{np,\mathbf{k}}+\tilde{\omega})E_{nm,\mathbf{k}}E_{np,\mathbf{k}}} + \frac{f_{pm,\mathbf{k}}(8E_{nm,\mathbf{k}}+3E_{pm,\mathbf{k}})}{4(E_{pm,\mathbf{k}}+\tilde{\omega})E_{pm,\mathbf{k}}^4} \\
&\qquad + \frac{f_{pm,\mathbf{k}}(5E_{nm,\mathbf{k}}+3E_{pm,\mathbf{k}})}{4(E_{pm,\mathbf{k}}+\tilde{\omega})^2E_{pm,\mathbf{k}}^3} + \frac{f_{pm,\mathbf{k}}(E_{nm,\mathbf{k}}+E_{pm,\mathbf{k}})}{2(E_{pm,\mathbf{k}}+\tilde{\omega})^3E_{pm,\mathbf{k}}^2} + \frac{f_{pm,\mathbf{k}}}{(E_{pm,\mathbf{k}}+\tilde{\omega})^3(E_{np,\mathbf{k}}+\tilde{\omega})} \\
&+ \frac{f_{pm,\mathbf{k}}}{(E_{pm,\mathbf{k}}+\tilde{\omega})^2(E_{np,\mathbf{k}}+\tilde{\omega})E_{pm,\mathbf{k}}} + \frac{f_{pm,\mathbf{k}}}{(E_{pm,\mathbf{k}}+\tilde{\omega})(E_{np,\mathbf{k}}+\tilde{\omega})E_{pm,\mathbf{k}}^2} + \frac{f_{pm,\mathbf{k}}}{(E_{np,\mathbf{k}}+\tilde{\omega})E_{nm,\mathbf{k}}E_{pm,\mathbf{k}}^2} \\
&\qquad - \frac{f_{pm,\mathbf{k}}}{(E_{pm,\mathbf{k}}+\tilde{\omega})(E_{np,\mathbf{k}}+\tilde{\omega})E_{nm,\mathbf{k}}E_{pm,\mathbf{k}}}\Bigg]
\end{aligned}
\tag{F.8}
$$

The two-band term is

$$
\begin{aligned}
\chi_0^{(3),2bnd}(\hat{\mathbf{q}},\hat{\mathbf{q}}_1,\hat{\mathbf{q}}_2,\hat{\mathbf{q}}_3,\omega,\omega,0) &= \hat{\mathbf{r}}_{nm,\mathbf{k}}(\hat{\mathbf{q}})\,\hat{\mathbf{r}}_{mn,\mathbf{k}}(\hat{\mathbf{q}}_1)\,\hat{\mathbf{r}}_{nm,\mathbf{k}}(\hat{\mathbf{q}}_2)\,\hat{\mathbf{r}}_{mn,\mathbf{k}}(\hat{\mathbf{q}}_3)\Bigg[-\frac{16f_{nm,\mathbf{k}}}{(E_{nm,\mathbf{k}}+2\tilde{\omega})^2E_{nm,\mathbf{k}}} \\
&\quad - \frac{32f_{nm,\mathbf{k}}}{(E_{nm,\mathbf{k}}+2\tilde{\omega})E_{nm,\mathbf{k}}^2}\Bigg] + \hat{\mathbf{r}}_{nm,\mathbf{k}}(\hat{\mathbf{q}})\,\hat{\mathbf{r}}_{mn,\mathbf{k}}(\hat{\mathbf{q}}_1)\,\hat{\mathbf{r}}_{mn,\mathbf{k}}(\hat{\mathbf{q}}_2)\,\hat{\mathbf{r}}_{nm,\mathbf{k}}(\hat{\mathbf{q}}_3)\Bigg[-\frac{5f_{nm,\mathbf{k}}}{2(E_{nm,\mathbf{k}}+\tilde{\omega})E_{nm,\mathbf{k}}^2} \\
&\quad - \frac{16f_{nm,\mathbf{k}}}{(E_{nm,\mathbf{k}}+2\tilde{\omega})^2E_{nm,\mathbf{k}}}\Bigg] + \Delta_{nm,\mathbf{k}}(\hat{\mathbf{q}})\,\Delta_{nm,\mathbf{k}}(\hat{\mathbf{q}}_1)\,\hat{\mathbf{r}}_{nm,\mathbf{k}}(\hat{\mathbf{q}}_2)\,\hat{\mathbf{r}}_{mn,\mathbf{k}}(\hat{\mathbf{q}}_3)\Bigg[\frac{16f_{nm,\mathbf{k}}}{(E_{nm,\mathbf{k}}+2\tilde{\omega})E_{nm,\mathbf{k}}^4} \\
&\qquad - \frac{f_{nm,\mathbf{k}}}{4(E_{nm,\mathbf{k}}+\tilde{\omega})^2E_{nm,\mathbf{k}}^3} - \frac{5f_{nm,\mathbf{k}}}{4(E_{nm,\mathbf{k}}+\tilde{\omega})E_{nm,\mathbf{k}}^4}\Bigg] \\
&+ \hat{\mathbf{r}}_{nm,\mathbf{k}}(\hat{\mathbf{q}})\,\hat{\mathbf{r}}_{mn,\mathbf{k}}(\hat{\mathbf{q}}_1)\,\Delta_{nm,\mathbf{k}}(\hat{\mathbf{q}}_2)\,\Delta_{nm,\mathbf{k}}(\hat{\mathbf{q}}_3)\Bigg[\frac{15f_{nm,\mathbf{k}}}{4(E_{nm,\mathbf{k}}+\tilde{\omega})E_{nm,\mathbf{k}}^4} + \frac{7f_{nm,\mathbf{k}}}{4(E_{nm,\mathbf{k}}+\tilde{\omega})^2E_{nm,\mathbf{k}}^3} \\
&+ \frac{f_{nm,\mathbf{k}}}{2(E_{nm,\mathbf{k}}+\tilde{\omega})^3E_{nm,\mathbf{k}}^2} - \frac{40f_{nm,\mathbf{k}}}{(E_{nm,\mathbf{k}}+2\tilde{\omega})E_{nm,\mathbf{k}}^4} - \frac{24f_{nm,\mathbf{k}}}{(E_{nm,\mathbf{k}}+2\tilde{\omega})^2E_{nm,\mathbf{k}}^3} - \frac{8f_{nm,\mathbf{k}}}{(E_{nm,\mathbf{k}}+2\tilde{\omega})^3E_{nm,\mathbf{k}}^2}\Bigg] \\
&- \Delta_{nm,\mathbf{k}}(\hat{\mathbf{q}})\,\hat{\mathbf{r}}_{nm,\mathbf{k}}(\hat{\mathbf{q}}_1)\,\hat{\mathbf{r}}_{mn,\mathbf{k}}(\hat{\mathbf{q}}_2)\,\Delta_{nm,\mathbf{k}}(\hat{\mathbf{q}}_3)\Bigg[\frac{5f_{nm,\mathbf{k}}}{4(E_{nm,\mathbf{k}}+\tilde{\omega})E_{nm,\mathbf{k}}^4} + \frac{3f_{nm,\mathbf{k}}}{4(E_{nm,\mathbf{k}}+\tilde{\omega})^2E_{nm,\mathbf{k}}^3} \\
&+ \frac{f_{nm,\mathbf{k}}}{4(E_{nm,\mathbf{k}}+\tilde{\omega})^3E_{nm,\mathbf{k}}^2}\Bigg] + \hat{\mathbf{r}}_{nm,\mathbf{k}}(\hat{\mathbf{q}})\,\Delta_{nm,\mathbf{k}}(\hat{\mathbf{q}}_1)\,\Delta_{nm,\mathbf{k}}(\hat{\mathbf{q}}_2)\,\hat{\mathbf{r}}_{mn,\mathbf{k}}(\hat{\mathbf{q}}_3)\Bigg[\frac{9f_{nm,\mathbf{k}}}{4(E_{nm,\mathbf{k}}+\tilde{\omega})E_{nm,\mathbf{k}}^4} \\
&\qquad + \frac{f_{nm,\mathbf{k}}}{2(E_{nm,\mathbf{k}}+\tilde{\omega})^2E_{nm,\mathbf{k}}^3} - \frac{32f_{nm,\mathbf{k}}}{(E_{nm,\mathbf{k}}+2\tilde{\omega})E_{nm,\mathbf{k}}^4} - \frac{8f_{nm,\mathbf{k}}}{(E_{nm,\mathbf{k}}+2\tilde{\omega})^2E_{nm,\mathbf{k}}^3}\Bigg]
\end{aligned}
\tag{F.9}
$$

Appendix G

Breakdown field

In this part, I discuss the intensity of the dc-electric field that one can use on the material without destroying it. Indeed, if the static field applied is too strong, it induces an electrical breakdown inside the sample, which corresponds to an irreversible and practically always destructive sudden flow of current. In that case, the Zener tunneling, shown in Figure 4.1 is no longer negligible and the insulator material becomes electrically conductive.

material	symbol	breakdown field (V/cm)
silicon	Si	$3.0 \cdot 10^5$
cubic silicon carbide	3C-SiC	$1.0 \cdot 10^6$
hexagonal silicon carbide	2H-SiC	$6.0 \cdot 10^5$
gallium arsenide	GaAs	$4.0 \cdot 10^5$
germanium	Ge	$1.0 \cdot 10^5$
silicon germanium	$Si_{1-x}Ge_x$	$< 3.0 \cdot 10^5$

Table G.1: Values of the breakdown field for different materials.

Bibliography

[1] Hannes Hübener. *Second Harmonic Generation in Solids: Theory and Simulation*. PhD thesis, Ecole Polytechnique, 2010.

[2] Nicolas Tancogne-Dejean. *Ab initio description of second-harmonic generation from crystal surfaces*. PhD thesis, Ecole Polytechnique, 2015.

[3] Ivan P. Kaminow. *An Introduction to Electrooptic Devices: Selected Reprints and Introductory Text By*. Academic Press, October 2013.

[4] P. A. Franken, A. E. Hill, C. W. Peters, and G. Weinreich. Generation of Optical Harmonics. *Phys. Rev. Lett.*, 7(4):118–119, August 1961.

[5] G. H. C. New and J. F. Ward. Optical Third-Harmonic Generation in Gases. *Phys. Rev. Lett.*, 19(10):556–559, September 1967.

[6] C. H. Lee, R. K. Chang, and N. Bloembergen. Nonlinear Electroreflectance in Silicon and Silver. *Phys. Rev. Lett.*, 18(5):167–170, January 1967.

[7] James L. P. Hughes and J. E. Sipe. Calculation of second-order optical response in semiconductors. *Phys. Rev. B*, 53(16):10751–10763, April 1996.

[8] M. Izdebski, W. Kucharczyk, and R. E. Raab. On relationships between electro-optic coefficients for impermeability and nonlinear electric susceptibilities. *J. Opt. A: Pure Appl. Opt.*, 6(4):421, 2004.

[9] Eleonora Luppi, Hannes Hübener, and Valérie Véniard. Ab initio second order optics in solids. *Phys. Rev. B*, 82(23):235201, December 2010.

[10] Nicolas Tancogne-Dejean, Christine Giorgetti, and Valérie Véniard. Optical properties of surfaces with supercell ab initio calculations: Local-field effects. *Phys. Rev. B*, 92(24):245308, December 2015.

[11] Wilfrid I. Ndebeka, Herbert Stafast, Erich Rohwer, Christine Steenkamp, and Pieter Neethling. Investigation of Free Charge Carrier Effects in Silicon Membranes. In *Frontiers in Optics 2015 (2015), paper JTu4A.84*, page JTu4A.84. Optical Society of America, October 2015.

[12] Oksana Ostroverkhova, Andrew Stickrath, and Kenneth D. Singer. Electric field-induced second harmonic generation studies of chromophore orientational dynamics in photorefractive polymers. *Journal of Applied Physics*, 91(12):9481–9486, May 2002.

[13] Claudio Aversa and J. E. Sipe. Nonlinear optical susceptibilities of semiconductors: Results with a length-gauge analysis. *Phys. Rev. B*, 52(20):14636–14645, November 1995.

[14] C. Attaccalite and M. Grüning. Nonlinear optics from an ab initio approach by means of the dynamical Berry phase: Application to second- and third-harmonic generation in semiconductors. *Phys. Rev. B*, 88(23):235113, December 2013.

[15] M. Grüning, D. Sangalli, and C. Attaccalite. Dielectrics in a time-dependent electric field: A real-time approach based on density-polarization functional theory. *Phys. Rev. B*, 94(3):035149, July 2016.

[16] Richard M. Martin. *Electronic structure: basic theory and practical methods*. Cambridge University Press, 2004.

[17] P. Hohenberg and W. Kohn. Inhomogeneous Electron Gas. *Phys. Rev.*, 136(3B):B864–B871, November 1964.

[18] W. Kohn and L. J. Sham. Self-Consistent Equations Including Exchange and Correlation Effects. *Phys. Rev.*, 140(4A):A1133–A1138, November 1965.

[19] P. A. Dirac. Note on exchange phenomena in the thomas atom. *Mathematical Proc. Cambridge Phil. Soc.*, 26(03):376–385, July 1930.

[20] D. R. Hamann, M. Schlüter, and C. Chiang. Norm-Conserving Pseudopotentials. *Phys. Rev. Lett.*, 43(20):1494–1497, November 1979.

[21] David Vanderbilt. Soft self-consistent pseudopotentials in a generalized eigenvalue formalism. *Phys. Rev. B*, 41(11):7892–7895, April 1990.

[22] Erich Runge and E. K. U. Gross. Density-Functional Theory for Time-Dependent Systems. *Phys. Rev. Lett.*, 52(12):997–1000, March 1984.

[23] Silvana Botti, Arno Schindlmayr, Rodolfo Del Sole, and Lucia Reining. Time-dependent density-functional theory for extended systems. *Rep. Prog. Phys.*, 70(3):357, 2007.

[24] Robert van Leeuwen. Mapping from Densities to Potentials in Time-Dependent Density-Functional Theory. *Phys. Rev. Lett.*, 82(19):3863–3866, May 1999.

[25] Giovanni Vignale. Real-time resolution of the causality paradox of time-dependent density-functional theory. *Phys. Rev. A*, 77(6):062511, June 2008.

[26] Robert van Leeuwen. Causality and Symmetry in Time-Dependent Density-Functional Theory. *Phys. Rev. Lett.*, 80(6):1280–1283, February 1998.

[27] Xavier Andrade, David Strubbe, Umberto De Giovannini, Ask Hjorth Larsen, Micael J. T. Oliveira, Joseba Alberdi-Rodriguez, Alejandro Varas, Iris Theophilou, Nicole Helbig, Matthieu J. Verstraete, Lorenzo Stella, Fernando Nogueira, Alán Aspuru-Guzik, Alberto Castro, Miguel A. L. Marques, and Angel Rubio. Real-space grids and the Octopus code as tools for the development of new simulation approaches for electronic systems. *Phys. Chem. Chem. Phys.*, 17(47):31371–31396, November 2015.

[28] R Kubo. Linear response theory and fluctuafion. dissipation theorem. *J. Phys. Soc. Japan*, 12:570586, 1957.

[29] R. van Leeuwen. Introduction to time-dependent density functional theory, 2006. *Available at* `http://www.tddft.org/TDDFT2006/2006tddft/docs/school/vanLeeuwen-I+II.pdf`.

[30] H. Ehrenreich. *The optical properties of solids*. Academic, New York, 1965.

[31] Sohrab Ismail-Beigi, Eric K. Chang, and Steven G. Louie. Coupling of Nonlocal Potentials to Electromagnetic Fields. *Phys. Rev. Lett.*, 87(8):087402, August 2001.

[32] R. Del Sole and E. Fiorino. Macroscopic dielectric tensor at crystal surfaces. *Phys. Rev. B*, 29(8):4631–4645, April 1984.

[33] R. W. Nunes and Xavier Gonze. Berry-phase treatment of the homogeneous electric field perturbation in insulators. *Phys. Rev. B*, 63(15):155107, March 2001.

[34] R. D. King-Smith and David Vanderbilt. Theory of polarization of crystalline solids. *Phys. Rev. B*, 47(3):1651–1654, January 1993.

[35] Raffaele Resta. Macroscopic polarization in crystalline dielectrics: the geometric phase approach. *Rev. Mod. Phys.*, 66(3):899–915, July 1994.

[36] The abinit code is a common project of the université catholique de louvain, corning incorporated, and other contributors (url http://www.abinit.org).

[37] Sabine Körbel, David Kammerlander, Rafael Sarmiento-Pérez, Claudio Attaccalite, Miguel A. L. Marques, and Silvana Botti. Optical properties of Cu-chalcogenide photovoltaic absorbers from self-consistent GW and the Bethe-Salpeter equation. *Phys. Rev. B*, 91(7):075134, February 2015.

[38] Michael Springborg and Bernard Kirtman. Analysis of vector potential approach for calculating linear and nonlinear responses of infinite periodic systems to a finite static external electric field. *Phys. Rev. B*, 77(4):045102, January 2008.

[39] Eleonora Luppi, Hans-Christian Weissker, Sandro Bottaro, Francesco Sottile, Valérie Veniard, Lucia Reining, and Giovanni Onida. Accuracy of the pseudopotential approximation in ab initio theoretical spectroscopies. *Phys. Rev. B*, 78(24):245124, December 2008.

[40] Sean M. Anderson, Nicolas Tancogne-Dejean, Bernardo S. Mendoza, and Valérie Véniard. Theory of surface second-harmonic generation for semiconductors including effects of nonlocal operators. *Phys. Rev. B*, 91(7):075302, February 2015.

[41] Valérie Véniard, Eleonora Luppi, and Hannes Hübener. (unpublished).

[42] S. Sharma, J. K. Dewhurst, and C. Ambrosch-Draxl. Linear and second-order optical response of the III-V monolayer superlattices. *Physical Review B*, 67(16), April 2003. arXiv: cond-mat/0211512.

[43] F. Nastos, B. Olejnik, K. Schwarz, and J. E. Sipe. Scissors implementation within length-gauge formulations of the frequency-dependent nonlinear optical response of semiconductors. *Phys. Rev. B*, 72(4):045223, July 2005.

[44] Ed Ghahramani, D. J. Moss, and J. E. Sipe. Full-band-structure calculation of second-harmonic generation in odd-period strained $(\mathrm{Si})_n/(\mathrm{Ge})_n$ superlattices. *Phys. Rev. B*, 43(11):8990–9002, April 1991.

[45] Xiao Tang, Kenneth G. Irvine, Dongping Zhang, and Michael G. Spencer. Linear electrooptic effect in cubic silicon carbide. *Applied Physics Letters*, 59(16):1938–1939, October 1991.

[46] Silvana Botti, Francesco Sottile, Nathalie Vast, Valerio Olevano, Lucia Reining, Hans-Christian Weissker, Angel Rubio, Giovanni Onida, Rodolfo Del Sole, and R. W. Godby. Long-range contribution to the exchange-correlation kernel of time-dependent density functional theory. *Phys. Rev. B*, 69(15):155112, April 2004.

[47] S. Adachi. *GaAs and related materials: Bulk Semiconducting and Superlattice properties*. World Scientific, Teaneck, NJ, 1994.

[48] F. S. Hickernell. The piezoelectric semiconductor and acoustoelectronic device development in the sixties. In *IEEE International Frequency Control Symposium and PDA Exhibition Jointly with the 17th European Frequency and Time Forum, 2003. Proceedings of the 2003*, pages 1012–1020, May 2003.

[49] Matteo Bertocchi. *First principles Second Harmonic Generation in quantum confined silicon based systems*. PhD thesis, Ecole Polytechnique, 2013.

[50] D. J. Bottomley, G. Lüpke, M. L. Ledgerwood, X. Q. Zhou, and H. M. van Driel. Second harmonic generation from SimGen superlattices. *Appl. Phys. Lett.*, 63(17):2324–2326, October 1993.

[51] Xinhui Zhang, Zhenghao Chen, Linzhen Xuan, Shaohua Pan, and Guozhen Yang. Enhancement of bulklike second-order nonlinear susceptibility in SiGe/Si step wells and biasing-field controlled $(\mathrm{Si}_5\mathrm{Ge}_5)_{100}$ superlattices. *Phys. Rev. B*, 56(24):15842–15846, December 1997.

[52] Chun Zhang, Xudong Xiao, N. Wang, K. K. Fung, M. M. T. Loy, Zhenghao Chen, and Junming Zhou. Defect-enhanced second-harmonic generation in $(\mathrm{Si}_m\mathrm{Ge}_n)_p$ superlattices. *Appl. Phys. Lett.*, 72(17):2072–2074, April 1998.

[53] Xudong Xiao, Chun Zhang, A. B. Fedotov, Zhenghao Chen, and M. M. T. Loy. Interfaces of strained layer $(\mathrm{Ge}_n\mathrm{Si}_m)_p$ superlattices studied by second-harmonic generation. *Journal of Vacuum Science & Technology B: Microelectronics and Nanometer Structures Processing, Measurement, and Phenomena*, 15(4):1112–1116, July 1997.

[54] Matteo Bertocchi, Eleonora Luppi, Elena Degoli, Valérie Véniard, and Stefano Ossicini. Defects and strain enhancements of second-harmonic generation in Si/Ge superlattices. *The Journal of Chemical Physics*, 140(21):214705, June 2014.

[55] J. Frigerio, P. Chaisakul, D. Marris-Morini, S. Cecchi, M. S. Roufied, G. Isella, and L. Vivien. Electro-refractive effect in Ge/SiGe multiple quantum wells. *Applied Physics Letters*, 102(6):061102, February 2013.

[56] M. Cazzanelli, F. Bianco, E. Borga, G. Pucker, M. Ghulinyan, E. Degoli, E. Luppi, V. Véniard, S. Ossicini, D. Modotto, S. Wabnitz, R. Pierobon, and L. Pavesi. Second-harmonic generation in silicon waveguides strained by silicon nitride. *Nat Mater*, 11(2):148–154, February 2012.

[57] Eleonora Luppi, Elena Degoli, Matteo Bertocchi, Stefano Ossicini, and Valérie Véniard. Strain-designed strategy to induce and enhance second-harmonic generation in centrosymmetric and noncentrosymmetric materials. *Phys. Rev. B*, 92(7):075204, August 2015.

[58] Rune S. Jacobsen, Karin N. Andersen, Peter I. Borel, Jacob Fage-Pedersen, Lars H. Frandsen, Ole Hansen, Martin Kristensen, Andrei V. Lavrinenko, Gaid Moulin, Haiyan Ou, Christophe Peucheret, Beáta Zsigri, and Anders Bjarklev. Strained silicon as a new electro-optic material. *Nature*, 441(7090):199–202, May 2006.

[59] O. A. Aktsipetrov, A. A. Fedyanin, E. D. Mishina, A. N. Rubtsov, C. W. van Hasselt, M. A. C. Devillers, and Th. Rasing. dc-electric-field-induced second-harmonic generation in Si(111)-SiO_2-Cr metal-oxide-semiconductor structures. *Phys. Rev. B*, 54(3):1825–1832, July 1996.

[60] P. Godefroy, W. de Jong, C. W. van Hasselt, M. a. C. Devillers, and Th. Rasing. Electric field induced second harmonic generation spectroscopy on a metaloxidesilicon structure. *Appl. Phys. Lett.*, 68(14):1981–1983, April 1996.

[61] O. A. Aktsipetrov, A. A. Fedyanin, A. V. Melnikov, E. D. Mishina, A. N. Rubtsov, M. H. Anderson, P. T. Wilson, M. ter Beek, X. F. Hu, J. I. Dadap, and M. C. Downer. dc-electric-field-induced and low-frequency electromodulation second-harmonic generation spectroscopy of Si(001)-SiO2 interfaces. *Phys. Rev. B*, 60(12):8924–8938, September 1999.

[62] J. G. Mihaychuk, N. Shamir, and H. M. van Driel. Multiphoton photoemission and electric-field-induced optical second-harmonic generation as probes of charge transfer across the si/sio$_2$ interface. *Phys. Rev. B*, 59(3):2164–2173, January 1999.

[63] D. A. Kleinman. Nonlinear Dielectric Polarization in Optical Media. *Phys. Rev.*, 126(6):1977–1979, June 1962.

Acknowledgements

There are many people I would like to thank. First of all, I am very grateful to my supervisor Valérie Véniard for the continuous support of my PhD work, for her motivation, patience and vast knowledge. Her guidance really helped me through my research.
I would also like to address my gratitude to the whole group of Theoretical Spectroscopy for creating a friendly and productive environment and in particular a former PhD student of our group, Nicolas Tancogne-Dejean, for helping me at the beginning of my PhD by answering all my questions. I am also thankful to Christine Giorgetti for her advices in the preparation of my talks both for conferences and for the defense of this thesis.
And finally, I would like to thank my friends and fellow PhD students in the Theoretical Spectroscopy group, Marco Vanzini and Jianqiang (Sky) Zhou for relaxing and fun discussions.

Abstract

A deep understanding of the optical properties of solids is crucial for the improvement of nonlinear materials and devices. It offers the opportunity to search for new materials with specific properties. One way to tune some of those properties is to apply an electrostatic field on materials, giving rise to electro-optic effects. This electrostatic field can be applied voluntarily on the system either to deform the material or to generate new electro-optic responses. But it is also possible that this dc-field was already present due to the structure of the material: for instance, an accumulation of charge can be created at an interface, effectively generating an electrostatic field inside the material. In that case, it becomes necessary to take into account the presence of this static field, which can induce corrections during the measurement of different susceptibilities. Furthermore, the measurement of susceptibilities that depend on the dc-field can be used as a tool to determine the value of this static field naturally generated at an interface.

In this thesis, two optical phenomena were studied: (i) the linear response (LR) that can be generated with a low intensity light and includes the one-photon absorption (OPA), where a photon is absorbed at the energy of of the input electric field and (ii) the second harmonic generation (SHG) that can only be generated from an intense light such as a laser, where two photons are absorbed by the material and a photon is emitted at twice the energy of the incoming photon. This process, as all second-order susceptibilities, is very sensitive to the symmetry of the material. Indeed, if the system studied presents an inversion symmetry then the second harmonic response will be zero.

Using a laser to generate a second-harmonic response will also generate a linear response. But, considering that these two phenomena happen at different energies, it becomes relatively easy to distinguish them. However, applying a static field amounts to induce new nonlinear processes happening at the same energy since it can be viewed as absorbing one or more photons of energy zero. Considering that these responses are generated at the same energy, it is no longer possible to look at them separately. Those new susceptibilities induced by the static field are then considered as corrections to the initial response.

The first-order correction in terms of the static field to the optical linear response corresponds to one of the most known electro-optic effect, namely the Pockel or linear electro-optic effect (LEO). It is a second order response since it is induced by both an optical field $E(\omega)$ and a static field E(0), and it is described by the susceptibility $\chi^{(2)}(-\omega;\omega,0)$. Likewise, the first-order correction in terms of the static field to the second-harmonic generation corresponds to a third order process, named EFISH (Electric Field Induced Second Harmonic) for which the susceptibility of interest is $\chi^{(3)}(-2\omega;\omega,\omega,0)$. The static field inside the material is breaking the centrosymmetry which then enable the generation of a "second-harmonic response" from every material, whether it has or not an inversion symmetry.

The aim of my thesis was to calculate theoretically and numerically these corrections to the linear and nonlinear (2^{nd} harmonic) optical responses of materials induced by an electrostatic field, namely the second- and third-order susceptibilities LEO and EFISH. I calculated those two responses in an ab-initio framework based on TDDFT (Time-dependent Density Functional Theory), for insulator or semiconductor materials. It was first applied on simple bulk materials, such as silicon carbide (SiC),

gallium arsenide (GaAs), etc, to validate the formalism. It has then been applied on more complex materials of technological interest like Si/Ge superlattices and strained materials.

Résumé

La connaissance des propriétés optiques est fondamentale pour l'amélioration des matériaux et des dispositifs non-linéaires. Elle offre la possibilité de chercher de nouveaux matériaux ayant des propriétés bien spécifiques. Une façon de moduler certaines de ces propriétés est d'appliquer un champ électrostatique sur les matériaux, donnant lieu à des effets électro-optiques. Ce champs statique peut être appliqué volontairement sur le système, soit pour déformer le matériau ou pour générer de nouvelles réponses électro-optiques. Mais il se peut également que ce champs statique soit déjà présent dû à la structure du matériau : par exemple, une accumulation de charges peut se créer à une interface générant un champ électrostatique à l'intérieur du matériau. Dans ce cas de figure, il devient alors nécessaire de prendre en compte la présence de ce champ statique qui peut induire des corrections lors de la mesure de différentes susceptibilités. De plus, la mesure de susceptibilités dépendantes du champ statique peut être utiliser comme un outil pour déterminer la valeur de ce champ statique naturellement générer à une interface.

Dans cette thèse, deux phénomènes optiques ont été étudiés : (i) la réponse linéaire, pouvant être générer avec une lumière de faible intensitité, qui comprend l'absorption à un photon (OPA) où un photon est absorbé à l'énergie correspondant à celle du champ électrique incident et (ii) la génération de seconde harmonique (SHG), qui ne peut être généré qu'avec une lumière très intense tel qu'un laser, où deux photons sont absorbés par le matériau et un photon est émis à une énergie deux fois plus grande que celle du photon incident. Ce processus, comme toute susceptibilité du second ordre, est très sensible à la symétrie du matériau. En effet, si le système étudié présente une symétrie d'inversion alors la réponse de seconde harmonique sera nulle.

Utiliser un laser pour générer une réponse de seconde harmonique va aussi avoir pour effet de générer une réponse linéaire. Mais étant donné que ces deux phénomènes se produisent à des énergies différentes, il devient relativement facile de les distinguer. Cependant appliquer un champ électrostatique revient à induire de nouveaux processus non-linéaire ayant lieu à la même énergie puisque cela peut être vu comme absorber un ou plusieurs photons d'énergie nulle. Etant donné que ces réponses sont générer à la même énergie, il n'est plus possible de les observer séparémment. Ces nouvelles susceptibilités induites par le champ statique sont donc considérées comme des corrections à la réponse initiale.

La correction au premier ordre de la réponse optique linéaire en fonction du champ statique correspond à l'un des effets électrostatiques les plus connus, à savoir l'effet Pockels ou effet électro-optique linéaire (LEO). Il s'agit d'une réponse du second ordre étant donnée qu'elle est induite à la fois par un champ optique $E(\omega)$ et par un champ statique $E(0)$. Ce processus est décrit par la susceptibilité $\chi^{(2)}(-\omega;\omega,0)$. De même, la correction au premier ordre en fonction du champ statique de la génération de seconde harmonique correspond à un processus de troisième ordre appelé EFISH (Electric Field Induced Second Harmonic) et décrit par la susceptibilité $\chi^{(3)}(-2\omega;\omega,\omega,0)$. Le champ statique à l'intérieur du matériau permet de briser la centrosymétrie du matériau et ainsi de générer une réponse de "seconde harmonique" dans n'importe quels matériaux, qu'ils possèdent ou non un centre d'inversion.

Le but de ma thèse était de calculer théoriquement et numériquement ces corrections aux réponses optiques linéraires et non-linéaires (deuxième harmonique) induite par un champ statique, soient les susceptibilités du second et troisième ordre LEO et EFISH. J'ai calculé ces deux réponses dans le cadre d'un formalisme ab-initio, reposant sur la TDDFT (Time-Dependent Density Functional Theory), pour des matériaux semi-conducteurs ou isolants. Ces calculs ont, dans un premier temps, été appliqués à des matériaux massifs simples de type carbure de silicium (SiC), arséniure de gallium (GaAs), etc, pour valider notre formalisme. Ils ont ensuite été appliqués à des matériaux plus complexes d'intérêt technologiques comme $(Si)_n/(Ge)_n$ et des matériaux sous contrainte.

université PARIS-SACLAY | ÉCOLE DOCTORALE Ondes et Matière (EDOM)

Titre: Description ab-initio de propriétés optiques non-linéaires de matériaux semi-conducteurs soumis à un champ électrostatique

Mots clés: physique du solide, optique non-linéaire, physique théorique, simulation numérique

Résumé: La connaissance des propriétés optiques est fondamentale pour l'amélioration des matériaux et des dispositifs non-linéaires. Une façon de moduler certaines de ces propriétés est d'appliquer un champ électrostatique sur les matériaux, donnant lieu à des effets électro-optiques. Un de ces effets les plus connus est l'effet Pockels ou effet électro-optique linéaire (LEO). Il s'agit d'une réponse du second ordre, qui correspond à une correction à la réponse optique linéaire en présence d'un champ statique. Un important processus non-linéaire est la génération de seconde harmonique (SHG), qui est très sensible à la symétrie du matériau. En effet, si le système étudié présente une symétrie d'inversion alors la réponse de seconde harmonique sera nulle. Cependant ajouter un champ statique à l'intérieur du matériau permettrait de générer une réponse du second ordre dans n'importe quels matériaux. Ce phénomène est un processus de troisième ordre appelé EFISH (Electric Field Induced Second Harmonic).
Dans cette thèse sont calculées les réponses optiques linéraires et non-linéaires (deuxième harmonique) de matériaux soumis à un champ électrostatique, soient les corrections au premier et second ordre LEO et EFISH. Ces deux réponses sont évaluées dans le cadre d'un formalisme ab-initio, reposant sur la TDDFT, pour des matériaux semi-conducteurs ou isolants. Ces calculs ont, dans un premier temps, été appliqués à des matériaux massifs simples de type carbure de silicium (SiC) et arséniure de gallium (GaAs). Ils ont ensuite été appliqués à des matériaux plus complexes d'intérêt technologiques comme des interfaces Si/Ge et des matériaux sous contrainte.

Titre: Ab-initio description of optical nonlinear properties of semiconductors in the presence of an electrostatic field

Mots clés: solid state physics, nonlinear optics, theoretical physics, numerical simulation

Résumé: A deep understanding of the optical properties of solids is crucial for the improvement of nonlinear materials and devices. One way to tune some of those properties is to apply an electrostatic field on materials, giving rise to electro-optic effects. One of the most known is the Pockel or linear electro-optic effect (LEO). It is a second order response property, which corresponds to a correction to the linear response in the presence of a static field. An important nonlinear process is the second harmonic generation (SHG), which is very sensitive to the symmetry of the material. Indeed, if the system studied presents an inversion symmetry then the second harmonic response will be zero. However, adding a static field inside the material would enable a second-order nonlinear response from every material, whether it is centrosymmetric or not. This happens through a third order process, named EFISH (Electric Field Induced Second Harmonic).
In this thesis, the linear and nonlinear (2^{nd} harmonic) optical responses of materials submitted to an electrostatic field are calculated, corresponding to the first and second order correction LEO and EFISH. Those two responses are evaluated in an ab-initio framework based on TDDFT, for insulator or semiconductor materials. It was first applied on simple bulk materials, such as silicon carbide (SiC) and gallium arsenide (GaAs), before being applied on more complex materials of technological interest like Si/Ge superlattices and strained materials.

Université Paris-Saclay
Espace Technologique / Immeuble Discovery
Route de l'Orme aux Merisiers RD 128 / 91190 Saint-Aubin, France